https://www.sciencedirect.com/science/article/abs/pii/B978012822944600058X
https://doi.org/10.1016/B978-0-12-822944-6.00058-X
Comprehensive Structural Integrity (Second Edition)
Volume 2, 2023, Pages 610-679

Shape Memory Alloys – Frontier Developments

Hüseyin Sehitoglu, Gunay Anlas[1], and Ahmed Sameer Khan Mohammed, Department of Mechanical Science and Engineering, University of Illinois Urbana-Champaign, Urbana, IL, United States

Abstract

This article is mainly concerned with summarizing the recent discoveries in the deformation physics of shape memory materials with special emphasis on (1) the need to develop fundamental understanding of twinning, slip, shear/shuffle at atomic scales, martensite twin boundary topologies, atomic stacking and stable/metastable fault structures in shape memory materials, and (2) factors that result in performance degradation and accumulation of residual strains leading to fatigue and fracture. The fundamental understanding has benefitted from ab-initio modeling of atomic-electronic structures and the fault energetics of stable/metastable crystal structures. Especially, the slip phenomenon during nucleation of martensite needs further elaboration, as it exercises a strong influence on hysteresis, functional and mechanical degradation of the shape memory alloys Finally, we discourse on studies of fatigue and fracture of shape memory alloys from the literature and outline efforts to explain the complex experimental trends with respect to fatigue thresholds and nucleation. It is in the fatigue area where advancing the understanding of cycle by cycle accumulation of the irreversibilities, the strong orientation dependence of slip resistance (i.e., non-Schmid behavior), complex evolution of elastic moduli,

[1]Permanent Address: Department of Mechanical Engineering, Bogazici University, Bebek, Istanbul, Turkey.

strain sensitive evolution of interfaces with terrace-disconnection energy minimal nanostructures, and asymmetric stress-strain response will lead to the development of a comprehensive model. In the case of fracture, continuum models employ LEFM concepts and the results need corrections for martensite-induced tractions which are rather complex with localized variants. Overall, deeper scientific activities, with potential use of lattice scale theories and ab-initio based empirical atomic potentials, are paramount to advance the field to the next level.

Key Points

- Modeling approaches accross length scales from continuum to atomistics in shape memory alloys (primarily in NiTi).
- Understanding of interfaces, transformation-induced slip, martensite twinning and elastic moduli.
- New developments in high-temperature, high-entropy, titanium- and iron-based shape memory alloys.
- Functional and structural fatigue in shape memory alloys, the complexity of driving force determination in fracture.
- Basics of operation of ferro-magnetic, elasto-caloric shape memory materials, and observations of hysteresis in super-elasticity and isobaric shape memory.

Introduction to Shape Memory Alloys

Shape memory alloys recover large strains under thermo-mechanical loadings (Bhattacharya, 2003; Christian, 2002; Lagoudas, 2008b; Otsuka and Wayman, 1999; Perkins, 1975; Funakubo and Kennedy, 1987) and have many potential applications (Yamauchi *et al.*, 2011; Hartl and Lagoudas, 2007; Jani *et al.*, 2014; Duerig *et al.*, 2013) in biomedical, aerospace, mechanical and civil engineering fields. The reversible austenite $\rightleftharpoons$ martensite transformation at the microstructural level (Knowles and Smith, 1981; Olson and Cohen, 1982) is mainly responsible for the large recoverability (Chowdhury *et al.*, 2016; Chowdhury and Sehitoglu, 2017a; Gall *et al.*, 1999c; Ishida and Hiwatari, 2007; Ko *et al.*, 2017; Lai *et al.*, 2000; Miyazaki *et al.*, 1984; Sato *et al.*, 2006; Tang *et al.*, 2010) in SMAs. The SMAs in applications undergo multiple cycles of reversible transformation and could suffer from loss of functionality and fatigue damage (Norfleet *et al.*, 2009; Malarría *et al.*, 2009) primarily due to localized slip deformation and accumulation (Delville *et al.*, 2011; Mohammed and Sehitoglu, 2020a,b, 2021; Simon *et al.*, 2010; Treppmann and Hornbogen, 1995). Internal interfaces (Hamilton *et al.*, 2004), precipitates (Tirry and Schryvers, 2005) and grain boundaries can form barriers (Wang and Sehitoglu, 2013, 2014a; Sehitoglu *et al.*, 2002) that assist the accumulation of localization. Many of the critical stress magnitudes for martensite formation (Alkan and Sehitoglu, 2019a; Alkan *et al.*, 2018a) and slip nucleation (Alkan and Sehitoglu, 2017b; Ojha and Sehitoglu, 2016b), and twinning (Wang and Sehitoglu, 2013, 2014a) have been established from experiments and modeling. Ideally, a very high slip resistance, high transformation strains and low transformation stresses would be desirable (Sehitoglu *et al.*, 2002) to develop new SMAs (Abuzaid *et al.*, 2019; Duerig *et al.*, 2013; Lagoudas, 2008a; Yamauchi *et al.*, 2011). These properties hold the key to formulating new theories for functionality and fatigue resistance although this goal has not been achieved yet. The resistance to fatigue and fracture require a better understanding of dislocation formation and intrinsic slip propensity in SMAs that originate from interfaces. Many treatments have been continuum based and phenomenological (Auricchio and Taylor, 1997; Boyd and Lagoudas, 1996; Brinson, 1993; Christ and Reese, 2009; Hartl and Lagoudas, 2008; Lagoudas *et al.*, 2012; Patoor *et al.*, 1996; Shaw, 2000; Stebner and Brinson, 2013; Zaki and Moumni, 2007) including studies on grain size, plastic strain effects, and assumptions on driving forces (Bouvet *et al.*, 2004; Gall *et al.*, 2000a; Gall and Sehitoglu, 1999; Sedlak *et al.*, 2012; Thamburaja and Anand, 2001). The advent of molecular dynamics (Parrinello and Rahman, 1981) tools, and quantum length scale tools such as the density functional theory revealed insight at subatomic scales (Engel and Dreizler, 2011; Ezaz and Sehitoglu, 2011; Ren and Sehitoglu, 2016). In the current paper, we summarize past work and frontier developments in atomic scale calculations, experiments and studies on new alloys and outline basic and detailed concepts for understanding the SMAs. It is our intention to put the new developments and tools in perspective to guide future developments.

Major Issues in Shape Memory Alloys

The field of shape memory alloys has been an intriguing topic. There are new alloys that are being developed that exhibit shape memory behavior. The rate of publications remains strong. The purpose of this overview is two-fold: The *first purpose* is to put forth the fundamental concepts in shape memory behavior that differ from our understanding of conventional (untransforming) materials (Sections "Key Quantities in Shape Memory and Superelasticity", "Summary of Classes of Shape Memory Alloys", "Superelasticity-Examples", "Shape Memory Response (ISME)-Examples") and follow with explanation of the mechanisms (Section "Explanation of the Mechanisms"). Early textbooks covered the crystallography of shape memory alloys (Section "Summary of Classes of Shape Memory Alloys"), but new developments including atomistic modeling need to be emphasized in new texts covering topics such as "Energy Barriers", "Elastic Modulus", "Slip Behavior- Slip Systems and Non-Schmid Effects", "Transformation Stress- Non-Schmid Effects", The Use of MD potentials in SMA Research the Use of MD potentials in SMA Research", "Twinning", "Irrational Twin Planes and the Origin of the Irrationality (Comparison With Experiments) and Slip Emission that are emphasized in this chapter. The

atomistic modeling provided insights into displacements at the lattice level, and contributed to key information on elastic moduli and energy barriers for transformation and twinning that continuum models require. New materials with shape memory characteristics emerged adding to the traditional Ni-, Cu-, and Fe- based shape memory alloys (Section "New SMAs – Fe based SMAs, High temperature SMAs, Ferromagnetic SMAs, High Entropy SMAs"). These new compositions resulted in different crystallography, higher transformation strains, crystal orientation dependence, and higher stress magnitudes in some cases. We will show new findings and current challenges in the shape memory field and discuss them throughout the paper. Some of the new materials and their behavior are complex and intriguing such as:

(1) the very wide range of superelasticity in the new Fe based SMAs (Section "Fe Based SMAsFe Based SMAs"),
(2) the high fatigue thresholds in Ni_2FeGa SMAs (Section "Fatigue Crack Growth"),
(3) very low twinning stresses in ferromagnetic SMAs and in martensites (Sections "Ferromagnetic Shape Memory Behavior"and "Twinning")
(4) the discovery of new high temperature SMAs with moderate strength (Section "High Temperature Shape Memory alloys")
(5) the source of hysteresis and its dependence on strain rate and temperature (Sections "Stress and Thermal Hysteresis"and "Irrational Twin Planes and the Origin of the Irrationality (Comparison With Experiments) and Slip Emission")
(6) the discovery of high entropy shape memory alloys with wide superelastic window (Section "High Entropy-Shape Memory Alloy Synergy")
(7) the use of SMAs as elastocaloric materials, and the development of new compositions for environmentally friendly cooling technologies (Section "Elasto-caloric Behavior").

Now, the *second purpose of this contribution* is to clarify some of the confusion in the shape memory field such as:

(1) the non-Schmid behavior for slip and transformation and variant selection criteria (Sections "Slip Behavior- Slip Systems and Non-Schmid Effects" and "Transformation Stress- Non-Schmid Effects")
(2) the meaning of elastic modulus in an environment when martensite is twinned and detwinned (Section "Elastic Modulus"),
(3) the toughening versus non-toughening in fatigue depending on the variant orientation near the crack tip (Section "Fatigue Crack Growth"),
(4) the source of slip in shape memory alloys (Section "Irrational Twin Planes and the Origin of the Irrationality (Comparison With Experiments) and Slip Emission"),
(5) the reliability of atomic potentials and their performance for SMAs (Section "The Use of MD potentials in SMA Research"),
(6) the irrational interface planes and the confusion surrounding them (Section "Irrational Twin Planes and the Origin of the Irrationality (Comparison With Experiments) and Slip Emission").
(7) the complexity associated with determination of driving forces in fracture (Section "Fracture of Shape Memory Alloys").
(8) the complexity in understanding fatigue crack initiation and development of a theory for fatigue (Section "Fatigue Crack Initiation (LCF and HCF)").

Some of the intriguing behaviors such as tension-compression asymmetry, crystal orientation dependence, stress and thermal hysteresis and the role of precipitates are well documented especially for NiTi (Section "Explanation of the Mechanisms") even though they are not completely understood (Sections "Slip Behavior- Slip Systems and Non-Schmid Effects" and "Transformation Stress- Non-Schmid Effects"). What emerges from these findings is the following: The shape memory alloys are a special class of materials that present behaviors that are more complex compared to conventional cubic (fcc/bcc) and hexagonal close packed (hcp) materials. Their crystal structure, transformation displacements (paths), slip and twin mechanisms (including non-crystallographic planes), internal misfit strains bring about additional sources of complication. Therefore, we will first provide an overview of shape memory alloys and then will undertake a discussion of the items listed above.

The purpose of **Fig. 1** is to illustrate why shape memory alloys are so important and some of the deep understanding that is necessary for their widespread use. The majority of the engineering applications of shape memory alloys (upper portion of **Fig. 1**) utilize the NiTi alloy. The most important use of the NiTi material is in cardiovascular stents. There are other biomedical applications including staples and anchor locks. There are emerging structural applications such as torque tubes for flow modification in jet engines in aerospace industry, resilient tire development, and in addition there are several applications that utilize SMAs as switches in automotive industry. Other potential applications are in civil engineering as dampers and concrete reinforcement which utilize iron-based shape memory materials. On the theoretical side, there are new developments in understanding the twinning interfaces and their migration, elastic moduli, the energy barriers, precise positioning of atoms in crystal structures that affect the properties. On the experimental front, the use of digital image correlation at micro- and meso-scales, high resolution transmission electron microscopy (HRTEM) complemented the existing tools such as X-ray diffraction, conventional TEM, SEM and EBSD to gain insight into our understanding. Some of these tools are listed in the bottom portion of **Fig. 1**.

Key Quantities in Shape Memory and Superelasticity

Three types of response for shape memory alloys (Otsuka and Wayman, 1998) have been investigated (shown in **Fig. 2**): (i) shape memory, (ii) superelasticity, and (iii) constrained recovery. The shape memory effect refers to forward and reverse transformation

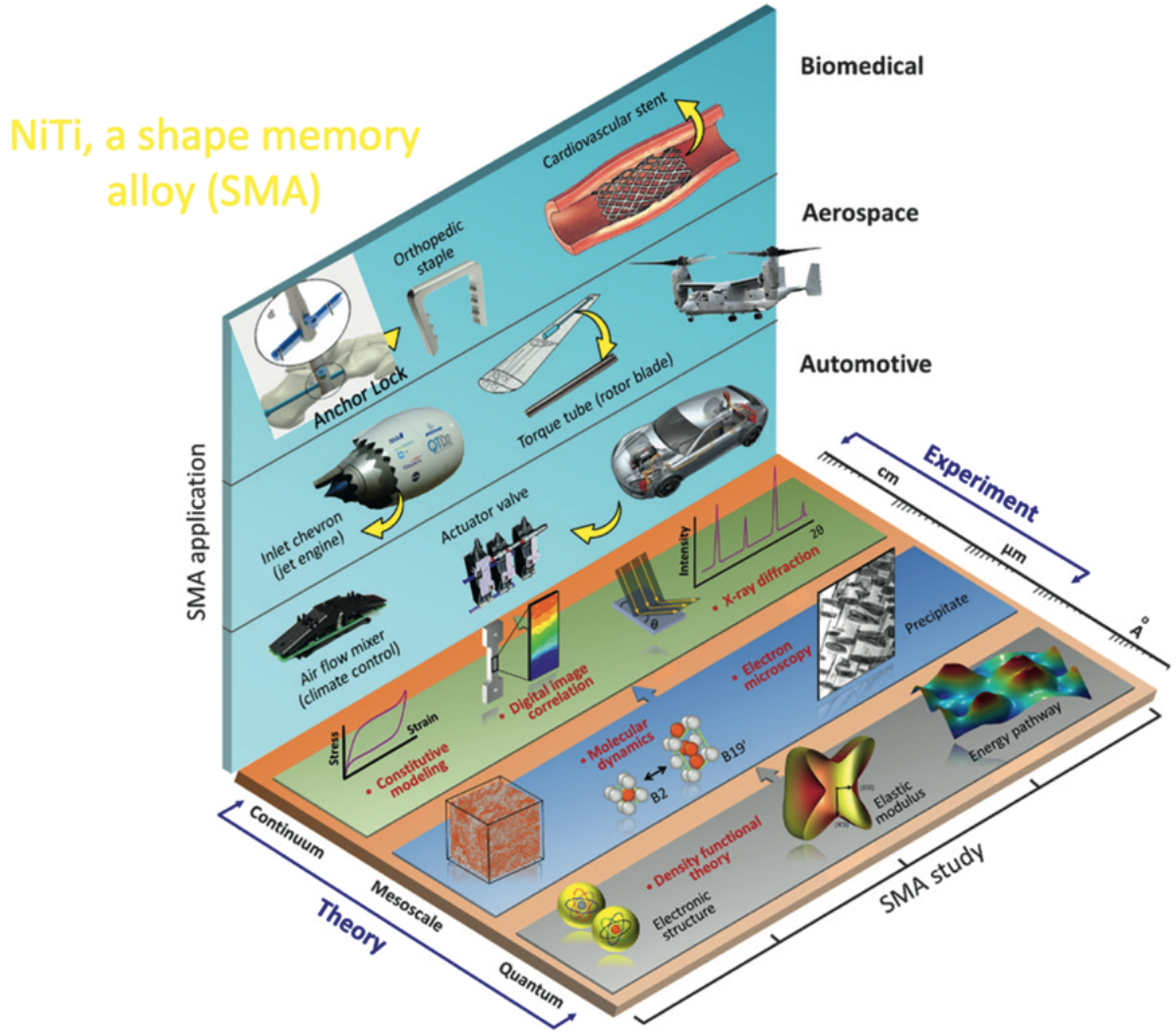

Fig. 1 Applications of shape memory alloys are shown in multiple sectors in the upper part of the diagram. The bottom half depicts the theoretical and experimental developments. Reproduced from Chowdhury, P., Ren, G., Sehitoglu, H., 2015. NiTi superelasticity via atomistic simulations. Philosophical Magazine Letters 95, 574-586, doi:10.1080/09500839.2015.1123819.

under stress (actuator type response) upon cycling the temperature (isobaric SME). The superelasticity (SE) is the forward transformation upon loading and reverse transformation upon unloading at a constant temperature (rubber like behavior).

The SME is the recovery of strains at zero external load (marked as SME) in **Fig. 2**. In the case of shape memory, the deformed martensite reverts to austenite upon heating and upon cooling back to twinned martensite. The difference between isobaric SME and SME is whether this happens at zero load or at finite load (tension and compression) respectively. The strains in (i) and (ii) can be fully or partially recovered depending on the alloy. The application in stents requires understanding of primarily SE. The actuator applications (including thin films) utilize the isobaric SME effect. In constrained recovery, the SMA is heated and cooled under constant strain and the stress developed as a result is called the 'recovery stress' marked as level B in **Fig. 2**(a). In this case, the recovery stress can impose a preload on structural components (such as prestressing concrete). Note the characteristic temperatures shown in **Fig. 2**(a). The subscripts s and f refer to start and finish and M and A refer to martensite and austenite respectively. At the M_d temperature substantial slip in the austenite occurs limiting the reversibility. Only four temperature levels, characterizing the austenite and martensite start and finish temperatures, are shown in **Fig. 2**(a). When a single transformation temperature is given, this refers to the equilibrium temperature, i.e., the average of peak temperatures observed in the DSC experiment.

Scientifically, the crystallography of transformation from the austenite phase to the martensite phase has been one of the first developments in shape memory field. The advance of the phenomenological theory of martensitic transformation from Wechsler, Lieberman and Read (WLR) (Wechsler *et al.*, 1953) permitted the determination of the habit plane (austenite-

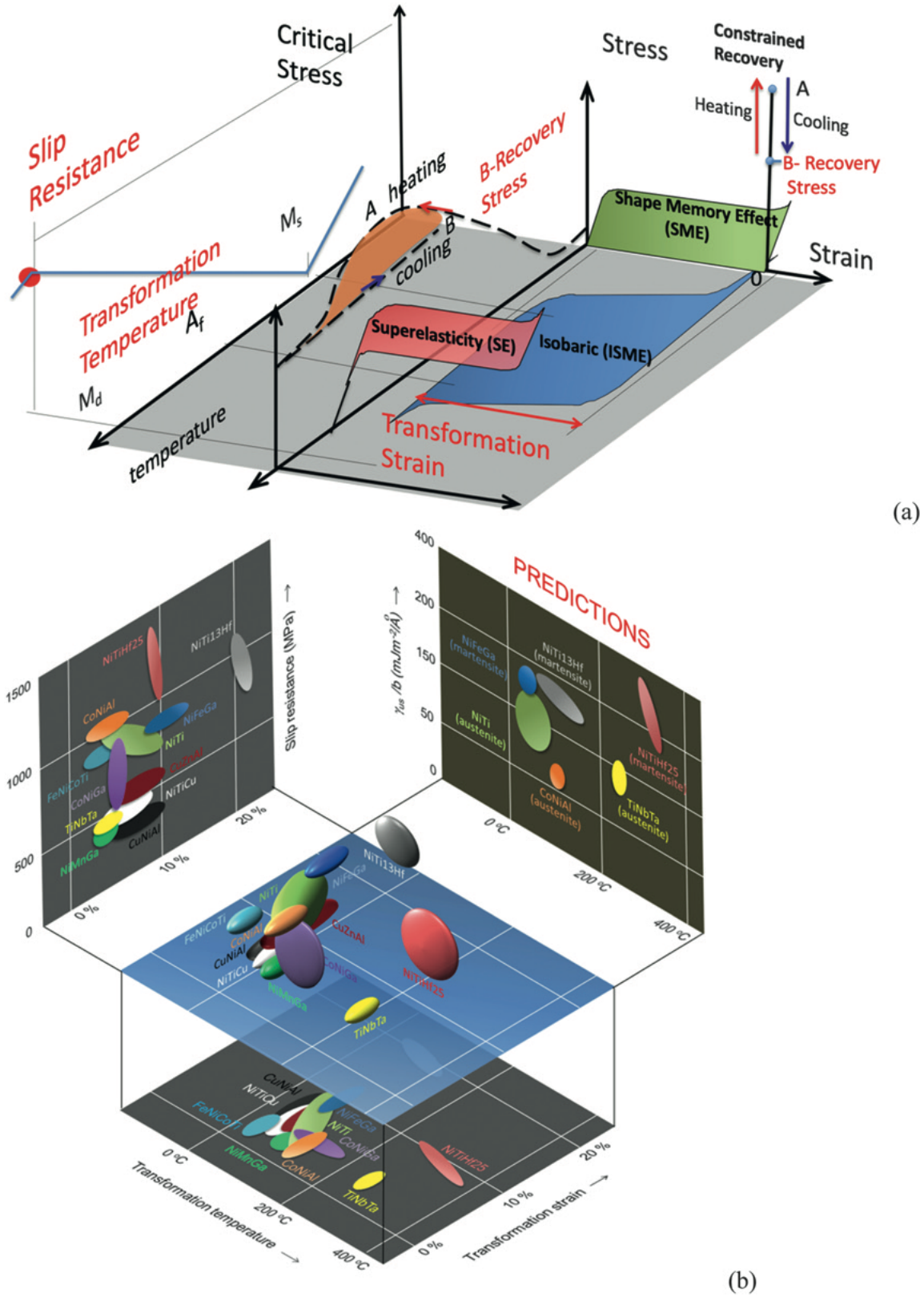

Fig. 2 (a) SMA response under (i) shape memory effect (SME), (ii) isobaric shape memory behavior (ISME), (iii) superelasticity (SE), constrained recovery (path AB). Critical stress for initiating plasticity, marked as "Slip Resistance", controls the maximum stresses achievable in SMAs during their operation, transformation temperatures are noted on the figure, (b) Transformation temperatures, transformation strains, slip resistance and unstable fault energies (theory) of most well-known shape memory alloys. Reproduced from Chowdhury, P., Sehitoglu, H., 2016. Significance of slip propensity determination in shape memory alloys. Scripta Materialia 119, 82–87.

martensite interface plane) indices with a full understanding of the orientation dependence as martensite evolves and spreads across the whole austenite domain. The equilibrium transformation temperatures, the transformation temperatures, the transformation strains, the slip resistance, unstable fault energies are marked in **Fig. 2**(b). The slip resistance is proportional to the unstable fault energy for dislocation mediated slip. In **Fig. 2**(b), the most important shape memory alloys are listed which are further discussed below.

Summary of Classes of Shape Memory Alloys

In **Table 1**, we provide a summary of the most important shape memory alloys. The main alloy that has been investigated and utilized in many applications is NiTi. More than 85% of the papers in the literature are on NiTi. The CuZnAl and CuAlNi also exhibit excellent strains but they are not suitable for bio-applications. There has been significant amount of work on Cu based

Table 1 Summary of the shape memory alloys and their key attributes

Major shape memory materials	*Comments*
NiTi	NiTi is the most widely studied SMA. It exhibits excellent cyclic stability, and moderate fatigue resistance. Higher Ni content provides higher transformation stress but with loss of recoverability (ie.transformation strain). It exhibits strong dependence on crystal orientation (texture) and also high anisotropy (Benafan *et al.*, 2014a; Buehler *et al.*, 1963; Chumlyakov *et al.*, 2013; Delville *et al.*, 2011; Hamilton *et al.*, 2004; Liu *et al.*, 1998; Miller and Lagoudas, 2001; Miyazaki *et al.*, 1981; Pelton *et al.*, 2012; Pfetzing-Micklich *et al.*, 2012; Sehitoglu *et al.*, 2000, 2001a; Shaw and Kyriakides, 1995; Simon *et al.*, 2010; Xie *et al.*, 1998; Ishida *et al.*)
CuZnAl/ CuAlNi	This is the next widely studied class of SMAs after NiTi. The results depend strongly on composition. They exhibit high recoverable strains ($>10\%$), high elastic anisotropy, and low fatigue resistance especially as polycrystals. Slip resistance is not adequate resulting in loss of functionality (Ahlers, 1986; Delaey *et al.*, 1981; Gall *et al.*, 1998a; Gil and Guilemany, 1992; Lexcellent *et al.*, 1996; Melton and Mercier, 1979a; Patoor *et al.*, 1995a; Perkins 1975; Pons *et al.*, 1993; Saburi *et al.*, 1982; Sade *et al.* 2007; Sade and Hornbogen, 1988; Schroeder and Wayman, 1979; Thumann and Hornbogen, 1988; Vinals *et al.*, 1984; Vivet and Lexcellent, 1999; Warlimont and Delaey, 1974; Wu *et al.*, 1989).
NiTiCu/Fe/Nb/Hf/Pd	Variations of NiTi are primarily designed to alter the transformation temperatures, stress leve. With Hf, the equilibrium temperature can reach 500°C making it a potential high temperature shape memory alloy (Ball and James, 1992; Bhattacharya *et al.*, 2004; Bigelow *et al.*, 2010, 2011; Coughlin *et al.*, 2012; Cui *et al.*, 2006; Golberg, 1995a, b, Gou *et al.*, 2014, 2015; Han *et al.*, 1996; Karaca *et al.*, 2013a; Karaca *et al.*, 2014; Kockar *et al.*, 2010; Kockar *et al.*, 2006; Kotil *et al.*, 2003; Kumar and Lagoudas, 2010; Lagoudas, 2008b; Lin *et al.*, 2009; Meng *et al.*, 2006; Miyazaki *et al.*, 1999; Nam *et al.*, 1990a,b; Nishida *et al.*, 1990; Noebe *et al.*, 2006; Otsuka *et al.*, 1993; Sandu *et al.*, 2006; Sehitoglu *et al.* 2017b,c; Soboyejo and Srivatsan, 2006; Tadaki and Wayman, 1982; Tang *et al.*, 2000; Teng *et al.*, 2007; Yang *et al.* 2013; Cai *et al.*, 2000; Hatcher, 2010; Hatcher *et al.*, 2009c)
FeNiCoTi/Al FeMnSi	FeNiCoTi/Al shape memory alloys exhibit higher stiffnesses and high recovery stresses compared to NiTi. The addition of Al imparts superelasticity. They exhibit larger thermal hysteresis compared to NiTi (Sato and Mori, 1991; Sato *et al.*, 1984; Bergeon *et al.*, 1998a, 1998b; Sato *et al.*, 1982; Sehitoglu *et al.*, 2005)
FeMnNiAl	FeMnNiAl based SMAs that show remarkable superelasticity over 500°C extending to low temperatures. Functionality decays with cycles, and the elastic anisotropy is high. So far, they have excellent attributes as single crystals. Strain rate insensitivity can be harnessed in some applications (Abuzaid *et al.*, 2019; Omori *et al.*, 2011; Tseng *et al.*, 2015a,b; Tseng *et al.*, 2016; Vollmer *et al.*, 2016, 2019)
Ni_2FeGa	These SMAs undergo two stage transformation they exhibit good fatigue resistance, but the results are highly orientation dependent making the polycrystalline versions prone to early fracture. Ni_2FeGa SMAs are known to possess considerably larger transformation strains ($>12\%$ in tension and >6 in compression) compared to NiTi (Omori *et al.*, 2004; Barandiarán *et al.*, 2008; Oikawa *et al.*, 2002; Sutou *et al.*, 2004; Sehitoglu *et al.*, 2012; Hamilton *et al.*, 2007a; Wang *et al.*, 2014; Hamilton *et al.*, 2007b; Chumlyakov *et al.*, 2008)
CoNiAl/CoNiGa	These SMAs exhibit superelasticity above 100°C, and recoverable strains are moderate, $\sim 6\%$. The microstructure is complex with secondary phases that do not transform (Efstathiou *et al.*, 2004; Pun *et al.*, 2015; Yamakov *et al.*, 2016; Hamilton *et al.*, 2005).
Ni_2MnGa	Ferromagnetic shape memory alloys undergo twin variant motion under magnetic fields. These materials exhibit very low twin migration stresses. They are too brittle to operate under tension and are expensive (O'Handley, 2000; O'Handley *et al.*, 2000; Söderberg *et al.*, 2005; Webster *et al.*, 1984; Enkovaara *et al.*, 2003; Ullakko *et al.*, 1996; Khovailo *et al.*, 2001; Brown *et al.*, 2002; Pons *et al.*, 2003, 2005; Zayak *et al.*, 2002, 2003; Zayak and Entel, 2004; Planes *et al.*, 2009; Dunand and Müllner, 2011; Chmielus *et al.*, 2009; Solomon *et al.*, 2005; De Graef *et al.*, 2001; Venkateswaran *et al.*, 2007)
TiNb/Zr/Ta/Al	The Ti based SMAs are developed for bio- applications or for high temperature. The loss of functionality with repeated transformation is the main concern. Alloying can improve the functionality (Ahmed and Rack, 1996; Al-Zain *et al.*, 2010; Biesiekierski *et al.*, 2012; Bönisch, 2013; Fukui *et al.*, 2004; Geetha *et al.*, 2009; Kim *et al.*, 2004, 2006a, 2015; Moffat and Kattner, 1988; Pathak *et al.*, 2014; Prokoshkin *et al.*, 2016; Tahara *et al.*, 2009; Takahashi *et al.*, 2002)
(TiZrHf)50Ni25Co10Cu15	The high entropy shape memory alloys exhibit high strength and wide range of superelasticity although the transformation strains are modest ($<3\%$) (Chen and Chen, 2019; Firstov *et al.*, 2015c)

Table 2 Summary of the crystallography of the most common shape memory alloys

NiTi (Kibey *et al.*, 2009)	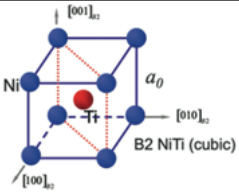	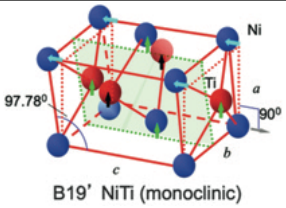
NiTiX (Kibey *et al.*, 2009; Wang and Sehitoglu, 2014a,c) X=Hf, Cu…	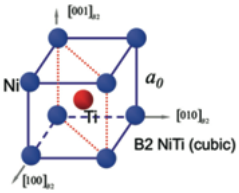	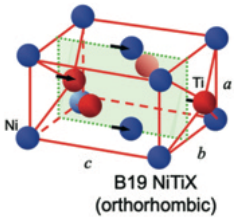
Ni_2FeGa (Chowdhury and Sehitoglu, 2017a)	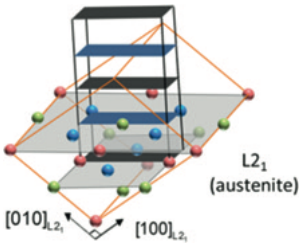 (L2$_1$ cubic)	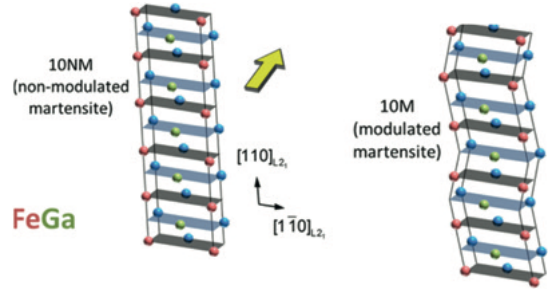 Monoclinic
FeMnNiAl (Chowdhury *et al.*, 2017)	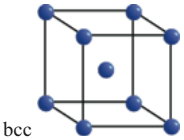 bcc	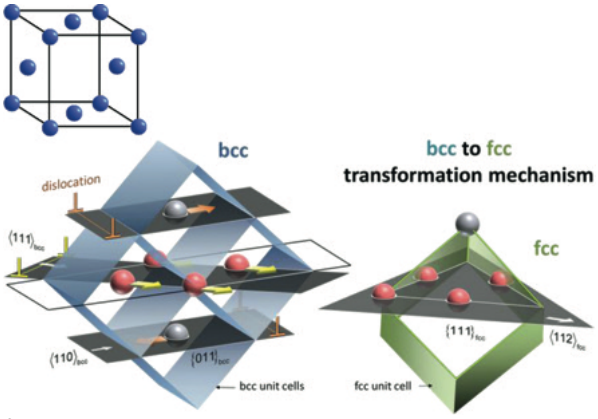 fcc
FeMnSi (Chowdhury *et al.*, 2017)	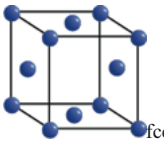 fcc	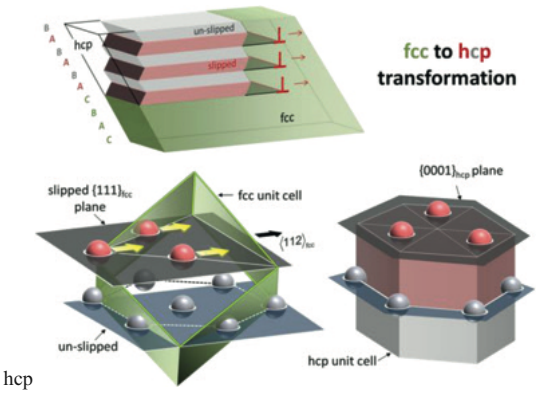 hcp

Table 2 Continued

CuZnAl(adapted from (Alkan *et al.*, 2018a)	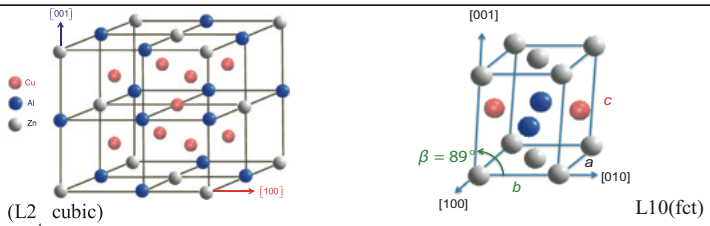 (L2$_1$ cubic) L10(fct)
CuNiAl (Otsuka *et al.*, 1976; Shield, 1995; Xiangyang *et al.*, 2000; Otsuka *et al.*, 1974)	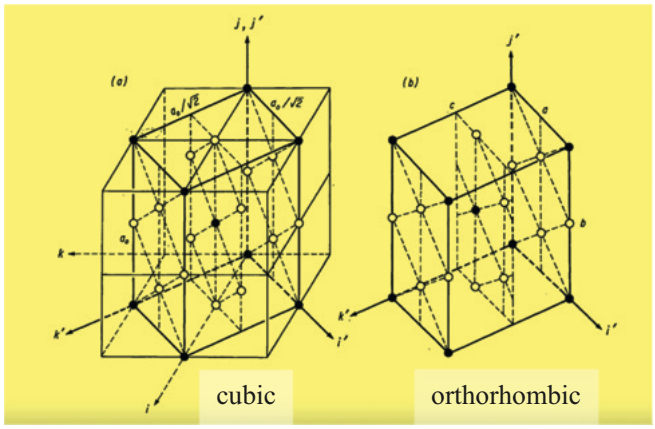 DO3 (cubic) austenite to Orthorhombic martensite phase (thermal induced, SME) -from [203]. Also, monoclinic martensite phase (stress-induced, SE) with 18R structure can format high stresses (not shown above)-closed circles Al, open circles-Cu, Ni
CoNiAl (Hamilton *et al.*, 2006b, 2005)	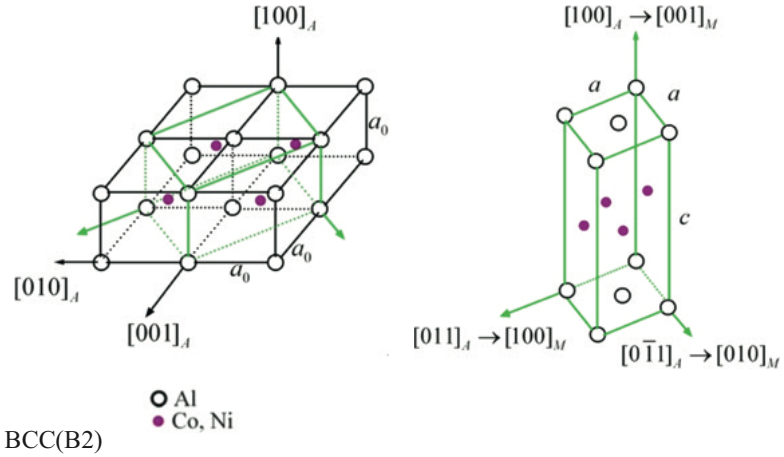 BCC(B2) $L1_0$(FCT)
FeNiCoTi (Sehitoglu *et al.*, 2002)	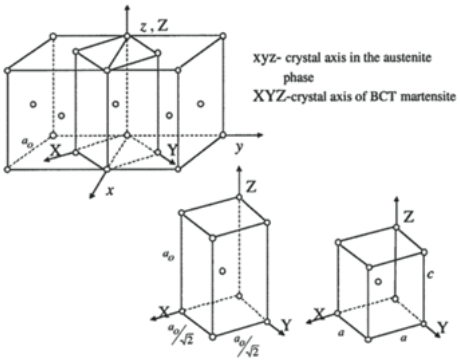 cubic tetragonal

(*Continued*)

Table 2 Continued

TiNb/Zr (Ojha and Sehitoglu, 2016a)	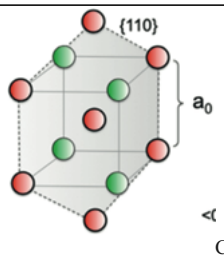	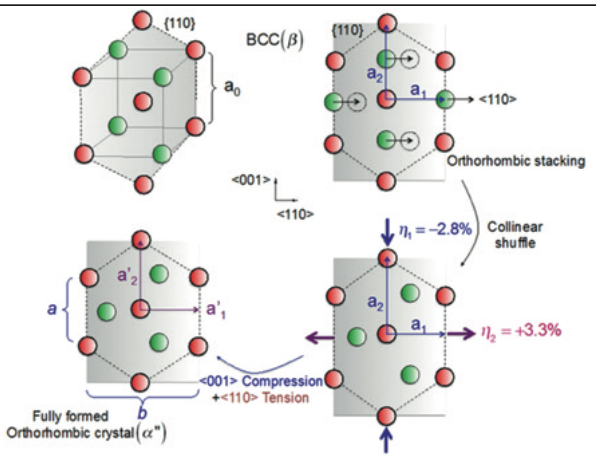

alloys in the 1970–1990 period but the interest waned somewhat except for potential elastocaloric applications. The NiTiCu and other ternary additions to NiTi can provide more stable transformation temperatures than NiTi but exhibit lower transformation strains. The transformation strains are lower in ternary NiTi compared to the binary NiTi alloys except the NiTiHf that has shown higher strains and high transformation temperatures. There has been developing interest on Fe based shape memory alloys. The first class of iron based SMAs was the FeMnSi variety that exhibits shape memory (SME) only. The FeNiCoTi was the next developed alloy which also exhibited SME and high transformation stresses. The FeNiCoAl/Ti/Ta alloys exhibit superelasticity, but are somewhat brittle. The most recent FeMnNiAl alloys are intriguing because the transformation strains are rather high (10%) and the superelasticity develops over a very wide temperature range but are susceptible to blockage of transformation at grain boundaries which leads to cracking. In addition, shape memory and superelasticity have been observed in Ni_2FeGa, CoNiAl, Co_2NiGa, Ni_2MnGa, Ti based shape memory alloys such as TiNbZr/Al/Ta and the high entropy alloys, such as (TiZrHf) 50Ni25Co10Cu15. To our knowledge, only NiTi alloys are commercially available among all these SMAs listed above. The others are custom made for research and specific application purposes. We should note that for majority of these alloys, with the exception of NiTi and Cu based varieties which are well established, the discovery of exact composition and the heat treatment to achieve superelasticity and/or shape memory is an onerous task. The results are very sensitive to austenitizing temperature, the quenching conditions and the following heat treatments. For the case of polycrystals the dependence on texture (especially for the case of rods and wires) is very significant.

The crystallography associated with the shape memory alloys is summarized in **Table 2**. For each material, we presented the austenite and martensite crystal structures and note the large variety of crystal structures. It is worth noting that the shape memory alloys exhibit crystallographically ordered structures and also low symmetries, so their behavior deviates from the well-known fcc and bcc crystals. For example, for the NiTi martensite the atoms inside the martensite crystal are not in center positions of the lattice and they are shifted as shown with arrows. This shift of the atoms in motif positions can only be realized via atomistic simulations, and it has a considerable influence on elastic modulus determination. The shape memory experiments probe: (1) the functionality (transformation stresses, strains, hysteresis) (2) the response over many transformation cycles, (3) transformation temperatures and the response at different temperatures, (4) response under magnetic fields, (5) durability under repeated loadings, and (6) fracture toughness. Therefore, the repertoire of experiments can be exceedingly large compared to conventional materials. We list below (**Table 3**) some of the experimental tools that are utilized to uncover shape memory material properties. They range from stress-strain and strain-temperature measurements (Bewerse *et al.*, 2013; Efstathiou and Sehitoglu, 2008; Reedlunn *et al.*, 2013) in test machines with special software control, electrical resistivity, magnetic field, DSC, X-ray diffraction (Kudoh *et al.*, 1985; Pons *et al.*, 2000; Sedmák *et al.*, 2016), advanced microscopy (Liu *et al.*, 1998; Liu and Xie, 2003; Nishida, 2006; Nishida *et al.*, 1988) to fatigue experiments (Robertson *et al.*, 2007; Robertson and Ritchie, 2007). We note that intermediate phases are present in some cases. In select NiTi compositions, the B19′ martensite can be obtained by a two-step transformation of $B_2 \rightarrow$ R-phase $\rightarrow$ B19′ where the R-phase is designated as a "premartensitic" rhombohedral phase. The most important finding is that when R phase is incorporated in calculations the compound twinning is offered as a solution of the phenomenological theory of martensite (Zhang and Sehitoglu, 2004). The two-step transformation, A $\rightarrow$ R $\rightarrow$ M, has been linked to internal stresses such as those induced by plastic deformation or coherent Ti_3Ni_4 precipitates (Chrobak and Morawiec, 2001; Favier and Liu, 2000; Liu and McCormick, 1996; Gall *et al.*, 1998c, 1999a; Tadaki *et al.*, 1987; Treppmann and Hornbogen, 1995; Mari and Dunand, 1995; Bataillard *et al.*, 1998). This could assist the two way shape memory effect.

Major developments were made in recent years in the theoretical arena. The type of models can be divided into three categories: (1) continuum models, (2) micro-mechanical models, and (3) atomistic modeling. The continuum models were the first to be

Table 3 Summary of experimental techniques in studying shape memory materials

Experiments to Probe Shape Memory Functionality and Endurance	*Comments*
Stress-strain response under deformation at constant temperature (twinning, superelasticity (SE) and plasticity).	Observation of superelasticity over a wide temperature curve, establishing the Clausius-Clapeyron (CC) curve and M_d temperature
Temperature Cycling under Constant Stress (isobaric thermal cycling, ISME)	Transformation temperatures under stress, thermal hysteresis.
Differential Scanning Calorimetry (DSC)	A very effective tool for determination of transformation temperatures. Also, using the second law, one can determine the entropy change hence predict the Clauisius-Clapeyron slope
Cycling the Magnetic Field under Constant Stress	This set up allows determination of the martensite reorientation induced strain associated with magnetic fields
Electrical Resistivity /Magnetization Measurements/ Nanocalorimetry on single and polycrystals	Transformation temperatures can be established from resistivity measurements. Magnetization and magnetic anisotropy experiments can assess the potential for ferromagnetic shape memory alloys.
Scanning/Transmission Electron Microscopy/EBSD/ High Energy Diffraction Microscopy	Lattice orientation relations, dislocation (slip) emission, twin and habit planes, grain orientations, and elastic strain tensor.
Fatigue Crack Growth/Initiation Experiments	Measurement of fatigue crack growth rate leads to the determination of the Paris constants and the fatigue threshold which are key parameters in design. The high cycle fatigue behavior is useful in determining the allowable stress (fatigue limit) corresponding to long lives.
Fracture Experiments	Load-displacement curves and determination of fracture initiation load and corresponding crack length.

Table 4 Theoretical models for transformation, plasticity, atomistic energy barriers

Theoretical Approaches/Tools for Superelasticity/Twinning Modeling	*Comments*
Crystal Plasticity for correspondent variant pairs.	Texture effects and hardening have been accounted for upon interaction of variants with semi-empirical constants (Patoor *et al.*, 1996; Gall *et al.*, 1998a; Patoor *et al.*, 1995a; Sehitoglu and Gall, 1999).
Thermodynamics/Continuum Approach	A number of semi-empirical continuum models some with thermo-mechanical coupling and FEM implementation have been developed (Boyd and Lagoudas, 1996; Zaki and Moumni, 2007; Lagoudas, 2008b)
Non-Schmid Transformation/ Slip Stress Models	Anisotropic Elasticity accounting for splitting of twin or transformation dislocations, atomistic simulation input via GPFE and GSFE (Alkan *et al.*, 2018a,b; Alkan and Sehitoglu, 2017b, 2017a, 2017b, 2019b; Ojha *et al.*, 2015).
Twinning Stress Models	Peierls stress calculation for twinning utilizing GPFE (Wang and Sehitoglu, 2013, 2014a; Ezaz and Sehitoglu, 2011; Ezaz *et al.*, 2012a; Wang and Sehitoglu, 2014b, 2014c; Ezaz *et al.*, 2011) has been implemented.
MD Simulations	Key issues are correct prediction of Ni and Ti atom positions, and correct elastic moduli determination. The MD models can predict superelasticity (Chowdhury *et al.*, 2016; Chowdhury and Sehitoglu, 2017a; Chowdhury *et al.*, 2015, 2017; Ren and Sehitoglu, 2016; Chowdhury and Sehitoglu, 2017b; Zhong *et al.*, 2011, 2012; Mirzaeifar *et al.*, 2014)
DFT (Ab-initio) Calculations	This is the most advanced model that predicts lattice constants, cohesive energy, elastic constants and fault energies (Ezaz and Sehitoglu, 2011; Hatcher *et al.*, 2009a,b; Huang *et al.*, 2003; Kibey *et al.*, 2009; Ko *et al.*, 2015, 2017; Wagner and Windl, 2008; Zayak *et al.*, 2002, 2003a,b; Zayak and Entel, 2004; Hatcher *et al.*, 2009c) accurately. The results can feed to continuum models.

developed as constitutive equations including a transformation strain term. The transformation strain was allowed to evolve with increase in martensite volume fraction according to an empirical relation. These phenomenological laws were consistent with the first and second law and relied on constants to fit the experimental results. The micro-mechanical models also relied on experimental constants but discretized the microstructure (an RVE) as a collection of grains with austenite and martensite domains. These models predicted the tension-compression asymmetry and texture effects which is prevalent in NiTi and other SMAs. Finally, the atomistic models can be divided into two categories: the MD models and the DFT models. The DFT models can deliver the energy barriers associated with twinning and phase transformation accurately. Further calculations are needed to relate these energy barriers to stresses. The MD models, on the other hand, have to be constructed with utmost care to match the DFT results, but have the advantage of bridging the DFT results to continuum. A summary of these models is given in **Table 4** and the results from these models will be discussed throughout this review.

Superelasticity-Examples

The aim in this section is to show examples of the superelastic response for various SMAs.

In **Fig. 3**, we consider a wide range of shape memory materials. This figure does not encompass all SMAs, but the most important ones. We start with the most famous shape memory alloy, Ni(50.8%at.)Ti, (**Fig. 3**(a)), and also show NiTiCu, CuZnAl, NiMnGa, FeMnNiAl, CoNiAl, Ni_2FeGa, TiZrNbSn, FeNiCoAlTi and 51.5%Ni-Ti (**Fig. 3**(j)). Note that the NiTi results (a) vs (j) depend on the exact chemical composition near the stoichiometric one (note the difference between 50.8%Ni and 51.5%Ni results) and the heat treatments which will be discussed later. Key parameters to note are the transformation stress, transformation strain and the stress hysteresis. Elastic moduli upon loading and unloading are also important and could be substantially different. The transformation strains are smaller for NiTiCu compared to NiTi ((a) vs (g)). The CuZnAl system was one of the earliest shape memory alloys that exhibited very high transformation strains and small hysteresis (d). There are some limitations especially the degradation in functionality because of cycling and also the high elastic anisotropy that precludes their use as polycrystals. Nevertheless, in single crystal form, they exhibit excellent properties. The NiMnGa is a ferromagnetic shape memory alloy that undergoes switching from one variant to another in the martensitic phase. The material can also be utilized in shape memory or superelasticity (**Fig. 3**(f)) mode but there are limitations because of lack of ductility. The CoNiAl and FeNiGa materials also exhibit large transformation strains (as high as 14% for FeNiGa case) and extend the temperature of superelasticity to 100°C and above. The FeMnNiAl shape memory materials that have been discovered recently display large transformation strains exceeding 10% (Abuzaid *et al.*, 2019; Omori, 2011; Vollmer, 2016, 2019) and superelasticity over a wide temperature range. It is too early to judge all the attributes of this class of Fe-based alloys. There are other SMA classes which have been studied including the high temperature shape memory alloys, such as NiTiHf, and various compositions of Ti (without Ni) based SMAs which provide distinct advantages. We will discuss these alloys in a later section.

It is important to name the groups who worked on these shape memory alloys over the years: Navy Ordinance Lab worked on NiTi (Buehler *et al.*, 1963), Otsuka and Miyazaki (Otsuka and Wayman, 1998; Miyazaki *et al.*, 1981; Otsuka *et al.*, 1993; Miyazaki *et al.*, 1986, 1984, 1982; Morii *et al.*, 1991; Onda *et al.*, 1992; Otsuka *et al.*, 1990; Otsuka and Ren, 2005; Otsuka *et al.*, 1971) also focused on NiTi, Univ. of Illinois worked on Cu- and NiTi alloys originally with Wayman (Otsuka and Wayman, 1999, 1998; Schroeder and Wayman, 1979; Wu *et al.*, 1989; Tadaki and Wayman, 1982; Adachi *et al.*, 1986; Au and Wayman, 1972; Jian and Wayman, 1992, 1994; Nishida *et al.*, 1988, 1986; Saburi *et al.*, 1981; Wayman, 1964, 1993; Yang and Wayman, 1994) and then with Sehitoglu (Chowdhury and Sehitoglu, 2017a; Hamilton *et al.*, 2004; Alkan *et al.*, 2018a; Wang and Sehitoglu, 2013; Sehitoglu *et al.*, 2001a; Gall *et al.*, 1998a; Sehitoglu *et al.*, 2000; Abuzaid *et al.*, 2019; Hamilton *et al.*, 2006b, 2005; Sehitoglu *et al.*, 2002; Ojha and Sehitoglu, 2016a; Alkan *et al.*, 2018b; Alkan and Sehitoglu, 2017b, 2019b; Ojha *et al.*, 2015; Wu *et al.*, 2019; Sidharth *et al.*, 2020a; Hamilton *et al.*, 2006b; Callaway *et al.*, 2006; Ezaz *et al.*, 2013; Gall *et al.*, 1999e, 2001; Hamilton *et al.*, 2006a, 2007a, 2006b; Patriarca *et al.*, 2016a; Ojha and Sehitoglu, 2015, 2016c,b; Patriarca and Sehitoglu, 2015; Patriarca *et al.*, 2016a,b; Sehitoglu *et al.*, 2001a,c, 2017a,b,c; Sgambitterra *et al.*, 2019; Sidharth *et al.*, 2020b; Wang and Sehitoglu, 2014c; Wang *et al.*, 2014; Wu *et al.*, 2015, 2016; Yaacoub and Sehitoglu, 2019). Texas AM group worked on NiTi and NiTiHf class of alloys with Lagoudas and Karaman (Haghgouyan *et al.*, 2019; Karaca *et al.*, 2004, 2003; Karaman and Lagoudas, 2006; Kumar *et al.*; Monroe *et al.*, 2011). UC Berkeley's Ritchie (Cao *et al.*, 2020; Gall *et al.*, 2008; Gludovatz *et al.*, 2014; McKelvey and Ritchie, 1999, 2001; Robertson *et al.*, 2007, 2012; Robertson and Ritchie, 2007) studied fatigue of NiTi. Industrial groups such as Duerig and Pelton primarily worked on NiTi (Duerig *et al.*, 2013; Pelton *et al.*, 2008, 2012; Goo *et al.*, 1985; Moberly *et al.*, 1990; Pelton, 2011). In Europe, Hornbogen and then Eggeler (Simon *et al.*, 2010; Pfetzing-Micklich *et al.*, 2012; Eggeler *et al.*, 2004; Gollerthan *et al.*, 2008, 2009; Hornbogen and Eggeler, 2004; Khalil-Allafi *et al.*, 2002; Krooß *et al.*, 2014; Pfetzing-Micklich *et al.*, 2013; Schmidt *et al.*, 2015; Simon *et al.*, 2010; Zhang *et al.*, 2012) and Maier (Lin *et al.*, 2009; Gall and Maier, 2002; Gerstein *et al.*, 2018; Meyer *et al.*, 2006) worked on NiTi. In Spain, Cesari and colleagues (Pons *et al.*, 1993; Barandiarán *et al.*, 2008; Pons *et al.*, 2003, 2005, 2000; Kireeva *et al.*, 2010; Seguí *et al.*, 2004; Chumlyakov *et al.*, 2008) worked on Cu based and Fe based SMAs, Manosa and Planes worked on NiTi and Cu based SMAs (Bonnot *et al.*, 2008; Manosa *et al.*, 1993, 2009, 2013a,b; Mañosa and Planes, 2017; Planes *et al.*, 2005, 2009; Vives, 2011), Patoor and Berveiller (Patoor *et al.*, 1996, 1995a; Lagoudas *et al.*, 2006; Niclaeys *et al.*, 2002; Patoor *et al.*, 1995b) worked on Cu and NiTi based materials. In Russia, Chumlyakov and Prokoshkin (Chumlyakov *et al.*, 2013; Prokoshkin *et al.*, 2016; Patriarca *et al.*, 2016a; Timofeeva *et al.*, 2012; Chumlyakov *et al.*, 2008) worked primarily on NiTi and in Czech Republic Sittner (Delville *et al.*, 2011; Heller *et al.*, 2009; Sedlak *et al.*, 2012; Sedmák, 2016; Sedmák *et al.*, 2015; Sittner, 2014) worked on Cu based and then NiTi, and in Belgium, Delaey and then Van Humbeeck studied Cu based SMAs and NiTi (Delaey, 1981; Firstov *et al.*, 2004a,b; Humbeeck and Kustov, 2005; Liu *et al.*, 1998; Van Humbeeck, 2001, 2003; Van Humbeeck and Delaey, 1981; Xie *et al.*, 1998; Delaey *et al.*, 1987). In South America, Ahlers, Sade and colleagues (Malarría *et al.*, 2009; Pons *et al.*, 1993; Sade and Hornbogen, 1988; Ahlers, 1986; Sade *et al.*, 2007; Ahlers, 2004; Pelegrina and Ahlers, 1992; Romero *et al.*, 1988, 1988; Sade *et al.*, 1985; Damiani *et al.*, 2002, 2003; Malarría *et al.*, 2001; Sade *et al.*, 1987) worked on Cu based and Fe based SMAs. Miyazaki and Nishida worked on Ti based SMAs (Fukui *et al.*, 2004; Al-Zain *et al.*, 2010; Tahara *et al.*, 2009; Kim *et al.*, 2015; Buenconsejo *et al.*, 2009), Kainuma and colleagues worked on Co based and Fe based SMAs (Omori *et al.*, 2011; Kainuma *et al.*, 1996; Omori and Kainuma, 2017). Recently, there are groups working on fracture in Italy with Furgiuele (Sgambitterra *et al.*, 2019; Falvo *et al.*, 2009; Maletta *et al.*, 2013; Sgambitterra *et al.*, 2018) and on constitutive simulations in Rome with Auricchio (Auricchio and Taylor, 1997) and in France-Turkey with Moumni and Anlas respectively (Zaki and Moumni, 2007; Chen *et al.*, 2014a; Hazar *et al.*, 2016, 2015; Moumni *et al.*, 2005; Mutlu *et al.*, 2020; Özerim *et al.*, 2018; Zhang *et al.*, 2017). Most companies such as SAES Getters, Cofluent, Medtronic, Boston Scientific, Edwards, Johnson and Johnson and Fort Wayne Metals are primarily working on producing NiTi relevant to and utilizing NiTi for biomedical applications, and NASA (Glenn) is pursuing actuation applications and high temperature SMAs. There are certainly other groups who published on SMAs, but we summarized above the main groups who are active currently.

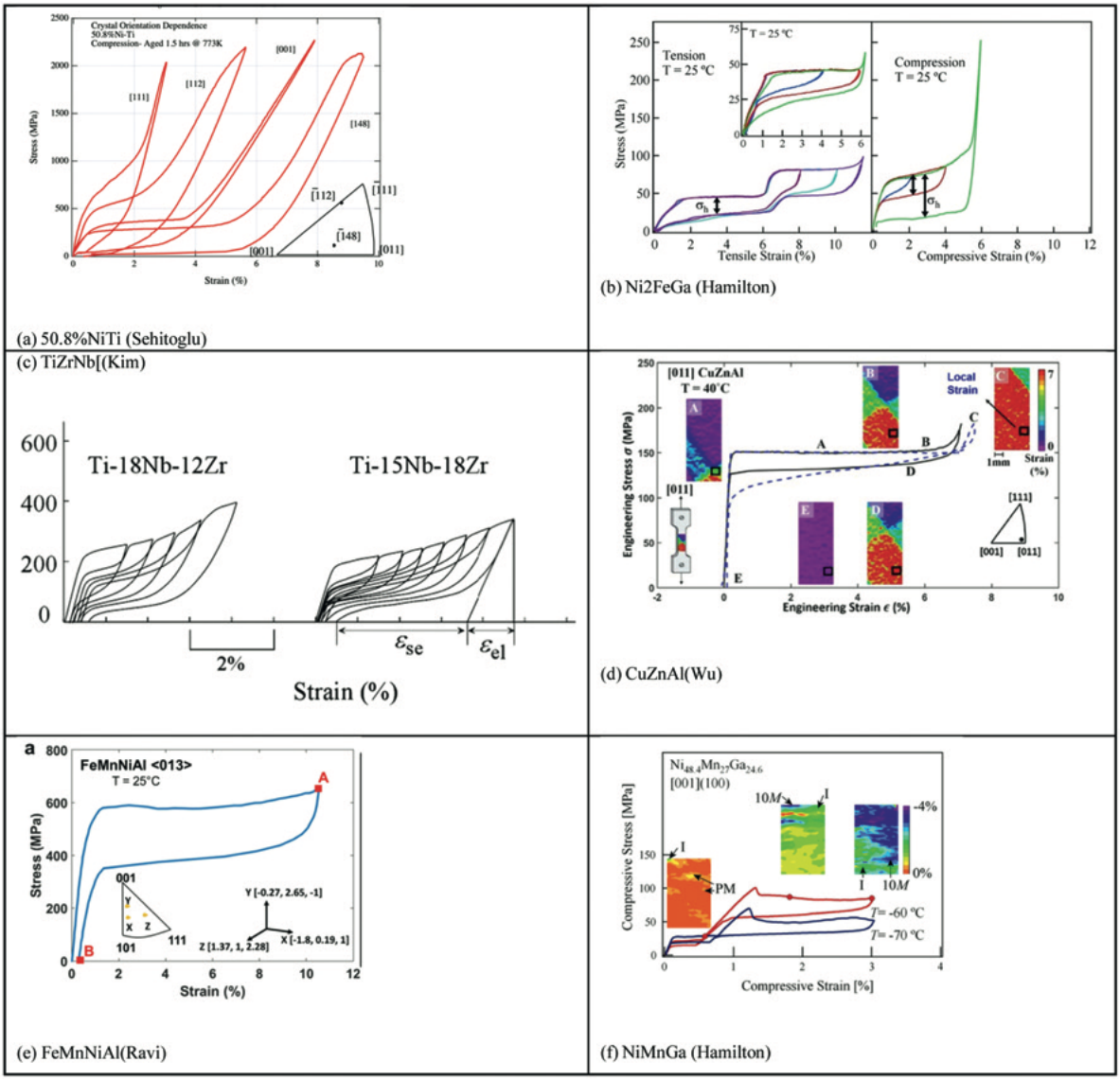

Fig. 3 Superelastic response of various shape memory materials. For details, see the references in the text and the annotations embedded in the figures; (a) NiTi (Sehitoglu *et al.*, 2000) (b) Ni_2FeGa (Hamilton *et al.*, 2007b) (c) TiNbZr (Kim *et al.*, 2015) (d) CuZnAl (Wu *et al.*, 2019) (e) FeMnNiAl (Sidharth *et al.*, 2020a) (f) Ni_2MnGa (Hamilton *et al.*, 2008).

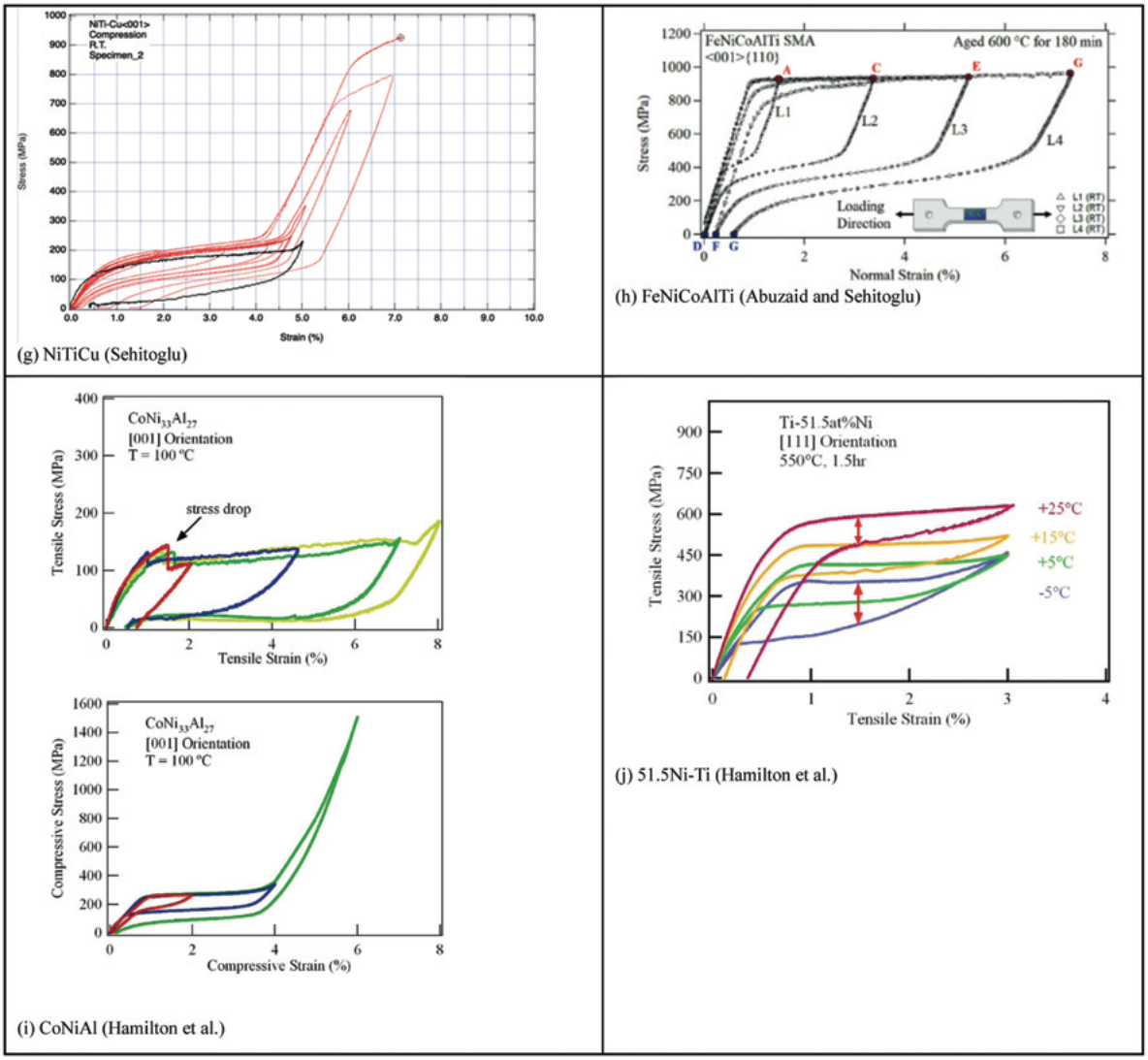

Fig. 3 Continued. (g) NiTiCu (Sehitoglu *et al.*, 2001b) (h) feNiCoAlTi (Abuzaid and Sehitoglu, 2018) (i) CoNiAl (Hamilton *et al.*, 2006b) (j) 51.5NiTi (Hamilton *et al.*, 2004).

Shape Memory Response (ISME)-Examples

In the next set of figures (**Fig. 4**), we provide the temperature cycling results for several shape memory alloys referred to as ISME (isobaric shape memory effect). The thermal hysteresis is shown with red arrows in **Fig. 4**(a)–(c), and the magnitude of constant stress during these experiments is indicated in the annotation. The constant stress that can be sustained in 51.5%Ni is higher than 50.4%Ni and 50.1%Ni but at the expense of transformation strain. The horizontal lines are strain predictions from CVP formation and CVP + detwinning respectively.

Iron based materials such as FeNiCoTi do not display superelasticity but they could be exploited for applications requiring high thermal hysteresis (such as in civil engineering for reinforcements (Chen *et al.*, 2014b)). The experimental transformation strain results for FeNiCoTi (**Fig. 4**(d)) fall considerably short of theoretical strain values. In general, the NiTi based alloys have narrow hysteresis while FeNiCoTi and FeMnNiAl based alloys have wider hysteresis. The transformation strains and transformation temperatures can be also noted from these figures. The shape of the curves can vary depending on the temperature. One of the intriguing temperature cycling behavior is that the hysteresis magnitude changes with applied stress. The thermal hysteresis increases with applied stress in low Ni compositions while it decreases with applied stress in higher Ni compositions (Hamilton *et al.*, 2004) (**Fig. 4**(b) vs (c)). The results for NiTiHf (with 24.7% at. Hf) are impressive (**Fig. 4**(h)) resulting in high strains at high temperatures and at high stress levels.

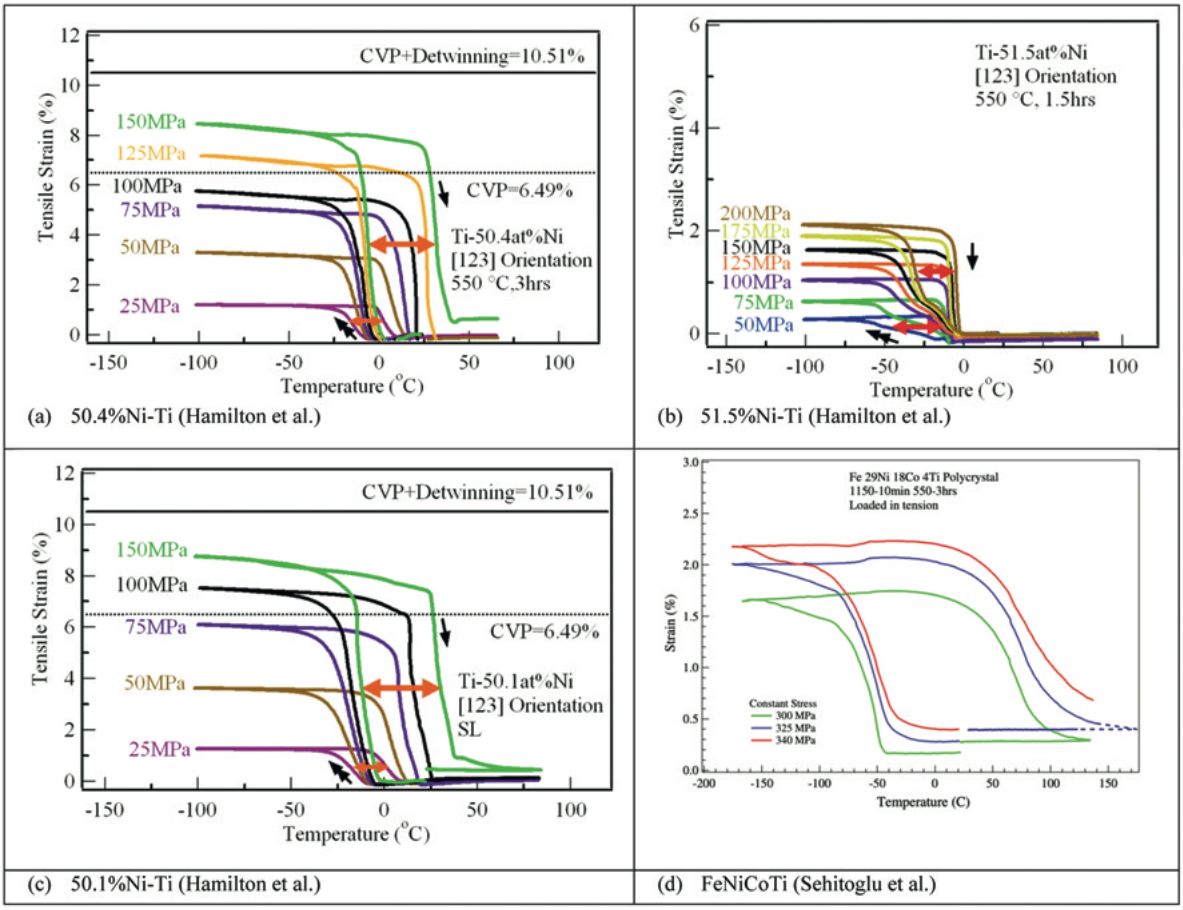

Fig. 4 Isobaric shape memory response of various shape memory materials. For details, see the references in the text. (a) 50.4%NiTi (Hamilton *et al.*, 2004) (b) 51.5%NiTi (Hamilton *et al.*, 2004) (c) 50.1%NiTi (Hamilton *et al.*, 2004) (d) FeNiCoTi (Sehitoglu *et al.*, 2005).

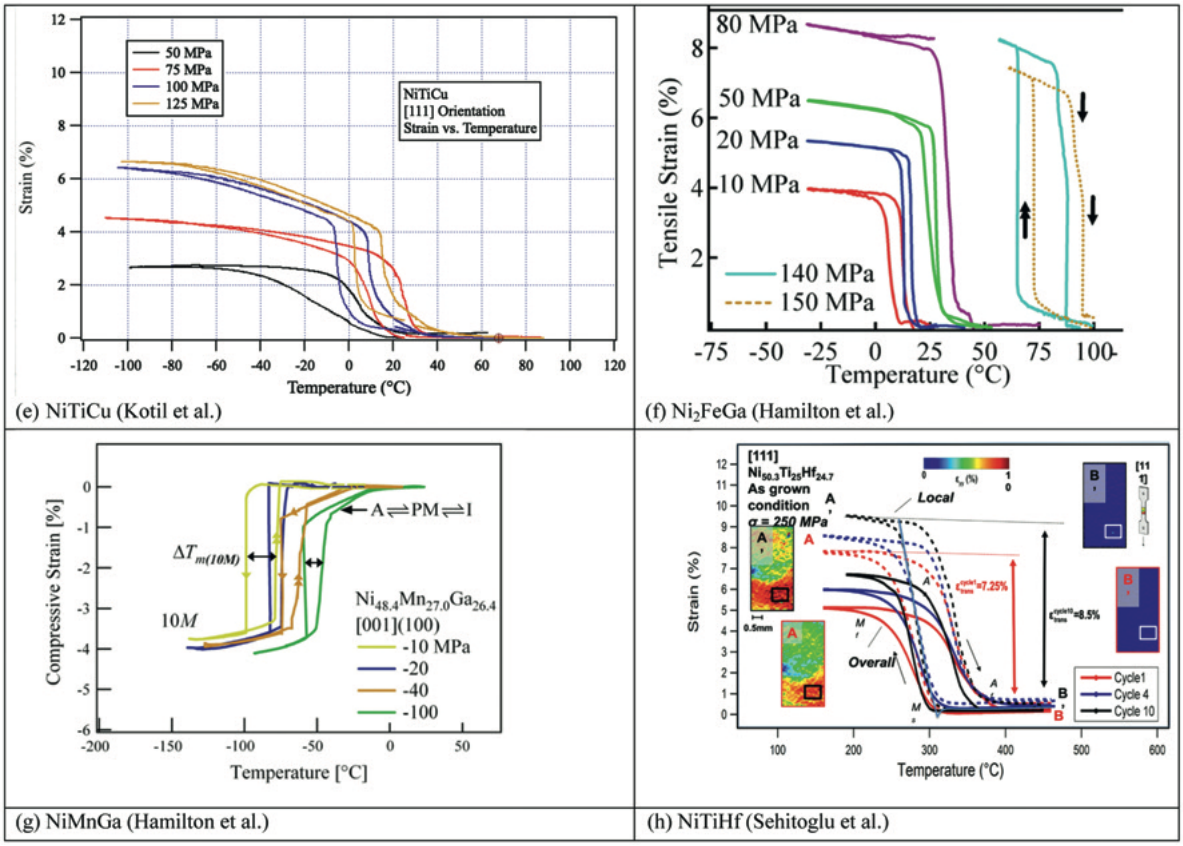

Fig. 4 Continued. (e) NiTiCu (Kotil *et al.*, 2003) (f) Ni_2FeGa (Hamilton *et al.*, 2007b) (g) Ni_2MnGa (Hamilton *et al.*, 2008) (h) NiTiHf (Sehitoglu *et al.*, 2017b)

Explanation of the Mechanisms

Stress and Thermal Hysteresis

A fundamental and critical property in shape memory alloys is the recoverability of transformation albeit with transformation hysteresis. The hysteresis observed in martensitic transformations results from energy dissipative (irreversible) processes. Although irreversiblities are inherent to martensitic transformations, the origin of the energy dissipative processes is still not well understood. The irreversible component of the non-chemical energy is mainly related to two energy dissipative processes. One process is attributed to energy dissipated in the form of frictional work (Niclaeys *et al.*, 2002; Ortin and Planes, 1988; Patoor *et al.*, 1995b; Delaey *et al.*, 1987). The frictional work is spent overcoming resistance to interfacial motion that is associated with the strength of the parent phase. The second dissipative process is due to the dissipation of elastic strain energy. Stored elastic strain energy is dissipated when the coherency strains of martensite-austenite interfaces relax. Therefore, plastic accommodation causes dissipation of elastic strain energy. Relaxation of coherency strains as an interface advances will also occur when it interacts with dislocations or precipitates (Liu and McCormick, 1996; Delaey *et al.*, 1987; Sehitoglu *et al.*, 2004). Hamilton *et al.* (2004) provides a detailed discussion of the hysteresis through continuum energetics, which is now briefly summarized to highlight the role of dissipation. Dissipative mechanisms are non-chemical contributions to the total Gibbs free energy of the system. Thermo-elastic equilibrium at a transforming interface requires a local balance between chemical and non-chemical contributions to the total Gibbs free energy (Olson and Cohen, 1975; Ortin and Planes, 1988; Delaey *et al.*, 1987). The non-chemical constituent is comprised of reversible and irreversible components, and the chemical constituent results from the chemical energy difference due to the nature of bonding in the crystalline phases. The mechanical strain energy provides the reversible non-chemical contribution. When dissipation occurs the mechanical strain energy needs to be modified. Since the state variables in martensitic transformations are stress and temperature dependent, the complementary free energy is chosen as the representative thermodynamic potential (Gall, 1998; Hamilton *et al.*, 2004; Lagoudas, 2006; Patoor *et al.*, 1995b; Patoor *et al.*, 1995):

$$\Psi(\Sigma_{ij}, T, f) = -\Delta G_{chem} - W_{mech} - W_{inter} + \Sigma_{ij}E_{ij}$$

where ΔG_{chem} is the chemical free energy difference between the parent phase and the martensitic phase $\left(=B(T_o - T)\sum_n f^n\right)$, W_{mech} is the total elastic strain energy associated with the transformation. In Equation (1), The last three terms represent non-chemical

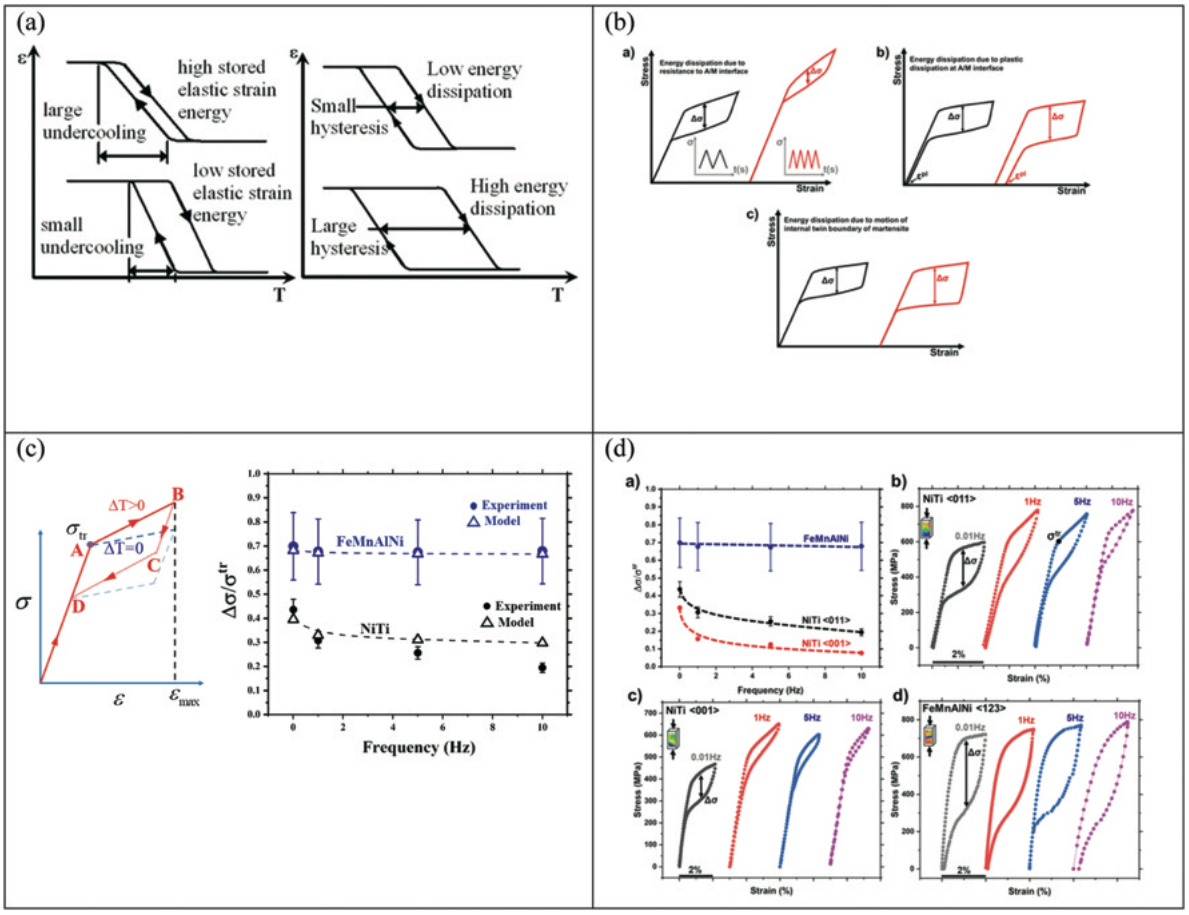

Fig. 5 (a) Illustration of strain-temperature response and the role of high and low elastic strain energy (b) multiple contributions to the generation of hysteresis in shape memory alloys, (c) prediction of hysteresis based on the thermodynamics model as a function of frequency, (d) the stress-strain responses showing the dramatic effect of frequency and material (NiTi versus FeMnNiAl). Reproduced from (a) Hamilton, R.F., Sehitoglu, H., Chumlyakov, Y., Maier, H.J., 2004. Stress dependence of the hysteresis in single crystal NiTi alloys. Acta Materialia 52, 3383–3402. (b), (c) and (d) Sidharth, R., Mohammed, A., Abuzaid, W., Sehitoglu, H., 2021. Unraveling frequency effects in shape memory alloys: NiTi and FeMnAlNi. Shape Memory and Superelasticity, 1–15.

contributions. The chemical energy difference is evaluated from calorimetry experiments. In our study, atomistic simulations will be used to evaluate this quantity and identify B and T_o. The W_{inter} is the interfacial energy between the new martensite and parent phase, and $\Sigma_{ij}E_{ij}$ represents macroscopic applied stresses and strain product. The interfacial energy can be calculated from atomistic simulations. The volume fraction of nth variant is denoted as f^n and B is a measure of transformation enthalpy. When Equation (1) is greater than zero, then the transformation from the parent phase to the martensitic phase occurs.

The W_{mech} opposes the transformation through elastic strain energy and variant-variant interaction terms. In the presence of plastic strain, there would be an additional term within W_{mech}. The term $\Sigma_{ij}E_{ij}$ promotes the transformation, while the resultant elastic strain energy, W_{mech}, and interfacial energy, W_{inter}, of the transformation prevent it. The continuum models based on micromechanics do not predict dislocation emission hence cannot consider plastic relaxation of elastic strain energy. If the physical dissipative processes are modeled, the CRSS for transformation should change and the reverse transformation and the forward transformation stress magnitudes will be altered. Clearly, the underlying physics of the transformation requires solutions that extends beyond the published literature, especially if hysteresis is to be predicted.

Shape memory alloys exhibit hysteresis even under fully recoverability (Van Humbeeck, 2001; Müller and Xu, 1991; Blanter *et al.*, 2007; San Juan and Nó, 2003), the hysteresis is a form of a damping mechanism (Kumar and Lagoudas, 2008). The high damping capacity of SMAs being much higher than steels (Van Humbeeck, 2001; Juan *et al.*, 2009) can potentially be utilized in engineering applications. The hysteresis depends on the frequency of loading (or strain rate) and on the exact composition of the SMA alloy. Previous work has studied damping by measuring the phase-lag between the oscillatory load-input and output strain-response (Seguí *et al.*, 2004; Van Humbeeck, 2001, 2003; Blanter *et al.*, 2007; San Juan and Nó, 2003; Bidaux *et al.*, 1989; San Juan and Perez-Saez, 2001; Chen *et al.*, 2009) such as in dynamic analyzer tests. It is more common to study superelastic mechanical response via conventional mechanical tests (Shaw and Kyriakides, 1995; Heller *et al.*, 2009; Van Humbeeck and Delaey, 1981; He *et al.*, 2010;

Dayananda and Rao, 2008; Dolce and Cardone, 2001; DesRoches *et al.*, 2004; Nemat-Nasser *et al.*, 2005a; Malécot *et al.*, 2006; Tobushi *et al.*, 1998; Yin *et al.*, 2014; Zhang *et al.*, 2010; Hartl and Lagoudas, 2008; Leo *et al.*, 1993; Yin *et al.*, 2013) where the dissipated energy (area under the stress strain loop) and the total stored elastic strain energy (Zener, 1938) ratio is indicative of the internal friction. The internal friction influences the fatigue life of the SMA (Moumni *et al.*, 2005; Zhang *et al.*, 2017; Sateesh *et al.*, 2014).

The variation of hysteresis is shown schematically in **Fig. 5**(a). It is intuitive to analyze the superelastic hysteresis due to three contributions (Van Humbeeck, 2001; San Juan and Nó, 2003; Bidaux *et al.*, 1989): (1) transitory part, (2) phase transformation part and (3) intrinsic part. **Fig. 5**(b) outlines each contribution under superelastic conditions. The transitory term arises from the latent heat of transformation which raises the temperature levels. This effect is often considered to be small (Van Humbeeck, 2001; San Juan and Nó, 2003; Dejonghe and Batist, 1976) but it depends on the alloy. Because the temperature evolution can be asymmetric, this differential would produce hysteresis. The heat is transferred to the surrounding medium at low frequencies (Tobushi *et al.*, 1998; Zhang *et al.*, 2010) and while at higher frequencies (>20 Hz), nearly adiabatic conditions prevail. Secondly, the phase transformation (San Juan and Nó, 2003; Bidaux *et al.*, 1989; Perez-Saez *et al.*, 1998) creates dislocation generation at the A/M transformation fronts (Mercier and Melton, 1976) and is affected by the crystallography, internally twinned martensite and misfit strains at the A/M interface (Bhattacharya, 2003; Bhattacharya *et al.*, 2004; Olson and Cohen, 1975; Hornbogen, 1985, 2004; Roitburd and Kurdjumov, 1979; Kajiwara, 1999; Kajiwara and Owen, 1977). Under mechanical cycling the dislocation accumulation (Simon *et al.*, 2010; Kajiwara, 1999; Mohammed and Sehitoglu, 2020a) will affect the dissipation.

The third contribution originates from intrinsic damping capacity of austenite and of internally twinned martensite (Van Humbeeck, 2001). The interfaces are decorated with twin partials (Humbeeck and Kustov, 2005). If twinning is fully reversible in martensite (Humbeeck and Kustov, 2005; Van Humbeeck, 2001; San Juan and Nó, 2003) the contribution can be small, but locally higher twin modes can become activated which are not reversible.

In summary, the formulation for hysteresis in shape memory alloys has a number of terms that cannot be readily determined. The source of the hysteresis is due to three main reasons: (1) energy dissipation due to resistance at A/M interface, (2) energy dissipation due to plastic dissipation (slip emission) at interface, (3) energy dissipation due to motion of internal twin boundaries in martensite. Among these three mechanisms, the twin boundary motion can be reversible, the slip emission is not reversible, and the A/M motion can be reversible but with hysteresis. Similarly, in thermal cycling case one could obtain hysteresis and the strain energy dictates the amount of undercooling, high amount of dissipation can produce hysteresis upon cycling. This is a known limitation in Ti shape memory alloys and iron-based shape memory alloys, for example. The results are a function of frequency and crystal orientation of the material.

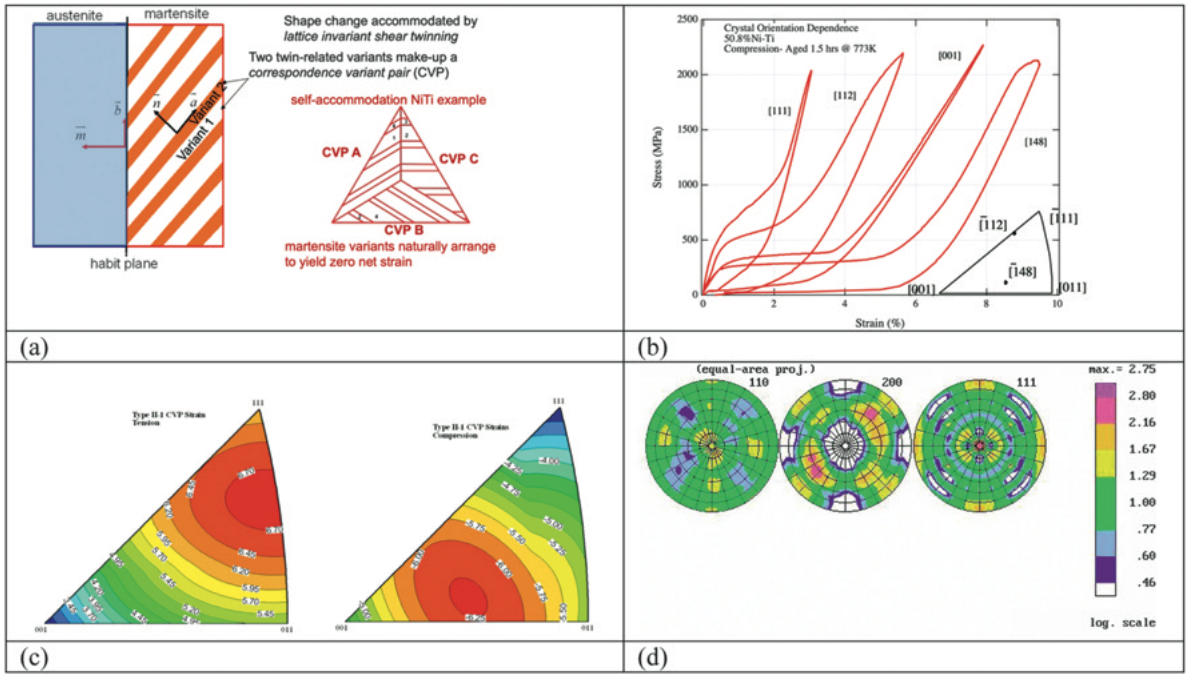

Fig. 6 (a) PTMT provides the habit plane and the internal twin details in martensite, (b) crystal orientation dependence of the transformation strains and the critical stress of NiTi, (c) the transformation strains (the CVP part without detwinning) for NiTi, (d) illustration of strong $<111>$ texture in polycrystals of NiTi. Reproduced from (b) Sehitoglu, H., *et al.* Proceedings of the IUTAM Symposium on Mechanics of Martensitic Phase Transformation in Solids, pp. 103–109. Dordrecht: Springer. (c) Sehitoglu, H., *et al.*, 2003. Detwinning in NiTi alloys. Metallurgical and Materials Transactions A 34, 5–13. (d) Gall, K., Sehitoglu, H., 1999. The role of texture in tension-compression asymmetry in polycrystalline NiTi (vol 15, pg 69, 1999). International Journal of Plasticity 15, 781–781.

Crystal Orientation Dependence of Mechanical Response

The origin of the modeling required to predict the orientation dependence of transformation strains and critical stress for a single crystal undergoing a martensitic phase transformation dates back to the phenomenological theory of martensitic transformations (PTMT) (Wechsler *et al.*, 1953; Miyazaki *et al.*, 1981; Knowles and Smith, 1981). The key outcomes from PTMT are illustrated in **Fig. 6**(a). The twinning mode, habit plane, orientation relationship, magnitude and direction of shape strain have been well documented for the well-known SMAs. We note that the martensite-austenite transformation plane shown in **Fig. 6**(a) and the martensite is internally twinned with twin plane and direction indicated. The thermally induced self-accommodating microstructure consisted of multiple three plate groups or CVPs (correspondent variant pairs). The martensite plates formed are called correspondence variant pairs (CVP's) because they represent stacking of different type II twin related single crystal variants. The habit plane of the martensite is a low symmetry plane, this results in considerable orientation dependence of the transformation stress and transformation strain. Strong crystal orientation dependence can be explained based on the low symmetry of the habit planes and the variant selection (**Fig. 6**(b)) as well as the non-planar transformation dislocation cores (Alkan *et al.*, 2018a; Alkan and Sehitoglu, 2019a). In solutionized NiTi single crystals, the maximum recoverable strains predicted (Buchheit and Wert, 1996) are consistent with experimental results on single crystal NiTi loaded under tension (Miyazaki *et al.*, 1984). Although the deformation behavior of solutionized NiTi single crystals obeys the PTMT, aged NiTi single crystals do not demonstrate such a favorable agreement. Several researchers (Miyazaki *et al.*, 1984) have observed that the recoverable strain levels under tension were significantly smaller in aged samples versus solutionized samples. It has been have proposed that the precipitates effectively inhibit the detwinning process (Buchheit and Wert, 1996; Sehitoglu *et al.*, 2003). An example of the transformation strains for CVP formation (no detwinning) is given in **Fig. 6**(c). These researchers noted that when detwinning strains were removed from the model, the predicted recoverable strains were closer to the experimental results for the aged NiTi single crystals.

The stress-strain behavior in metallic materials is often described by isotropic moduli, yield criteria and strain hardening flow rules in three-dimensional principal stress space. In metals that undergo dislocation-mediated slip, the deformation induced anisotropy is well known. The concept of crystallographic texture, or a so-called deformation texture at large strains is well known. These textures arise during processing, resulting in a strong orientation dependence of material properties resulting in a textured polycrystal exhibiting significant anisotropy. The NiTi wires have $<111>$ texture, so their behavior is very similar to $<111>$ single crystals (**Fig. 6**(d)). The strong crystal orientation dependence has ramifications in understanding the polycrystalline behavior. Also, the data displays the crystal orientation dependence of elastic moduli (from the stress-strain curves) in **Fig. 6**(b).

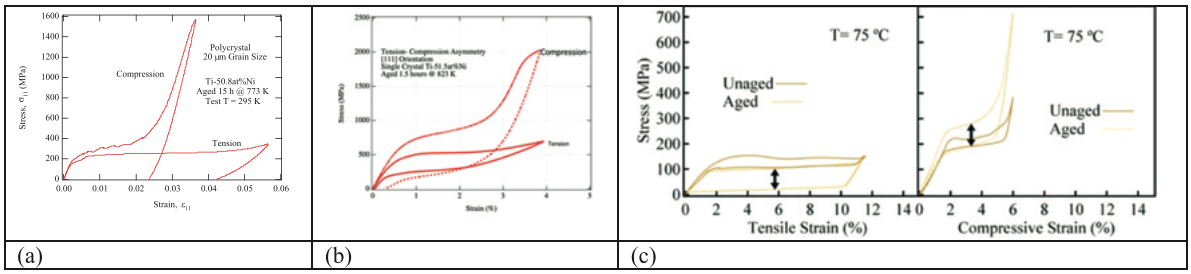

Fig. 7 (a) Tension-compression asymmetry of shape memory response in textured polycrystal, The corresponding pole figure is shown in **Fig. 6** (d), (b) Tension-compression asymmetry in $<111>$ oriented single crystals, (c) Tension compression asymmetry in Ni_2FeGa single crystals under superelasticity. Reproduced from (a) Gall, K., Sehitoglu, H., Chumlyakov, Y., Kireeva, I.V., Maier, H.J., 1999a. The influence of aging on critical transformation stress levels and martensite start temperatures in NiTi: Part II – Discussion of experimental results. Trans ASME 121, 28–37. Gall, K., Sehitoglu, H., Chumlyakov, Y.I., Kireeva, I.V., Maier, H.J., 1999b. The influence on critical transformation stress levels and martensite start temperatures in NiTi: Part I-aged microstructure and micro-mechanical modeling. ASME Journal of Engineering Materials and Technology 121, 19–27. (b) Sehitoglu, H., *et al.* Proceedings of the IUTAM Symposium on Mechanics of Martensitic Phase Transformation in Solids, pp. 103–109. Dordrecht: Springer. (d) Based on Hamilton, R.F., Sehitoglu, H., Efstathiou, C., Maier, H.J., 2007a. Mechanical response of NiFeGa alloys containing second-phase particles. Scripta Materialia 57, 497–499. doi: 10.1016/j.scriptamat.2007.05.024.

Tension-compression Asymmetry

In traditional metals, the mechanical properties will depend strongly on the loading axes; however, the material will not demonstrate strong tension-compression asymmetry because dislocations may move along the positive or negative slip direction with similar resistance. Contrary this trend, metals that deform by twinning demonstrateconsiderable tension-compression asymmetry at the single crystal level. This strong asymmetry is a result of the unidirectional nature of the shear strain across the twinning planes. The crystallography and energy barriers and the magnitude of shear prohibit deformation in the reverse sense. Similar to twinning, the martensitic transformation also is directional resulting in considerable asymmetry. The low symmetry of the habit planes creates a strong tension-compression asymmetry which translates to strong tension-compression asymmetry at the polycrystalline level (Saburi *et al.*, 1981). The drawn polycrystalline NiTi demonstrate anisotropic properties (Gall *et al.*, 1998a;

Jacobus *et al.*, 1996) and tension-compression asymmetry (Gall and Sehitoglu, 1999; Gall *et al.*, 1999b, 1999c). Previous research showed that under compression the polycrystalline NiTi demonstrates much smaller transformation strains and higher critical transformation stress levels, and steeper transformation stress-strain slopes.

Tension compression asymmetry is a well-known feature of shape memory alloys. This phenomenon is clearly illustrated in **Fig. 7**. It is often explained based on variant selection. In reality, there are dislocations on twin boundaries and also on habit plane boundaries. At the atomic level the transformation dislocation glide is crystal orientation dependent because the core of the dislocations is split on multiple planes. The plastic (slip) response in austenite is highly dependent on crystal orientation, i.e., stresses other than the glide stress dictate the flow behavior (Alkan and Sehitoglu, 2019a; Alkan *et al.*, 2018a). The slip behavior will be discussed in the later sections.

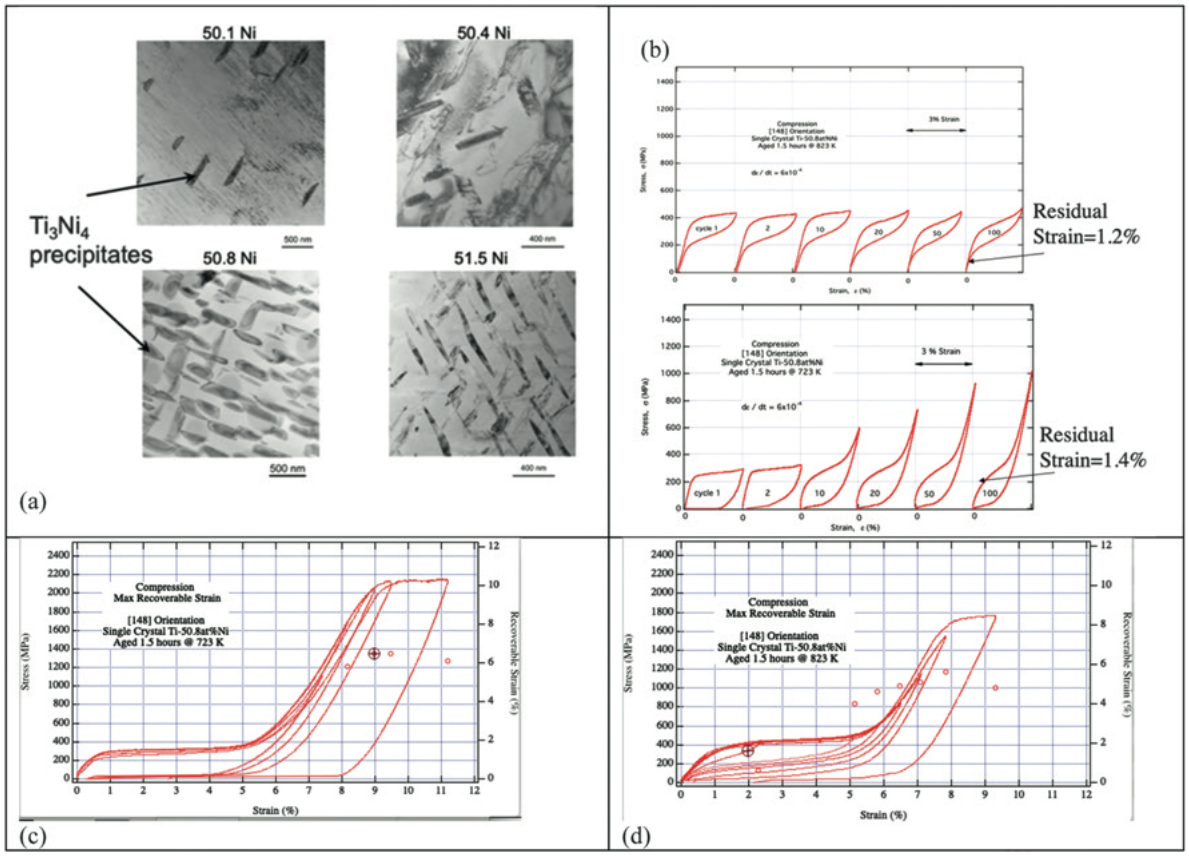

Fig. 8 (a) TEM microscopy of the NiTi precipitates as a function of Ni content, (b) Cyclic loading of overaged (823 K 1.5 h) and peak aged (723 1.5 h) superelastic curves showing substantially lower transformation stress for peak aged case and accumulation of residual strains under cyclic loading, (c) Superelasticity for peak aged case, (d) Superelasticity for overaged case. Note that the slip resistance (the upper plateau) is higher for peak aged case. On the other hand, the transformation stress (lower plateau) is higher for the overaged case. The recoverable strains are shown with data points and reach could exceed 6% in compression. Reproduced from (a) Hamilton, R.F., Sehitoglu, H., Chumlyakov, Y., Maier, H.J., 2004. Stress dependence of the hysteresis in single crystal NiTi alloys. Acta Materialia 52, 3383–3402. (b) Gall, K., Sehitoglu, H., Chumlyakov, Y.I., Kireeva, I.V., 1998b. Pseudoelastic cyclic stress-strain response of over-aged single crystal Ti-50.8 at% Ni. Scripta materialia 40, 7–12. (c) and (d) Sehitoglu, H., *et al.*, 2000. Compressive response of NiTi single crystals. Acta Materialia 48, 3311–3326.

The Role of Precipitates

It is well-known that when NiTi (and many other SMAs) are used in engineering applications they are frequently given some type of aging treatment that results in a precipitated microstructure. All present research efforts agree that the precipitation of semi-coherent Ti_3Ni_4 precipitates (Tadaki *et al.*, 1986) leads to a large change in the macroscopic mechanical properties of Ni rich NiTi alloys. Peak-aging treatments can lead to the most drastic changes in the mechanical properties of NiTi although solutionized and overaged states with precipitate free and incoherent precipitates respectively have been studied as well (Gall *et al.*, 1999a, 2000b, 1998b,c). In the peak aged samples the lattice parameter mismatch between the Ti_3Ni_4 precipitates and the B2 matrix produces strong local stress fields. These stress fields from the coherent precipitates contribute to martensite formation and hence assist the transformation. The local

stress fields resolve differently onto the martensite variants (Gall *et al.*, 1998c; Sehitoglu, 2001) and affect the preferred variant selection, effectively weakening the orientation dependence of critical stress. In the overaged state, the local lattice mismatch stress fields are diminished by interfacial dislocations and the transformation behavior should be similar to that of solutionized specimens. It is noted that the precipitates act as obstacles for dislocation motion, so they increase the critical stress for dislocation motion and decrease the critical transformation stress for inducing martensite (Treppmann and Hornbogen, 1995) converging towards optimal microstructures. Finally, superelasticity is not usually observed in solutionized NiTi (Miyazaki *et al.*, 1982) while observed for the aged case with precipitates. The aging may also create the conditions for the two-way shape memory effect (Nishida and Honma, 1984). It is also important to note that under aging the most common precipitate is the nickel rich Ti_3Ni_4 (Nishida *et al.*, 1986) and due to aging few other changes are noted: (1) the transformation temperatures (Johnson *et al.*, 2005) are modified, (2) the martensite morphology is dominated by a single plate growing from precipitate variants rather than the thermally-induced morphology, and (3) the martensite in aged alloys was comprised of compound twins (internal defects on (100) planes) rather than type II twins (internal defects on (110) planes).

Fine precipitates that are rich in Ni are observed in nickel rich NiTi alloys. **Fig. 8**(a) summarizes the precipitate images with increasing Ni content. **Fig. 8**(b) shows fatigue results and one notes the accumulation of residual strains and the reduction of transformation strains and stress hysteresis with cycles. The precipitates have been observed in other shape memory alloys as well and dramatically alter the transformation stresses and the slip resistance. The volume fraction of the precipitates increases with increasing Ni content. This increase ultimately limits the transformation strains in tension of 51.5% NiTi to less than 4%. The dramatic effect of the aging effect is shown in **Fig. 8**(c) and (d) below. Note that the lower temperature aging treatment produces a lower transformation stress and at the same time a higher slip stress which can produce a superior performance. Under fatigue conditions, the cyclic response also displays different trends as noted above.

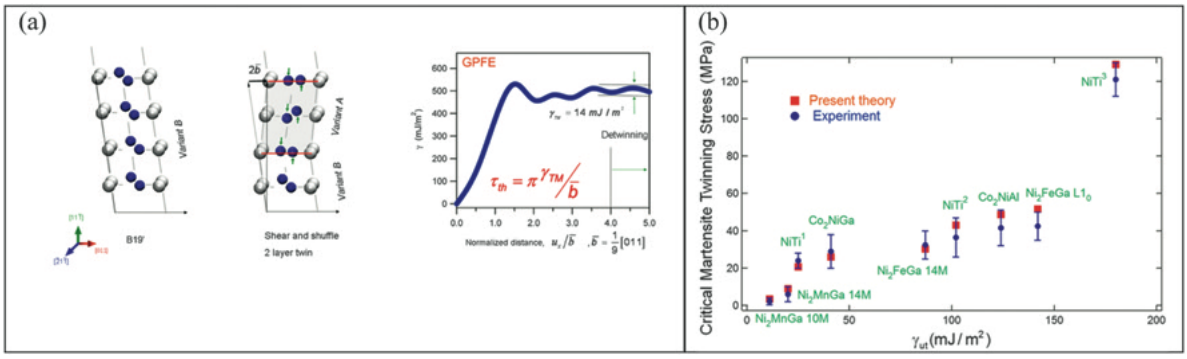

Fig. 9 (a) The growth of the Type II variant (GPFE) via combined shear and shuffle, (b) the martensite twinning stress for well-known SMAs. Reproduced from (a) Ezaz, T., Sehitoglu, H., 2011. Type II detwinning in NiTi. Applied Physics Letters 98, 141906. (b) Wang, J., Sehitoglu, H., 2013. Twinning stress in shape memory alloys: Theory and experiments. Acta Materialia 61, 6790–6801.

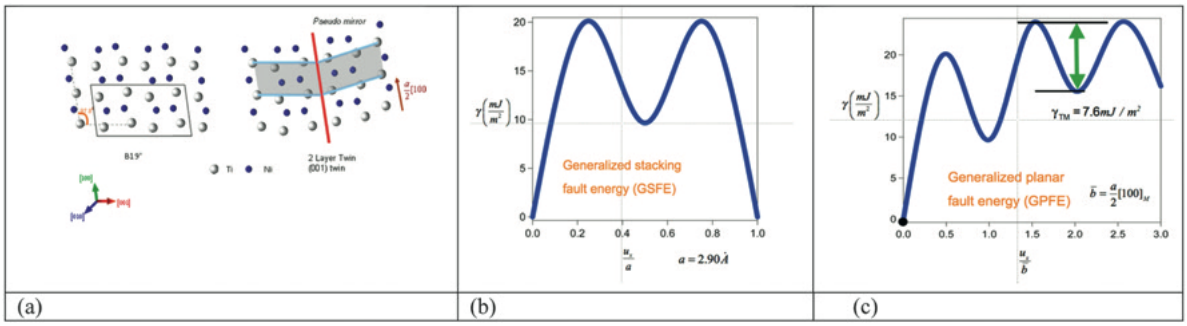

Fig. 10 (a) atomic positions during twinning process for (001) twin, (b) the GSFE curve corresponding to slip on the (001) plane, (c) the GPFE curve that shows that the twin boundary migration barrier is as low as 7.6 mJ/m^2. Reproduced from Ezaz, T., Sehitoglu, H., Maier, H.J., 2011. Energetics of twinning in martensitic NiTi. Acta Materialia 59, 5893–5904. doi:10.1016/j.actamat.2011.05.063.

Energy Barriers

The SMAs undergo reversible phase transformation (Bhattacharya, 2003; Ahlers, 2004) between austenite and martensite where martensite advances via twinning (Nishida *et al.*, 1995a; Kainuma *et al.*, 2006). The degradation of shape memory, on the other hand, is attributed to slip-mediated plastic deformation (Chowdhury and Sehitoglu, 2016, 2017b). These events involve atoms displacing to mirror symmetry positions for forming twins and lattice displacements to minimize energies at the transforming interfaces. The developments center on atomic shear and shuffle determinations. Since the experimental techniques are often limited to probe such sub-atomic length scale events the developments in density functional theory have been invaluable to understand the SMA properties with precise construction of energy landscapes (Entel, 2013; Ezaz and Sehitoglu, 2011; Huang *et al.*, 2003; Hatcher, 2010). Several new SMAs (NiTiPt, NiTiPd, Ni_2FeGa, Ni_2MnGa, Fe-Mn-Al-Ni) have been examined to understand the unstable or metastable and more stable structures (Hatcher *et al.*, 2009a; Vishnu and Strachan, 2010; Wang and Sehitoglu, 2012). Examples are shown in **Figs. 9–11**.

The energy barriers associated with internal twinning play a key role in understanding the critical stress levels. The GPFE curve is obtained by shearing of consecutive layers starting with the twin plane, and by shearing all atoms above the next plane and so on. The slip barriers are characterized by the GSFE curve and the twinning barriers with the GPFE curve. We briefly discuss the energy barrier for the Type II twinning case in NiTi martensite (**Fig. 9**(a)). To achieve high strains the martensite undergoes detwinning and as noted in **Fig. 9**(a) the migration barriers are rather small in NiTi. Note that other SMAs that exhibit very low critical stress magnitudes are the Ni_2MnGa variety as shown below. The other main issue is what is the burgers vector associated with the twinning system of the martensite? This magnitude dictates the critical stress determination. This burgers vector can be inferred from the energy landscape determination. There are other methods to obtain the burgers vector, such as the topological model (Hirth and Pond, 1996), but then one must be very careful about the exact starting atomic structure at the interfaces (i.e., lattice offsets). A summary of the martensite twin stress for well known SMAs is summarized in **Fig. 9**(b). The agreement between theory and experiment is remarkably good.

A two layer (001) twin with a shear strain of 0.2385 is constructed in **Fig. 10**(a)-(b). Initially, we show the GSFE curve in **Fig. 10**(b), then the GPFE curve in **Fig. 10**(c). Because the twin shear is small, the twin related planes are close which requires careful experiments to identify. The direction of shear is the [100] or '*a*' direction, which is the shortest lattice vector in B19′.

The, $\gamma_{TM} = 7.6$ mJ/m^2 (shown with green vertical arrow in **Fig. 10**(c)) decides the twin migration stress.

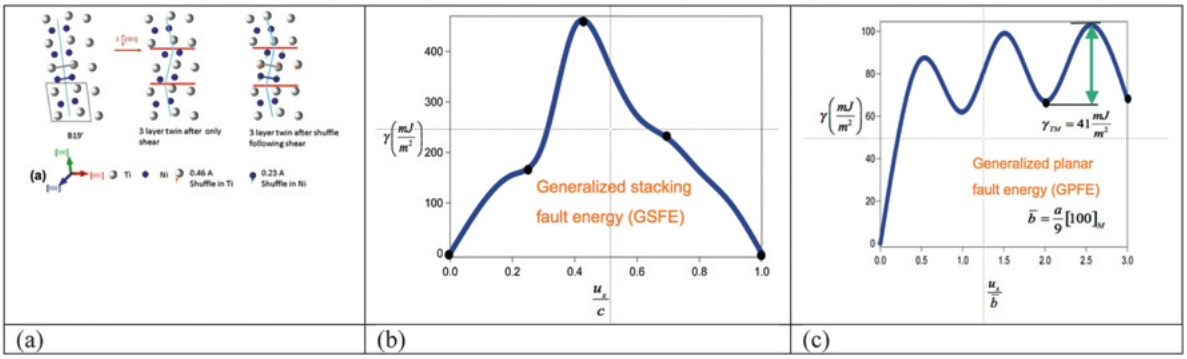

Fig. 11 (a) Shear and shuffles associated with creation of the (100) twin (shuffles are shown with arrows), (b) GSFE for the (100) slip showing very high unstable stacking fault energy, see also Section "Twinning", (c) GPFE for (100) twinning displaying the twin migration energy. Reproduced from (b) and (c) Ezaz, T., Sehitoglu, H., Maier, H.J., 2011. Energetics of twinning in martensitic NiTi. Acta Materialia 59, 5893–5904. doi:10.1016/j.actamat.2011.05.063.

As deformation proceeds, higher order twin modes such as {100} twins can occur at moderate strains (**Fig. 11**) and has been experimentally observed (Onda *et al.*, 1992). The {100} and {001} are from the same family, hence they are difficult to distinguish experimentally, but the barriers are different because the *c*-axis and *a*-axis dimensions differ in monoclinic structure. This twinning mode involves a shuffle making the atomic displacements rather complicated. Also, an additional shuffle is required for Ni and Ti to obtain mirror symmetry along the boundary plane. The shuffling direction is nearly normal to the [001] direction and the magnitude is 0.46 $\dot{A}$ and 0.23 $\dot{A}$ for Ti atoms and Ni atoms, respectively.

Note that in GSFE, shuffles are not permitted and the GSFE barriers are much higher than GPFE. Also for the (100)[001] GSFE, there is no metastable energy position, and the higher barriers in the GSFE compared to GPFE preclude the propensity of slip in this case. Then, twinning for the (100) case can develop because of lower GPFE energy barriers.

Elastic Modulus

This elastic moduli of austenite and martensite remain a topic of current interest (Benafan, 2013a; Brill *et al.*, 1991; Mercier *et al.*, 1980; Rajagopalan *et al.*, 2005; Sittner, 2014; Stebner *et al.*, 2013; Wagner and Windl, 2008; Wang and Sehitoglu, 2014d; Ye *et al.*, 1997;

Hatcher *et al.*, 2009) since the elastic moduli differ in austenite and martensite. The NiTi austenite phase, has three elastic constants (C_{11}, C_{12} and C_{44}) (Ren *et al.*, 2001) while the monoclinic martensite has thirteen constants (Wagner and Windl, 2008) (C_{11}, C_{12}, C_{13}, C_{15}, C_{22}, C_{23}, C_{25}, C_{33}, C_{35}, C_{44}, C_{46}, C_{55}, C_{66}) computed by a select group of researchers (Wang and Sehitoglu, 2014d; Hatcher *et al.*, 2009b). The elastic moduli in micromechanical models is often deficient and can be improved with these constants. Also, good molecular dynamics potentials must predict these moduli correctly which is a difficult task. In fact, the moduli can be used to optimize the potentials (Yamakov *et al.*, 2016; Ren and Sehitoglu, 2016; Daw and Baskes, 1984; Baskes, 1997). To transition to polycrystals, theorems have been developed (Hill, 1952; Reuss, 1929; Voigt, 1928; Nye, 1985; Hashin and Shtrikman, 1963) for calculation, but one must note that the SMAs are often textured so the random texture assumption will not hold. In addition, in the martensitic phase the twinned variants undergo detwinning creating a directional moduli. Furthermore, the twinning/detwinning stress strongly depends on the shear moduli.

We draw attention to an important dichotomy in the literature. The inelastic deformation of twinned martensite which is made up of correspondence-variant pairs involves growth of the preferred variant. Therefore, the initial slope during loading is the stretching of the twinned lattice (and twinned and detwinned lattice have different moduli (Wagner and Windl, 2008; Wang and Sehitoglu, 2014d) with twinned lattice having a lower moduli). Hence a lower ground state exists for twinned martensite compared to detwinned martensite stress-induced. In comparison, the austenite moduli do not depend on the initial microstructural state. The notion that martensite moduli is lower than austenite moduli is fundamentally wrong because the moduli in martensite is altered by the presence of twin interfaces.

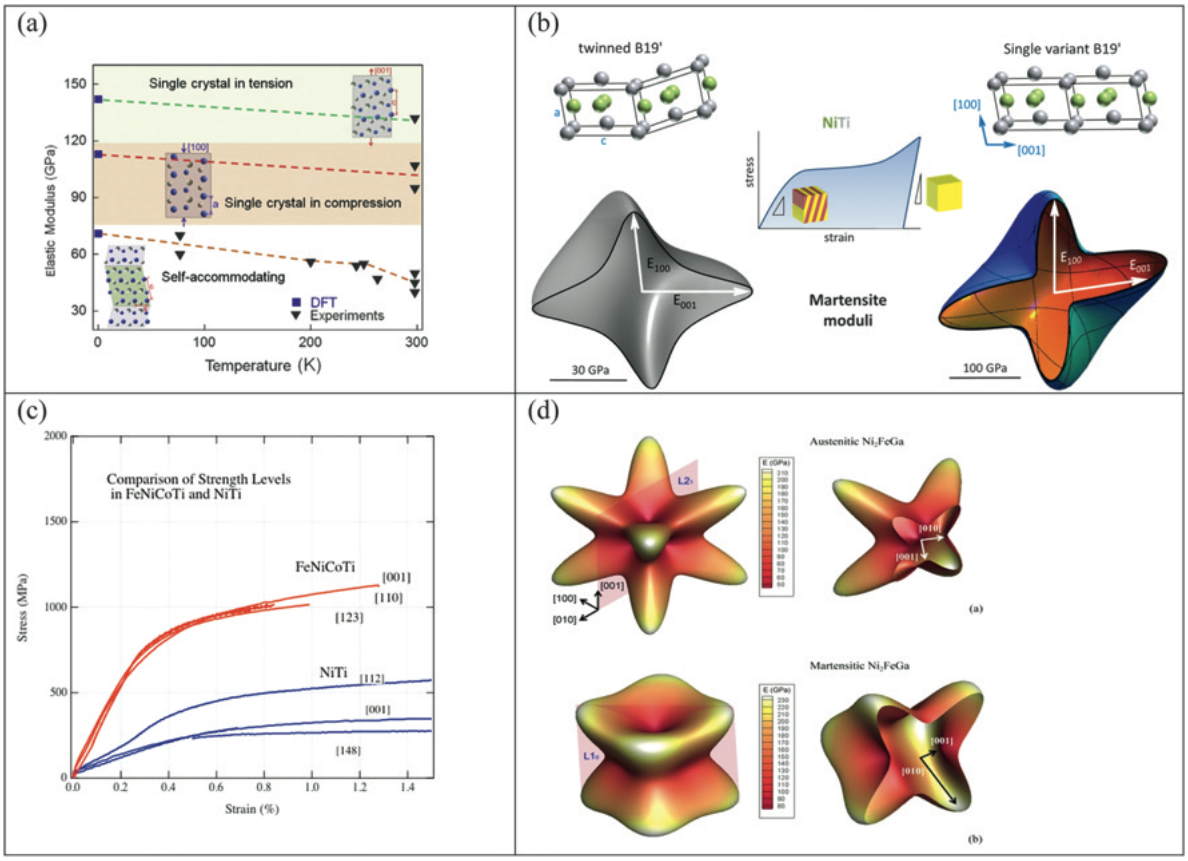

Fig. 12 (a) The elastic moduli of self accommodating twinned martensite in comparison with the martensite modulus in tension and in compression, (b) Comparison of elastic moduli of twinned variant and single crystal of martensite. Note the scale difference between the two cases (30 GPa vs 100 GPa), (c) experiments showing the difference between NiTi moduli and FeNiCoTi moduli for single crystals, and (d) 3D comparison of the anisotropy of the moduli for Ni_2FeGa austenite and martensite. Reproduced from (a) Wang, J., Sehitoglu, H., 2014d. Martensite modulus dilemma in monoclinic NiTi-theory and experiments. International Journal of Plasticity 61, 17–31. (b) Chowdhury, P., Sehitoglu, H., 2017a. Deformation physics of shape memory alloys – Fundamentals at atomistic frontier. Progress in Materials Science 88, 49–88. Available at: https://doi.org/10.1016/j.pmatsci.2017.03.003. (c) Wu, Y., Ojha, A., Patriarca, L., Sehitoglu, H., 2015. Fatigue crack growth fundamentals in shape memory alloys. Shape Memory and Superelasticity 1, 18–40.

Overall, the moduli anisotropy has ramifications in determining constitutive response. Also, the elastic modulus is highly orientation dependent, i.e., anisotropic. It is difficult to comprehend the role of this anisotropy because many of the textbooks covering fatigue, fracture and related topics treat the elastic modulus as a scalar. The results from DFT caculations for self accommodated, and detwinned martensites are given in **Fig. 12**(a). The problem is complicated because the martensite detwinning can start at low stresses and the detwinning process in reality is not an elastic response but is a consequence of twin variant motion. So, trying to extract an elastic modulus from the detwinning process may lead to erroneous results. In fact, the moduli of martensite may be underpredicted with this approach with many consequences. For example, when trying to determine the driving forces in fatigue and fracture from displacement measurements (such as DIC), one needs an accurate value of the elastic moduli. The anisotropy of elastic moduli in NiTi is illustrated in **Fig. 12**(b). The difference in iron and NiTi based SMAs modulus is shown in **Fig. 12**(c). Finally, we illustrate the dramatic anisotropy in Ni2FeGa austenite and martensite in **Fig. 12**(d).

Slip Behavior- Slip Systems and Non-Schmid Effects

In early work, the austenite stresses predicted from theory for several important shape memory alloys in austenite phase and compared to the experimental slip stress data (**Table 5**). The martensite slip stress levels are rather high. The austenite slip stress levels, on the other hand, are more readily available in the experiments and are also very important. The austenite of these materials (Ni_2FeGa, Co_2NiGa, Co_2NiAl, NiTi, CuZn and Ni_2TiHf) possess the $L2_1$ and B2 cubic structures. For each material, the lattice type, the slip system, and the experimental range of critical slip stresses and the theory are shown. If the ideal stress levels are included, these exceed several GPa and are much higher than experiments. Interestingly, the critical stress for CuZnAl, which has excellent transformation properties, but suffers from plastic deformation, exhibits the lowest levels. For austenitic NiTi the most likely slip system is $(011)[100]$ with a slip stress level of 0.71 GPa which is higher than experiments. This difference is expected because in the theory the calculation of the core width is based on a fraction of interplanar spacing (consistent with classical PN (Peierls-Nabarro) theory) which produces higher stresses than experiments. For further discussion, the reader is referred to Mohammed *et al.* (2022).

Table 5 Predicted Peierls stresses for shape memory alloys are compared to known reported experimental values. The slip systems and crystal structures of SMAs are given. ($L2_1$ and B2 are the crystal structures in austenite phase)

Material	*Crystal Structure*	*Slip system*	*Critical Shear Stress-Present Theory (GPa)*	*Critical Shear Stress-Experiment (GPa)*
Ni_2FeGa	$L2_1$	$(1\bar{1}0)\frac{1}{4}[111]$	0.63	0.40–0.65 (Timofeeva *et al.*, 2012)
Co_2NiGa	B2	$(011)[100]$	0.76	0.40–0.70 (Karaman and Lagoudas, 2006; Chumlyakov *et al.*, 2008)
Co_2NiAl	B2	$(011)[100]$	0.72	0.60–0.80 (Chumlyakov *et al.*, 2008; Dilibal *et al.*, 2011a)
NiTi	B2	$(011)[100]$	0.71	0.40–0.80 (Ezaz *et al.*, 2013; Sehitoglu *et al.*, 2001a; Chumlyakov *et al.*, 2008;
		$(011)[1\bar{1}1]$	1.2	Efstathiou and Sehitoglu, 2008)
Ni_2TiHf	B2	$(011)[100]$	0.78	0.55–0.75 (Coughlin *et al.*, 2012; Wang *et al.*, 1999)
CuZn	B2	$(011)[1\bar{1}1]$	0.08	0.03–0.07 (Romero *et al.*, 1988; Wollmershauser *et al.*, 2009)

The experimental slip stress data are taken from the plot of critical stress vs. temperature. The critical austenite slip stress at M_d is considered as the experimental data for austenite slip and compared to the (Peierls based) theory. Since the calculations represented the lattice resistance with no thermal activation one must keep this difference in mind.

The slip behavior of shape memory materials is rather complex. The crystal structures display non-Schmid behavior and the Schmid law is not applicable. So, the slip behavior is orientation dependent. Plastic slip develops mainly at the interfaces and progresses to the austenite phase during phase transformation and limits the functionality of SMAs. The well-known Schmid law utilizes a CRSS value independent of slip system orientation and the sense of loading (Schmid and Boas, 1950). While this law holds for fcc metals, it is considered an exception because most other crystal structures do not obey the Schmid law including the well-known body centered cubic (bcc) cases (Christian, 1983; Duesbery, 1989). The main reason for the deviation from the Schmid law is that non-glide shear (NGS) stresses affect the dislocation core displacements hence the critical stress magnitudes (Alkan and Sehitoglu, 2017b, 2019b; Ojha *et al.*, 2015; Ezaz and Sehitoglu, 2011; Ezaz *et al.*, 2012a, 2011). Another factor in non-Schmid behavior via twining or antitwinning direction of slip in $<111>$ direction in bcc crystals (Duesbery, 1984; Taylor, 1928; Guiu, 1969) (**Fig. 13**(a)) reflected through the antisymmetry of the Generalized Stacking Fault Energy (GSFE) ,or γ, surface (Duesbery and Vitek, 1998; Dezerald *et al.*, 2016).

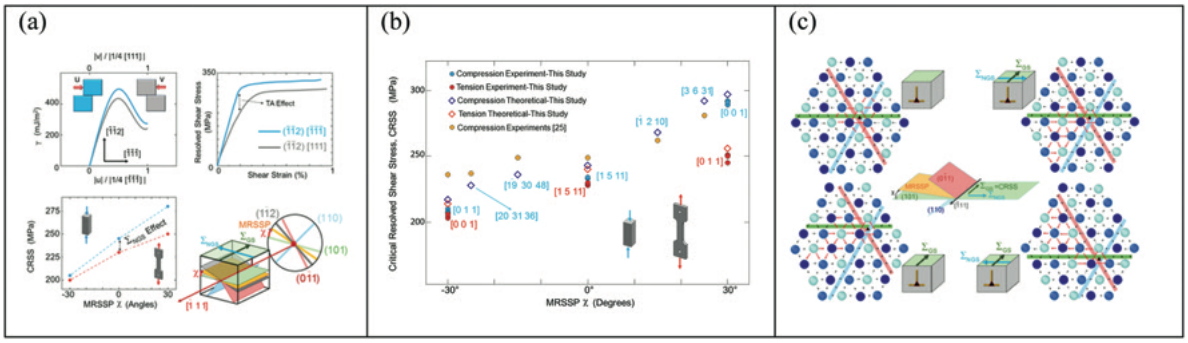

Fig. 13 Dislocation-mediated Slip :(a) the twin, anti-twin asymmetry, (b) Non-Schmid Slip response of Fe_3Al, (c) the core displacements, the CRSS as a function of orientation in (d) CuZnAl and (e) NiTi. The orientation dependence is very significant in both of these most well-known SMAs. If Schmid law was obeyed then CRSS would have been independent of MRSSP (Maximum Resolved Shear Stress Plane) angle, (f) the difference of core displacements for tension and compression in NiTi slip, (g) shows the geometry of the leading partial core in CuZnAl, (h) the resolved shear stresses τ_1, τ_2 and τ_3 acting on the core fractionals, (i) dislocation density distributions on the three planes at the dislocation core. Reproduced from Alkan, S., Sehitoglu, H., 2019a. Prediction of transformation stresses in NiTi shape memory alloy. Acta Materialia 175, 182–195. Alkan, S., Wu, Y., Ojha, A., Sehitoglu, H., 2018a. Transformation stress of shape memory alloy CuZnAl: Non-Schmid behavior. Acta Materialia 149, 220–234. Available at: https://doi.org/10.1016/j.actamat.2018.02.011. Alkan, S., Ojha, A., Sehitoglu, H., 2018b. The complexity of non-Schmid behavior in the CuZnAl shape memory alloy. Journal of the Mechanics and Physics of Solids 114, 238–257. Alkan, S., Sehitoglu, H., 2017b. Dislocation core effects on slip response of NiTi- a key to understanding shape memory. International Journal of Plasticity 97, 126–144. Available at: http://doi.org/10.1016/j.ijplas.2017.05.012. Alkan, S., Sehitoglu, H., 2017a. Non-Schmid response of Fe3Al: The twin-antitwin slip asymmetry and non-glide shear stress effects. Acta Materialia 125, 550–566. Available at: https://doi.org/10.1016/j.actamat.2016.12.019. Alkan, S., Sehitoglu, H., 2019b. Plastic flow resistance of NiTiCu shape memory alloy-theory and experiments. Acta Materialia 163, 173–188. Available at: https://doi.org/10.1016/j.actamat.2018.09.063. (d) Alkan, S., Wu, Y., Ojha, A., Sehitoglu, H., 2018b. Transformation stress of shape memory alloy CuZnAl: Non-Schmid behavior. Acta Materialia 149, 220–234. Available at: https://doi.org/10.1016/j.actamat.2018.02.011. (e) Alkan, S., Sehitoglu, H., 2017b. Dislocation core effects on slip response of NiTi- a key to understanding shape memory. International Journal of Plasticity 97, 126–144. Available at: http://doi.org/10.1016/j.ijplas.2017.05.012. Alkan, S., Wu, Y., Sehitoglu, H., 2017. Giant non-Schmid effect in NiTi. Extreme Mechanics Letters 15, 38–43. Available at: https://doi.org/10.1016/j.eml.2017.05.003.

A simple illustration of the GS and NGS stress components, i.e., Σ_{GS} and Σ_{NGS}, which act along a parallel and perpendicular direction to the Burgers' vector on the active glide plane. The bcc-based ordered structures, e.g., DO_3, B2, $L2_1$, which are common in shape memory alloys, exhibit non-Schmid behavior (Paidar, 1976; Umakoshi *et al.*, 1985; Yamaguchi *et al.*, 1981; Yamaguchi and Umakoshi, 1984, 1990) including DO_3-Fe_3Al undergoing reversible slip (Ojha *et al.*, 2015; Yasuda *et al.*, 2005, 2007, 2003; Yasuda and Umakoshi, 2010) with dissociated four $1/4<111>$ superpartials (Marcinkowski and Brown, 1961; Kubin *et al.*, 1982) (**Fig. 13**(b)). This alloy exhibits both Σ_{GS} and Σ_{NGS} effects (Yasuda *et al.*, 2003; Yasuda and Umakoshi, 2010; Hanada *et al.*, 1981) (**Fig. 13**(c)-(d). The orientation relationship of crystals and the applied loading are designated via the conventional angle χ (Duesbery, 1989). Physically, χ corresponds the angle between the{110}family plane with the highest resolved shear stress along the slip vector and the maximum resolved shear stress plane (MRSSP). The angleχ is bounded between $\pm 30^{\circ}$ owing to the bcc crystal symmetry for Fe_3Al and CuZnAl, for the case of NiTi the range of the angle is 45°.

The slip response of NiTi is of significant interest, and there has been attempts to understand it in detail based on experimental and theoretical treatments (Ezaz *et al.*, 2013; Simon *et al.*, 2010; Benafan *et al.*, 2013b; Sehitoglu *et al.*, 2017d). It is well known that $\{110\}$ $<001>$ slip is dominant in the NiTi alloy. The detailed experimental measurements suggest the non-Schmid behavior of B2 ordered NiTi and a theory has been developed to predict the non-Schmid behavior (**Fig. 13**(e) and (f)).

As shown in **Fig. 13**(f), the screw core in NiTi is non-planar, and depends on the entire stress tensor acting under uniaxial tension and compression. The dislocation core is affected by the sense of loading- a more compact core resulting in higher slip resistance. The deviatoric stress tensor **S** tensor has components of S_{11}, S_{22}, S_{21}, S_{13} and the glide component is designated as S_{23}, i.e., CRSS (see **Table 6** for the constants).

$$\tau_{cr} = \mathrm{CRSS} + a_1 S_{11} + a_2 S_{22} + a_3 S_{21} + a_4 S_{13}$$

where the parameters τ_{cr}, a_1, a_2, a_3 and a_4 are obtained from theory. The simulation results are given in **Fig. 13**(d) and (e) . We show experimental data on 3 orientations under uniaxial tension-compression (6 cases) loading for NiTi, i.e., $<111>$, $<249>$ and $<011>$. We predict the significant tension-compression asymmetry of the slip and the orientation (including non-glide and normal stress) dependence.

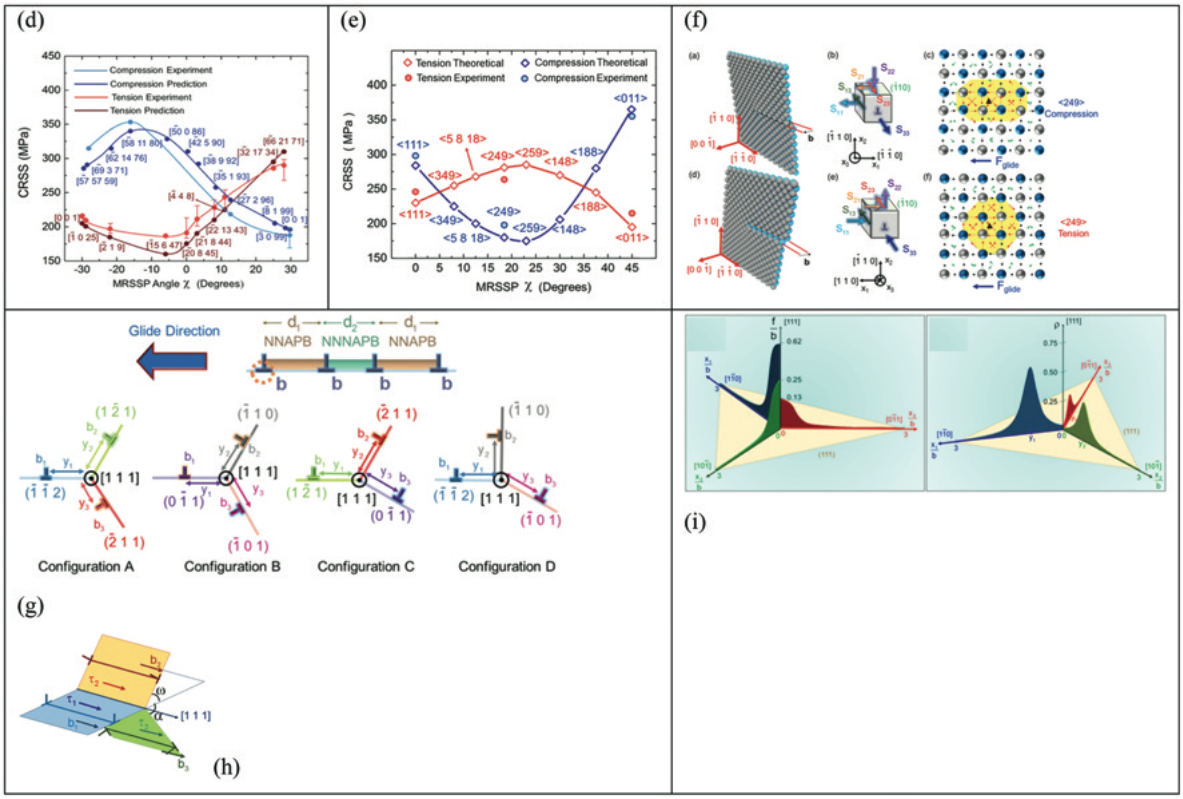

Fig. 13 Continued.

Table 6 Multiaxial yield criteria for NiTi incorporating both glide and non-glide shear stress components

τ_{cr} (MPa)	a_1	a_2	a_3	a_4
240	0.14	0.11	−0.19	0.22

Note: Alkan, S., Sehitoglu, H., 2017b. Dislocation core effects on slip response of NiTi- a key to understanding shape memory. International Journal of Plasticity 97, 126–144. Available at: http://doi.org/10.1016/j.ijplas.2017.05.012.

We consider CuZnAl next which exhibits considerable non-Schmid behavior (**Fig. 13**(d)). Earlier literature on CuZnAl addresses that significant CRSS differentials can be observed as a function of the single crystal orientation under uniaxial loading (Romero *et al.*, 1988). In the case of CuZnAl, the super-lattice dislocation dissociates into the four partial dislocations of each having a/4<111> Burgers vector. The partials are joint by the Nearest Neighbor (NN) and Next Nearest Neighbor (NNN) Antiphase boundary (APB) faults (**Fig. 13**(g)). The core structure of the screw character partials in $L2_1$ ordered lattices exhibit non-planar extension on {110} and/or {112} family planes (four configurations are shown in **Fig. 13**(g)) within the glide zone of <111> (Duesbery and Richardson, 1991; Yamaguchi and Umakoshi, 1983) (**Fig. 13**(h)). The distribution of slip (**Fig. 13**(i)) inside the non-planar core structure is affected by the external stress tensor (stress components other than the glide stress play a role) which results in significant deviations from the Schmid Law (Romero *et al.*, 1988). The huge orientation dependence is evident in the CuZnAl case. There are no fitting parameters or adjustments in the modified Peierls-Nabarro model that predicts the nonlinear CRSS trends (**Fig. 13**(d)).

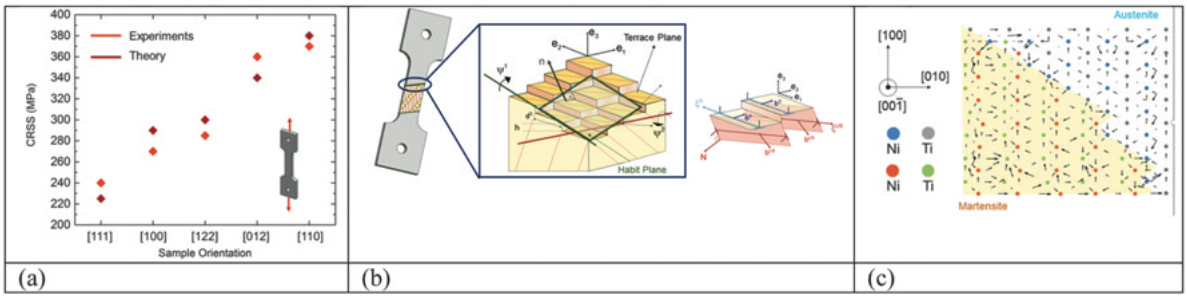

Fig. 14 Transformation Stress Calculation: (a) The variation of CRSS with crystal orientation, (b) the stepped austenite martensite-interface and illustration of twinning dislocations and austenite-martensite interfacial dislocations, (c) differential displacement map illustrating the austenite-martensite interface. Reproduced from Alkan, S., Sehitoglu, H., 2019a. Prediction of transformation stresses in NiTi shape memory alloy. Acta Materialia 175, 182–195.

Transformation Stress- Non-Schmid Effects

The magnitude of the transformation stress is a key quantity that characterizes the constitutive response of a shape memory alloy. The transformation stress is considered as one of the input parameters for the constitutive model. Previous studies presume the validity of Schmid Law, i.e., also known Critical Resolved Shear Stress-CRSS Law, but it is well known that the shape memory alloys do not obey the Schmid law. The most recent approach uses a Peierls Nabarro framework (Alkan and Sehitoglu, 2017a; Wang *et al.*, 2014) to characterize the stress required for advancing the transformation dislocations (**Fig. 14**). It predicts the correct trend for orientation dependence of the transformation stress in NiTi. The treatment is based on the defect network (periodic dislocation arrays) considering the discrete lattice structure generated on the interface at the austenite-martensite boundaries (Zhou *et al.*, 2018; Koch, 2007). This is an advancement over the phenomenological theory of martensite crystallography (PTMC). This treatment is consistent with dislocation motion (Dalle *et al.*, 2002; Sinclair and Mohamed, 1978) at austenite-martensite transformation front. The topological model (Pond, 1989) or other treatments provide the boundary structure, and local displacement fields and stress fields are established via Stroh formulation (Stroh, 1958). The motion of the dislocations depend on the stress state because their cores are non-planar resulting in a coupling between the applied loading direction and the non-planar core structure (Alkan and Sehitoglu, 2017b; Alkan *et al.*, 2017). The interfacial dislocations produce a non-Schmid transformation stress consistent with earlier experimental works (Gall, 1998; Sehitoglu *et al.*, 2001a; Surikova and Chumlyakov, 2000). The derivation has accounted for the energy barriers associated with austenite (B2) to martensite (B19′) crystallographic change. The transformation interface treatment and the molecular statics (MS) simulations reveal the non-Schmid dislocation glide behavior of NiTi (Chowdhury *et al.*, 2015; Alkan and Sehitoglu, 2017b). These theoretical formulations, accounting for the fundamental variables, are expected to advance our understanding of SMAs. This type of formulation will predict the anisotropy of the slip resistance depending on the grain orientation; hence it will advance modeling of polycrystals.

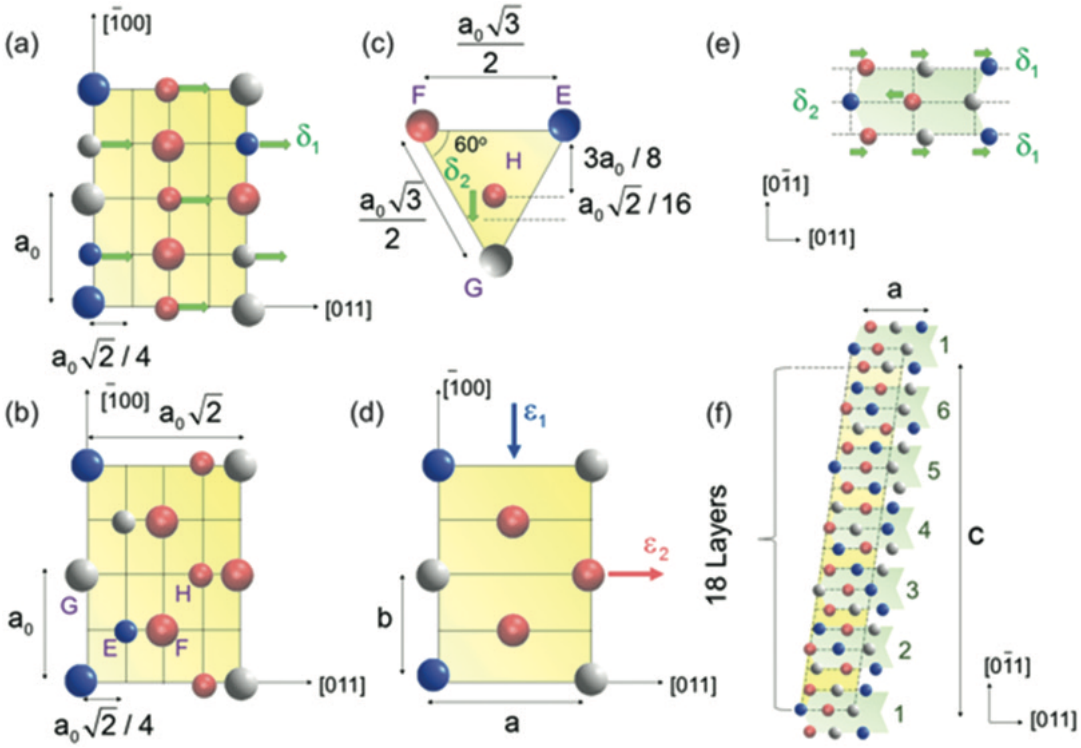

Fig. 15 CuZnAl Transformation- The schematic illustrates the sequential shuffle and shear mechanisms for $L2_1$–18R transformation. (a) shows the primary glide along $\delta_1 = a_0/4[011]$ on each consecutive $(0\bar{1}1)$ plane. The smaller atoms are located on a neighboring plane of $(0\bar{1}1)$. (b) the intermediate displaced positions of the atoms are shown in the undeformed coordinates. (c) shows the secondary shuffling (d) shows the accompanying principle Bain strain components, ε_1 and ε_2 (e) shows the three layer formed as a result of primary shearing and the shuffling mechanism. (f) The 18 R structure involves six of these packing layers. Reproduced from Alkan, S., Wu, Y., Ojha, A., Sehitoglu, H., 2018a. Transformation stress of shape memory alloy CuZnAl: Non-Schmid behavior. Acta Materialia 149, 220–234. Available at: https://doi.org/10.1016/j.actamat.2018.02.011.

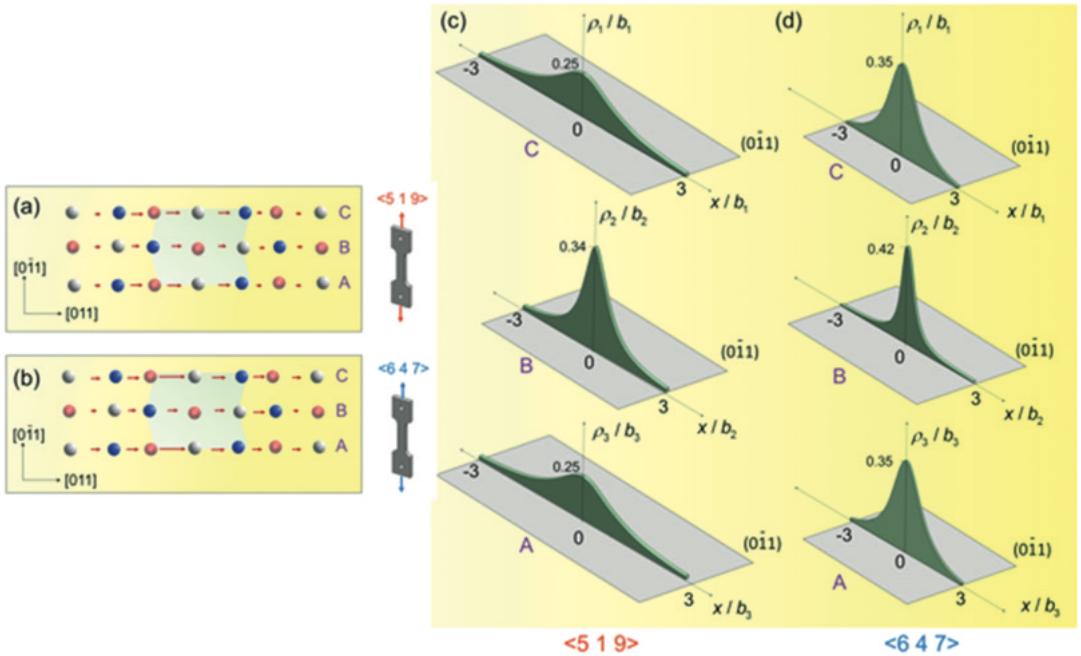

Fig. 16 (a) and (b) illustrates the atomistic scale relative displacements parallel to [011] along the (011) planes of C, B and A for the uniaxial tensile loading directions $<519>$ and $<647>$. It is noted that they are normalized with respect to $\max\{\rho_1 b_1\}$. (c) and (d) shows the resulting dislocation densities along the planes C, B and A for the uniaxial tensile directions along $<519>$ and $<647>$ respectively. From Alkan, S., Wu, Y., Ojha, A., Sehitoglu, H., 2018a. Transformation stress of shape memory alloy CuZnAl: Non-Schmid behavior. Acta Materialia 149, 220–234. Available at: https://doi.org/10.1016/j.actamat.2018.02.011.

A stacking fault mechanism for $L2_1$ to 18R transformation in CuZnAl has been also modeled by considering the shears and shuffles in the underlying process (**Fig. 15**). Both the shear and normal applied stress components contribute to the non-Schmid criteria. The results are strongly orientation dependent and also exhibit tension-compression asymmetry of the CRSS values as a function of crystal orientation by a factor of almost 2.5. The austenitic β phase in CuZnAl (Ahlers, 1986) is essentially an ordered cubic crystal structure- the $L2_1$ structure. The martensite has an 18R structure - denoted as β' phase (Pelegrina and Ahlers, 1992). The transformation stress calculation is based on glide of $a_0/2<111>$ dislocations which upon (Rodriguez *et al.*, 1996) dislocation dissociation result in a pair of $a_0/4[011]$ dislocations gliding on each consecutive (011) planes and $a_0/2[100]$dislocations as explained earlier (Malarría *et al.*, 2001; Sade *et al.*, 1987). **Fig. 16** below illustrates the motion of the dissociated dislocations. The core widths of these three imperfect dislocations with Burgers vectors of $b_1 = a_0/4[011]$, $b_2 = a_0/2[100]$ and $b_3 = a_0/4[011]$are derived which then provide the critical stress for transformation. The experimental and predicted results are given in **Table 7** below. The trends are correct.

Table 7 Transformation stress magnitudes in tension and compression for CuZnAl as a function of orientation

Alloy	*<001> T*	*<001> C*	*<519> T*	*<849> T*	*<103> T*	*<17019> T*	*<647> T*
Cu-27Zn-13.8Al τ_{crit}^{trans} RT Theory, (Alkan *et al.*, 2018a)	25	25	25	33	39.7	41	55.2
Cu-23.7Zn-9.4Al τ_{crit}^{trans}(Exp.) RT (Lexcellent *et al.*, 1996)	25	25	29.5	48.4	50.7	51.9	70.8

Note: Alkan, S., Wu, Y., Ojha, A., Sehitoglu, H., 2018a. Transformation stress of shape memory alloy CuZnAl: Non-Schmid behavior. Acta Materialia 149, 220–234. Available at: https://doi.org/10.1016/j.actamat.2018.02.011. Alkan, S., Ojha, A., Sehitoglu, H., 2018b. The complexity of non-Schmid behavior in the CuZnAl shape memory alloy. Journal of the Mechanics and Physics of Solids 114, 238–257.

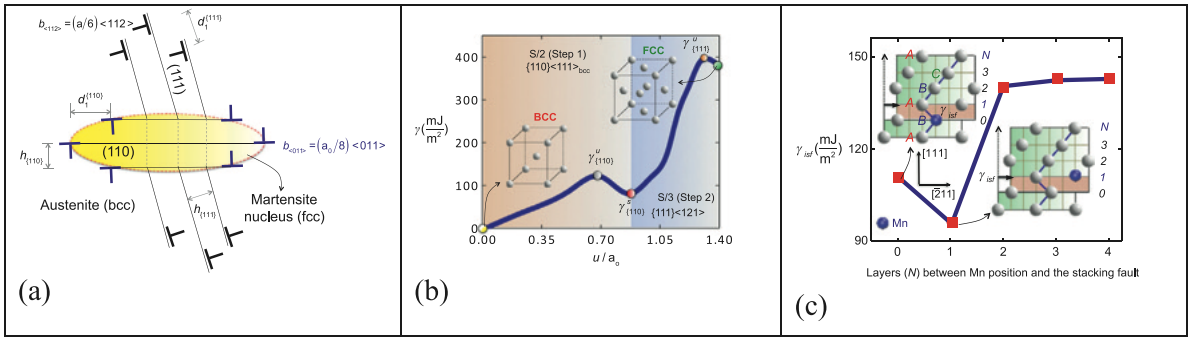

Fig. 17 The transformation in FeMnNiAl: (a) double slip to transition from a bcc to fcc structure, (b) the energy path indicating the barriers associated with the two shear steps, (c) the minimization of the energies upon segregation of Mn atoms near the transformation interface. Reproduced from Ojha, A., Sehitoglu, H., 2016c. Transformation stress modeling in new FeMnAlNi shape memory alloy. International Journal of Plasticity 86, 93–111. doi:10.1016/j.ijplas.2016.08.003.

Next, we consider FeMnNiAl which undergoes a bcc-fcc transformation via a dislocation-based shear glide on S/3 and S/2 systems (glide every third and second plane respectively). The double shear mechanism occurs via motion of two sets of dislocations, $a_0/8<110>$ and $a/6<112>$. The shear on the $\{110\}<110>$ system is termed *S*/2 shear and the shear on the $\{111\}<112>$ system is designated as *S*/3 shear. The energy barriers and the strain energy associated with the participating dislocations are considered to formulate the transformation stress in agreement with experiments. on different planes in a bcc crystal, the intersection of which forms the fcc crystal, as shown in **Fig. 17**. This is analogous to the Bogers-Burgers double shear mechanism (Bogers and Burgers, 1964). We note that the energy profile for the Bain path in this case is higher and not favored. The derivation is based on the modified Peierls Nabarro (PN) formalism (based on our early work on PN (Carrez *et al.*, 2007; Joos and Duesbery, 1997; Joós *et al.*, 1994; Lu *et al.*, 2000; Peierls, 1940) and forward a theoretical model for bcc-fcc transformation stress. The agreement between theory and experiment is excellent (**Table 8**). The martensite is internally twinned so one must include the twinning stress in fcc martensite (Wang and Sehitoglu, 2013) for further insight. Since the solute atoms close to the fault can reduce the stacking fault energy (Suzuki, 1962; Finkenstadt and Johnson, 2006), the GPFE with the minimum value of stacking fault energy is utilized for critical twinning stress calculations (**Table 8**).

Table 8 Comparison of theoretical and experimental critical transformation stress and the twinning stress in the martensite (fcc phase)

Alloy	*Critical transformation stress (τ_{crit}^{trans}, MPa)*		*Critical twinning stress (τ_{crit}^{trans}, MPa)*
	Theory	*Experiment (Tseng et al., 2016)*	*Theory (study Ojha and Sehitoglu)*
FeMnAlNi	191	200	201

Note: Ojha, A., Sehitoglu, H., 2016c. Transformation stress modeling in new FeMnAlNi shape memory alloy. International Journal of Plasticity 86, 93–111. doi:10.1016/j.ijplas.2016.08.003.

The Use of MD Potentials in SMA Research

The solution of the interatomic bonding is most accurately given by the Schrödinger's equation, the basis of the quantum mechanics (Tadmor and Miller, 2011). To determine millions of electronic positions by simultaneously solving the same number of Schrödinger's equations is beyond the capabilities of supercomputers! Therefore, the first principle calculations using density functional theory have been employed for extracting certain properties (e.g., elastic constants, energy of phases, transformation energy pathways etc.) (Wagner and Windl, 2008; Huang *et al.*, 2003). It is crucial to establish the transformation response at the continuum and mesoscales. Using the *first principle* extracted properties as a basis one can develop molecular dynamics simulations describing the interatomic force-fields through the so-called "pair-potential". Despite the critical need, there have been limited progress on development of pair potentials for shape memory alloys at mesoscale (Zhong *et al.*, 2012; Lai and Liu, 2000).

One of the first potentials for NiTi B2 phase was developed by Farkas *et al.* (1996) which predicted the cohesive energy (4.93 eV/atom) and the lattice constant of stable B2 NiTi ($a_{B2} = 3.00A^o$) in agreement with DFT results (Hultgren *et al.*, 1973). The studies of transformation from the B2 to the B19′ phase have been undertaken later by Lai and Liu (Lai *et al.*, 2000; Lai and Liu, 2000) and then utilized by Sato *et al.* (2006), Ishida and Hiwatari (2007) to evaluate shape memory behavior. Others utilizing this potential (Zhong *et al.*, 2011; Mirzaeifar *et al.*, 2014; Mutter and Nielaba, 2011, 2013) made good progress for understanding the equiatomic NiTi response. Hysteresis and two-way transformations were predicted in Mutter and Nielaba (2011, 2010) as well as detwinning (Mutter and Nielaba, 2013). Lower energy structures were proposed B33 (BCO) where superelasticity was predicted (Zhong *et al.*, 2011, 2012), including abrupt stress drop upon martensite nucleation. When internal stress-fields are present, the B19' phase dominates instead of B33′ and B19′ has been observed experimentally without exception.

In summary, there are very few MD potentials that can predict the NiTi behavior (stress levels, atom positions and elastic moduli) accurately (**Fig. 18**(a)-(d)). The major challenge has been to obtain the correct elastic moduli, the correct lattice-motif atom positions from the MD simulations. The next issue is to predict superelasticity, and then the correct transformation stress magnitudes. Among several MD potentials that have been published, the one closest to experimental findings is Ren and Sehitoglu (2016) (**Fig. 18**(a)). It predicts the tension-compression asymmetry and temperature dependence. This is a newly developed Finnis-Sinclair type pair-potential. This new potential is an improvement over other potentials in the literature (Zhong *et al.*, 2012; Lai and Liu, 2000; Mutter and Nielaba, 2010), in that it can predict, for example, a better level of elastic constants among other important crystal properties. In fact, this potential was used to determine the energy barriers in conformity with DFT calculations. The model is also used to determine the lattice offsets in Type II twinning and the migration mechanism by exchange of atoms in lattice and motif points (Mohammed and Sehitoglu, 2020a, 2020b, 2021).

Since the response of SMAs is extremely complex, to our knowledge, the NiTi is the only SMA with MD potentials that have been tested under different loading scenarios. The CoNiAl shape memory alloy, which also exhibits superelasticity, has also been considered in the literature (Pun *et al.*, 2015; Yamakov *et al.*, 2016). However, further work is necessary to evaluate the CoNiAl potentials.

The stress-strain response from MD simulations (Ren-Sehitoglu potential) are summarized in **Fig. 18**(c) showing the role of precipitates on the results. A comparison of elastic moduli using the MD potentials by Ren-Sehitoglu and the one by Zhu are given in **Fig. 18**(b). The stress-strain results for NiTi using the Zhu's potential are given in **Fig. 18**(e), and in **Fig. 18**(f) the results for CoNiAl are shown using the CoNiAl potential (Pun *et al.*, 2015; Yamakov *et al.*, 2016) from the literature.

Early x-ray diffraction studies affirmed that the lattice structure of the Ni_4Ti_3 precipitate is of rhombohedral type (Saburi *et al.*, 1986; Tadaki *et al.*, 1986). The Ni_4Ti_3 precipitates are typically found to be of oblate spheroid geometry, lying on the $\{111\}_{B2}$ family of planes. Schryvers (Tirry and Schryvers, 2005; Schryvers *et al.*, 2006) have measured the strain gradient near a Ni_4Ti_3 particle in an austenitic matrix using TEM and GPA methods, revealing a complex spatial variation. The MD (Chowdhury *et al.*, 2016) accurately capture the local stress gradient at the precipitate-matrix interface in agreement with the experimentally determined trend.

Given the important role of Ni_4Ti_3 precipitates, a number of theoretical approaches have been undertaken in the earlier literature. Most of these models based on the principles of thermodynamics, finite element and self-consistent methods address the continuum aspects of the problem (Bhattacharya, 2003; Boyd and Lagoudas, 1996; Patoor *et al.*, 1996). Most noteworthy among them are the Eshelby-type analyses (Mura, 2012) capturing the internal/external stress/strain distributions for various precipitate geometries. Sehitoglu et al explained the biased variants due to the precipitate fields with micro-mechanical calculations (Gall *et al.*, 1999d). On the other hand, the fundamental effects of a precipitate disturbance fields originate from the atomistic interactions (Khalil-Allafi *et al.*, 2002) at the discrete lattice level. Most recently, ab-initio calculations were made showing the elastic anisotropy of the Ni_4Ti_3 lattice founded on the sub-lattice electronic structure (Wagner and Windl, 2009). However, ab-initio calculations deal with finite number of atoms (Tadmor and Miller, 2011), and MD approaches more

(a)

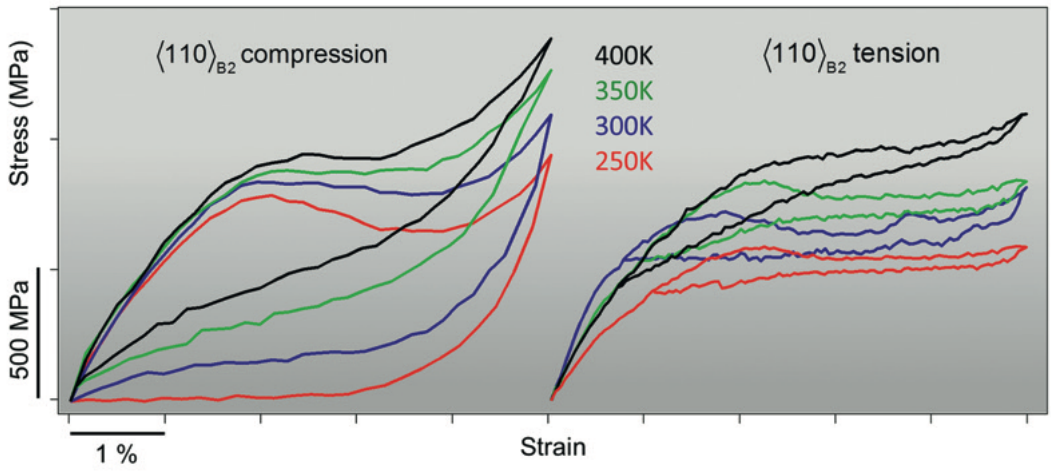

(b)

Martensite Elastic Moduli	DFT Results Hatcher	Wang	MD Results Zhong	Ren
C11	223	238	303	218
C12	129	139	222	120
C13	99	102	326	103
C15	27	27	175	−16
C22	241	234	1135	252
C23	125	114	400	72
C25	−9	−7	125	−7
C33	200	209	692	206
C35	4	1	292	2
C44	76	77	286	37
C46	−4	−5	110	−2
C55	21	23	215	41
C66	77	72	114	43
B	152	154	447	141
G	56	56	202	50
E	149	150	526	133
ν	0.34	0.34	0.30	0.34

Fig. 18 (a) The simulations of compression and tension with the MD potential, (b) comparison of martensite elastic constants utilizing the MD potentials of Sehitoglu-Ren, the DFT results, and based on the proposed potential by Zhu *et al* (c) the role of precipitates on the stress-strain response via MD simulations, (d) precipitate dimensions for NiTi utilized in the simulations shown in (c), (e) another example of MD simulations of stress-strain response from the literature, (f) MD simulations for CoNiAl shape memory alloy. Reproduced from (a) Chowdhury, P., Ren, G., Sehitoglu, H., 2015. NiTi superelasticity via atomistic simulations. Philosophical Magazine Letters 95, 574–586. doi: 10.1080/09500839.2015.1123819. (b) Based on Ren, G., Sehitoglu, H., Interatomic potential for the NiTi alloy and its application. Computational Materials Science 123, 19–25. Zhong, Y., Gall, K., Zhu, T., 2012. Atomistic characterization of pseudoelasticity and shape memory in NiTi nanopillars. Acta Materialia 60, 6301–6311. (c) Chowdhury, P., Patriarca, L., Ren, G., Sehitoglu, H., 2016. Molecular dynamics modeling of NiTi superelasticity in presence of nanoprecipitates. International Journal of Plasticity 81, 152–167. (e) Zhong, Y., Gall, K., Zhu, T., 2011. Atomistic study of nanotwins in NiTi shape memory alloys. Journal of Applied Physics 110, 033532. Zhong, Y., Gall, K., Zhu, T., 2012. Atomistic characterization of pseudoelasticity and shape memory in NiTi nanopillars. Acta Materialia 60, 6301–6311. (f) Based on the potential proposed in references Pun, G.P., Yamakov, V., Mishin, Y., 2015. Interatomic potential for the ternary Ni–Al–Co system and application to atomistic modeling of the B2–L10 martensitic transformation. Modelling and Simulation in Materials Science and Engineering 23, 065006. Yamakov, V., *et al.*, 2016. Multiscale modeling of sensory properties of Co–Ni–Al shape memory particles embedded in an Al metal matrix. Journal of Materials Science 51, 1204–1216.

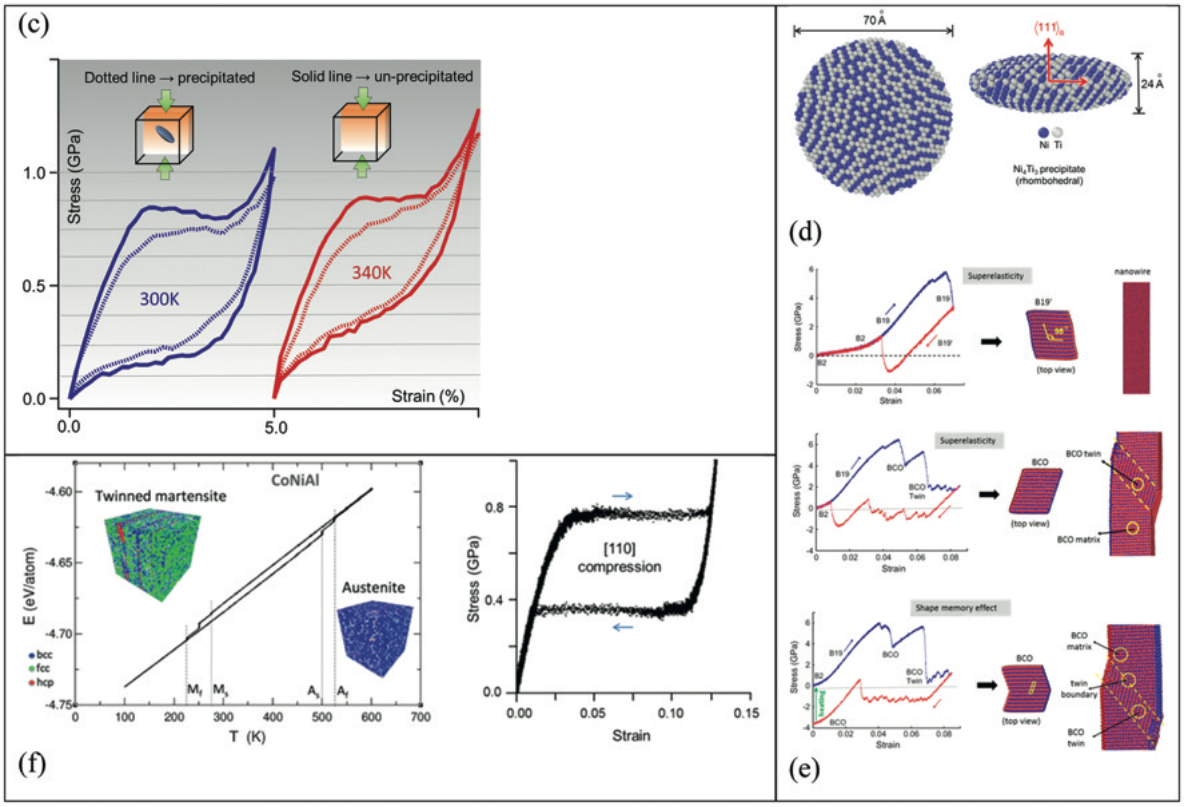

Fig. 18 Continued.

suitable for studying nm size domains. Since the previous MD studies (Zhong *et al.*, 2012; Lai and Liu, 2000; Mutter and Nielaba, 2010) were for pristine NiTi austenite utilizing the MD potential produced insightful results.

The results in **Fig. 18**(c) give insight to the role of precipitates (Chowdhury *et al.*, 2016; Sato *et al.*, 2006) in NiTi. The aging treatments can lower transformation stress and the hysteresis. The presence of precipitates create internal strain fields, which affects variant selection for the Ni_4Ti_3 particle. The stress-strain fields and the overall stress-strain behavior has been simulated in recent works and the non-linear internal fields associated with misfit of the precipitates create a different response than expected based on the matrix. The results are in agreement with experiments (Tirry and Schryvers, 2005) and the observation of preferred martensite variants near the precipitate (Bataillard *et al.*, 1998). In the presence of precipitates forming on different planes (multi-variants), there would be disturbance fields that overlap and potentially produce a more isotropic response.

Twinning

The martensite NiTi which is cooled under no external stress is internally twinned and this is often called a self-accommodated state (Otsuka and Ren, 2005). Among the multiple twin modes, Type II twins (with {111} terraces) are the most common (Knowles and Smith, 1981; Otsuka *et al.*, 1971) for solutionized cases while (001) twins exist in the aged alloys (Nishida *et al.*, 1988; Miyazaki *et al.*, 1981) or in fine grained NiTi (Waitz *et al.*, 2004, 2005). Upon application of stress, the transformation twin boundaries migrate and this typically occurs at low stresses. Deformation twins such as {012} are activated at higher strains. We illustrate the martensite (B19') load/unload curve (red curve) stress-strain curve in **Fig. 19**(a). Upon heating above A_f (blue curve) the deformation is recovered and the martensite returns to the self-accommodated state. In NiTi martensite, Type I, Type II and compound twins (Otsuka *et al.*, 1971; Knowles and Smith, 1981; Gupta and Johnson, 1973) have been encountered upon transformation- the Type II being the most common one. Type II twin is achieved via rotation (180° rotational symmetry) about the η_1 axis([011] direction) . Upon deformation one variant of Type II twin overtakes the other variant, and this process is called detwinning. There has been debate whether the (001) twins are also possible initially, at higher stresses, these twins, called compound twins, have been observed (Kudoh *et al.*, 1985). Higher order twins $(\bar{2}01)$ and (113) can also form (Onda *et al.*, 1992; Nishida *et al.*, 1998) (**Fig. 19**(b)) but they may not be recoverable upon unloading or upon heating. Finally, in the austenite phase, twins of types (114) and (112) (Goo *et al.*, 1985; Nishida *et al.*, 2006; Moberly *et al.*, 1991; Tyumentsev *et al.*, 2004) are reported (**Fig. 19**(c)). It has been shown that there is a direct correspondence between the austenite twins and the higher order martensite twins ({114}A to {012}M).

Experimentally, Type II type twins are most commonly observed for solutionized NiTi (Onda *et al.*, 1992; Xie and Liu, 2004) and rearrange during the stress plateau of the martensite deformation. The study of Type II twins in NiTi martensite has remained a topic of considerable debate, and a general consensus regarding its unique interface morphology has emerged recently (Nishida *et al.*, 1995b). Specifically, phenomenological models (Wayman, 1964; Lieberman *et al.*, 1955; Bowles and Mackenzie, 1954) widely consider the twinning plane as irrational (Bilby and Crocker, 288AD), i.e. $K_1 = (0.72051\ \overline{1})$, while high resolution TEM analyses (Knowles, 1982; Liu and Xie, 2003) suggest a rational yet stepped geometry. The origin of rather unusual boundary geometry is attributed to a need to minimize the total interfacial energy (Liu and Xie, 2003; Christian, 2002). Both shear and shuffle displacements contribute to this type of twinning (Ezaz and Sehitoglu, 2011). Additional straining can be achieved via activation of (001) and (100) twinning modes (Kudoh *et al.*, 1985; Onda *et al.*, 1992; Waitz *et al.*, 2004, 2005; Nishida *et al.*, 1998; Waitz *et al.*, 2007). Higher order twins such as {201} type twins, impart additional ductility to the deformed martensite. In addition, dislocation activities can also accompany the deformation at this stage (Liu *et al.*, 1998; Chumlyakov *et al.*, 2013). The twinning energy landscapes for the (001) and (100) modes (based on (Ezaz *et al.*, 2011)) were illustrated in **Figs. 10** and **11** and they produce different barriers 7.6 mJ m^{-2} and 41 mJ m^{-2} respectively for (001) and (100) twins. We note that a 20 mJ m^{-2} of barrier magnitude is required for (001) slip, which points to potential slip occurring in concurrence with twinning.

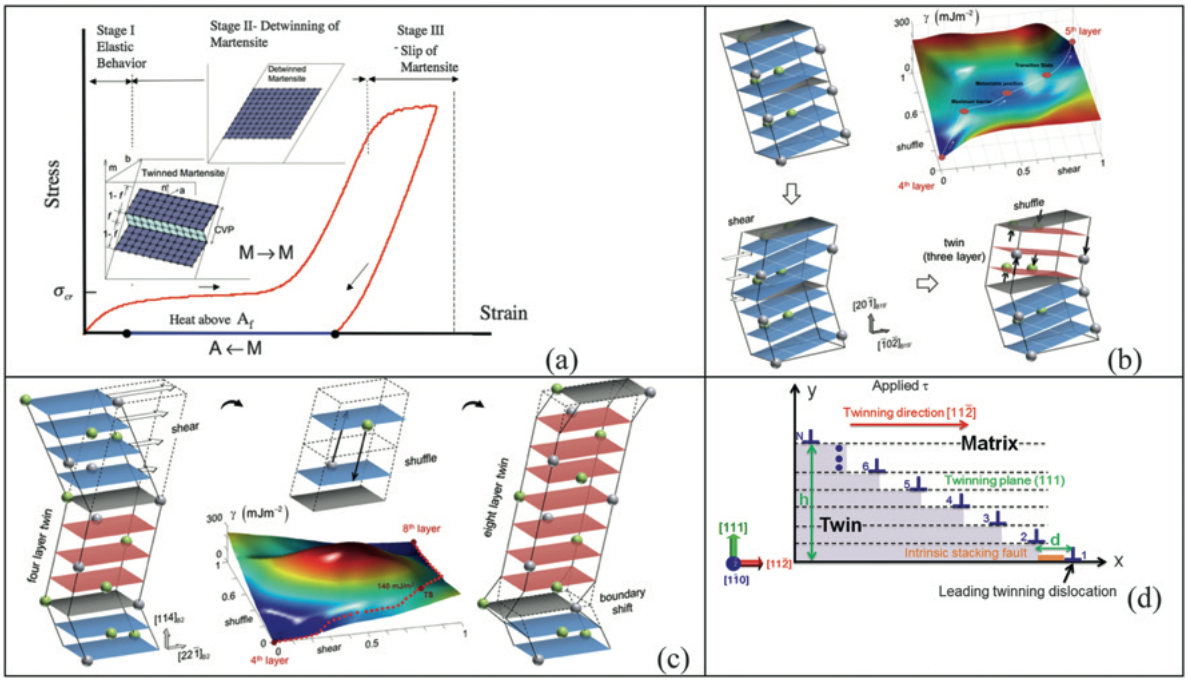

Fig. 19 (a) Stress-strain response in the martensitic phase (M to M (martensite to martensite), and M to A (martensite to austenite) upon heating at zero stress to a temperature above the austenite finish temperature is shown with a blue line), a schematic for NiTi martensite showing the detwinning of martensite upon progressive deformation as the inset figures, (b) a higher order twin in NiTi, the {201} system, (c) the {114} twin in NiTi austenite, (d) a generalized theoretical model for twinning. Reproduced from (b) Chowdhury, P., Sehitoglu, H., 2017a. Deformation physics of shape memory alloys – Fundamentals at atomistic frontier. Progress in Materials Science 88, 49–88, Available at: https://doi.org/10.1016/j.pmatsci.2017.03.003. (c) Ezaz, T., Sehitoglu, H., Maier, H.J., 2012a. Energetics of (114) twinning in B2 NiTi under coupled shear and shuffle. Acta Materialia 60, 339–348. Wang, J., Sehitoglu, H., 2013. Twinning stress in shape memory alloys: Theory and experiments. Acta Materialia 61, 6790–6801.

Table 9 Predicted critical twin nucleation stresses τ_{crit}^{theory} for shape memory alloys are compared to known reported experimental values τ_{crit}^{expt}. The twin systems, equilibrium spacing d and unstable twin nucleation energy γ_{ut} corresponding to SMAs are given. (10M, 14M, $L1_0$ and B19' are the martensitic crystal structures explained in the text)

Material	*Twin system*	$\gamma_{ut}(mJ/m^2)$ *(pred.)*	*d (Å) (pred.)*	τ_{crit}^{theory} *(MPa) (pred.)*	τ_{crit}^{expt} *(MPa) (experiment)*
Ni_2MnGa 10M	[100](010)	11	38	3.5	0.5–4 (Callaway *et al.*, 2006; Chulist *et al.*, 2012; Müllner *et al.*, 2003; Müllner and King, 2010; Straka *et al.*, 2004; Soolshenko *et al.*, 2003; Sozinov *et al.*, 2001)
Ni_2MnGa 14M	[100](010)	20	21	9	2–10 (Sozinov *et al.*, 2002; Soolshenko *et al.*, 2003)
NiTi[1] B19'	(001)[100]	25	45	20	20–28 (Sehitoglu *et al.*, 2000; Ezaz *et al.*, 2011)
Co_2NiGa $L1_0$	$(111)[11\bar{2}]$	41	42	26	22–38 (Kireeva *et al.*, 2010; Chumlyakov *et al.*, 2008)
Ni_2FeGa 14M	[100](010)	87	17	30	25–40 (Timofeeva *et al.*, 2012; Sutou *et al.*, 2004)
NiTi[2] B19'	(100)[001]	102	35	43	26–47 (Sehitoglu *et al.*, 2000; Ezaz *et al.*, 2011)
Co_2NiAl $L1_0$	$(111)[11\bar{2}]$	124	37	48	32–51 (Chumlyakov *et al.*, 2008; Dilibal *et al.*, 2011a)
Ni_2FeGa $L1_0$	$(111)[11\bar{2}]$	142	24	51	35–50 (Timofeeva *et al.*, 2012; Sutou *et al.*, 2004)
NiTi[3] B19'	$(20\bar{1})[\bar{1}0\bar{2}]$	180	9	129	112–130 (Ezaz *et al.*, 2011, 2012b)

There is also experimental evidence of twins in the B2 phase, the existence of the {114}twin system (Goo *et al.*, 1985; Moberly *et al.*, 1990; Chumlyakov *et al.*, 2008; Nishida *et al.*, 2006; Moberly, 1991; Moberly *et al.*, 1991; Surikova and Chumlyakov, 2000; Ii *et al.*, 2003; Krishnan and Maji, 2001; Zheng *et al.*, 1999), involving both the energy pathway as a function of shear and shuffle is reported in **Fig. 19**(b) and (c) (Ezaz *et al.*, 2012a). The fault energy (γ) is the maximum (148 mJ m^{-2}) and such a low energy barrier can be the preferred mode delaying slip in the austenite.

The critical twinning stress (for martensite) τ_{crit} was predicted for several important shape memory alloys (based on the Peierls-Nabarro formulations schematically shown in **Fig. 19**(d) and the results are given in **Table 9**) and compared to experimental twinning stress data. The martensitic crystal structures of these materials present 10M (five-layered modulated tetragonal structure for Ni_2MnGa and five-layered modulated monoclinic structure for Ni_2FeGa), 14M (seven-layered modulated monoclinic structure), $L1_0$ (non-modulated tetragonal structure) and B19' (monoclinic structure). There is excellent agreement between the predicted values and experimental data without any fitting parameters in theory as shown in **Table 9**. The equilibrium d (separation width) corresponding to the minimum total energy for different materials is also shown. This study important crystal structures 10M and 14M in Ni_2MnGa, and the monoclinic B19′ structure of NiTi. In all cases, we determined the lattice constants prior to our simulations. The twin system and unstable twin nucleation energy γ_{ut} corresponding to SMAs are also given. We should note that because the core width of the twin partials is calculated from simplified considerations, its magnitude is slightly smaller than reality which gives higher theoretical values. Further work is needed in this area. It is experimentally observed that the morphology of twinning dislocations array near the twin tip is thin and semi-lenticularly shaped (Jin and Bieler, 1995; Zhang, 1999; Müllner and Romanov, 2000; Gutkin *et al.*, 2007). The critical stage of twin nucleation is the activation of the first twinning partial dislocation on twin plane involving an intrinsic stacking fault (Jin and Bieler, 1995; Gutkin *et al.*, 2007; Marcinkowski and Sree Harsha, 1968; Appel *et al.*, 2011). This can occur in a region of high stress concentration (Marcinkowski and Sree Harsha, 1968). The h is the twin thickness and N is the number of twin-layers, and d is the spacing between two adjacent twinning dislocations and varies depending on their locations relative to the twin tip (**Fig. 19**(d)). It is experimentally observed that twinning partials near the twin tip are more closely spaced (d is smaller) compared to the dislocations far away from the twin tip (d is larger) (Jin and Bieler, 1995). The minimum shear stress to form a twin is called critical twin nucleation stress, τ_{crit}. Once the first twinning partial (leading twinning dislocation) has nucleated, subsequent partials readily form on successive twin planes (Appel *et al.*, 2011). We note that a three-layer fault forms the twin nucleus in $L1_0$ Ni_2FeGa, which reproduces the $L1_0$ structure. Thus, the number of twin-layers, N, equals to 3 in the models.

Irrational Twin Planes and the Origin of the Irrationality (Comparison With Experiments) and Slip Emission

It is well known that the cause of functional fatigue in shape memory alloys is transformation-induced slip (Norfleet *et al.*, 2009; Delville *et al.*, 2011; Pelton *et al.*, 2012; Simon *et al.*, 2010; Sade *et al.*, 1985; Damiani *et al.*, 2003; Kajiware and Owen, 1973; Kajiwara and Kikuchi, 1982; Jiang *et al.*, 1997). It is the accumulation of these slip dislocations over multiple cycles of transformation that leads to accumulating residual strain, degrading functionality, and eventually structural failure. However, the mechanism that leads to the formation of the slip dislocations during transformation is not well understood. It is indeed perplexing to fathom why slip-dislocation activity is observed when the stress-levels associated with transformation are far lower than that required for austenitic slip (Sehitoglu *et al.*, 2000). Given this disparity, there must be a slip-dislocation "source" from the transformation to explain the induced slip. An early hypothesis of such a mechanism was offered Kajiwara and Kikuchi (1982). The mechanism was based on a consistent observation regarding the observed slip dislocations. It was evidenced that not all slip-systems are activated in the austenite phase and only a preferential slip system selected by the transformation is active. The activated slip system exhibits a consistency with the internal lattice-invariant deformation mode of the martensite, most commonly twinning. In other words, the Burgers vector of

the emitted slip dislocation and the plane of slip were consistent with the martensitic direction of twinning shear and the plane of twinning respectively (Norfleet *et al.*, 2009; Simon *et al.*, 2010; Zhang *et al.*, 2012).

This observation pointed to the possibility of the slip-dislocations originating from the internal twin boundary within the martensitic phase. And the mechanism proposed by Kajiwara-Kikuchi (K-K) was founded on this idea. A brief description is provided here and the reader is referred to reference Kajiwara and Kikuchi (1982) for a more detailed exposition. The mechanism involves the role of two critical interfaces during the martensitic transformation namely the habit-plane and the internal twinning interface within martensite. During the forward transformation, the habit-plane sweeps into the austenite and the internal martensitic twin boundary is also mobile leading to the growth of one martensitic twin variant at the expense of the other. This growth is achieved by twinning dislocations on the twin boundary, gliding under the stress of forward transformation. During the reverse transformation, the twinning dislocations are immobilized due to a lower prevailing stress of transformation. And now the habit-plane is mobile in the reverse direction closing down and shrinking the martensitic phase. The twinning dislocations cannot readily slip into the austenitic phase since the corresponding slip-system has a much higher glide resistance. It was hypothesized that the twinning dislocations build-up on the habit-plane until at a certain critical point, a dislocation reaction is triggered. This reaction leads to the emission of slip-dislocations into the austenitic phase. The possibility of twin-dislocation build-up and slip-emission reaction proposed by the K-K mechanism offered a plausible explanation for occurrence of slip at far lower stress levels than the native slip-stress of the austenitic phase. Furthermore, the importance of twinning dislocations and their role during the martensitic transformation was brought to the fore.

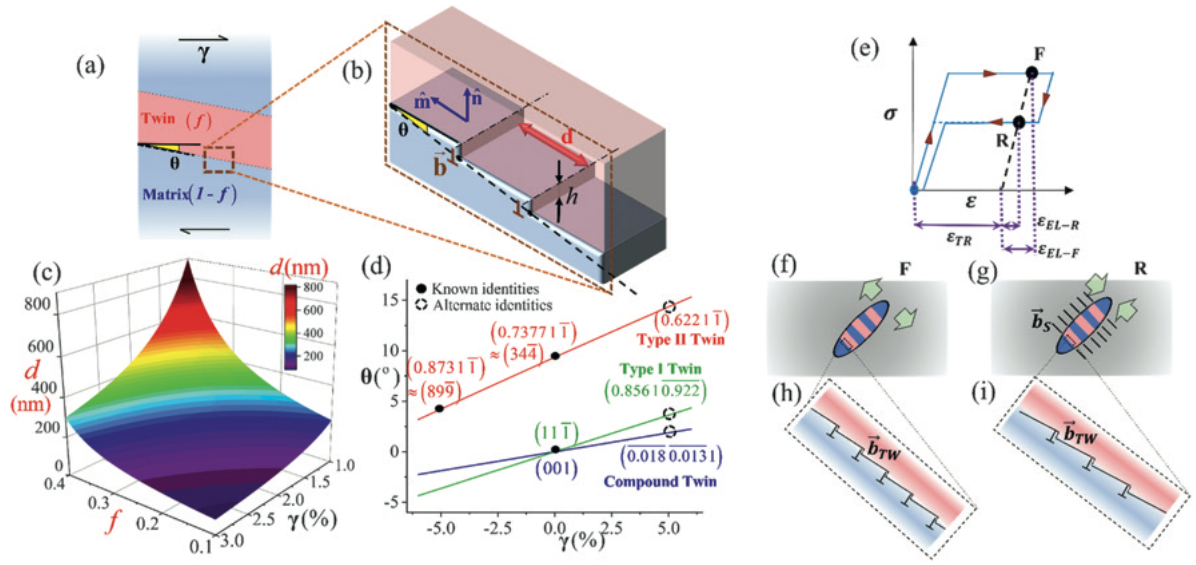

Fig. 20 Strain-sensitive twin interface evolution and relevance to slip-emission: (a) Schematic of the martensitic twinned structure where one twin variant has volume fraction f and is subject to a shear-strain γ (b) Terrace-disconnection topology of the twin interface illustrating the disconnection spacing d, the Burgers vector $\vec{b}$, step height h and angle of inclination from rational terrace θ (c) Prediction of strain-sensitive evolution of dislocation-spacing with variation of strain γ and volume-fraction f (d) Prediction of evolving θ for all twin-types in NiTi illustrating the varying Miller-index identities that the twin interfaces can exhibit, also explaining the two experimentally proposed identities of the Type II twin (e) Schematic illustration of a superelastic response of a Shape Memory Alloy, also showing the partitioning of the prevailing strain-state at any point based on the transformation-strain ε_{TR} and elastic-strain ε_{EL} (f) Nucleated martensitic inclusion within the austenitic phase growing outward, and the internal twinned morphology of the martensite (g) Receding martensitic inclusion and the internal twinned morphology along with emitted slip-lines, with Burgers vector $\vec{b}_S$ (h) martensitic twin interface under higher elastic-strain at F, given by ε_{EL-F}, consequently exhibiting higher twin-disconnection density, with Burgers vector $\vec{b}_{TW}$ (i) martensitic twin interface under lower elastic-strain at R, given by ε_{EL-R}, consequently exhibiting lower twin-disconnection density; the deficit in twin-disconnection density is used to explain the emitted slip based on the law of conservation of Burgers vectors in the system. Reproduced from Mohammed, A.S.K., Sehitoglu, H., 2020a. Martensitic twin boundary migration as a source of irreversible slip in shape memory alloys. Acta Materialia 186, 50–67. Mohammed, A.S.K., Sehitoglu, H., 2020b. Modeling the interface structure of type II twin boundary in B19′ NiTi from an atomistic and topological standpoint. Acta Materialia 183, 93–109. Available at: https://doi.org/10.1016/j.actamat.2019.10.048.

Despite such an early proposition of the mechanism, several aspects remained unaddressed. A clear understanding of the internal martensitic twin boundary is only currently emerging. The primary impediment which delayed this development was the complex low-symmetry crystal structure often exhibited by the martensite, distinguishing them from simpler twins in fcc and bcc materials. Furthermore, the internal twin boundaries of martensite often exhibit "irrational" Miller indices as observed in NiTi, CuZnAl, CuAlNi and other alloys (Morii *et al.*, 1991; Adachi *et al.*, 1986; Xie and Liu, 2004; Knowles, 1982; Okamoto *et al.*, 1986; Hara *et al.*, 1992; Nishida *et al.*, 1997; Liu and Dunne, 2003; Nishida *et al.*, 2008; Zou *et al.*, 2018). These irrational twins are

classified under "Type II" twin boundaries under the classical theory of deformation twinning (Bilby and Crocker). The topology of such irrational twin boundaries has been a recent topic of significant research interest particularly in the last few years (Mohammed and Sehitoglu, 2020b, 2021; Pond and Hirth, 2018; Pond *et al.*, 2019; Karki *et al.*, 2020; Hirth and Wang, 2021). The development of reliable interatomic potentials, as discussed previously in the chapter, and methods such as Topological Modeling (Pond *et al.*, 2007) in recent times has led to much needed advancements in understanding of the martensitic twin boundary.

Using atomistic and topological methods it was shown that the irrational plane of the twin boundary can be explained as a stepped topology over rational terrace planes with periodically spaced twinning dislocations or "disconnections" (Mohammed and Sehitoglu, 2020b, 2021). Thus, the involvement of twinning disconnections on the equilibrium topology of the twin boundary was established. The crystal structure on the rational terraces were clarified using atomistic simulations, establishing new concepts of lattice-motif shuffles in the detwinning mechanism and lattice-offset required for the equilibrium twin structure. This advancement opened avenues for more exploratory research along the lines of the K-K mechanism within atomistic frameworks. The mechanism of twin migration via motion of the twinning disconnection was simulated and an emissary dislocation-reaction upon interaction with a barrier was shown to occur, justifying the K-K proposition (Mohammed and Sehitoglu, 2020a).

Furthermore, the terrace-disconnection topological model of the type II twin was shown to be relevant to other twin modes in general. A new "Evolving Interface (EI)" theory was proposed showing that all twin topologies, irrespective of type and rationality, can evolve under the influence of local elastic lattice strains to exhibit varying arrangement of twin-disconnection densities (Mohammed and Sehitoglu, 2021). As shown in **Fig. 20**(a)-(d), the twin-disconnection spacing reduces (or equivalently disconnection density increases) with increasing elastic-strain and vice versa. Such behavior has direct implications on twin-dislocation activity during the martensitic transformation. For instance, consider a superelastic cycle under external stress as schematically represented in **Fig. 20**(e). Consider two analogous points during the forward and reverse transformation, F and R, where the total-transformation strain ε_{TR} is the same, correlated with the same underlying martensitic volume fraction (refer **Fig. 20**(f) and (g)). During the forward transformation at F, the magnitude of elastic-strain is higher and therefore enforces a higher twin-disconnection density (refer **Fig. 20**(h)). During the reverse-transformation at R, the magnitude of elastic-strain is reduced and therefore enforces a lower twin-disconnection density (refer **Fig. 20**(i)). Thus, between the two analogous points F and R, the only difference is a deficit in the twin-disconnection density on the internal martensitic twin boundary. Then from the law of conservation of Burgers vectors, it is plausible to expect that this deficit is emitted as austenitic slip at the transformation front, during the reverse transformation, as represented in **Fig. 20**(g). This mechanism revamps and provides a modern interpretation of Kajiwara's mechanism following decades of development in understanding of the internal martensitic twin boundary and their behavior under strain. And such an understanding will be instrumental in narrowing future research focus on aspects such as the sensitivity of twin-boundary topology to external strain and the mobility of the twin-disconnection on the twin-boundary as tailorable parameters, in search of fatigue-resistant shape memory alloys.

New SMAs – Fe Based SMAs, High Temperature SMAs, Ferromagnetic SMAs, High Entropy SMAs

Fe Based SMAs

The Fe-based shape memory alloys have many desirable attributes. The FeMnSi alloys (Sato and Mori, 1991; Sato *et al.*, 1984, 1982) which exhibit shape memory response are potentially very significant because of their lower cost compared to other SMAs and their transformation strains as high as 8%. The development of the most recent FeMnNiAl (Omori *et al.*, 2011; Vollmer *et al.*, 2019, 2016; Ojha and Sehitoglu, 2016c; Omori and Kainuma, 2017; Ozcan *et al.*, 2018, 2017; Vollmer *et al.*, 2017a,b, 2015) alloys also exhibit huge potential with strains approaching 10% and they undergo superelasticity over a broad temperature range. Another class of iron based SMAs are the FeNiCoTiAl/Ta/Nb (Abuzaid and Sehitoglu, 2018; Krooß *et al.*, 2014; Chumlyakov *et al.*, 2016; Ma *et al.*, 2013) which are rather brittle. The early FePt, FePd (Wayman, 1993; Sohmura *et al.*, 1980; Oshima and Sugiyama, 1982; Sugiyama *et al.*, 1984a,b) alloys are prohibitive in

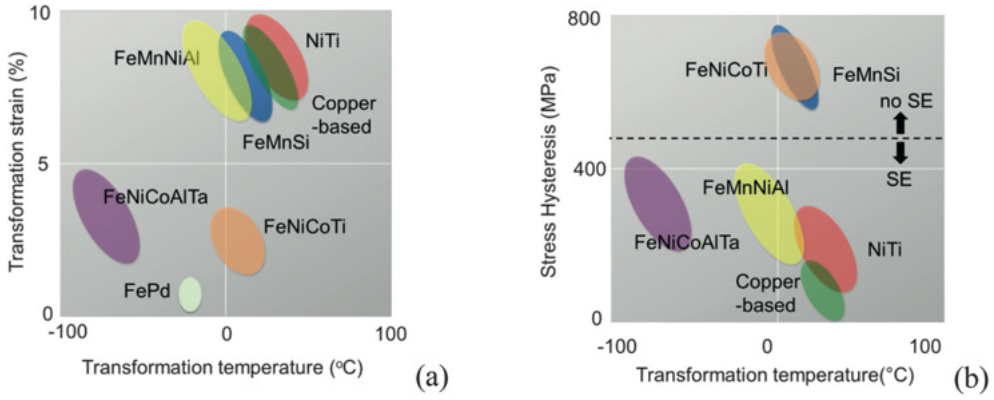

Fig. 21 The Fe based SMAs can exhibit (a) maximum transformation strains that can be achieved depending on the crystallographic texture, the horizontal axis shows the equilibrium temperature, and (b) stress hysteresis levels strongly depend on the chemical composition (see Table 10 for more details). Some of the alloy compositions such as FeMnSi and FeNiCoTi do not exhibit SE (superelasticity) but they show shape memory.

cost and exhibit transformation strains less than 3%. We summarize the iron based alloys in **Fig. 21**, and also in **Table 10**.

These FeMnNiAl alloys constitute a major advancement that is worthy of further studies (**Fig. 22**(a)–(b)). The results so far unequivocally showed that alloy FeMnNiAl exhibits superelasticity over a very wide temperature range, spanning from −100-−200°C (**Fig. 22**(a)). In **Fig. 22**(b) the stress-strain response is indicated and how the strain transfer from one grain to another is difficult (GB is indicated with a dashed line in **Fig. 22**(b)). Suitable crystallographic textures during processing will circumvent this issue. In **Fig. 22**(c), we illustrate the potentially high transformation strains in the case of FeMnNiAl with theoretical strains far exceeding 10%.

The onset of new variants is expected to impart additional superelasticity (**Fig. 22**(d)) when existing variants are exhausted. When the recoverable strain on a particular variant is exhausted, new variants are activated; this results in return of superelasticity. This phenomenon is illustrated after cycle 12780 in **Fig. 22**(d). The ramifications of such phenomenon are that activation of new variants produces transient deceleration of the fatigue crack growth rates and such a phenomenon imparts increased fatigue crack growth resistance (Sidharth *et al.*, 2020a).

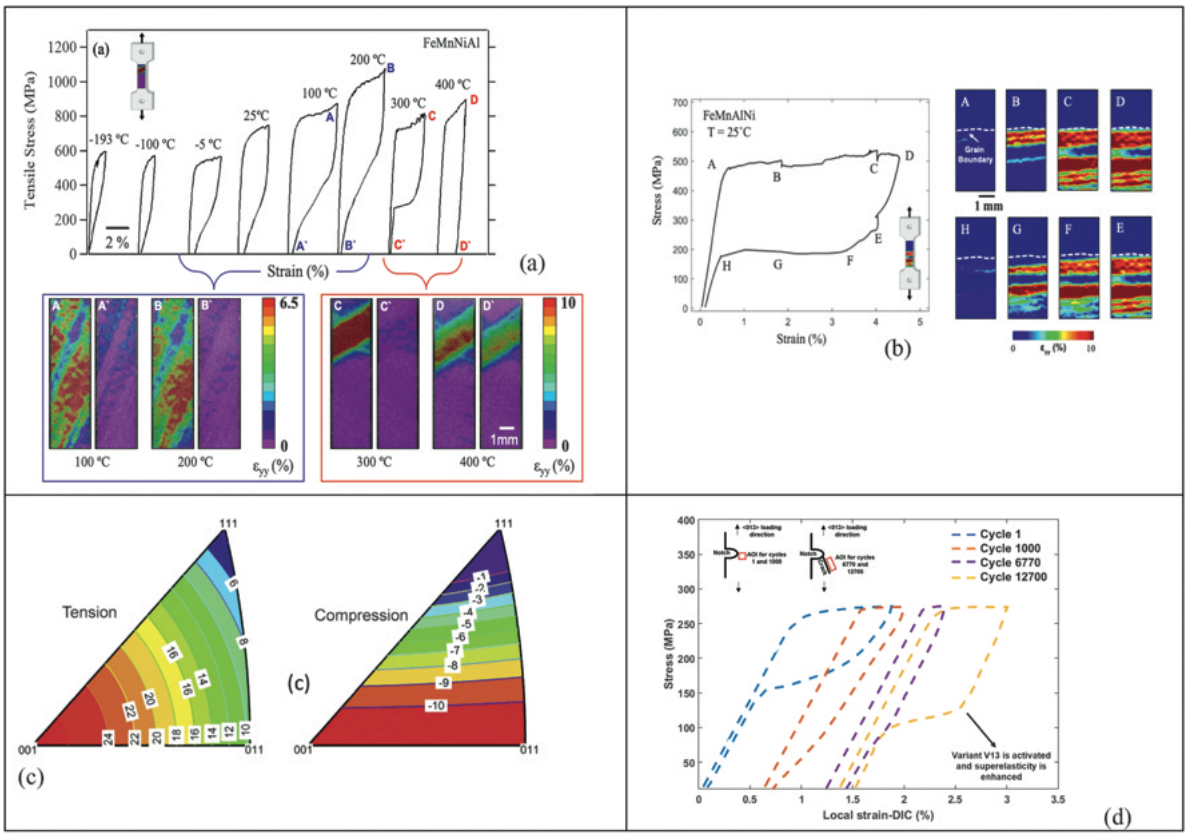

Fig. 22 The superelasticity observations over a wide temperature range in FeMnNAl, the local strains exceed 10%, (b) Stress-strain response where the transmission of transformation boundary (DIC images show the local strains) is inhibited at the grain boundary (the GB is shown as a dashed line), (c) theoretical transformation strains showing potentially very high strain levels in FeMnNiAl, (d) illustrates the return of superelasticity upon activation of a new variant (V13) in FeMnNiAl upon exhaustion of the primary variant and the subsequent return of superelasticity (after cycle 12,700). Such behavior is beneficial as it imparts FCG deceleration. Reproduced from (b) Abuzaid, W., *et al.*, 2019. FeMnNiAl iron-based shape memory alloy: Promises and challenges. Shape Memory and Superelasticity 5, 263–277, doi:10.1007/s40830-019-00230-9. (c) Ojha, A., Sehitoglu, H., 2016c. Transformation stress modeling in new FeMnAlNi shape memory alloy. International Journal of Plasticity 86, 93–111, doi:10.1016/j.ijplas.2016.08.003. (d) See reference Sidharth, R., Wu, Y., Brenne, F., Abuzaid, W., Sehitoglu, H., 2020a. Relationship between functional fatigue and structural fatigue of iron-based shape memory alloy FeMnNiAl. Shape Memory and Superelasticity 6, 256–272.

Table 10 A summary of iron based shape memory alloys and comments on major findings

Fe- based SMAs	*Austenite and martensite phases - Major Findings*
FeNiCoTi (Sehitoglu *et al.*, 2002, 2001c; Maki *et al.*, 1984; Jost, 1999; Koval *et al.*, 1979)	-bcc to bct (3 variants), 33%Ni,10%Co,4%Ti, Observations of Shape Memory Behavior with strains as high as 4%, high strength, [001] texture preferred, large hysteresis, low ductility in polycrystalline form
FeMnSi (Otsuka *et al.*, 1990; Jian and Wayman, 1992, 1994; Sato *et al.*, 1982)	-fcc to hcp, 30%Mn (12 variants), 5%Si. Observations of shape memory as high as 6%, moderate strength, large hysteresis, high ductility for poly and single crystals
FeMnNiAl/Ti (Omori *et al.*, 2011; Vollmer *et al.*, 2019, 2016; Ojha and Sehitoglu, 2016c; Omori and Kainuma, 2017; Ozcan *et al.*, 2018, 2017; Vollmer *et al.*, 2017a,b, 2015)	-bcc to fcc (3 variants), 34%Mn, 15%Al, 7.5%Ni. Observations of superelasticity with local strains near 10%, moderate to high strength, [001] texture preferred, small stress hysteresis, improved ductility for bamboo crystals
FeNiCoTiAl/Ta/Nb (Abuzaid and Sehitoglu, 2018; Krooß *et al.*, 2014; Chumlyakov *et al.*, 2016; Ma *et al.*, 2013)	-bcc to bct (3 variants), 30%Ni,15%Co,10%Al,2.5%Ti (Abuzaid and Sehitoglu, 2018) observations of superelasticity with local strains near 6%, high strength, small hysteresis, [001] texture preferred, poor ductility, brittle in polycrystalline form
FePt, FePd (Wayman, 1993; Sohmura *et al.*, 1980; Oshima and Sugiyama, 1982; Sugiyama *et al.*, 1984a, 1984b)	25%Pt- Ll_2 to ordered bct and 30%Pd-fcc to fct (3 variants, disordered), transformation strains less than 3%, small hysteresis, moderate ductility

High Entropy-Shape Memory Alloy Synergy

High entropy alloys are a new class of materials that defy the strength and ductility tradeoff well known in materials science and mechanics (Cantor *et al.,* 2004). Often they include multiple elements and result in the formation of a single phase solid solution with an fcc, hcp or bcc crystal structure. High entropy alloys have the characteristics to impart unusually high slip resistance (Gludovatz *et al.,* 2014; Cantor *et al.,* 2004; Abuzaid and Sehitoglu, 2017a; Tong *et al.,* 2005a), so developing high entropy shape memory alloys can potentially achieve properties not realized previously. A summary of the previous works on high entropy shape memory alloys are summarized in **Table 11**. We note that there are few works that have appeared despite the tremendous potential of these alloys. The first proposed composition was derived from the NiTi (Firstov *et al.,* 2015a,b,c). The compositions based on the NiTi composition has given very promising results with shape memory strain near 5% (Chen and Chen, 2019). Very preliminary work on compositions based on NiAl and CoNiAl have been reported (Gerstein *et al.,* 2018). As noted in **Table 11**, several of these compositions have the B2 austenite phase similar to NiTi and NiAl. The thermal hysteresis of 40°C is comparable to NiTi alloys. The shape memory strains of 5% are comparable to CoNiAl behavior and is excellent as long as functionality could be maintained with cycles. The degradation in functionality is the drawback of most SMAs and imparting HEA characteristics may address this concern.

The idea of high entropy alloys first started by building on the successful and well explored NiTi system. The NiTi based systems have essentially B2 type crystal structure, on the other hand the HEA B2 exhibits triclinic distortion (Firstov *et al.,* 2015a, b,c). The composition that is considered in **Fig. 23** is the $(TiZrHf)_{50}(CoNiCu)_{50}$ type. The M_s temperature and the volume of the phases can be adjusted with the Ni and Cu replacement of cobalt. The best shape memory attributes include : (1) small volume change, (2) small lattice invariant shear, (3) high flow (slip) resistance of the austenite and martensite phases and (4) low twin boundary energy in martensite to minimize irreversibilities. Whether the HEA-SMA performance is superior in the metrics above needs to be determined over time. The compositions, and the role of the Cu and Ni replacement of Co on the volume of austenite are shown in **Fig. 23**(a) and (b). The composition effect on volume/atom of austenite is significant. The lattice is considerably distorted and deviated from the B2 structure to a triclinic one (**Fig. 23**(c)). In **Fig. 23**(d) the experimental stresses

Table 11 Summary of selected works on high entropy shape memory alloys (HESMAs). The major results are included and the shape memory strains of >5% are impressive

Investigator	*Material*	*Crystal phases*	*Major results*	
		Austenite to martensite	*Thermal hysteresis (°C)*	*Shape memory or superelastic strains (%)*
Firstov *et al.* (Firstov *et al.*, 2015a,b,c)	$(TiZrHf)_{50}Co_{10}Ni_{20}Cu_{20}$	B2 to B19′	90	0.6–1.84
Wang/Hui (Wang *et al.*, 2019)	$Ti_{49}Zr_{20}Hf_{15}Al_{10}Nb_6$	BCC to B19	150	>3
Chen *et al.* (Chen and Chen, 2019)	$(TiZrHf)_{50}Ni_{25}Co_{10}Cu_{15}$	B2 to B19′	40	>5
Maier *et al.* (Gerstein *et al.*, 2018)	$(CoNiCu)_{67}(AlGaIn)_{33}$	B2 to $L1_0$	15	Not Reported

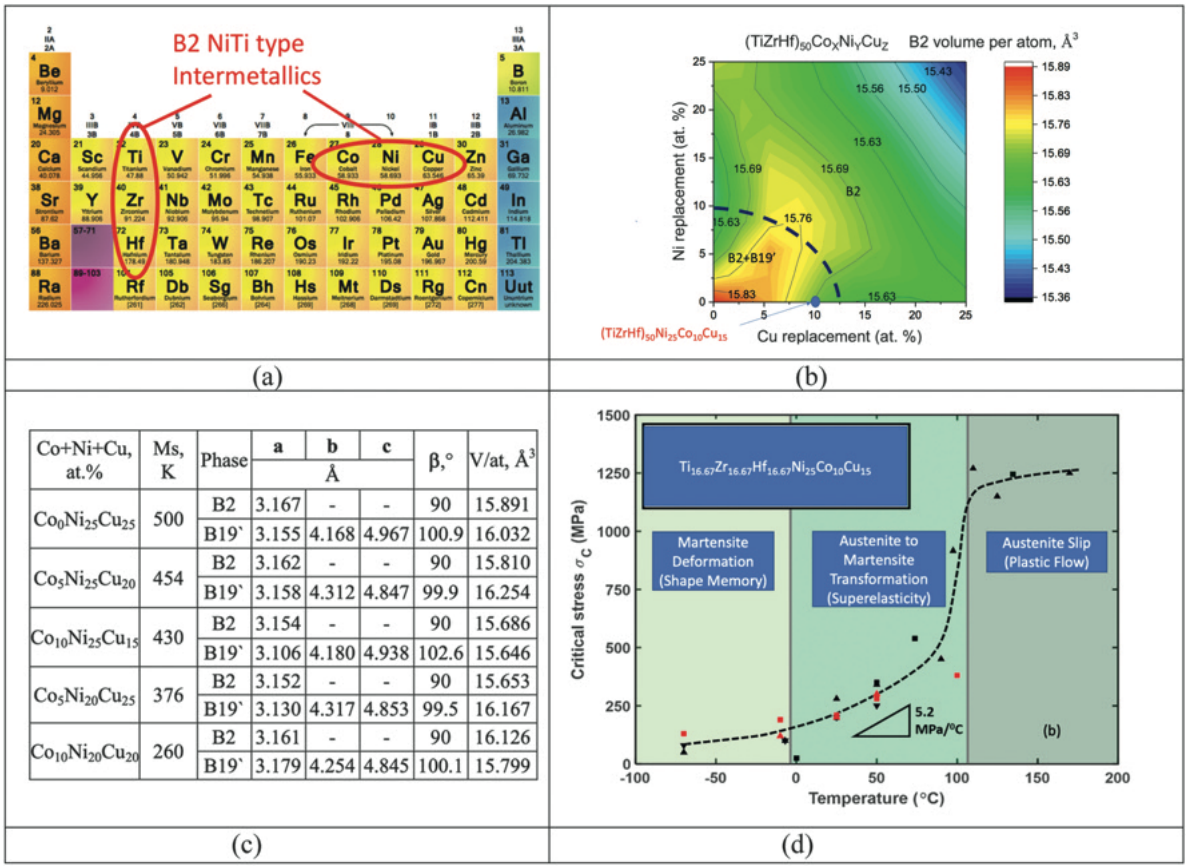

Co+Ni+Cu, at.%	Ms, K	Phase	a	b	c	β,°	V/at, Å^3
			Å				
$Co_0Ni_{25}Cu_{25}$	500	B2	3.167	-	-	90	15.891
		B19`	3.155	4.168	4.967	100.9	16.032
$Co_5Ni_{25}Cu_{20}$	454	B2	3.162	-	-	90	15.810
		B19`	3.158	4.312	4.847	99.9	16.254
$Co_{10}Ni_{25}Cu_{15}$	430	B2	3.154	-	-	90	15.686
		B19`	3.106	4.180	4.938	102.6	15.646
$Co_5Ni_{20}Cu_{25}$	376	B2	3.152	-	-	90	15.653
		B19`	3.130	4.317	4.853	99.5	16.167
$Co_{10}Ni_{20}Cu_{20}$	260	B2	3.161	-	-	90	16.126
		B19`	3.179	4.254	4.845	100.1	15.799

Fig. 23 (a) Periodic table with pseudo NiTi HEASMA alloy compositions, (b) the volume of the B2 volume per atom for the CoNiCu elements of the $(TiZrHf)_{50}(CoNiCu)_{50}$ system, minimizing the volume difference between B2 and B19′ is an important consideration, the $(TiZrHf)_{50}Ni_{25}Co_{10}Cu_{15}$ is marked on the volume map with a blue dot, (c) a table showing the summary of Co + Ni + Cu compositions for M_s for $(TiZrHf)_{50}(CoNiCu)_{50}$ and the lattice constants, note the finite monoclinic angle as high as 102.6°, (d) the transformation stress as a function of temperature. Reproduced from (a) Firstov, G., Van Humbeeck, J., Koval, Y.N., 2004b. Comparison of high temperature shape memory behaviour for ZrCu-based, Ti–Ni–Zr and Ti–Ni–Hf alloys. Scripta Materialia 50, 243–248. (a)–(c) Firstov, G., *et al.*, 2015c. Electronic and crystal structure of the high entropy TiZrHfCoNiCu intermetallics undergoing martensitic transformation. MATEC Web of Conferences 33, 06006. Yaacoub, J., Abuzaid, W., Brenne, F., Sehitoglu, H., 2020. Superelasticity of (TiZrHf) 50Ni25Co10Cu15 high entropy shape memory alloy. Scripta Materialia 186, 43–47.

for $Ti_{16.67}Zr_{16.67}Hf_{16.67}Ni_{25}Co_{10}Cu_{15}$ are shown for martensite deformation (twinning), austenite to martensite transformation, and austenite slip (plastic flow) respectively. The slip resistance is very high, consistent with fcc and bcc HEA alloys.

There are several important remarks on this structure:

(1) The crystal structure is heavily distorted and deviates from B2 to a P1 triclinic one.
(2) Interatomic distances among Co, Ni and Ti, Zr, Hf deviate from ideal levels, while the bond lengths between Cu and Ti, Zr and Hf are near ideal levels.
(3) The volume change difference is a strong function of Co substitution by Ni and Cu. The volume change is smallest for the $Co_{10}Ni_{25}Cu_{15}$ case. This small volume change being slightly negative is similar to NiTi.
(4) The multi-element HEA possesses high lattice friction stress and should reduce the degradation observed in shape memory alloys. This has not been studied experimentally or with theory yet.

Another class of high entropy alloys are emerging based on the NiAl structure (**Fig. 24**). First observations of shape memory characteristics in Ni-Al dates back to 1970s (Au and Wayman, 1972; Enami *et al.*, 1973). A major drawback has been the extreme brittleness and the formation of Ni_5Al_3 phase that does not transform (Yang and Wayman, 1994). The addition of Co to NiAl has been introduced that significantly advanced the shape memory and superelasticity characteristics (Hamilton *et al.*, 2006b, 2005; Oikawa *et al.*, 2001). This was followed by CoNiGa with excellent high temperature properties. The CoNiAl and CoNiGa share similar characteristics. To achieve HESMAs, for each binary element equiatomic distribution of elements have been adopted- the CoNiCu for Ni67 and AlGaIn for Al33. The lattice distortions in this case are expected to be significant and indeed a yield stress near 1400 MPa was achieved. Such a high strength could be very beneficial in addressing the limitations in the functionality of CoNiAl systems.

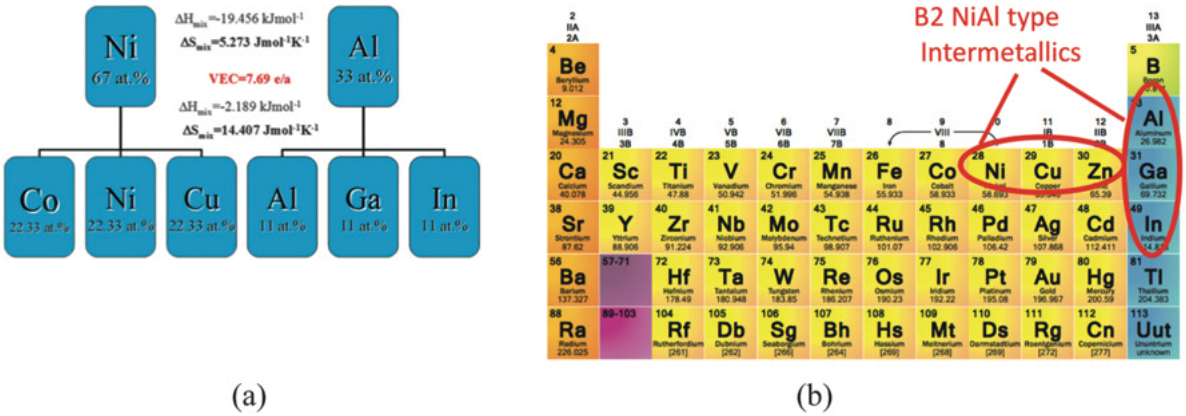

Fig. 24 The development of high entropy alloys based on the intermetallic NiAl, CoNiAl systems, (a) the $(CoNiCu)_{67}(AlGaIn)_{33}$ (Gerstein *et al.*, 2018), (b) the periodic table with illustration of the compositional design of NiAl type intermetallics. Reproduced from Gerstein G., Firstov G.S., Kosorukova T.A., Koval Y.N., Maier H.J., 2018. Development of B2 shape memory intermetallics beyond NiAl, CoNiAl and CoNiGa Shape Memory and Superelasticity 360–368.

Preliminary HEASMA compositions are illustrated in **Fig. 24**(a) and (b) showing the mixing entropies and the elements. The composition that has been explored are given in Ref (Kainuma *et al.*, 1996). Preliminary DSC results have been established achieving high temperature SMA characteristics with the $(CoNiCu)_{67}(AlGaIn)_{33}$.

High Temperature Shape Memory Alloys

Despite the commercial dominance of NiTi in biomedical industry, it is only applicable for low to intermediate stress and low-temperature applications (<100°C). This limitation excludes its utilization in most of aerospace applications. The NiTi's irrecoverability under cycling due to lack of slip resistance and small range of transformation temperatures (TTs) limits its potential use in aerospace applications. Shape memory materials with higher strength and higher TTs, especially above 100°C, are needed for compact actuators for flow and controls, actuation tubes for rotors, moving or morphing surfaces as well as inlet/exhaust configurations (Schetky, 1991; Webster, 2006; Benafan and Gaydosh, 2017) in aeronautics.

Recently, there has been significant emphasis on high temperature shape memory alloys with potential applications. These materials are either the NiTi with ternary additions such as NiTiHf (Dalle *et al.*, 2002; Potapov *et al.*, 1997; Bigelow *et al.*, 2011; Dalle *et al.*, 2003; Karaca *et al.*, 2011; Kockar *et al.*, 2006; López *et al.*, 1996; Liu *et al.*, 2002; Pozzi and Airoldi, 1999; Rao *et al.*, 2010; Sanjabi *et al.*, 2005; Tong *et al.*, 2009, 2008, 2005b; Zarinejad *et al.*, 2009, 2008), NiTiPd (Kumar *et al.* 2011; Monroe *et al.*, 2011; Atli *et al.*, 2011; Bozzolo *et al.*, 2005; Kockar *et al.*, 2010; Kumar and Lagoudas, 2010; Yang and Mikkola, 1993), NiTiPt (Lin *et al.*, 2009; Kovarik *et al.*, 2010; O'Donoghue *et al.*, 2010) or Ni_2FeGa (Hamilton *et al.*, 2006a, 2007a; Biswas and Krishnan, 2010; Dilibal *et al.*, 2011a; Efstathiou *et al.*, 2007, 2010; Morito *et al.*, 2005; Yu *et al.*, 2009a,b; Zhu and Dui, 2010), Co_2NiGa (Arróyave *et al.*, 2010; Craciunescu *et al.*, 2002; Dadda *et al.*, 2006; Dogan *et al.*, 2011; Fu *et al.*, 2009; Kishi *et al.*, 2003, 2008; Liu *et al.*, 2006a,b, 2005a; Monroe *et al.*, 2010) or CoNiAl (Hamilton *et al.*, 2006b; Karaca *et al.*, 2004, 2003; Meyer *et al.*, 2006; Dilibal *et al.*, 2011a; Bartova *et al.*, 2008; Dilibal *et al.*, 2011b; Liu *et al.*, 2005b, 2008; Rajini Kanth *et al.*, 2010; Wang *et al.*, 2005; Xu *et al.*, 2006) or Ti based shape memory alloys (Buenconsejo *et al.*, 2009; Niendorf *et al.*, 2015) (**Fig. 25**(a)). Their widespread utilization is limited primarily due to the lack of understanding of their shape memory response. The NiTiHf alloys have emerged as a promising shape memory alloy system. In 2010, there was a major review article in International Materials Reviews that summarized the state of the art (Ma *et al.*, 2010). Since then, many papers have appeared with compositions as high as 25%Hf and strength levels exceeding 1.5 GPa (Patriarca *et al.*, 2016a; Patriarca and Sehitoglu, 2015; Patriarca *et al.*, 2016b; Wang and Sehitoglu, 2014c; Wu *et al.*, 2016; Santamarta *et al.*, 2013; Evirgen *et al.*, 2015; Benafan *et al.*, 2014b). The fundamental and critical properties in shape memory alloys are the following (**Fig. 25**(b)-(d)): (1) transformation stress, (2) twinning stress, (3) slip stress, and (4) stress and/or thermal hysteresis. Theoretical models for slip stress of austenite have been studied recently with some promising results (Alkan and Sehitoglu, 2017a, 2019b), while the determination of transformation stress is far more complicated (Alkan *et al.*, 2018a) and is also the subject of current theoretical studies. The potential advantage of NiTiHf alloys is that the addition of Hf raises the slip strength considerably. These alloys enable potential aerospace actuators that can be part of the structure (Benafan and Gaydosh, 2017; Calkins *et al.*, 2008).

SMAs functionalities are sensitive to variation in composition as well as microstructural morphology (Elahinia *et al.*, 2012) depending on the processing route. Ternary or quarterly elemental addition to binary NiTi, has been used to achieve raised TTs

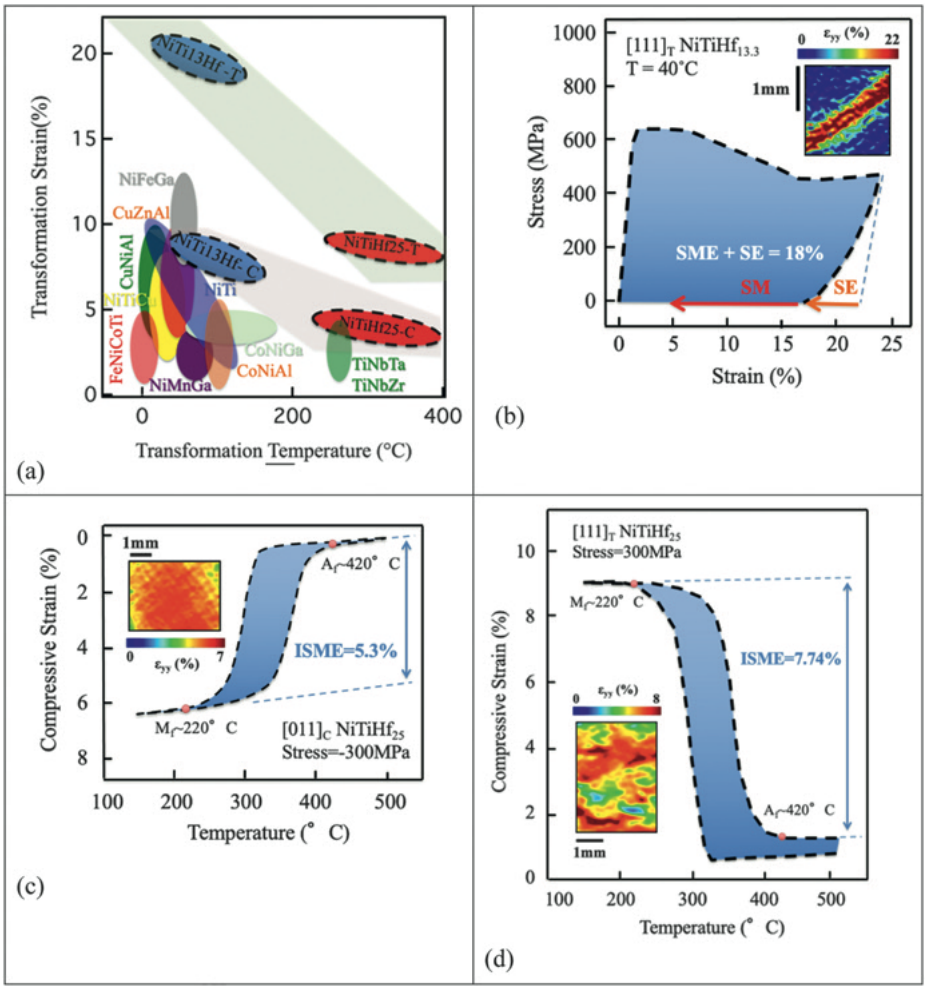

Fig. 25 From reference (Sehitoglu, H., Patriarca, L., Wu, Y., 2017a. Shape memory strains and temperatures in the extreme. Current Opinion in Solid State and Materials Science 21, 113–120), (a) High temperature capability of NiTiHf alloys (with 13% and 25%Hf), (b) Shape memory response of NiTi with 13%Hf, note that the recoverable strains exceed 15%, (c) illustration of high temperature capabilities of $NiTiHf_{25}$ showing A_f temperature of 420°C, transformation strains exceed 5%, (d) Isobaric shape memory (ISME) response under tension of $NiTiHf_{25}$. The strains exceed 7.7%. Reproduced from (a) Sehitoglu, H., Patriarca, L., Wu, Y., 2017a. Shape memory strains and temperatures in the extreme. Current Opinion in Solid State and Materials Science 21, 113–120.

based on the type of element and concentration. These higher temperature and strength ordered intermetallic compounds are achieved via partial or complete substitution of Ni or Ti by a third element such as Hf, Zr, Pt, Pd, and Au (Ma *et al.*, 2010; Ojha and Sehitoglu, 2016a,b; Sehitoglu *et al.*, 2017b,c) . A discussion is provided in **Table 12**.

Ideally, higher transformation temperatures (near 400°C) could open significant applications in various industries. In **Fig. 25** the results on NiTiHf alloys martensite start temperatures and actuation strains for common (Sehitoglu *et al.*, 2017a) 13Hf and 25Hf alloys are given. But, there are myriad of compositions to explore in the future.

Table 12 The primary NiTiHf alloys systems with a summary of main features and performance of each alloy

(Ti + Hf) rich NiTiHf (Firstov *et al.*, 2004b; Kockar *et al.*, 2006; Meng *et al.*, 2002)	-cubic B2 to monoclinic B19′ , Peak martensite temperature as high as 300°C, large thermal hysteresis of transformation, poor thermal and dimensional stability, lack of a superelastic response
$Ni_{50.3}Ti_{34.7}Hf_{15}$ (Canadinc *et al.*, 2017; Olier *et al.*, 1995; Moshref-Javadi *et al.*, 2013; Evirgen *et al.*, 2015)	-cubic B2 to monoclinic B19′, transformation temperatures decreased below room temperature when the precipitate size, and thus the interparticle distance, was below ∼20 nm, excellent dimensional stability under stress levels as high as 300 MPa, maximum fully recoverable strain of 4.5% after aging, Peak martensite temperature as high as 175°C, Thermal hysteresis in the range of 35–75°C
$Ni_{50.3/50.6}Ti_{29.7/29}.4Hf_{20}$ (Karaca *et al.*, 2013a; Coughlin *et al.*, 2012; Bigelow *et al.*, 2011; Benafan *et al.*, 2014b, 2012; Karaca *et al.*, 2011)	-cubic B2 to monoclinic B19′, Actuation strains up to 5%, excellent dimensional and cyclic stability at high stress levels without training, perfect superelastic behavior (at 210°C by Coughlin *et al.* (2012), at 220°C by Bigelow *et al.* (2011), and at 240°C by Benafan *et al.* (2014b) and Karaca *et al.* (2013a)), Thermal hysteresis in the range of 30–60°C, Work output up to 30 J/cm^3, Peak martensite temperature as high as 230°C, Martensite phase is resistant to plastic deformation at stresses greater than 1 GPa.
$Ni_{50.3}Ti_{25}Hf_{24.7}$ (Abuzaid and Sehitoglu, 2017b; Patriarca *et al.*, 2016b)	-cubic B2 to orthorhombic B19, local transformation strains in tension up to 7.74% and 5.3% in compression alongside the austenite finish temperature of 422°C, thermal hysteresis in the range of 50–65°C
$Ni_{50.6}Ti_{24.4}Hf_{25.0}$ (Patriarca and Sehitoglu, 2015)	-cubic B2 to orthorhombic B19, Peak martensite temperature as high as 288°C, Local actuation strains up to 3.25%, thermal hysteresis of 29–60°C Near perfect superelastic behavior at (255–300)°C range, Peak martensite temperature of 224°C
$Ni_{51.2}Ti_{23.4}Hf_{25.4}$ (Patriarca *et al.*, 2016a)	-cubic B2 to orthorhombic B19, high TTs (>250°C) along with high strength (>1000 MPa), Local actuation strains up to 4.04%, thermal hysteresis of 55–72°C,
NiTiHf(Pd/Nb) (Karaca *et al.*, 2012, 2013b; Kim *et al.*, 2011; Acar *et al.*, 2015)	-cubic B2 to monoclinic B19′, perfect superelastic loop with 4.2% actuation strain, ultrahigh yield strength of more than 2500 MPa, Peak martensite temperature up to 180°C, high work outputs and damping capacities reaching up to 30–35 J/cm^3

Ti Based SMAs

The original developments in this field were through the development of Ti-Nb based SMAs with the impetus to remove Ni-related toxicity in medical applications (Kim *et al.*, 2006a; Biesiekierski *et al.*, 2012; Geetha *et al.*, 2009; Prokoshkin *et al.*, 2016). Several experiments (Kim *et al.*, 2015, 2006b, 2005; Miyazaki *et al.*, 2006), and recent theoretical calculations (Ojha and Sehitoglu, 2015) have shown that upon alloying Ti-alloys with Nb, Ta, and Zr, high transformation strains (11%) can be achieved. Further advancements focused on alloying with Zr, Ta, Al (Bönisch, 2013; Kim *et al.*, 2004) to modify stress hysteresis, slip resistance and transformation strains (Takahashi *et al.*, 2002; Fukui *et al.*, 2004; Al-Zain *et al.*, 2010; Tahara *et al.*, 2009; Kim *et al.*, 2015). We note that alloys with Nb less than 7.2% have an hcp structure (Ahmed and Rack, 1996; Moffat and Kattner, 1988) while higher Nb contents develop a bcc structure. The transformation is from cubic to orthorhombic crystal structure. We also note that the use of NiTi is limited to less than 100°C (Sehitoglu *et al.*, 2000). In fact, the transformation temperatures in SMAs with good functional properties are typically less than 150°C for most cases (**Fig. 26**(a)). At elevated temperatures, the activation of slip impedes the reversibility of transformation (Ma *et al.*, 2010). On the other hand, the TiNb, TiPd, TiAu, TiPdX, TiAuX (X = Nb,Ta) alloys can permit high transformation temperatures (see **Fig. 26**(a)), but their twin/slip stresses with respect to transformation stress is available only in limited studies (Ojha and Sehitoglu, 2016a,b) (**Fig. 26**(b)–(c)). In fact, **Fig. 26** (c) shows why these alloys are successful, because the twin/slip stresses exceed the transformation stress. The complex variation with increasing Zr is illustrated in **Fig. 26**(d).

Although the Ni2FeGa and CoNiGa (Al) alloys can exhibit superelasticity at temperatures above 75°C (Hamilton *et al.*, 2007a, 2006b), their austenite finish temperature is less than 50°C. Therefore, they cannot be used as an actuator at high temperatures. The CuZnAl, CuNiAl, and FeNiCoTi alloys are limited to temperatures less than 100°C. Previous work explored the transformation temperatures of less than 250°C with Hf contents in the range 15%–20% (Evirgen *et al.*, 2015; Karaca *et al.*, 2011; Stebner *et al.*, 2014). Most recently, the use of 25%Hf NiTi25Hf (Patriarca and Sehitoglu, 2015) resulted in higher transformation temperatures (near 400°C, see **Fig. 26**(a)). On the other hand, the recent introduction of Nb, Ta, and Zr ternary elements in TiTa and TiNb (Kim *et al.*, 2015; Buenconsejo *et al.*, 2009; Miyazaki *et al.*, 2006) alloys have opened new possibilities. The Ti alloys can reach high transformation temperatures exceeding 450°C but these alloys with potential combinations with Pd,Au,Ta,Nb needs further study.

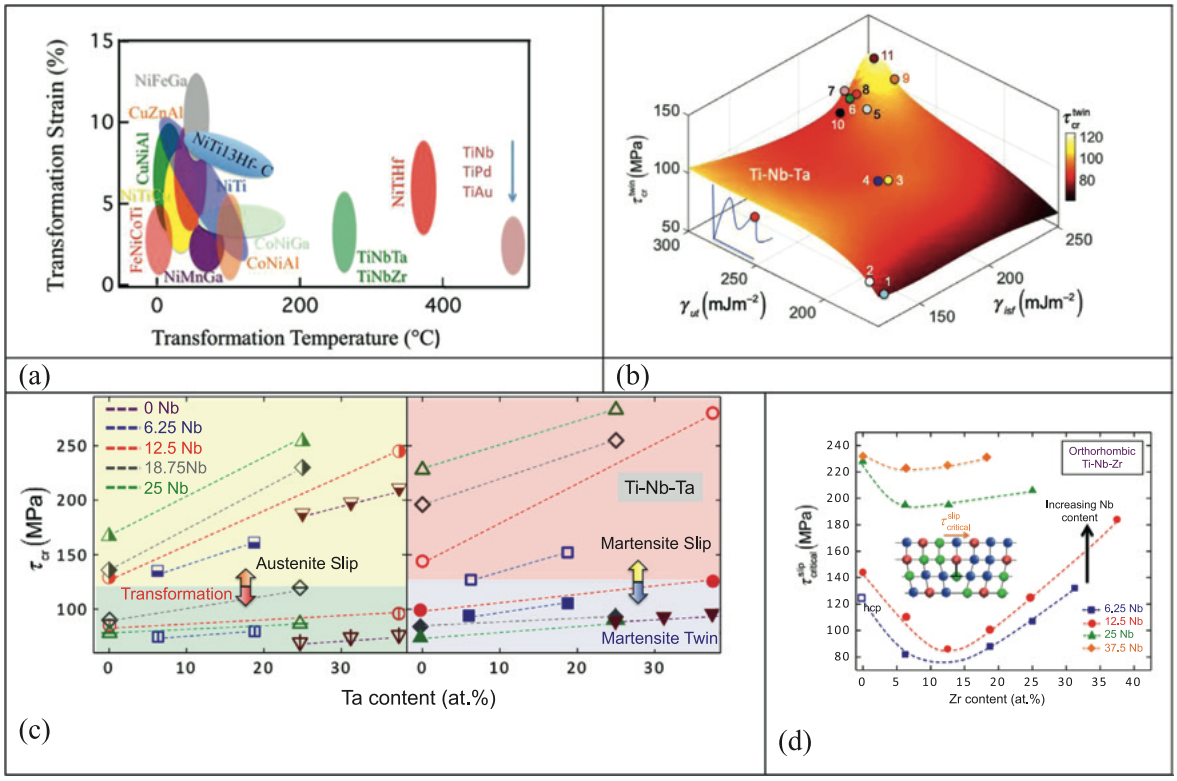

Fig. 26 (a) Transformation temperatures of SMAs in comparison with Ti based alloys, (b) Critical stress levels of Ti based SMAs as a function of composition, 1: Ti-25Nb, 2: Ti-18.75Nb, 3: Ti-6.25Nb-6.25Ta, 4:Ti-25Nb-25Ta 5: Ti-12.5Nb, 6: Ti-31.25Ta, 7: Ti-37.5Ta, 8: Ti-18.75Nb-25Ta, 9: Ti-6.25Nb-18.75Ta, 10: Ti-25Ta, 11: Ti-12.5Nb-37.5Ta, (c) Critical stresses as a function of composition, (d) the nonlinear dependence of critical stresses as a function of chemical composition. Reproduced from (b) and (c) Ojha, A., Sehitoglu, H., 2016a. Critical stresses for twinning, slip, and transformation in Ti-based shape memory alloys. Shape Memory and Superelasticity 2, 180–195. (d) Ojha, A., Sehitoglu, H., 2015. Slip resistance of Ti based high temperature shape memory alloys. Shape Memory and Superelasticity. Ahead of print.

Elasto-Caloric Behavior

Solid state refrigeration technology has been significant in reducing the dependence on vapor compression with harmful refrigerants (such as the common hydrofluorocarbon (HFC) HFC-134a). The solid state refrigeration utilizes the well-known magnetocaloric effect (MCE) (Mañosa and Planes, 2017; Moya *et al.*, 2014). Elastocaloric cooling with shape memory alloys (SMA) is an alternative solid state refrigeration solution without the necessity of a large magnetic field (Qian *et al.*, 2016; Kirsch *et al.*, 2018). Recent works focused on elasto-caloric effect have been published (Schmidt *et al.*, 2015; Bonnot *et al.*, 2008; Manosa *et al.*, 2013, 1993, 2009; Pataky *et al.*, 2015; Ossmer *et al.*, 2015). Cu-Zn-Al has shown a temperature change of 6°C and the NiTi wires (Cui *et al.*, 2012) and thin films (Ossmer *et al.*, 2014; Bechtold *et al.*, 2012) displayed higher temperature changes reaching 20°C. An ideal SMA refrigerant (one that produces the largest ΔT) for elastocaloric cooling would maximize the entropy change: $\Delta S(T) = S_A(T) - S_M(T)$, where $S_A(T)$ is the entropy of the austenite phase and $S_M(T)$ is the entropy of the martensite phase at temperature T. The ΔT results from the inverse relationship between ΔS and the specific heat, C_p, so SMAs that have the largest ΔS with the smallest C_p are the best candidates for EC cooling. Previous work on SMAs are summarized in **Fig. 27**(a) for $Ni_{50.8}Ti_{49.2}$ (at%) single crystals (Pataky *et al.*, 2015), $Ni_{50}Ti_{50}$ (at%) wire (Cui *et al.*, 2012), $Ni_{50}Ti_{50}$ (at%) thin film (Ossmer *et al.*, 2014), $Ni_{32.5}Ti_{59.4}Cu_{12.6}$ (at%) thin film (Bechtold *et al.*, 2012), NiTiCuCo (Ossmer *et al.*, 2015), and NiTiCuV (Schmidt *et al.*, 2015), CuZnAl (Bonnot *et al.*, 2008; Manosa *et al.*, 2013; Vives, 2011), Ni_2FeGa (Pataky *et al.*, 2015), Ni2FeGaCo (Xiao *et al.*, 2015), CoNiAl (Pataky *et al.*, 2015), FePd (Xiao *et al.*, 2013), NiMnInCo (Lu *et al.*, 2014), NiMnIn (Huang *et al.*, 2015), and NiMnSn (Sun *et al.*, 2016). The quantity ΔT_{th} is related to ΔS by the relationship $\Delta T_{th} = -\frac{T\Delta S}{C_p}$, where T is the deformation temperature and C_p is the heat capacity (Mañosa and Planes, 2017; Moya *et al.*, 2014). Elastocaloric (EC) effect refers to the temperature decrease in shape memory alloys (SMAs) during reverse transformation from martensite to austenite (**Fig. 27**(b)).

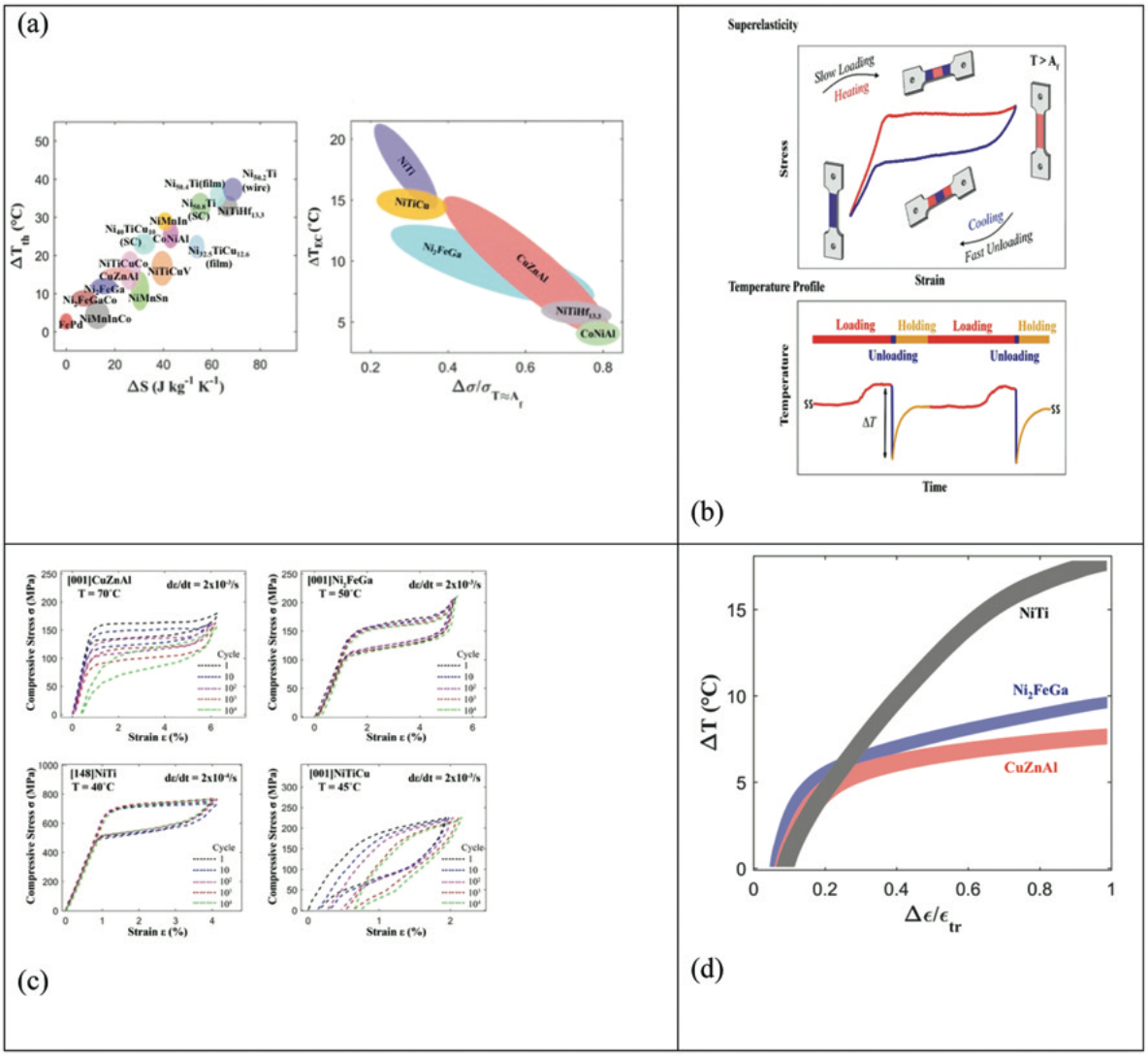

Fig. 27 (a) The linear correlation between theoretical change in temperature and the entropy change, (b) stress-strain and temperature profile that illustrates the EC effect, (c) Cyclic stress-strain curves for SMAs that have been tested to study the EC effect, (d) the increase in temperature due to EC effect as a function of applied strain showing that the effect is maximized when applied strain is near maximum transformation strain, (e) A 3D plot showing the dependence of the temperature change as a function of applied strain, entropy change and maximum applied stress. Reproduced from (a) and (d) Sehitoglu, H., Wu, Y., Ertekin, E., 2018. Elastocaloric effects in the extreme. Scripta Materialia 148, 122–126. (b) and (e) Wu, Y., Ertekin, E., Sehitoglu, H., 2017. Elastocaloric cooling capacity of shape memory alloys – Role of deformation temperatures, mechanical cycling, stress hysteresis and inhomogeneity of transformation. Acta Materialia 135, 158–176.

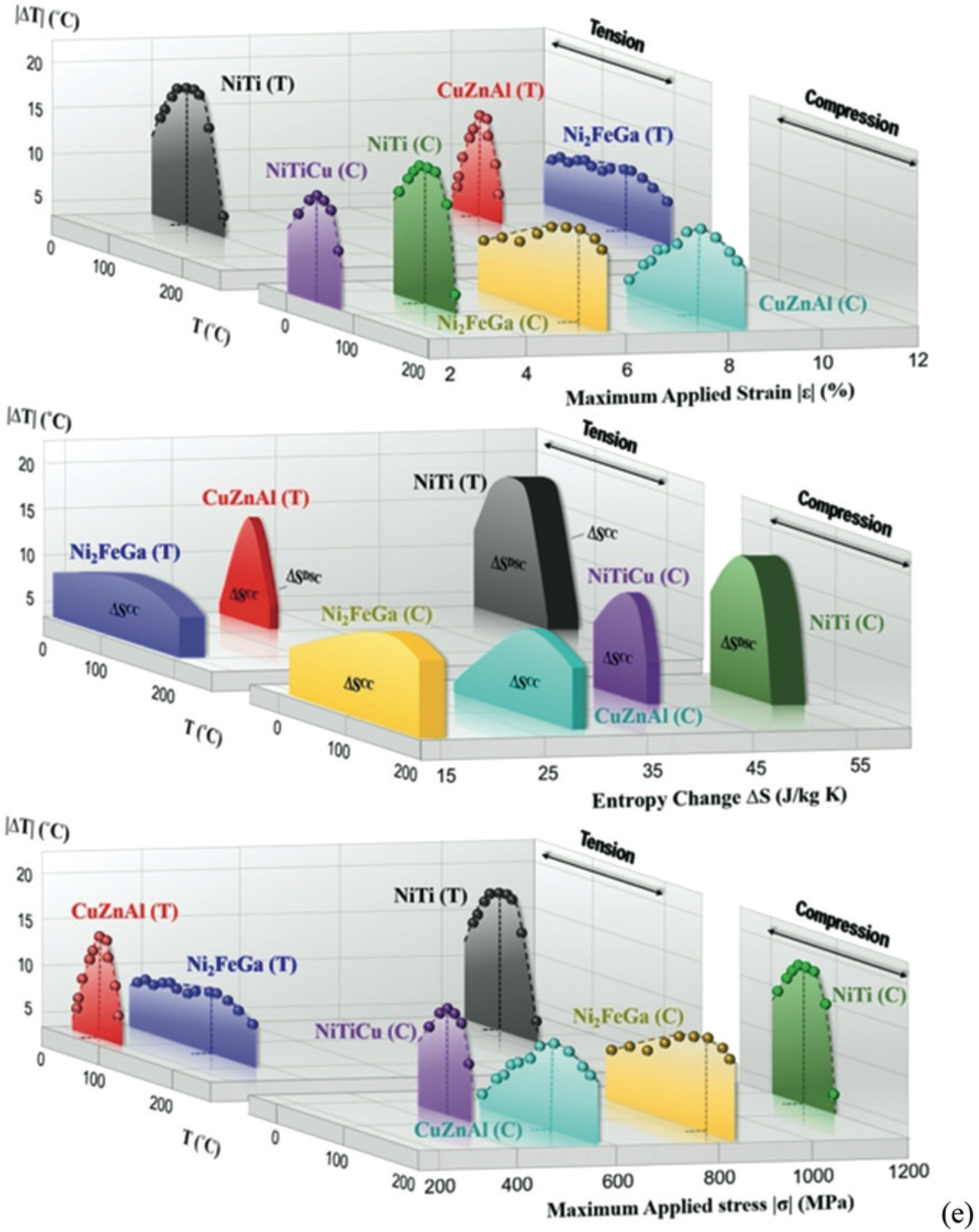

Fig. 27 Continued.

The EC effect occurs under phase transformation due to an entropy change under adiabatic conditions. It is important to know if the EC effect is stable under multi-cycles (Manosa *et al.*, 2013) and the range of deformation temperatures over which the effect is active. Several experiments were conducted to study this effect because as noted in **Fig. 27**(c) the measured temperature change is a function of the normalized cycling strain with the largest temperature changes corresponding to application of high strain near the transformation strain (**Fig. 27**(d)). If the rate of unloading is fast, the cooling is nearly adiabatic which produces a temperature drop of nearly 25°C in NiTi. Such a temperature change can open potentially new applications and avoid the expensive rare earth materials which are inherently brittle. The results show that under long-term cyclic deformation the response of NiTi and Ni_2FeGa are stable under loading and unloading but the failure under fatigue conditions remain a concern. In the case of NiTi-based SMAs, many papers have been published regarding the fatigue lives of NiTi (Pelton *et al.*, 2008; Miyazaki *et al.*, 1999; Pelton, 2011; Eggeler *et al.*, 2004; Melton and Mercier, 1979c; Nakahara *et al.*, 2000; Figueiredo *et al.*, 2009) and polycrystalline NiTiCu (Miyazaki *et al.*, 1999). For practical usage EC operation must exceed millions of cycles and longer fatigue lives are obtained for smaller $\Delta\varepsilon/\varepsilon_{tr}$ (**Fig. 27**(d)). A 3D plot showing the dependence of the temperature change as a function of applied strain, entropy change and maximum applied stress is given in **Fig. 27**(e).

Ferromagnetic Shape Memory Behavior

The magnetically induced shape changes occur primarily in the martensitic regime in nickel manganese gallium and iron palladium alloys (Chen *et al.*, 2014a; Heczko *et al.*, 2000; Kainuma, 2006; Manosa *et al.*, 1993; Müllner *et al.*, 2003; Müllner and Kostorz, 2008; Murray *et al.*, 2000; O'Handley, 2000; O'Handley *et al.*, 2000; Sozinov *et al.*, 2002; Straka *et al.*, 2004; Sun *et al.*, 2016; Tickle, 2000; Ullakko *et al.*, 1996; Webster *et al.*, 1984; Yu, 2009b; Zayak *et al.*, 2003; Karaman and Lagoudas, 2006; Sozinov *et al.*, 2001). The martensite domains have internal twin variants to minimize the energy of the system. The orientation of the variants with respect to the crystallographic axis is known. If the sample is cooled under an applied stress a single variant of martensite will form. The ferromagnetic shape memory alloys undergo the largest shape change when the rearrangement of a single martensitic variant occurs under an applied magnetic field. It is the rearrangement of the martensite at relatively low fields that has attracted considerable scientific attention. The levels of strain in magnetic shape memory alloys are much higher than the small strains of the order of 0.1% encountered in magnetostrictive and piezoelectric materials.

The twin boundary motion is the key and is dependent on the different magnetic anisotropy (the difference in area between the M-H curves for easy and hard axis), which undergoes alignments under the applied magnetic field. The $L1_o$ is the martensitic ground state (Ayuela *et al.*, 2002; Zayak *et al.*, 2003), The process can proceed at low stresses via disconnection-assisted migration (Müllner and Kostorz, 2008; Pond and Celotto, 2003).

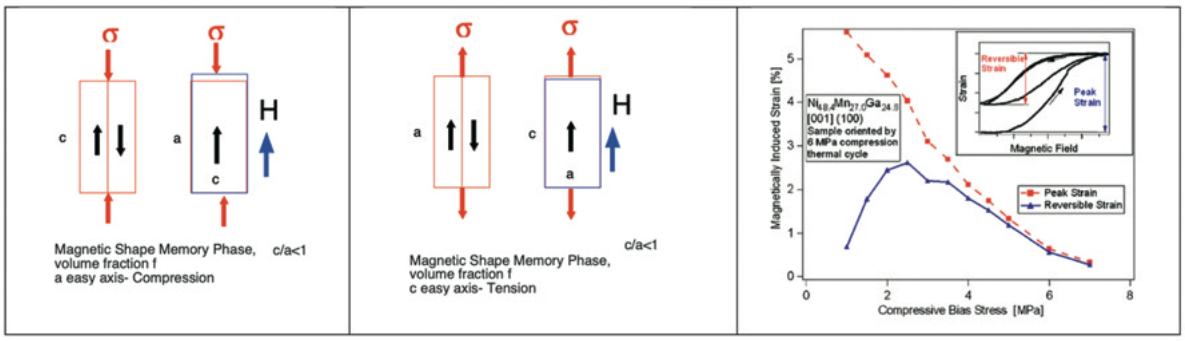

Fig. 28 (a) If c/a < 1 upon cooling under compression, the c axis is vertical. Upon application of magnetic field a axis becomes vertical if a axis is the easy axis, (b) Under tension a-axis is vertical, if c-axis is easy axis, the magnetic field shifts vertical axis to c-axis, (c) the measurements of magnetically induced strain as a function of biasing stress. Reproduced from Callaway, J.D., *et al.*, 2006. Magnetic shape memory in Ni2MnGa as influenced by applied stress. Applied Physics Letters 89, 221905–221901.

In the case of ferromagnetic shape memory, the strain is derived from a switch of the martensite domains from 'a' axis vertical to 'c' axis vertical (or vice versa) under the application of a magnetic field (**Fig. 28**(a)). If compression was applied as biasing stress, then 'a-axis' vertical would form because c/a < 1. Since the magnetically easy axis is the 'c-axis' the applied vertical field will switch the martensite to vertical 'c- axis' resulting in a large dimensional change. A high magnetic anisotropy and a low energy barrier for twin boundary motion is conducive to reorientation and magnetic shape memory. If during magnetization the boundary movement is not reversible the magnetization versus field strength curves exhibit considerable hysteresis. The absence of a hysteresis is an indication of reversible boundary motion, a desirable attribute in ferromagnetic shape memory alloys.

An overview of magnetic shape memory developments is given (Ullakko *et al.*, 1996; Murray *et al.*, 2000). The accompanying strain change can be a few percent as sown in **Fig. 28**(c). We note that MSM alloys produce large strains but not high stresses. The ferromagnetic shape memory materials have several characteristics that make them unique. They have to: (a) exhibit low twinning stress, (b) high magnetic anisotropy, and (c) high strains due to variant orientation change. The major drawbacks have been: (a) inherent brittleness of these materials, (b) the high cost of producing these materials, (c) extreme sensitivity to the compositional variations and (d) operation at low bias stress levels while higher stress is desirable in structures.

This field of research received considerable emphasis in the 1990s and over time continuous efforts by teams in Germany, Japan, Spain, and Czech Republic continue. The major advantage of these materials is the speed of actuation due to magnetic field application compared to the relatively slow actuation under temperature application (shape memory). The majority of the works in this field were undertaken on the well-known NiMnGa alloys (Callaway *et al.*, 2006; Heczko *et al.*, 2000) but other alloys have also been utilized (such as FePd) (Tickle, 2000).

Fatigue of Shape Memory Alloys

Fatigue Crack Growth

There have been early attempts to generate fatigue crack growth characterization of NiTi (Melton and Mercier, 1979b) (**Fig. 29**(a)). The well-known fatigue crack growth experiments on NiTi SMAs have been conducted by Ritchie and his students (McKelvey and Ritchie, 1999, 2001; Robertson *et al.*, 2007, 2012) who documented the threshold stress intensity, the Paris Regime for austenite and martensite microstructures (**Fig. 29**(b)). The general consensus that emerged from their experiments is that the martensite exhibits superior fatigue crack growth response compared to austenite. Since the work of Ritchie (**Table 13** first row), there has been a paucity of experimental works in shape memory fatigue crack growth. Later experiments on fatigue crack growth were undertaken by Sehitoglu and his students (Wu *et al.*, 2019; Sidharth *et al.*, 2020a; Sgambitterra *et al.*, 2019; Sidharth *et al.*, 2020b; Wu *et al.*, 2015; Yaacoub and Sehitoglu, 2019; Sgambitterra *et al.*, 2018) on Ni_2FeGa, NiTi, CuZnAl and FeMnNiAl (**Fig. 29**(c)-(g)). The stress intensity has been derived by regression of the displacement fields. This provided insight into the local driving forces accounting for the transformation strain of the initially austenitic specimens. Three observations are noted from these experiments:

(1) The local driving force differs from the handbook solutions because of shielding effects for Ni_2FeGa (Wu *et al.*, 2015) and NiTi (Sgambitterra *et al.*, 2018) (**Fig. 29**(c)–(e)). The closure forces due to transformation are more substantial in Ni_2FeGa resulting in higher thresholds.
(2) Non-shielding effects were observed in CuZnAl (Wu *et al.*, 2019) and FeMnNiAl (Sidharth *et al.*, 2020a) in view of the asymmetric transformation zones contributing to higher fatigue crack growth rates compared to other SMAs (**Fig. 29**(d–g)).
(3) In FeMnNiAl, when new variants are activated ahead of the crack tip, transient retardation effects were observed (Sidharth *et al.*, 2020a) (**Fig. 29**(g)).
(4) The fatigue crack growth rates are crystal orientation dependent in NiTi (Yaacoub and Sehitoglu, 2019) and the local accumulation of strain that produces irreversible displacements is also orientation dependent (**Fig. 29**(h)).
(5) The driving forces in shape memory alloys have a Mode II component that must be considered especially when the transformation zone is not symmetric with respect to the crack plane (**Fig. 29**(f and g)).
(6) The major finding in these studies is that the load carrying capacity of CuZnAl (**Fig. 29**(f)) is far lower than other SMAs. This is unfortunate because the CuZnAl has excellent transformation strains and low hysteresis.
(7) Intrinsic threshold stress intensity could be high in shape memory alloys but the extrinsic value could be lower in FeMnNiAl and CuZnAl (Wu *et al.*, 2019; Sidharth *et al.*, 2020a) due to non-shielding effects. Further work is needed along the lines of the schematic shown in **Fig. 29**(i).

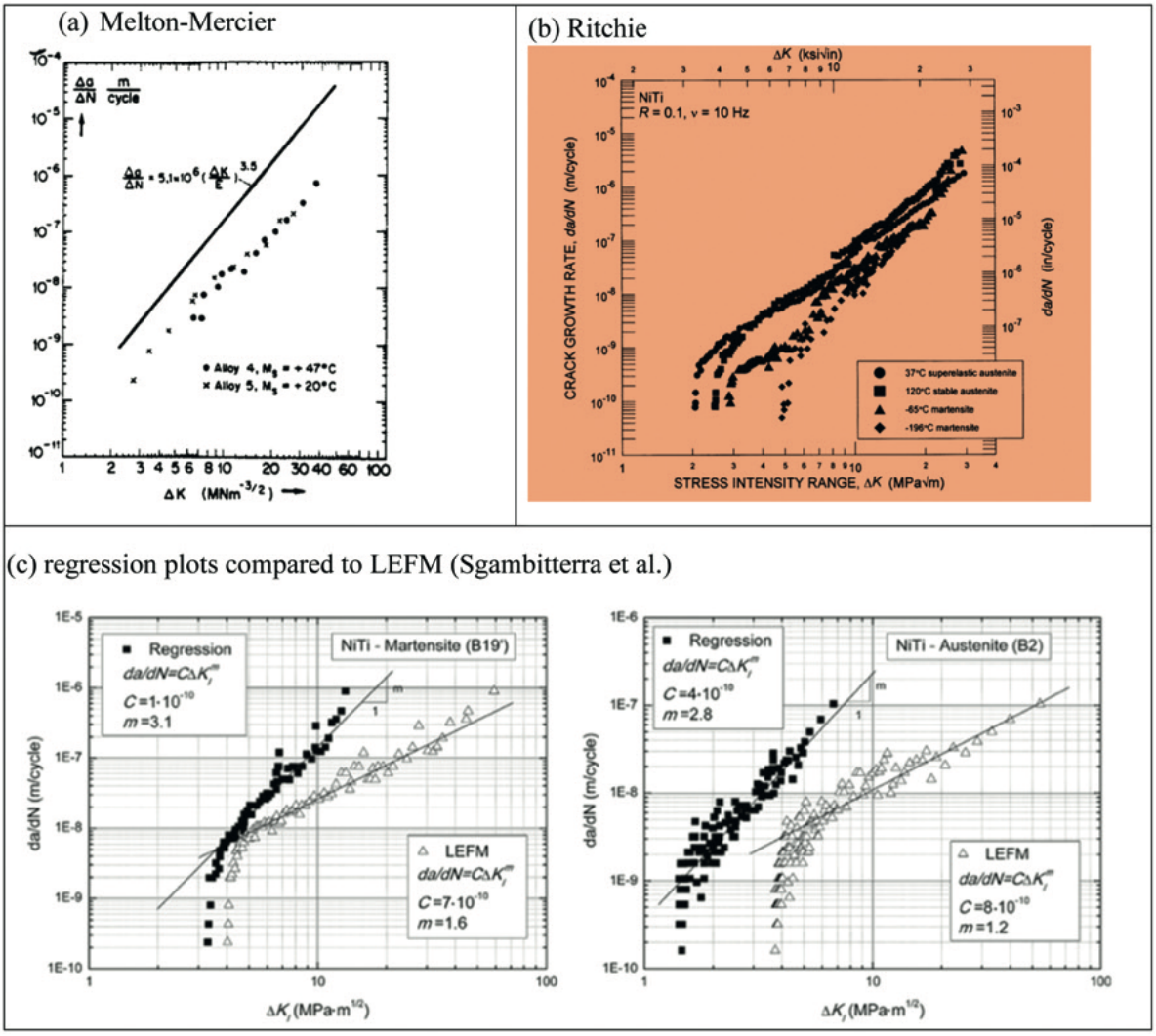

Fig. 29 (a) Early works on fatigue crack growth display rather low threshold stress intensity, (b) results that show superior FCG in martensite compared to austenite, (c) comparison of martensite and austenite fatigue crack growth data, (d) asymmetric transformation zones near the crack tip, (e) Fatigue Crack growth (the effective stress intensity range is arrived at by regression of the displacement fields), CuZnAl FCG curves showing the deshielding effect (i.e., the effective values of stress intensity are higher than the LEFM solution), (e) fatigue crack growyth data on Ni2FeGa class of SMAs, (f) fatigue crack growth experiments on a new SMA (FeMnNiAl), details of the stress-intensity range calculation is given in reference (Sidharth, R., Wu, Y., Brenne, F., Abuzaid, W., Sehitoglu, H., 2020a. Relationship between functional fatigue and structural fatigue of iron-based shape memory alloy FeMnNiAl. Shape Memory and Superelasticity 6, 256–272) (g) the evolution of irreversible displacements as crack growth occurs, (g) accumulation of residual strains at the crack tip with ffatigue cycling, (h) potential modeling strategies of dislocation emission at the crack tip in an inhomogeneous microstructure with plastic zone in martensite, the matrix is austenitic. Reproduced from (a) Melton, K.N., Mercier, O., 1979b. Fatigue of NITI thermoelastic martensites. Acta Metallurgica 27, 137–144. Available at: http://doi.org/10.1016/0001-6160(79)90065-8. (b) McKelvey, A.L., Ritchie, R.O., 2001. Fatigue-crack growth behavior in the superelastic and shape-memory alloy nitinol. Metallurgical and Materials Transactions A 32, 731–743. doi: 10.1007/s11661-001-1008-7. Sgambitterra, E., Maletta, C., Furgiuele, F., Sehitoglu, H., 2018. Fatigue crack propagation in [0 1 2] NiTi single crystal alloy. International Journal of Fatigue 112, 9–20). (d) Wu, Y., *et al.*, 2019. Deshielding effects on fatigue crack growth in shape memory alloys-A study on CuZnAl single-crystalline materials. Acta Materialia 176, 155–166. (e) Wu, Y., Ojha, A., Patriarca, L., Sehitoglu, H., 2015. Fatigue crack growth fundamentals in shape memory alloys. Shape Memory and Superelasticity 1, 18–40.

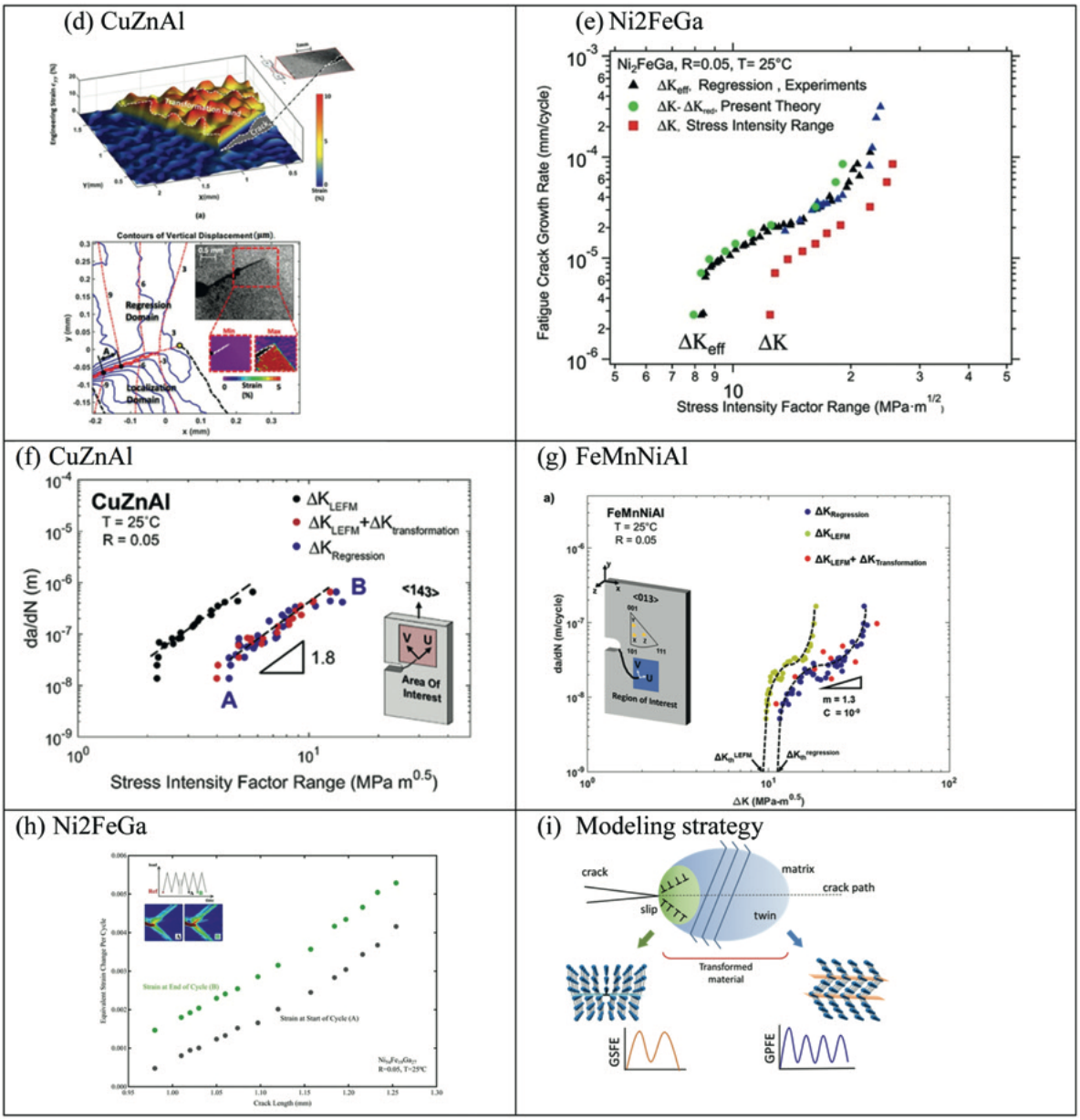

Fig. 29 Continued.

Table 13 Summary of the FCG and LCF/HCF research on shape memory materials

Melton-Mercier (Melton and Mercier, 1979b), Ritchie *et al* (McKelvey and Ritchie, 1999, 2001; Robertson *et al*., 2007, 2012), Sehitoglu *et al* (Wu *et al*., 2019; Sidharth *et al*., 2020a; Sgambitterra *et al*., 2019; Sidharth *et al*., 2020b; Wu *et al*., 2015; Yaacoub and Sehitoglu, 2019; Sgambitterra *et al*., 2018), Daly-LePage (LePage *et al*., 2021)	NiTi, CuZnAl Ni2FeGa	Very low crack thresholds less than $3MPa\sqrt{m}$ in NiTi and CuZnAl, higher thresholds ($10MPa\sqrt{m}$) in Ni_2FeGa. Martensite has higher thresholds compared to austenite.
Sade *et al* (Sade and Hornbogen, 1988; Damiani *et al*., 2002) , Gall-Sehitoglu-Maier (Gall *et al*., 1999d, 2001, 2008; Gall and Maier, 2002; Gall *et al*., 1998b), Miyazaki *et al* (Miyazaki *et al*., 1986, 1998), Hornbogen-Eggeler *et al* (Hornbogen and Eggeler, 2004; Hornbogen, 1978), Pelton *et al* (Pelton *et al*., 2008), Ritchie *et al* (Cao *et al*., 2020), Petrini *et al* (Berti *et al*., 2021), Moumni *et al* (Moumni *et al*., 2005)	CuZnAl, NiTi	Demonstrated residual martensite and irreversibility at microscale, interaction of dislocation tangles with martensites lowering of transformation stress and significant hardening in fatigue, emerging debate on mean strain effects in HCF.
Brown *et al* (Brown, 1979, 1982), Laird *et al* (Ritter *et al*., 1979; Yang *et al*., 1977), Delaey et al (Andrade *et al*., 1985; Delaey *et al*., 1978; Janssen *et al*., 1979)	CuAlNi	Fatigue crack initiation at matrix-martensite and grain boundary interfaces, incompatibility among grains, local rise in temperature during fatigue.

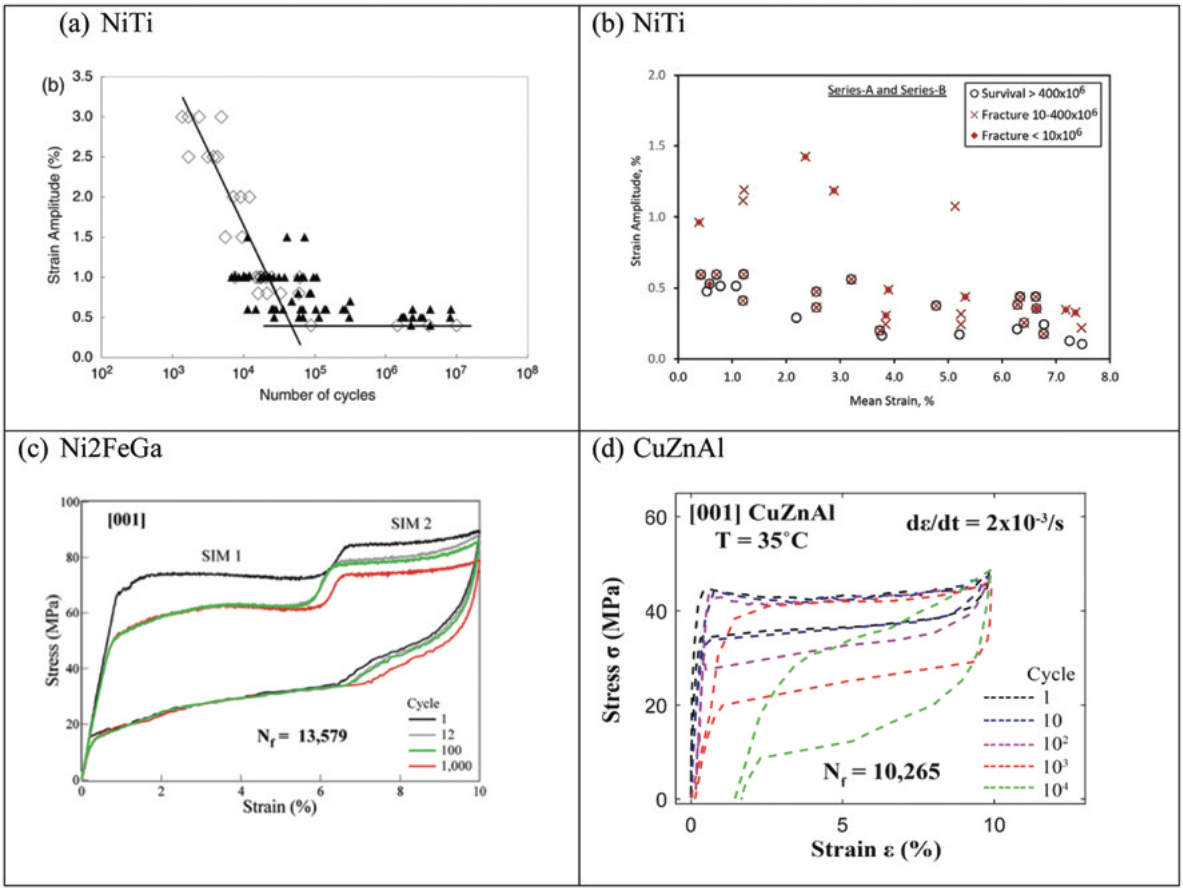

Fig. 30 (a) Strain amplitude vs fatigue life displaying the LCF and HCF regimes, (b) the strain amplitude versus mean strain corresponding to the fatigue limit region, (c) Stress-strain response of Ni_2FeGa showing fatigue lives over 13,000 cycles at a strain range exceeding 10%, (d) the stress-strain response of CuZnAl showing fatigue lives exceeding 10,000 cycles for a strain range of 10%, (e) Ni_2FeGa results, (f) Slip in Austenite displaying localization at austenite-martensite interfaces as evidenced by many research groups. NiTi is one of the most researched SMAs as well as most widely used in commercial applications., (g) Slip in martensite, dislocations are noted on twin variant interfaces. (h) nucleation and growth of fatigue cracks at austenite-martensite interfaces in FeMnNiAl. Reproduced from (a) Pelton, A., *et al.*, 2008. Fatigue and durability of Nitinol stents. Journal of the Mechanical Behavior of Biomedical Materials 1, 153–164. (b) Cao, H., Wu, M.H., Zhou, F., McMeeking, R.M. & Ritchie, R.O., 2020. The influence of mean strain on the high-cycle fatigue of Nitinol with application to medical devices. Journal of the Mechanics and Physics of Solids 143, 104057, https://doi.org/10.1016/j.jmps.2020.104057. (c) Efstathiou, C., Sehitoglu, H., Kurath, P., Foletti, S., Davoli, P., 2007. Fatigue response of NiFeGa single crystals. Scripta materialia 57, 409–412. (d) and (e) Wu, Y., Ertekin, E., Sehitoglu, H., 2017. Elastocaloric cooling capacity of shape memory alloys – Role of deformation temperatures, mechanical cycling, stress hysteresis and inhomogeneity of transformation. Acta Materialia 135, 158–176. (f) Chowdhury, P., Sehitoglu, H., 2017b. A revisit to atomistic rationale for slip in shape memory alloys. Progress in Materials Science 85, 1–42. Norfleet, D., *et al.*, 2009. Transformation-induced plasticity during pseudoelastic deformation in Ni–Ti microcrystals. Acta Materialia 57, 3549–3561. Delville, R., Malard, B., Pilch, J., Sittner, P., Schryvers, D., 2011. Transmission electron microscopy investigation of dislocation slip during superelastic cycling of Ni–Ti wires. International Journal of Plasticity 27, 282–297. Hamilton, R. F., Sehitoglu, H., Chumlyakov, Y., Maier, H.J., 2004. Stress dependence of the hysteresis in single crystal NiTi alloys. Acta Materialia 52, 3383–3402. Pfetzing-Micklich, J., *et al.*, 2012. Orientation dependence of stress-induced phase transformation and dislocation plasticity in NiTi shape memory alloys on the micro scale. Materials Science and Engineering: A 538, 265–271. Pelton, A., Huang, G., Moine, P., Sinclair, R., 2012. Effects of thermal cycling on microstructure and properties in Nitinol. Materials Science and Engineering: A 532, 130–138. Nemat-Nasser, S., Choi, J.-Y., Guo, W.-G., Isaacs, J.B., 2005b. Very high strain-rate response of a NiTi shape-memory alloy. Mechanics of materials 37, 287–298. (g) Chowdhury, P., Sehitoglu, H., 2017b. A revisit to atomistic rationale for slip in shape memory alloys. Progress in Materials Science 85, 1–42. From Liu, Y., Xie, Z., Van Humbeeck, J., Delaey, L., 1998. Asymmetry of stress–strain curves under tension and compression for NiTi shape memory alloys. Acta Materialia 46, 4325–4338. Chumlyakov, Y., *et al.* Shape memory effect and high-temperature superelasticity in high-strength single crystals. Journal of Alloys and Compounds 577, S393–S398. (h) Sidharth, R., Abuzaid, W., Vollmer, M., Niendorf, T., Sehitoglu, H., 2020b. Fatigue crack initiation in the iron-based shape memory alloy FeMnAlNiTi. Shape Memory and Superelasticity 6, 323–331.

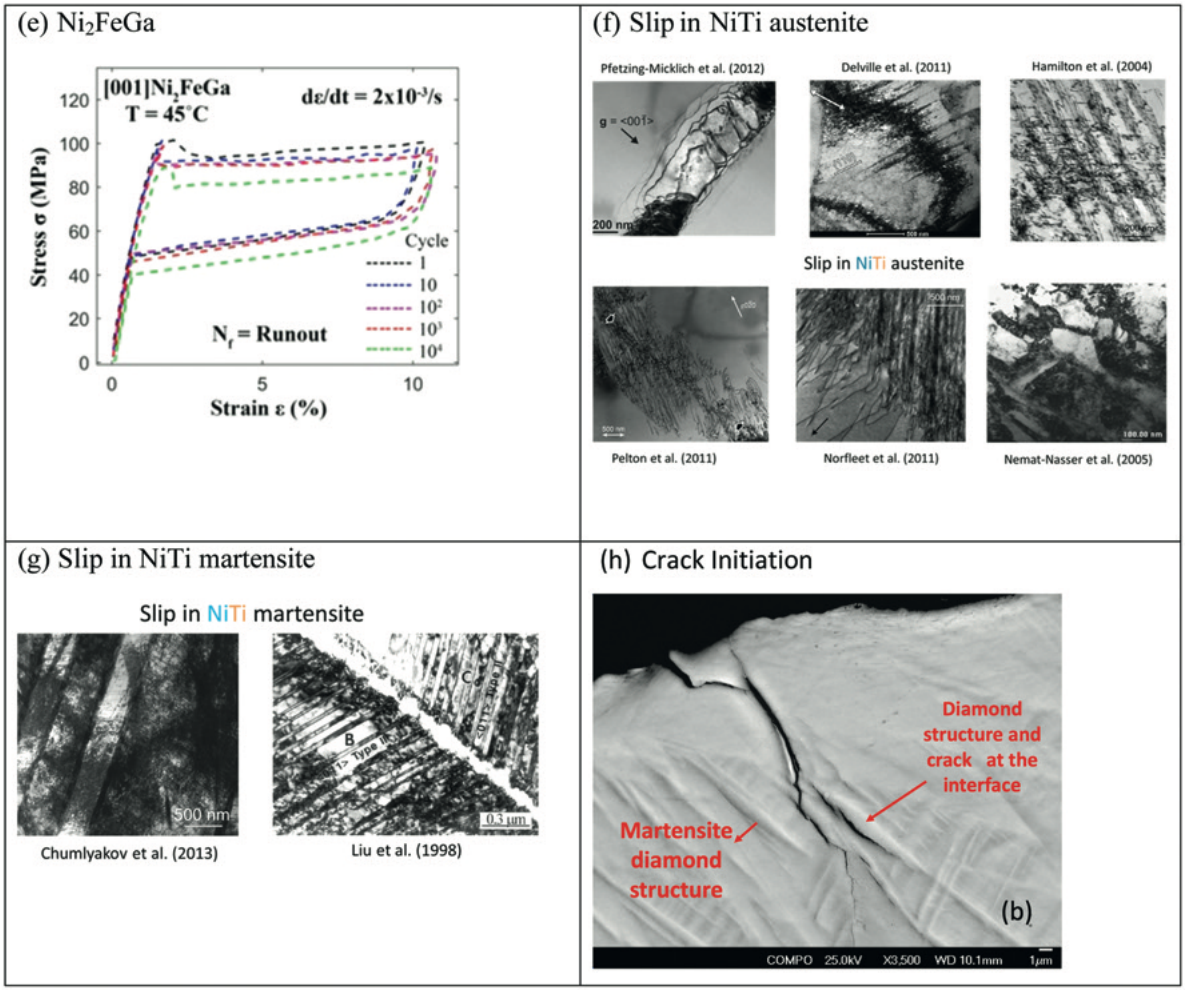

Fig. 30 Continued.

Fatigue Crack Initiation (LCF and HCF)

There are many studies which have focused on experiments (in LCF and HCF regimes- **Table 13**–2nd and 3rd rows) and collected fatigue data. Then, plots of strain-life and stress-life curves have been generated. These fatigue experiments were conducted on polycrystals, and often in the superelastic regime. Majority of the works have been conducted on NiTi; however, there are early experiments on Cu based alloys and more recent work on Ni_2FeGa and others. The recent results on NiTi stent wires subjected to axial-bending loading showed that the strain amplitudes corresponding to the fatigue limit is of the order of 0.4% (**Fig. 30**(a)). There has been debate on the dependence of this strain amplitude on the mean strain, one study proposing an increase in the allowable strain with increasing mean strain (Pelton *et al.*, 2008) while others proposing a decrease in the strain amplitude from 0.4% to 0.16% for mean strains higher than 3% (Cao *et al.*, 2020) (**Fig. 30**(a) and (b)). Nevertheless, two observations are noteworthy: (1) the strain amplitude limit of 0.4% corresponding to long lives in HCF is still relatively high compared to conventional metals but is significantly lower compared to the maximum recoverable strains which can be of the order of 6%–10% in NiTi polycrystals, (2) there is considerable scatter in fatigue lives in the very high cycle fatigue regime of the order of three orders of magnitude. Further work is needed to explain the source of this variation in lives. The variations in grain size, grain misorientations, dislocation emission and nucleation at austenite/martensite boundaries, internal stresses at matrix/precipitate boundaries, the origin of cracking (surface where there are high image stresses versus the interior of the sample) need to be incorporated in a comprehensive fatigue model.

There has been previous fatigue work on other shape memory compositions. The results shown in **Fig. 30**(c)–(e) are for Ni2FeGa and CuZnAl single crystals respectively. We note that the fatigue lives exceeded 10^4 cycles for a strain amplitude of 5% in Ni2FeGa. Note that the Ni2FeGa alloy undergoes two stage transformation and the maximum transformation strains can reach 14%. We note that the absence of grain boundaries is conducive to long fatigue lives in CuZnAl alloys as well pointing to the role

strain accumulation at the boundaries. While a preferred variant forms in single crystals the variant selection changes from grain to grain in the case of polycrystals. There has been also interest in NiTiCu as it could produce a lower hysteresis compared to NiTi and other SMAs, but its fatigue response could be inferior to the alloys discussed in this section.

Using electron microscopy, the fatigue-induced dislocation slip structures and the prevailing systems have been identified and shown in **Fig. 30**(f) for the austenitic phase of NiTi SMA (Norfleet *et al.*, 2009; Delville *et al.*, 2011; Hamilton *et al.*, 2004; Pfetzing-Micklich *et al.*, 2012; Pelton *et al.*, 2012; Nemat-Nasser *et al.*, 2005b). The lattice resistance to slip operative at the sub-lattice scale has been established in theoretical works from Ezaz *et al.* and Hatcher et al (Ezaz *et al.*, 2013; Hatcher *et al.*, 2009b) based on fault energetics of NiTi austenite. The slip in martensite is generally more difficult and occurs only at higher stress magnitudes than in austenite (Liu *et al.*, 1998; Chumlyakov *et al.*, 2013; Xie *et al.*, 1998) (**Fig. 30**(g)). On the other hand, the martensitic twinning can occur at relatively low stresses and different modes of twinning have been discussed earlier. The images in **Fig. 30**(f) and (g) point to localization (or high density of dislocations and entanglements) at interfaces. **Fig. 30**(h) shows the nucleation of the fatigue cracks at the austenite-martensite interfaces in FeMnNiAl where localization develops consistent with the early observations from Section "Irrational Twin Planes and the Origin of the Irrationality (Comparison With Experiments) and Slip Emission".

Fracture of Shape Memory Alloys

The fracture of conventional materials has been studied in depth from a continuum viewpoint over several decades. Measures such as critical stress intensity (K_{IC}) and critical energy release rate (G_C or J_{IC}) emerged as engineering tools to measure cracking resistance. From the continuum viewpoint, the driving forces such as stress intensity (LEFM) have been computed with finite elements for different crack geometries, and their critical values, often related to the surface energy for cleavage, correspond to the material toughness. On the experimental side, the load displacement curves in cracked specimens have been measured to establish the critical load that corresponds to nucleation (initiation) of fracture. The occurrence of plasticity is known to raise the resistance to fracture and measures such as J-integral have been introduced to account for nonlinear material behavior. The main issue with the shape memory alloys is that primary deformation mechanism is via crystallographic transformation with internal twinning and concurrent plasticity. The transformation is mainly due to shear and can be as high as 10% strain. One would expect relatively high toughness with such high levels of crack tip shear, but shape memory materials have low intrinsic toughness. This is partly because of the crystallographic order and higher unstable fault energies (which control slip mediated plasticity) compared to the surface energy (Rice and Thomson, 1974). The onset of slip can result in crack blunting hence ductile behavior. Plastic slip can occur in shape memory alloys during transformation and is expected to affect the

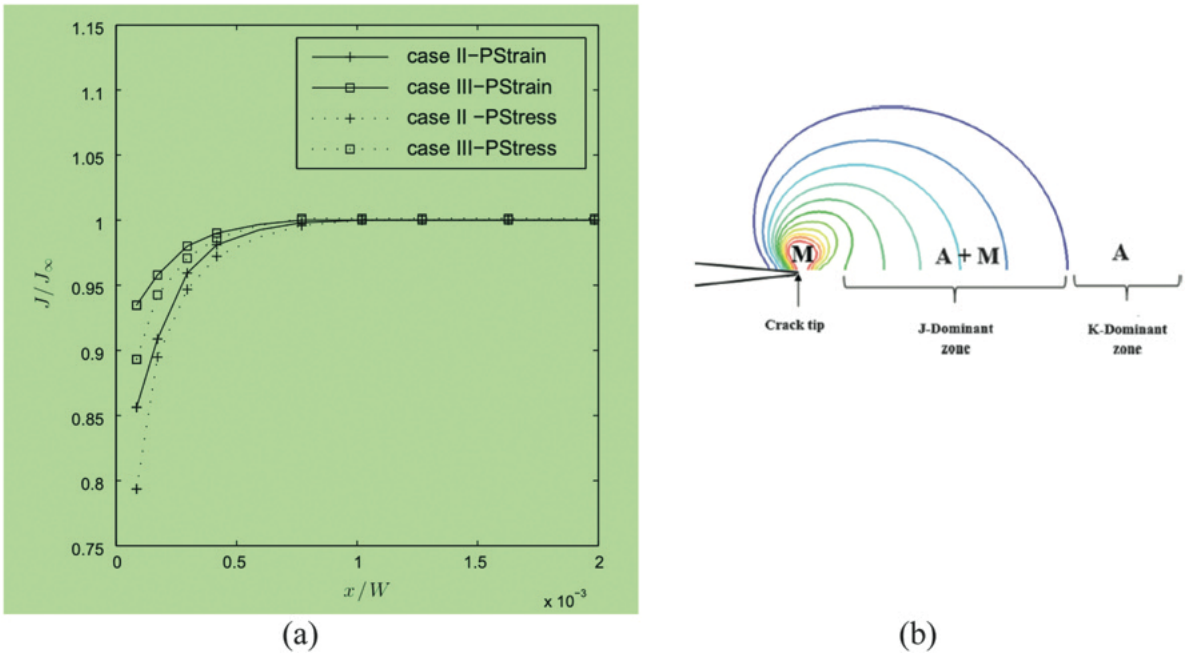

Fig. 31 (a) The magnitude of J varies near the crack tip (M and A + M domains) and reaches a steady state, J_∞, far from the crack tip (in the austenite regime), (b) nonlinear crack tip asymptotic equations were derived in Özerim *et al.* Reproduced from (a) Hazar, S., Zaki, W., Moumni, Z., Anlas, G., 2015. Modeling of steady-state crack growth in shape memory alloys using a stationary method. International Journal of Plasticity 67, 26–38. Available at: https://doi.org/10.1016/j.ijplas.2014.08.018. (b) Özerim, G., Anlaş, G., Moumni, Z., 2018. On crack tip stress fields in pseudoelastic shape memory alloys. International Journal of Fracture 212, 205–217. doi:10.1007/s10704-018-0300-0.

fracture behavior but the phenomenon is not well understood. The design of high toughness SMAs has eluded current researchers with most SMAs exhibiting toughness levels less than 50 MPa $m^{1/2}$. This is a topic to be investigated in future studies. In this article, we will review the existing works on both experimental and theoretical (mainly continuum) fronts on fracture behavior of SMAs.

Several continuum formulations of stress-strain response of shape memory alloys have been proposed but they have considerable limitations to predict a wide range of material behavior over a broad range of strains, temperatures, strain rates. These thermo-mechanical models are phenomenological in nature and have several internal variables such as volume fraction of martensite, the critical stress for transformation, and temperature. They have been used in simulations to formulate a fracture criteria. We note that forward transformation results in a temperature rise and cooling upon reverse transformation which alters the stress-strain response considerably. The plastic strains are handled as additive in these models which is a huge approximation because the plastic strain must be coupled with transformation. The strain energies depend on the elastic moduli (with large number of anisotropic constants) which is evolving during the deformation as martensite forms and is distinct from austenite as illustrated earlier in the paper (Wang and Sehitoglu, 2014d). These details complicate the interpretation of numerical results and can potentially be resolved in future treatments.

Determination of Driving Forces

When a crack is present in a structure made of a superelastic shape memory alloy, high stresses that occur at the crack tip induce almost an immediate phase transformation, and the crack tip is surrounded by a non-homogeneous region of martensite and austenite + martensite. The parent austenite surrounds this zone further away. Even for a simple crack geometry and loading state, the resulting problem to be studied is a nonhomogeneous cracked domain which deviates significantly from the homogenous continuum treatments. Standard linear elastic fracture mechanics solutions do not apply to determine the driving forces in these cases.

Asymptotic equations of (LEFM), as $r \to 0$, describe the stress field around the crack tip (Williams, 1957) in homogenous bodies. Assuming the transformation region is small with respect to crack dimensions, the far field stress field is described by

$$\sigma_{ij}(\mathrm{r},\theta) = \frac{K_I}{\sqrt{2\pi r}} f_{ij}(\theta).$$

The asymptotic equations above require the knowledge of the Mode I stress intensity factor (SIF), K_I, i.e., the driving force. Although results for SIFs for several different geometries and loadings are presented in the literature in detail for LEFM (Sih, 1973; Murakami, 1992) for homogeneous elastic deformations, studies on the precise evaluation of the driving forces in SMAs are limited because one must account for transformation-induced strains and tractions which are difficult to determine.

Several approaches from finite elements have been undertaken for evaluation of SIFs. In general, the J- contour integral was determined and the stress intensity factor determination follows; but in the case of an SMA this integral is contour dependent as a result of nonhomogeneity around the crack tip (Hazar *et al.*, 2015) (**Fig. 31**(a)). The steady state levels correspond to contours obtained in the austenite regime and results stabilize. In the constitutive model utilized in Hazar *et al.* (2015), there is provision for martensite reorientation upon unloading which modifies the results (Case II vs Case III from Hazar *et al.* (2015)), nevertheless the non-uniqueness in J-integral near the crack front is noted in both cases. Using nonlinear crack tip asymptotic equations, a J-dominant region was derived (Özerim *et al.*, 2018) similar to the Hutchinson's asymptotic treatment (Hutchinson, 1968) as shown in **Fig. 31**(b).

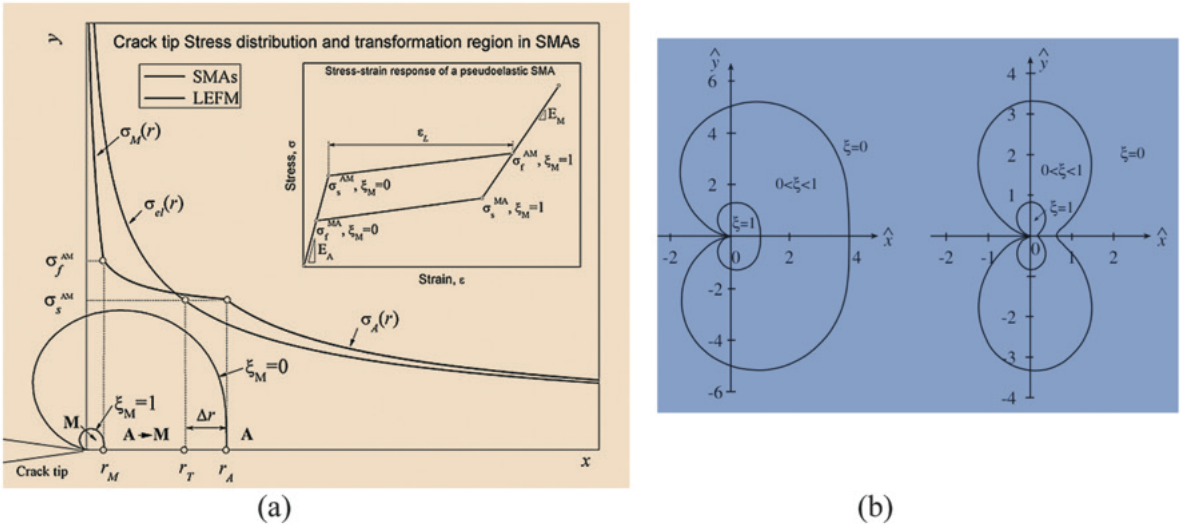

Fig. 32 (a) The stress distribution ahead of a crack tip based on the constitutive model shown in the inset, (b) the transformation zones based on a multiaxial transformation surface - the difference in plane stress and plane strain case and the evolution of the zone as volume fraction of martensite increases is noted. From (a) Maletta, C., Sgambitterra, E., Furgiuele, F., 2013. Crack tip stress distribution and stress intensity factor in shape memory alloys. Fatigue & Fracture of Engineering Materials & Structures 36, 903–912. doi:10.1111/ffe.12055. (b) Freed, Y., Bankssills, L., 2007. Crack growth resistance of shape memory alloys by means of a cohesive zone model. Journal of the Mechanics and Physics of Solids 55, 2157–2180. doi:10.1016/j.jmps.2007.03.002.

Furthermore, due to the dislocation-mediated localized plasticity as noted earlier, an accurate J_{tip} value cannot be readily established. This is because the martensite is often in the form of a band with a given orientation and may not be symmetric around the crack tip. Further advances in constitutive formulations (energy or other criteria) are needed which could be then applied to crack tip transformation to identify the shear band propensity (Crone and Shield, 2001) and ensuing plasticity and driving force determination. Since the elastic moduli at the tip of a stationary crack (which immediately transformed into martensite) is also needed for conversion of energy release rate, J, to stress intensity, K which is especially difficult for monoclinic martensites with 13 constants in single crystal (orientation) (Ren and Sehitoglu, 2016). In the existing finite element formulations different phenomenological constitutive equations have been adopted to model the behavior of the SMAs (Lagoudas *et al.*, 2012; Stebner and Brinson, 2013; Zaki and Moumni, 2007; Gall *et al.*, 2000a; Lagoudas *et al.*, 2006; Baxevanis *et al.*, 2012). Commercial FE softwares have their own built in models (Auricchio *et al.*, 1997); and also permit user- defined subroutines, a code prepared separately by the user. In summary, a universally accepted methodology for K calculations has not emerged.

Transformation Zone

The phase transformation region (PTR) at the crack tip evolves as crack advances. Previous treatments in the literature employed the asymptotic equations of linear elastic fracture mechanics (LEFM) to predict the extent of the PTR (Birman, 1998) based on simple constitutive equations (Tanaka and Sato, 1986). The transformation zone can be determined as a function of r and θ (Falvo *et al.*, 2009; Xiong and Liu, 2007). In **Fig. 32**(a), the extent of the martensitic region and the two phase domain (A + M) and the remote austenite region (A) are shown (Maletta *et al.*, 2013). The stress redistribution at the crack tip due to transformation is noted and the extent of the transformation zone considers the equilibrium due to stress redistribution. The extent of the transformation zone is illustrated for plane stress and plane strain conditions in **Fig. 32**(b) without considering redistribution of stresses. Nevertheless, the results point to transformation zones that differ depending on the out-of-plane constraint (**Fig. 32**).

In most of the studies, the stress intensity factor, K, has been calculated using LEFM, but it is well known that the transformation-induced internal forces in the crack wake modify the stress intensity (McMeeking and Evans, 1982). Similar calculations have been undertaken for shape memory alloys to illustrate the closure forces under transformation eigen strains which are dictated by shear (Wu *et al.*, 2015) which modify the transformation zones. In other treatments, the stress state around the crack tip was accounted for based on a transformation function, or a thermodynamic force together with asymptotic equations of LEFM (Hazar *et al.*, 2016; Freed and Bankssills, 2007; Stam and van der Giessen, 1995; Yi and Gao, 2000; Yi *et al.*, 2001; Lexcellent and Thiebaud, 2008).

The validity of a square root singularity and the existence of a K Dominant region to calculate the stresses may be rather approximate, and non-linear response can be better characterized with energy release rate calculations (Hutchinson, 1968) . This is the impetus behind the J-integral formulations in recent work. However, the J-integral determination varies within the A + M zone as shown above (Özerim *et al.*, 2018). This result points to an ambiguity regarding the use of these standard measures in SMA analysis.

There have been previous attempts on experimental determination of the transformation zone (Daly *et al.*, 2007). Digital image correlation (DIC) is a powerful tool to obtain the displacement field, and to calculate local strains that provide an approximate measure (Mutlu *et al.*, 2020; Haghgouyan *et al.*, 2016; Ahadi and Sun, 2016). In-situ synchrotron measurements (Robertson *et al.*, 2007; Gollerthan *et al.*, 2009) provide valuable insight into the phase transformation region and the contours are illustrated in **Fig. 33**(a).

The full displacement data (the u-v field) obtained from DIC can be fitted into asymptotic equations to obtain the crack tip parameters., K_I, K_{II}, T-stress, etc (Sgambitterra *et al.*, 2018; Haghgouyan *et al.*, 2016). Using a similar approach, SIFs can be obtained numerically using the full displacement field obtained from finite elements, and fitting them into the asymptotic formulas (Hazar *et al.*, 2016; Mutlu *et al.*, 2020; Özerim *et al.*, 2018).

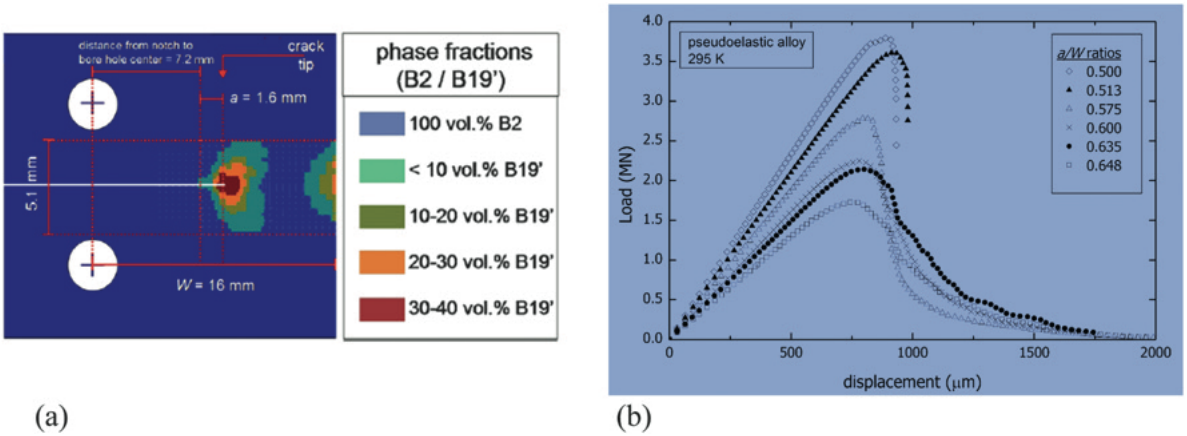

Fig. 33 (a) Phase fractions of the austenite B2 and martensite B19′ structures for the two transformation zones in a pseudoelastic NiTi SMA CT specimen obtained by in situ synchrotron measurements at high stress intensity, (b) The fracture toughness estimate is obtained by using the maximum load and the corresponding crack length and the standard stress intensity formulas for the CT specimen which relate stress intensity to load, crack length, and a/W ratio. Reproduced from (a) and (b) Gollerthan, S., 2009. Fracture mechanics and microstructure in NiTi shape memory alloys. Acta Materialia 57, 1015–1025. doi:10.1016/j.actamat.2008.10.055.

Fracture Toughness

There are well known methods and standards for the determination of fracture toughness for metallic materials. In the case of an SMA, no closed form solution is available for K_ι, and no standard method exists for the evaluation of fracture toughness: the maximum level of K may be extracted from a load displacement curve (from simulations or experiments) can be used as an estimate for the toughness. If an energy approach is undertaken then the need for elastic modulus arises which is harder to define for shape memory materials considering the crack tip zone is B19′ martensite and has preferred crystallographic orientation.

Experimental measurements of fracture toughness have been undertaken only in few studies (Robertson *et al.*, 2012; Robertson and Ritchie, 2007; Gollerthan *et al.*, 2008; Jiang and Vecchio, 2007; Wang *et al.*, 2008; Luo *et al.*, 2016; Baxevanis *et al.*, 2013a). A typical load vs displacement curve for pseudoelastic NiTi (Gollerthan *et al.*, 2009) is shown in **Fig. 33**(b), and the stress intensity is computed using the P, the maximum load, as the critical or the maximum stress intensity.

Table 14 Summary of fracture toughness results from the literature. Most experiments were conducted on NiTi

Material	*Pseudoelastic NiTi*	*T > Md Austenitic NiTi*	*Martensitic NiTi*	*Research Group*
49.2 at % Ni–Ti, 0.5 mm Thick NiTi Sheet	33.8 MPa.m$^{1/2}$			Maletta *et al* (Maletta *et al.*, 2013)
52 wt % Ni-Ti, 0.16 mm Thick NiTi Sheet	51.4 + -3.6 MPa.m$^{1/2}$			Daly *et al* (Daly *et al.*, 2007)
55.9 wt % Ni-Ti, 1.0 mm Thick NiTi Sheet	33.8 MPa.m$^{1/2}$ (DIC) 31.9 MPa.m$^{1/2}$ (E399)	28.1 MPa.m$^{1/2}$ at 373 K		Haghouyan *et al* (Haghgouyan *et al.*, 2016)
50.7 at % Ni-Ti, 2 mm Thick NiTi Sheet	34 MPa.m$^{1/2}$ (E399)	53 MPa.m$^{1/2}$ at 423 K	31 MPa.m$^{1/2}$ at 295 K (50.3 at % Ni)	Gollerthan *et al* (Gollerthan *et al.*, 2009)
50.9 at % Ni -Ti 1.7 mm Thick NiTi Sheet. Nanocrystalline SE Niti. GS *x*, Grain Size, "*x*" nanometer:	GS 10: 25 MPa.m$^{1/2}$ GS 18: 27 MPa.m$^{1/2}$ GS 42: 32 MPa.m$^{1/2}$ GS 64: 34 MPa.m$^{1/2}$ GS 80: 42.5 MPa.m$^{1/2}$ GS 1500: 44 MPa.m$^{1/2}$			Ahadi *et al* (Ahadi and Sun, 2016)
50.8 at % Ni–Ti, 0.4 mm Thick	34 MPa.m$^{1/2}$			Robertson *et al* (Robertson and Ritchie, 2007)
NiTi Alloy, Ni/Ti Ratio of 55/45	39.2 + -2.8 MPa.m$^{1/2}$			He *et al* (He *et al.*, 2004)
Compilation of Fracture Toughness Data for NiTi	All virtually identical steady state values of 30 MPa.m$^{1/2}$			Robertson *et al* (Robertson *et al.*, 2012)
49.9 at % Ni-Ti Hot Rolled NiTi Plates	40 MPa.m$^{1/2}$ at 25 ^{o}C	64 MPa.m$^{1/2}$ at 150 ^{o}C		Holtz, *et al* (Holtz, 1999)
50.0 at % Ni –Ti	39.0 MPa.m$^{1/2}$			Jiang *et al* (Jiang and Vecchio, 2007).
50.3 at % Ni –Ti	31.5 MPa.m$^{1/2}$			Gollerthan *et al* (Gollerthan *et al.*, 2008)
Ni 56.3 wt % - Ti NiTi	39.4 MPa.m$^{1/2}$			Wang *et al* (Wang *et al.*, 2008)
50.8 at % Ni –Ti NiTi Strips, 0.60–0.64 mm	18–35 MPa.m$^{1/2}$ when T < Md	40 MPa.m$^{1/2}$ at T ≈ 230 ^{o}C	At -40 ^{o}C: 30 MPa.m$^{1/2}$ At 0 ^{o}C: 18 MPa.m$^{1/2}$	Luo *et al* (Luo *et al.*, 2016)
50.8 at % Ni –Ti, NiTi Sheet, Thickness: 0.60–0.50 mm	30 MPa.m$^{1/2}$ at 293 K to 37.5 MPa.m$^{1/2}$ at 333 K.			Maletta *et al* (Maletta *et al.*, 2016)
50.8 at % Ni –Ti NiTi , Thickness: 6.0 mm	29.13 MPa.m$^{1/2}$			Katanchi *et al* (Katanchi *et al.*, 2018)
49.5 at % Ni -Ti NiTi	38 MPa.m$^{1/2}$ at 20^{o}C 41 MPa.m$^{1/2}$ at 80^{o}C From J_{IC} 95 MPa.m$^{1/2}$ at 20^{o}C 90 MPa.m$^{1/2}$ at 80^{o}C	50 MPa.m$^{1/2}$ at 170^{o}C From J_{IC} 110 MPa.m$^{1/2}$ at 170^{o}C		Haghouyan *et al*, (Haghgouyan *et al.*, 2019)
49.5 at % Ni -Ti NiTi Specimens With 2,3,4,5 mm Thicknesses	32 + − 1 MPa.m$^{1/2}$ From J_{IC} 93–94 MPa.m$^{1/2}$			Abut *et al* (Abut *et al.*, 2021)
Ni_2MnGa SMA (Using Vickers Hardness Test)	4–10 MPa. m$^{1/2}$			D'Silva *et al* (D'Silva *et al.*, 2021)
3–1.5 mm. thick CuAlBeMn Samples. Compositions differ.	34.81 MPa.m$^{1/2}$ 36.75 MPa.m$^{1/2}$ 41.94 MPa.m$^{1/2}$			Shivasiddarramaiah *et al* (Shivasiddaramaiah *et al.*, 2018)

In most studies, fracture tests have been carried out on non-standard specimen geometry and the value obtained does not correspond to that of plane strain fracture toughness (He *et al.*, 2004). Another approach to calculate the fracture toughness is to use the full displacement field obtained from Digital Image Correlation (DIC) at P_{max}, and to extract the SIF, K_{max} using the asymptotic equations of LEFM (Haghgouyan *et al.*, 2016). A summary of the results is provided in **Table 14**. In almost all of the studies the fracture toughness has been found superior in martensite compared to austenite.

It is possible to evaluate the driving forces such as J Integral from simulations, however, caution should be taken as there is path dependence. The crack tip energy release rate was established virtual crack closure technique (Baxevanis *et al.*, 2013a,b, 2014) incorporating the role of transformation. The maximum SIFs from critical J values for crack growth were found to be considerably higher than the ones reported in the literature (Haghgouyan *et al.*, 2019). Correlation has been sought between hardness to toughness, via Vickers micro indentation to evaluate the fracture toughness of Ni_2MnGa magnetic shape memory alloy (D'Silva *et al.*, 2021) but further work is needed to interpret the results.

In summary, most works of fracture of SMAs rely on stress intensity approaches; but the calculation of the SIF depends on the transformation zone and the modified crack tip stresses. The complexity of material behavior in the region ahead of the crack tip precludes simple remote loading based stress intensity determination. Since martensites exhibit internal twinning with twinning dislocations that are emitted to the austenite domains, prediction of ductile vs brittle behavior is complex, and this is left aside for future work. In the field of fracture, following the Rice and Thomson treatment (Rice and Thomson, 1974), recent efforts have considered atomistic level calculations of free surface and fault energies. The fault energy decides the propensity of slip nucleation from crack tips, hence this methodology incorporates the role of plasticity on fracture behavior. From the atomistic standpoint, the model of Rice-Thomson classified ductile vs brittle behaviors in untransforming materials upon comparison of unstable fault energies versus the surface energy. This is equivalent to comparing the dislocation core widths with the equilibrium distance of dislocation from the crack front. Such an approach has been applied to assess different crystal structures and environmental effects in recent years with considerable success. On the other hand, applying such a model to shape memory alloys is premature at this point due to the complexity of deformation behavior.

Concluding Remarks

This review article outlined the different modeling approaches across length scales providing a current understanding of lattice level and macroscopic SMA behaviors. The need for grain level atomic simulations via MD are needed to bridge the length scale from discrete physics to continuum. Because shape memory alloys pose complex elastic constants, lattice-motif sites, shears and shuffles the preparation of the MD potentials to match the atomistic approach are rather demanding. This pursuit is needed for unraveling the complexity of fatigue damage evolution in SMAs.

The Peierls barrier concept which energetically represented slip in the past has been extended to twinning and transformation fronts. These fault energy considerations hold considerable promise in unraveling the complexity in SMAs which have complex crystal structures and atomic positions at the atomic crystal lattice level. Mesoscale treatments to convert energy barriers to frictional (flow) stresses that can be used in continuum formulations must be the goals of future studies. These developments would replace the old empirical approaches especially in understandings of fatigue in SMAs.

In summary, theoretical developments must address the couplings of (Robertson *et al.*, 2012; Pelton, 2011; Eggeler *et al.*, 2004; Sedmák *et al.*, 2015): (1) functional fatigue and (2) structural fatigue. Functional fatigue refers to the drifting of superelastic or shape memory responses over cycles, which results from persistent accumulation of slip. As a result, the slip localization and formation of intense shear bands produce structural fatigue damage in the form of nucleation of cracks. Structural fatigue leads to gradual progression to catastrophic fracture. The branch of atomistic simulations that unveil the actual mechanism of concurrent plasticity and transformation is of significant interest (Pfetzing-Micklich *et al.*, 2013). The MD simulations have been insightful for understanding the concepts of slip emission and interactions with twins (Baker and Warner, 2014; Chowdhury *et al.*, 2013, 2014; Horstemeyer *et al.*, 2010; Tang *et al.*, 2010; Zamora *et al.*, 2015; Potirniche *et al.*, 2006) and further work is needed to extend these ideas towards a successful SMA fatigue modeling.

Regarding the understanding of fracture, the determination of driving force in the presence of asymmetric transformation zones, spatially varying phase fractions (martensite and austenite) ahead of the crack tip, and localized dislocation mediated slip remains a challenge. Since the fracture toughness of the SMAs are low compared to structural materials, the efforts to enhance the toughening by introducing secondary ductile phases and with compositionally complex microstructures (similar to developments in high entropy alloys) would be worthwhile.

Acknowledgments

This research is conducted with the financial support from the Nyquist Chair funds, the National Science Foundation (DMR 2104971 and CMMI- 2125821) and the Air Force Office of Scientific Research (FA9550-18-1-0198-Dr. Ali Sayir, PO). Efforts were made to list representative works, but inevitably we are unable to cover all works given the limited scope of the current paper. Particularly, some of the less well known SMAs that have been proposed and their response are not covered. The authors regret any omission that may have resulted for the sake of preserving brevity. Discussions with former graduate students and postdocs on SMA research are gratefully acknowledged.

References

Abut, B., Haghgouyan, B., Karaman, I., Lagoudas, D.C., 2021. Effect of specimen thickness on the fracture toughness of a NiTi shape memory alloy. Shape Memory and Superelasticity 7, 90–100. https://doi.org/10.1007/s40830-021-00312-7.

Abuzaid, W., Wu, Y, Sidharth, R, *et al.*, 2019. FeMnNiAl iron-based shape memory alloy: Promises and challenges. Shape Memory and Superelasticity 5, 263–277. https://doi.org/10.1007/s40830-019-00230-9.

Abuzaid, W., Sehitoglu, H., 2018. Superelasticity and functional fatigue of single crystalline FeNiCoAlTi iron-based shape memory alloy. Materials & Design 160, 642–651.

Abuzaid, W., Sehitoglu, H., 2017a. Critical resolved shear stress for slip and twin nucleation in single crystalline FeNiCoCrMn high entropy alloy. Materials Characterization 129, 288–299.

Abuzaid, W., Sehitoglu, H., 2017b. Functional fatigue of Ni50. 3Ti25Hf24. 7–Heterogeneities and evolution of local transformation strains. Materials Science and Engineering: A 696, 482–492.

Acar, E., Tobe, H., Kaya, I., Karaca, H., Chumlyakov, Y., 2015. Compressive response of Ni 45.3 Ti 34.7 Hf 15 Pd 5 and Ni 45.3 Ti 29.7 Hf 20 Pd 5 shape-memory alloys. Journal of Materials Science 50, 1924–1934.

Adachi, K., Perkins, J., Wayman, C.M., 1986. Type II twins in self-accommodating martensite plate variants in a Cu•Zn•Al shape memory alloy. Acta Metallurgica 34, 2471–2485. https://doi.org/10.1016/0001-6160(86)90150-1.

Ahadi, A., Sun, Q., 2016. Grain size dependence of fracture toughness and crack-growth resistance of superelastic NiTi. Scripta Materialia 113, 171–175. https://doi.org/10.1016/j.scriptamat.2015.10.036.

Ahlers, M., 1986. Martensite and equilibrium phases in Cu-Zn and Cu-Zn-Al alloys. Progress in Materials Science 30, 135–186.

Ahlers, M., 2004. The martensitic transformation. Revista Materia 9, 169–183.

Ahmed, T., Rack, H.J., 1996. Martensitic transformations in Ti-(16–26 at%) Nb alloys. Journal of Materials Science 31, 4267–4276.

Al-Zain, Y., Kim, H., Hosoda, H., Nam, T., Miyazaki, S., 2010. Shape memory properties of Ti–Nb–Mo biomedical alloys. Acta Materialia 58, 4212–4223.

Alkan, S., Sehitoglu, H., 2019a. Prediction of transformation stresses in NiTi shape memory alloy. Acta Materialia 175, 182–195.

Alkan, S., Sehitoglu, H., 2017a. Non-Schmid response of Fe3Al: The twin-antitwin slip asymmetry and non-glide shear stress effects. Acta Materialia 125, 550–566. https://doi.org/10.1016/j.actamat.2016.12.019.

Alkan, S., Sehitoglu, H., 2017b. Dislocation core effects on slip response of NiTi- a key to understanding shape memory. International Journal of Plasticity 97, 126–144. https://doi.org/10.1016/j.ijplas.2017.05.012.

Alkan, S., Sehitoglu, H., 2019b. Plastic flow resistance of NiTiCu shape memory alloy-theory and experiments. Acta Materialia 163, 173–188. https://doi.org/10.1016/j.actamat.2018.09.063.

Alkan, S., Wu, Y., Ojha, A., Sehitoglu, H., 2018a. Transformation stress of shape memory alloy CuZnAl: Non-Schmid behavior. Acta Materialia 149, 220–234. https://doi.org/10.1016/j.actamat.2018.02.011.

Alkan, S., Ojha, A., Sehitoglu, H., 2018b. The complexity of non-Schmid behavior in the CuZnAl shape memory alloy. Journal of the Mechanics and Physics of Solids 114, 238–257.

Alkan, S., Wu, Y., Sehitoglu, H., 2017. Giant non-Schmid effect in NiTi. Extreme Mechanics Letters 15, 38–43. https://doi.org/10.1016/j.eml.2017.05.003.

Andrade, M., Janssen, J., Delaey, L., 1985. Some TEM-observations of fatigued pseudoelastic Cu-Zn-Al alloys. Metallography 18, 107–113. https://doi.org/10.1016/0026-0800(85)90056-4.

Appel, F., Paul, J.D.H., Oehring, M., 2011. Gamma Titanium Aluminide Alloys: Science and Technology. Wiley.

Arróyave, R., *et al.*, 2010. Investigation of the structural stability of Co2NiGa shape memory alloys via ab initio methods. Acta Materialia 58, 5220–5231. https://doi.org/10.1016/j.actamat.2010.05.033.

Atli, K.C., Karaman, I., Noebe, R.D., Maier, H.J., 2011. Comparative analysis of the effects of severe plastic deformation and thermomechanical training on the functional stability of Ti50.5Ni24.5Pd25 high-temperature shape memory alloy. Scripta Materialia 64, 315–318. https://doi.org/10.1016/j.scriptamat.2010.10.022.

Auricchio, F., Taylor, R.L., 1997. Shape-memory alloys: Modelling and numerical simulations of the finite-strain superelastic behavior. Computer Methods in Applied Mechanics and Engineering 143, 175–194.

Auricchio, F., Taylor, R.L., Lubliner, J., 1997. Shape-memory alloys: Macromodelling and numerical simulations of the superelastic behavior. Computer Methods in Applied Mechanics and Engineering 146, 281–312. https://doi.org/10.1016/S0045-7825(96)01232-7.

Au, Y.K., Wayman, C.M., 1972. Thermoelastic behavior of the martensitic transformation in ß′ NiAl alloys. Scripta Metallurgica 6, 1209–1214. https://doi.org/10.1016/0036-9748(72)90233-5.

Ayuela, A., Enkovaara, J., Nieminen, R., 2002. Ab initio study of tetragonal variants in Ni_2MnGa alloy. Journal of Physics: Condensed Matter 14, 5325.

Baker, K.L., Warner, D., 2014. An atomistic investigation into the nature of near threshold fatigue crack growth in aluminum alloys. Engineering Fracture Mechanics 115, 111–121.

Ball, J.M., James, R.D., 1992. Proposed experimental tests of a theory of fine microstructure and the two-well problem. Philosophical Transactions of the Royal Society of London A: Mathematical, Physical and Engineering Sciences 338, 389–450.

Barandiarán, J., *et al.*, 2008. Martensitic transformation in Ni–Fe–Ga alloys. Materials Science and Engineering: A 478, 125–129.

Bartova, B., Wiese, N., Schryvers, D., Chapman, J.N., Ignacova, S., 2008. Microstructure of precipitates and magnetic domain structure in an annealed shape memory alloy. Acta Materialia 56, 4470–4476. https://doi.org/10.1016/j.actamat.2008.05.006.

Baskes, M., 1997. Determination of modified embedded atom method parameters for nickel. Materials Chemistry and Physics 50, 152–158.

Bataillard, L., Bidaux, J.-E., Gotthardt, R., 1998. Interaction between microstructure and multiple-step transformation in binary NiTi alloys using in-situ transmission electron microscopy observations. Philosophical magazine A 78, 327–344.

Baxevanis, T., Chemisky, Y., Lagoudas, D.C., 2012. Finite element analysis of the plane strain crack-tip mechanical fields in pseudoelastic shape memory alloys. Smart Materials and Structures 21. 094012. https://doi.org/10.1088/0964-1726/21/9/094012.

Baxevanis, T., Parrinello, A.F., Lagoudas, D.C., 2013a. On the fracture toughness enhancement due to stress-induced phase transformation in shape memory alloys. International Journal of Plasticity 50, 158–169. https://doi.org/10.1016/j.ijplas.2013.04.007.

Baxevanis, T., Landis, C.M., Lagoudas, D.C., 2013b. On the fracture toughness of pseudoelastic shape memory alloys. Journal of Applied Mechanics 81.https://doi.org/10.1115/1.4025139.

Baxevanis, T., Landis, C.M., Lagoudas, D.C., 2014. On the effect of latent heat on the fracture toughness of pseudoelastic shape memory alloys. Journal of Applied Mechanics 81.https://doi.org/10.1115/1.4028191.

Bechtold, C., Chluba, C., De Miranda, R.L., Quandt, E., 2012. High cyclic stability of the elastocaloric effect in sputtered TiNiCu shape memory films. Applied Physics Letters 101. 091903.

Benafan, O., *et al.*, 2014a. Thermomechanical cycling of a NiTi shape memory alloy-macroscopic response and microstructural evolution. International Journal of Plasticity 56, 99–118.

Benafan, O., *et al.*, 2013a. Temperature-dependent behavior of a polycrystalline NiTi shape memory alloy around the transformation regime. Scripta Materialia 68, 571–574.

Benafan, O., *et al.*, 2013b. Temperature dependent deformation of the B2 austenite phase of a NiTi shape memory alloy. International Journal of Plasticity 51, 103–121. https://doi.org/10.1016/j.ijplas.2013.06.003.

Benafan, O., Gaydosh, D.J., 2017. High temperature shape memory alloy Ni50.3Ti29.7Hf20 torque tube actuators. Smart Materials and Structures 26.https://doi.org/10.1088/1361-665X/aa7ef4.

Benafan, O., *et al.*, 2014b. Mechanical and functional behavior of a Ni-rich Ni50. 3Ti29. 7Hf20 high temperature shape memory alloy. Intermetallics 50, 94–107.

Benafan, O., Noebe, R., Padula, S., Vaidyanathan, R., 2012. Microstructural response during isothermal and isobaric loading of a precipitation-strengthened Ni-29.7 Ti-20Hf high-temperature shape memory alloy. Metallurgical and Materials Transactions A 43, 4539–4552.

Bergeon, N., Guenin, G., Esnouf, C., 1998a. Microstructural analysis of the stress-induced υ martensite in a Fe–Mn–Si–Cr–Ni shape memory alloy: Part I—calculated description of the microstructure. Materials Science and Engineering: A 242, 77–86.

Bergeon, N., Guenin, G., Esnouf, C., 1998b. Microstructural analysis of the stress-induced υ martensite in a Fe–Mn–Si–Cr–Ni shape memory alloy: Part II: Transformation reversibility. Materials Science and Engineering: A 242, 87–95.

Berti, F., *et al.*, 2021. Nickel–Titanium peripheral stents: Which is the best criterion for the multi-axial fatigue strength assessment. Journal of the Mechanical Behavior of Biomedical Materials 113. 104142. https://doi.org/10.1016/j.jmbbm.2020.104142.

Bewerse, C., Gall, K.R., McFarland, G.J., Zhu, P., Brinson, L.C., 2013. Local and global strains and strain ratios in shape memory alloys using digital imagecorrelation. Materials Science and Engineering: A 568, 134–142.

Bhattacharya, K., 2003. Microstructure of Martensite: Why it Forms and How it Gives Rise to the Shape-Memory Effect. vol. 2. Oxford University Press.

Bhattacharya, K., Conti, S., Zanzotto, G., Zimmer, J., 2004. Crystal symmetry and the reversibility of martensitic transformations. Nature 428, 55–59.

Bidaux, J.-E., Schaller, R., Benoit, W., 1989. Study of the hcp-fcc phase transition in cobalt by acoustic measurements. Acta Metallurgica 37, 803–811.

Biesiekierski, A., Wang, J., Gepreel, M.A.-H., Wen, C., 2012. A new look at biomedical Ti-based shape memory alloys. Acta Biomaterialia 8, 1661–1669.

Bigelow, G.S., Garg, A., Padula Ii, S.A., Gaydosh, D.J., Noebe, R.D., 2011. Load-biased shape-memory and superelastic properties of a precipitation strengthened high-temperature Ni50.3Ti29.7Hf20 alloy. Scripta Materialia 64, 725–728. https://doi.org/10.1016/j.scriptamat.2010.12.028.

Bigelow, G.S., Padula II, S.A., Garg, A., Gaydosh, D., Noebe, R.D., 2010. Characterization of ternary NiTiPd high-temperature shape-memory alloys under load-biased thermal cycling. Metallurgical and Materials Transactions A 41, 3065–3079.

Birman, V., 1998. On mode I fracture of shape memory alloy plates. Smart Materials and Structures 7, 433–437. https://doi.org/10.1088/0964-1726/7/4/001.

Biswas, A., Krishnan, M., 2010. Deformation studies of ferromagnetic shape memory alloy. Physics Procedia 10, 105–110. https://doi.org/10.1016/j.phpro.2010.11.083.

Blanter, M.S., Golovin, I.S., Neuhäuser, H., Sinning, H.-R., 2007. Internal Friction in Metallic Materials: A Handbook. Berlin Heidelberg: Springer, pp. 121–155.

Bogers, A.J., Burgers, W.G., 1964. Partial dislocations on the {110} planes in the BCC lattice and the transition of the FCC into the BCC lattice. Acta Metallurgica 12, 255–261.

Bönisch, M., *et al.*, 2013. Thermal stability and phase transformations of martensitic Ti–Nb alloys. Science and Technology of Advanced Materials 14 (5).

Bonnot, E., Romero, R., Manosa, L., Vives, E., Planes, A., 2008. Elastocaloric effect associated with the martensitic transition in shape-memory alloys. Physical Review Letters 100. 125901. https://doi.org/10.1103/PhysRevLett.100.125901.

Bouvet, C., Calloch, S., Lexcellent, C., 2004. A phenomenological model for pseudoelasticity of shape memory alloys under multiaxial proportional and nonproportional loadings. European Journal of Mechanics-A/Solids 23, 37–61.

Bowles, J., Mackenzie, J., 1954. The crystallography of martensite transformations I. Acta metallurgica 2, 129–137.

Boyd, J.G., Lagoudas, D.C., 1996. A thermodynamical constitutive model for shape memory materials. Part I. The monolithic shape memory alloy. International Journal of Plasticity 12, 805–842.

Bozzolo, G., Noebe, R.D., Mosca, H.O., 2005. Atomistic modeling of Pd site preference in NiTi. Journal of Alloys and Compounds 386, 125–138. https://doi.org/10.1016/j.jallcom.2004.05.015.

Brill, T., Mittelbach, S., Assmus, W., Mullner, M., Luthi, B., 1991. Elastic properties of NiTi. Journal of Physics: Condensed Matter 3, 9621.

Brinson, L.C., 1993. One-dimensional constitutive behavior of shape memory alloys: Thermomechanical derivation with non-constant material functions and redefined martensite internal variable. Journal of Intelligent Material Systems and Structures 4, 229–242. https://doi.org/10.1177/1045389x9300400213.

Brown, P., *et al.*, 2002. The crystal structure and phase transitions of the magnetic shape memory compound Ni2MnGa. Journal of Physics: Condensed Matter 14.10159.

Brown, L.C., 1979. The fatigue of pseudoelastic single crystals of α-CuAlNi. Metallurgical Transactions A 10, 217–224. https://doi.org/10.1007/BF02817631.

Brown, L.C., 1982. The fatigue of pseudoelastic polycrystalline β-cuznsn. Metallurgical Transactions A 13, 25–31. https://doi.org/10.1007/BF02642412.

Buchheit, T.E., Wert, J.A., 1996. Predicting the orientation-dependent stress-induced transformation and detwinning response of shape memory alloy single crystals. Metallurgical and Materials Transactions A (Physical Metallurgy and Materials Science) 27A, 269–279.

Buehler, W.J., Gilfrich, J., Wiley, R., 1963. Effect of low-temperature phase changes on the mechanical properties of alloys near composition TiNi. Journal of Applied Physics 34, 1475–1477.

Buenconsejo, P.J.S., Kim, H.Y., Hosoda, H., Miyazaki, S., 2009. Shape memory behavior of Ti–Ta and its potential as a high-temperature shape memory alloy. Acta Materialia 57, 1068–1077.

Burgers, W., 1934. On the process of transition of the cubic-body-centered modification into the hexagonal-close-packed modification of zirconium. Physica 1, 561–586.

Bilby, B., Crocker, A. ,1965. Proceedings of the Royal Society of London A: Mathematical, Physical and Engineering Sciences, 288, 1413, pp. 240–255. The Royal Society.

Cai, W., Tanaka, S., Otsuka, K., 2000. Materials Science Forum. Trans Tech Publ, 327-328; pp. 279-282

Calkins, F., Mabe, J., Ruggeri, R., 2008. ASME Conference on Smart Materials, Adaptive Structures and Intelligent Systems. American Society of Mechanical Engineers Digital Collection. pp. 885–895.

Callaway, J.D., *et al.*, 2006. Magnetic shape memory in Ni2MnGa as influenced by applied stress. Applied Physics Letters 89. 221905.

Canadinc, D., *et al.*, 2017. On the deformation response and cyclic stability of Ni50Ti35Hf15 high temperature shape memory alloy wires. Scripta Materialia 135, 92–96.

Cantor, B., Chang, I., Knight, P., Vincent, A., 2004. Microstructural development in equiatomic multicomponent alloys. Materials Science and Engineering: A 375, 213–218.

Cao, H., Wu, M.H., Zhou, F., McMeeking, R.M., Ritchie, R.O., 2020. The influence of mean strain on the high-cycle fatigue of Nitinol with application to medical devices. Journal of the Mechanics and Physics of Solids 143.https://doi.org/10.1016/j.jmps.2020.104057.104057.

Carrez, P., Ferré, D., Cordier, P., 2007. Peierls–Nabarro model for dislocations in MgSiO3 post-perovskite calculated at 120 GPa from first principles. Philosophical Magazine 87, 3229–3247.

Chen, C.-H., Chen, Y.-J., 2019. Shape memory characteristics of (TiZrHf)50Ni25Co10Cu15 high entropy shape memory alloy. Scripta Materialia 162, 185–189. https://doi.org/10.1016/j.scriptamat.2018.11.023.

Chen, Y., Jiang, H.C., Liu, S.W., Rong, L.J., Zhao, X.Q., 2009. Damping capacity of TiNi-based shape memory alloys. Journal of Alloys and Compounds 482, 151–154. https://doi.org/10.1016/j.jallcom.2009.03.148.

Chen, X., Moumni, Z., He, Y., Zhang, W., 2014a. A three-dimensional model of magneto-mechanical behaviors of martensite reorientation in ferromagnetic shape memory alloys. Journal of the Mechanics and Physics of Solids 64, 249–286. https://doi.org/10.1016/j.jmps.2013.11.005.

Chen, Q., Andrawes, B., Sehitoglu, H., 2014b. Thermomechanical testing of FeNiCoTi shape memory alloy for active confinement of concrete. Smart Materials and Structures 23. 055015.

Chmielus, M., Zhang, X., Witherspoon, C., Dunand, D., Müllner, P., 2009. Giant magnetic-field-induced strains in polycrystalline Ni–Mn–Ga foams. Nature Materials 8, 863–866.

Chowdhury, P., Canadinc, D., Sehitoglu, H., 2017. On deformation behavior of Fe-Mn based structural alloys. Materials Science and Engineering: R: Reports 122, 1–28.

Chowdhury, P., Patriarca, L., Ren, G., Sehitoglu, H., 2016. Molecular dynamics modeling of NiTi superelasticity in presence of nanoprecipitates. International Journal of Plasticity 81, 152–167.

Chowdhury, P., Ren, G., Sehitoglu, H., 2015. NiTi superelasticity via atomistic simulations. Philosophical Magazine Letters 95, 574–586. https://doi.org/10.1080/09500839.2015.1123819.

Chowdhury, P., Sehitoglu, H., 2017a. Deformation physics of shape memory alloys – Fundamentals at atomistic frontier. Progress in Materials Science 88, 49–88. https://doi.org/10.1016/j.pmatsci.2017.03.003.

Chowdhury, P., Sehitoglu, H., 2016. Significance of slip propensity determination in shape memory alloys. Scripta Materialia 119, 82–87.

Chowdhury, P., Sehitoglu, H., 2017b. A revisit to atomistic rationale for slip in shape memory alloys. Progress in Materials Science 85, 1–42.

Chowdhury, P.B., Sehitoglu, H., Rateick, R.G., Maier, H.J., 2013. Modeling fatigue crack growth resistance of nanocrystalline alloys. Acta materialia 61, 2531–2547.

Chowdhury, P.B., Sehitoglu, H., Rateick, R.G., 2014. Predicting fatigue resistance of nano-twinned materials: Part I–Role of cyclic slip irreversibility and Peierls stress. International Journal of Fatigue 68, 277–291.
Christian, J.W., 1983. Some surprising features of the plastic deformation of body-centered cubic metals and alloys. Metallurgical Transactions A 14, 1237–1256. https://doi.org/10.1007/BF02664806.
Christian, J.W., 2002. The Theory of Transformations in Metals and Alloys (Part 1 and Part 2). Pergamon.
Christ, D., Reese, S., 2009. A finite element model for shape memory alloys considering thermomechanical couplings at large strains. International Journal of solids and Structures 46, 3694–3709.
Chrobak, D., Morawiec, H., 2001. Thermodynamic analysis of the martensitic transformation in plastically deformed NiTi alloy. Scripta Materialia 44, 725–730.
Chulist, R., *et al*., 2012. Diffraction study of bending-induced polysynthetic twins in 10M modulated Ni-Mn-Ga martensite. Journal of Applied Physics 112.(063517-063517-063517).
Chumlyakov, Y., *et al*., 2013. Shape memory effect and high-temperature superelasticity in high-strength single crystals. Journal of Alloys and Compounds 577, S393–S398.
Chumlyakov, Y., *et al*., 2008. High-temperature superelasticity in CoNiGa, CoNiAl, NiFeGa, and TiNi monocrystals. Russian Physics Journal 51, 1016–1036. https://doi.org/10.1007/s11182-009-9143-5.
Chumlyakov, Y.I., *et al*., 2016. Unusual reversible twinning modes and giant superelastic strains in FeNiCoAlNb single crystals. Scripta Materialia 119, 43–46. https://doi.org/10.1016/j.scriptamat.2016.03.027.
Coughlin, D., *et al*., 2012. Characterization of the microstructure and mechanical properties of a 50.3 Ni–29.7 Ti–20Hf shape memory alloy. Scripta Materialia 67, 112–115.
Craciunescu, C., Kishi, Y., Lograsso, T.A., Wuttig, M., 2002. Martensitic transformation in Co2NiGa ferromagnetic shape memory alloys. Scripta Materialia 47, 285–288. https://doi.org/10.1016/s1359-6462(02)00148-3.
Crone, W.C., Shield, T.W., 2001. Experimental study of the deformation near a notch tip in copper and copper–beryllium single crystals. Journal of the Mechanics and Physics of Solids 49, 2819–2838. https://doi.org/10.1016/S0022-5096(01)00080-1.
Cui, J., *et al*., 2006. Combinatorial search of thermoelastic shape-memory alloys with extremely small hysteresis width. Nature materials 5, 286–290.
Cui, J., *et al*., 2012. Demonstration of high efficiency elastocaloric cooling with large ΔT using NiTi wires. Applied Physics Letters 101. 073904.
Dadda, J., Maier, H.J., Karaman, I., Karaca, H.E., Chumlyakov, Y.I., 2006. Pseudoelasticity at elevated temperatures in [0 0 1] oriented Co49Ni21Ga30 single crystals under compression. Scripta Materialia 55, 663–666. https://doi.org/10.1016/j.scriptamat.2006.07.005.
Dalle, F., Perrin, E., Vermaut, P., Masse, M., Portier, R., 2002. Interface mobility in Ni49.8Ti42.2Hf8 shape memory alloy. Acta Materialia 50, 3557–3565. https://doi.org/10.1016/S1359-6454(02)00151-9.
Dalle, F., *et al*., 2003. Ni49.8Ti42.2Hf8 shape memory alloy strips production by the twin roll casting technique. Materials Science and Engineering: A 346, 320–327. https://doi.org/10.1016/s0921-5093(02)00548-8.
Delaey, L., Ortin, J., Van Humbeeck 1987. Phase Transformations 87, 60–66.
Daly, S., Miller, A., Ravichandran, G., Bhattacharya, K., 2007. An experimental investigation of crack initiation in thin sheets of nitinol. Acta Materialia 55, 6322–6330. https://doi.org/10.1016/j.actamat.2007.07.038.
Damiani, C., Lovey, F.C., Sade, M., 2002. Plastic deformation under compression of Cu-Zn-Al martensitic single crystals. Materials Science and Engineering A (Structural Materials: Properties, Microstructure and Processing) A323, 436–444.
Damiani, C., Sade, M., Lovey, F.C., 2003. Fatigue in Cu-Zn-Al single crystals during pseudoelastic cycling: In situ observations by SEM and optical microscopy. Journal de Physique IV France 112, 623–626.
Daw, M.S., Baskes, M.I., 1984. Embedded-atom method: Derivation and application to impurities, surfaces, and other defects in metals. Physical Review B 29, 6443.
Dayananda, G.N., Rao, M.S., 2008. Effect of strain rate on properties of superelastic NiTi thin wires. Materials Science and Engineering: A 486, 96–103. https://doi.org/10.1016/j.msea.2007.09.006.
De Graef, M., Willard, M.A., McHenry, M.E., Zhu, Y., 2001. In-situ Lorentz TEM cooling study of magnetic domain configurations in Ni 2 MnGa. IEEE Transactions on Magnetics 37, 2663–2665.
Delaey, L., Janssen, J., Van de Mosselaer, D., Dullenkopf, G., Deruyttere, A., 1978. Fatigue properties of pseudoelastic Cu ■ Zn ■ Al alloys. Scripta Metallurgica 12, 373–376. https://doi.org/10.1016/0036-9748(78)90302-2.
Dejonghe, W., Batist, D., 1976. Factors Affecting the Internal Friction Peak Due to Thermoelastic Martensitic Transformation.
Delaey, L., *et al*., 1981. Cu-Zn-Al shape memory alloys. Metals Forum 4, 164–175.
Delville, R., Malard, B., Pilch, J., Sittner, P., Schryvers, D., 2011. Transmission electron microscopy investigation of dislocation slip during superelastic cycling of Ni–Ti wires. International Journal of Plasticity 27, 282–297.
DesRoches, R., McCormick, J., Delemont, M., 2004. Cyclic properties of superelastic shape memory alloy wires and bars. Journal of Structural Engineering 130, 38–46. https://doi.org/10.1061/(ASCE)0733-9445(2004)130:1(38).
Dezerald, L., Rodney, D., Clouet, E., Ventelon, L., Willaime, F., 2016. Plastic anisotropy and dislocation trajectory in bcc metals. Nature Communications 7.https://doi.org/10.1038/ncomms11695.11695.
Dilibal, S., Sehitoglu, H., Hamilton, R., Maier, H., Chumlyakov, Y., 2011a. On the volume change in Co–Ni–Al during pseudoelasticity. Materials Science and Engineering: A 528, 2875–2881.
Dilibal, S., Sehitoglu, H., Hamilton, R.F., Maier, H.J., Chumlyakov, Y., 2011b. Corrigendum to ‚ÄúOn the volume change in Co‚ÄìNi‚ÄìAl during pseudoelasticity‚Äù [Mater. Sci. Eng. A 528 (2011) 2875‚Äì2881]. Materials Science and Engineering: A 528, 4268. https://doi.org/10.1016/j.msea.2011.02.001.
Dogan, E., Karaman, I., Chumlyakov, Y.I., Luo, Z.P., 2011. Microstructure and martensitic transformation characteristics of CoNiGa high temperature shape memory alloys. Acta Materialia 59, 1168–1183. https://doi.org/10.1016/j.actamat.2010.10.050.
Dolce, M., Cardone, D., 2001. Mechanical behaviour of shape memory alloys for seismic applications 2. Austenite NiTi wires subjected to tension. International Journal of Mechanical Sciences 43, 2657–2677.
Duerig, T.W., Melton, K., Stöckel, D., 2013. Engineering Aspects of Shape Memory Alloys. Butterworth-Heinemann.
Duesbery, M.S., 1989. In: Nabarro, F.R.N. (Ed.), Dislocations in Solids, vol. 8. Elsevier Science Publishers B.V.
Duesbery, M.S., 1984. On non-glide stresses and their influence on the screw dislocation core in body-centred cubic metals. I. The Peierls stress. Proceedings of the Royal Society of London A: Mathematical, Physical and Engineering Sciences 392, 145–173.
Duesbery, M., Richardson, G., 1991. The dislocation core in crystalline materials. Critical Reviews in Solid State and Material Sciences 17, 1–46.
Duesbery, M.S., Vitek, V., 1998. Plastic anisotropy in b.c.c. transition metals. Acta Materialia 46, 1481–1492. https://doi.org/10.1016/S1359-6454(97)00367-4.
Dunand, D.C., Müllner, P., 2011. Size effects on magnetic actuation in Ni-Mn-Ga shape-memory alloys. Advanced Materials 23, 216–232.
D'Silva, G.J., Goanta, V., Ciocanel, C., 2021. Fracture toughness evaluation of Ni2MnGa magnetic shape memory alloys by Vickers micro indentation. Engineering Fracture Mechanics 247. 107655. https://doi.org/10.1016/j.engfracmech.2021.107655.
Efstathiou, C., *et al*., 2004. Large reduction in critical stress in Co–Ni–Al upon repeated transformation. Scripta Materialia 51, 979–985.
Efstathiou, C., Sehitoglu, H., 2008. Local transformation strain measurements in precipitated NiTi single crystals. Scripta Materialia 59, 1263–1266.
Efstathiou, C., Sehitoglu, H., Kurath, P., Foletti, S., Davoli, P., 2007. Fatigue response of NiFeGa single crystals. Scripta Materialia 57, 409–412.
Efstathiou, C., Sehitoglu, H., Lambros, J., 2010. Multiscale strain measurements of plastically deforming polycrystalline titanium: Role of deformation heterogeneities. International Journal of Plasticity 26, 93–106. https://doi.org/10.1016/j.ijplas.2009.04.006.
Eggeler, G., Hornbogen, E., Yawny, A., Heckmann, A., Wagner, M., 2004. Structural and functional fatigue of NiTi shape memory alloys. Materials Science and Engineering: A 378, 24–33.

Elahinia, M.H., Hashemi, M., Tabesh, M., Bhaduri, S.B., 2012. Manufacturing and processing of NiTi implants: A review. Progress in Materials Science 57, 911–946. https://doi.org/10.1016/j.pmatsci.2011.11.001.
Enami, K., Nenno, S., Shimizu, K., 1973. Crystal structure and internal twins of the Ni-36.8 at% Al martensite. Transactions of the Japan Institute of Metals 14, 161–165. https://doi.org/10.2320/matertrans1960.14.161.
Engel, E., Dreizler, R.M., 2011. Density Functional Theory: An Advanced Course. Springer Science & Business Media.
Enkovaara, J., Heczko, O., Ayuela, A., Nieminen, R.M., 2003. Coexistence of ferromagnetic and antiferromagnetic order in Mn-doped Ni 2 MnGa. Physical Review B 67. 212405.
Entel, P., *et al.*, 2013. Optimization of smart Heusler alloys from first principles. Journal of Alloys and Compounds 577, S107–S112.
Evirgen, A., Karaman, I., Santamarta, R., Pons, J., Noebe, R.D., 2015. Microstructural characterization and shape memory characteristics of the Ni50.3Ti34.7Hf15 shape memory alloy. Acta Materialia 83, 48–60. https://doi.org/10.1016/j.actamat.2014.09.027.
Ezaz, T., Sehitoglu, H., 2011. Type II detwinning in NiTi. Applied Physics Letters 98. 141906.
Ezaz, T., Sehitoglu, H., Maier, H.J., 2012a. Energetics of (114) twinning in B2 NiTi under coupled shear and shuffle. Acta Materialia 60, 339–348.
Ezaz, T., Sehitoglu, H., Abuzaid, W., Maier, H., 2012b. Higher order twin modes in martensitic NiTi-The (20-1) Case. Materials Science and Engineering: A.
Ezaz, T., Sehitoglu, H., Maier, H.J., 2011. Energetics of twinning in martensitic NiTi. Acta Materialia 59, 5893–5904. https://doi.org/10.1016/j.actamat.2011.05.063.
Ezaz, T., Wang, J., Sehitoglu, H., Maier, H.J., 2013. Plastic deformation of NiTi shape memory alloys. Acta Materialia 61, 67–78. https://doi.org/10.1016/j.actamat.2012.09.023.
Falvo, A., Furgiuele, F., Leonardi, A., Maletta, C., 2009. Stress-induced martensitic transformation in the crack tip region of a NiTi alloy. Journal of Materials Engineering and Performance 18, 679–685. https://doi.org/10.1007/s11665-009-9361-6.
Farkas, D., Roqueta, D., Vilette, A., Ternes, K., 1996. Atomistic simulations in ternary Ni-Ti-Al alloys. Modelling and Simulation in Materials Science and Engineering 4, 359.
Favier, D., Liu, Y., 2000. Restoration by rapid overheating of thermally stabilized martensite of NiTi shape memory alloys. Journal of Alloys & Compounds 297, 114–121.
Figueiredo, A.M., Modenesi, P., Buono, V., 2009. Low-cycle fatigue life of superelastic NiTi wires. International Journal of Fatigue 31, 751–758.
Finkenstadt, D., Johnson, D.D., 2006. Solute/defect-mediated pathway for rapid nanoprecipitation in solid solutions: γ surface analysis in fcc Al-Ag. Physical Review B 73. 024101.
Firstov, G.S., Kosorukova, T.A., Koval, Y.N., Odnosum, V.V., 2015a. High entropy shape memory alloys. Materials Today: Proceedings 2, S499–S503. https://doi.org/10.1016/j.matpr.2015.07.335.
Firstov, G.S., Kosorukova, T.A., Koval, Y.N., Verhovlyuk, P.A., 2015b. Directions for high-temperature shape memory alloys' improvement: Straight way to high-entropy materials? Shape Memory and Superelasticity 1, 400–407. https://doi.org/10.1007/s40830-015-0039-7.
Firstov, G.S., Van Humbeeck, J., Koval, Y.N., 2004a. High-temperature shape memory alloys: Some recent developments. Materials Science and Engineering: A 378, 2–10.
Firstov, G., *et al.*, 2015c. Electronic and crystal structure of the high entropy TiZrHfCoNiCu intermetallics undergoing martensitic transformation. MATEC Web of Conferences 33. 06006.
Firstov, G., Van Humbeeck, J., Koval, Y.N., 2004b. Comparison of high temperature shape memory behaviour for ZrCu-based, Ti–Ni–Zr and Ti–Ni–Hf alloys. Scripta Materialia 50, 243–248.
Freed, Y., Banksslls, L., 2007. Crack growth resistance of shape memory alloys by means of a cohesive zone model. Journal of the Mechanics and Physics of Solids 55, 2157–2180. https://doi.org/10.1016/j.jmps.2007.03.002.
Fukui, Y., Inamura, T., Hosoda, H., Wakashima, K., Miyazaki, S., 2004. Mechanical properties of a Ti-Nb-Al shape memory alloy. Materials Transactions 45, 1077–1082.
Funakubo, H., Kennedy, J., 1987. Shape memory alloys. Gordon and Breach, xii + 275, 15 x 22 cm, Illustrated.
Fu, H., Yu, H.J., Teng, B.H., Zhang, X.Y., Zu, X.T., 2009. Magnetic properties and magnetic entropy change of Co50Ni22Ga28 alloy. Journal of Alloys and Compounds 474, 595–597. https://doi.org/10.1016/j.jallcom.2008.07.028.
Gall, K., Jacobus, K., Sehitoglu, H., Maier, H.J., 1998a. Stress-induced martensitic phase transformations in polycrystalline CuZnAl shape memory alloys under different stress states. Metallurgical and Materials Transactions A 29, 765–773. https://doi.org/10.1007/s11661-998-0267-y.
Gall, K., Sehitoglu, H., Chumlyakov, Y.I., Kireeva, I.V., 1998b. Pseudoelastic cyclic stress-strain response of over-aged single crystal Ti-50.8 at% Ni. Scripta Materialia 40, 7–12.
Gall, K., Sehitoglu, H., Chumlyakov, Y.I., Zuev, Y.L., Karaman, I., 1998c. The role of coherent precipitates in martensitic transformations in single crystal and polycrystalline Ti-50.8at%Ni. Scripta Materialia 39, 699–705.
Gall, K., Sehitoglu, H., Chumlyakov, Y.I., Kireeva, I.V., Maier, H.J., 1999d. The influence of aging on critical transformation stress levels and martensite start temperatures in NiTi: Part II—discussion of experimental results. Journal of Engineering Materials and Technology 121, 28–37.
Gall, K., Lim, T.J., McDowell, D.L., Sehitoglu, H., Chumlyakov, Y.I., 2000a. The role of intergranular constraint on the stress-induced martensitic transformation in textured polycrystalline NiTi. International Journal of Plasticity 16, 1189–1214.
Gall, K., Maier, H., 2002. Cyclic deformation mechanisms in precipitated NiTi shape memory alloys. Acta Materialia 50, 4643–4657.
Gall, K., Sehitoglu, H., Chumlakov, Y., 2000b. SPIE's 7 th International Symposium on Smart Structures and Materials and SPIE's 5 th International Symposium on Nondestructive Evaluation and Health Monitoring of Aging Infrastructure.
Gall, K., Sehitoglu, H., Chumlyakov, Y., Kireeva, I.V., Maier, H.J., 1999a. The influence of aging on critical transformation stress levels and martensite start temperatures in NiTi: Part II - Discussion of experimental results. Trans ASME 121, 28–37.
Gall, K., Sehitoglu, H., Chumlyakov, Y.I., Kireeva, I.V., Maier, H.J., 1999b. The influence on critical transformation stress levels and martensite start temperatures in NiTi: Part I-aged microstructure and micro-mechanical modeling. ASME Journal of Engineering Materials and Technology 121, 19–27.
Gall, K., Sehitoglu, H., Chumlyakov, Y.I., Kireeva, I., 1999c. Tension–compression asymmetry of the stress–strain response in aged single crystal and polycrystalline NiTi. Acta Materialia 47, 1203–1217.
Gall, K., *et al.*, 1999d. Micromechanics and Micromechanisms of Deformation and Fracture: In Honor of Professor Ali S Argon, first to second ed. Elsevier. pp. 85–92.
Gall, K., Sehitoglu, H., 1999. The role of texture in tension-compression asymmetry in polycrystalline NiTi (vol 15, pg 69, 1999). International Journal of Plasticity 15, 781.
Gall, K., Yang, N., Sehitoglu, H., Chumlyakov, Y., 2001. Fracture of precipitated NiTi shape memory alloys. International Journal of Fracture 109, 189–207. https://doi.org/10.1023/A:1011069204123.
Gall, K., *et al.*, 2008. Effect of microstructure on the fatigue of hot-rolled and cold-drawn NiTi shape memory alloys. Materials Science and Engineering: A 486, 389–403. https://doi.org/10.1016/j.msea.2007.11.033.
Gall, K.A., 1998. The Effect of Stress State and Precipitation on Stress-Induced Martensitic Transformations in Polycrystalline and Single Crystal Shape Memory Alloys: Experiments and Micro-Mechanical Modeling Dissertation Thesis. University of Illinois at Urbana-Champaign.
Geetha, M., Singh, A., Asokamani, R., Gogia, A., 2009. Ti based biomaterials, the ultimate choice for orthopaedic implants–a review. Progress in Materials Science 54, 397–425.
Gerstein, G., Firstov, G.S., Kosorukova, T.A., Koval, Y.N., Maier, H.J., 2018. Development of B2 shape memory intermetallics beyond NiAl, CoNiAl and CoNiGa. Shape Memory and Superelasticity 4, 360–368. https://doi.org/10.1007/s40830-018-0180-1.
Gil, F., Guilemany, J., 1992. The determination of the electron to atom ratio interval corresponding to the change in the martensitic structure from α' to β' in Cuznal shape memory alloys. Materials Research Bulletin 27, 117–122.
Gludovatz, B., *et al.*, 2014. A fracture-resistant high-entropy alloy for cryogenic applications. Science 345, 1153–1158.
Golberg, D., *et al.*, 1995a. Characteristics of Ti 50 Pd 30 Ni 20 high-temperature shape memory alloy. Intermetallics 3, 35–46.
Golberg, D., *et al.*, 1995b. High-temperature shape memory effect in Ti 50 Pd 50 − x Ni x (x= 10, 15, 20) alloys. Materials Letters 22, 241–248.
Gollerthan, S., Herberg, D., Baruj, A., Eggeler, G., 2008. Compact tension testing of martensitic/pseudoplastic NiTi shape memory alloys. Materials Science and Engineering: A 481–482, 156–159. https://doi.org/10.1016/j.msea.2007.03.126.
Gollerthan, S., *et al.*, 2009. Fracture mechanics and microstructure in NiTi shape memory alloys. Acta Materialia 57, 1015–1025. https://doi.org/10.1016/j.actamat.2008.10.055.
Goo, E., Duerig, T., Melton, K., Sinclair, R., 1985. Mechanical twinning in Ti50Ni47Fe3 and Ti49Ni51 alloys. Acta Metallurgica 33, 1725–1733.

Gou, L., Liu, Y., Ng, T.Y., 2014. An investigation on the crystal structures of Ti 50 Ni 50 − x Cu x shape memory alloys based on density functional theory calculations. Intermetallics 53, 20–25.
Gou, L., Liu, Y., Ng, T.Y., 2015. Effect of Cu content on atomic positions of Ti50Ni50–xCux shape memory alloys based on density functional theory calculations. Metals 5, 2222–2235.
Guiu, F., 1969. Slip asymmetry in molybdenum single crystals deformed in direct shear. Scripta Metallurgica 3, 449–454. https://doi.org/10.1016/0036-9748(69)90129-X.
Gupta, S.P., Johnson, A.A., 1973. Morphology and crystallography of β' martensite in TiNi alloys. Transactions of the Japan Institute of Metals 14, 292–302.
Gutkin, M.Y., Ovid'ko, I., Skiba, N., 2007. Mechanism of deformation-twin formation in nanocrystalline metals. Physics of the Solid State 49, 874–882.
Haghgouyan, B., Hayrettin, C., Baxevanis, T., Karaman, I., Lagoudas, D.C., 2019. Fracture toughness of NiTi–Towards establishing standard test methods for phase transforming materials. Acta Materialia 162, 226–238. https://doi.org/10.1016/j.actamat.2018.09.048.
Haghgouyan, B., Shafaghi, N., Aydıner, C.C., Anlas, G., 2016. Experimental and computational investigation of the effect of phase transformation on fracture parameters of an SMA. Smart Materials and Structures 25.https://doi.org/10.1088/0964-1726/25/7/075010. 075010.
Hamilton, R.F., Efstathiou, C., Sehitoglu, H., Chumlyakov, Y., 2006a. Thermal and stress-induced martensitic transformations in NiFeGa single crystals under tension and compression. Scripta Materialia 54, 465–469. https://doi.org/10.1016/j.scriptamat.2005.10.003.
Hamilton, R., Sehitoglu, H., Aslantas, K., Efstathiou, C., Maier, H., 2008. Inter-martensite strain evolution in NiMnGa single crystals. Acta materialia 56, 2231–2236.
Hamilton, R.F., Sehitoglu, H., Chumlyakov, Y., Maier, H.J., 2004. Stress dependence of the hysteresis in single crystal NiTi alloys. Acta Materialia 52, 3383–3402.
Hamilton, R.F., Sehitoglu, H., Efstathiou, C., Maier, H.J., Chumlyakov, Y., 2006b. Pseudoelasticity in Co–Ni–Al single and polycrystals. Acta Materialia 54, 587–599. https://doi.org/10.1016/j.actamat.2005.09.025.
Hamilton, R.F., *et al*., 2005. Transformation of Co–Ni–Al single crystals in tension. Scripta Materialia 53, 131–136. https://doi.org/10.1016/j.scriptamat.2005.01.032.
Hamilton, R.F., Sehitoglu, H., Efstathiou, C., Maier, H.J., 2007a. Mechanical response of NiFeGa alloys containing second-phase particles. Scripta Materialia 57, 497–499. https://doi.org/10.1016/j.scriptamat.2007.05.024.
Hamilton, R.F., Sehitoglu, H., Efstathiou, C., Maier, H.J., 2007b. Inter-martensitic transitions in Ni–Fe–Ga single crystals. Acta Materialia 55, 4867–4876. https://doi.org/10.1016/j.actamat.2007.05.003.
Hanada, S., Watanabe, S., Sato, T., Izumi, O., 1981. Deformation of Fe3Al0.8Si0.2 with DO3 structure. Transactions of the Japan Institute of Metals 22, 873–881.
Han, X., Zou, W., Wang, R., Zhang, Z., Yang, D., 1996. Structure and substructure of martensite in a Ti 36.5 Ni 48.5 Hf 15 high temperature shape memory alloy. Acta Materialia 44, 3711–3721.
Hara, T., Ohba, T., Miyazaki, S., Otsuka, K., 1992. Electron microscopy study of type II twins in $\gamma <$SUB$>$1$<$/SUB$>'$ Cu–Al–Ni Martensite. Materials Transactions, JIM 33, 1105–1113. https://doi.org/10.2320/matertrans1989.33.1105.
Hartl, D.J., Lagoudas, D.C., 2007. Aerospace applications of shape memory alloys. Proceedings of the Institution of Mechanical Engineers, Part G: Journal of Aerospace Engineering 221, 535–552.
Hartl, D.J., Lagoudas, D.C., 2008. Shape Memory Alloys: Modeling and Engineering Applications. Springer. pp. 53–119.
Hashin, Z., Shtrikman, S., 1963. A variational approach to the theory of the elastic behaviour of multiphase materials. Journal of the Mechanics and Physics of Solids 11, 127–140.
Hatcher, N.B., 2010. Electronic and phononic origins of martensitic behavior in nickel titanium-based binary and ternary shape memory alloys, PhD Thesis, Northwestern University.
Hatcher, N., Kontsevoi, O.Y., Freeman, A.J., 2009a. Martensitic transformation path of NiTi. Physical Review B 79. 020202.
Hatcher, N., Kontsevoi, O.Y., Freeman, A.J., 2009b. Role of elastic and shear stabilities in the martensitic transformation path of NiTi. Physical Review B 80. 144203.
Hazar, S., Anlas, G., Moumni, Z., 2016. Evaluation of transformation region around crack tip in shape memory alloys. International Journal of Fracture 197, 99–110. https://doi.org/10.1007/s10704-015-0069-3.
Hazar, S., Zaki, W., Moumni, Z., Anlas, G., 2015. Modeling of steady-state crack growth in shape memory alloys using a stationary method. International Journal of Plasticity 67, 26–38. https://doi.org/10.1016/j.ijplas.2014.08.018.
Heczko, O., Sozinov, A., Ullakko, K., 2000. Giant field-induced reversible strain in magnetic shape memory NiMnGa alloy. IEEE Transactions on Magnetics 36, 3266–3268. https://doi.org/10.1109/20.908764.
Heller, L., Šittner, P., Pilch, J., Landa, M., 2009. Factors controlling superelastic damping capacity of SMAs. Journal of Materials Engineering and Performance 18, 603–611. https://doi.org/10.1007/s11665-009-9358-1.
He, J.Y., Gao, K.W., Su, Y.J., Qiao, L.J., Chu, W.Y., 2004. The role of hydride, martensite and atomic hydrogen in hydrogen-induced delayed fracture of TiNi alloy. Materials Science and Engineering: A 364, 333–338. https://doi.org/10.1016/j.msea.2003.08.062.
He, Y., Yin, H., Zhou, R., Sun, Q., 2010. Ambient effect on damping peak of NiTi shape memory alloy. Materials Letters 64, 1483–1486.
Hill, R., 1952. The elastic behaviour of a crystalline aggregate. Proceedings of the Physical Society. Section A 65, 349.
Hirth, J.P., Pond, R.C., 1996. Steps, dislocations and disconnections as interface defects relating to structure and phase transformations. Acta Materialia 44, 4749–4763. https://doi.org/10.1016/S1359-6454(96)00132-2.
Hirth, J.P., Wang, J., 2021. Extension of the classical theory for types I and II twinning. Journal of Materials Research 36, 2615–2622. https://doi.org/10.1557/s43578-020-00003-6.
Holtz, R., 1999. Fatigue thresholds of Ni-Ti alloy near the shape memory transition temperature. International Journal of Fatigue 21, 137–145. https://doi.org/10.1016/s0142-1123(99)00065-1.
Hornbogen, E., Eggeler, G., 2004. Surface aspects in fatigue of Shape Memory Alloys (SMA). Materialwissenschaft und Werkstofftechnik 35, 255–259. https://doi.org/10.1002/mawe.200400759.
Hornbogen, E., 1985. The effect of variables on martensitic transformation temperatures. Acta Metallurgica 33, 595–601.
Hornbogen, E., 2004. Review thermo-mechanical fatigue of shape memory alloys. Journal of Materials Science 39, 385–399.
Hornbogen, E., 1978. Martensitic transformation at a propagating crack. Acta Metallurgica 26, 147–152. https://doi.org/10.1016/0001-6160(78)90211-0.
Horstemeyer, M., Farkas, D., Kim, S., Tang, T., Potirniche, G., 2010. Nanostructurally small cracks (NSC): A review on atomistic modeling of fatigue. International Journal of Fatigue 32, 1473–1502.
Huang, X., Ackland, G.J., Rabe, K.M., 2003. Crystal structures and shape-memory behaviour of NiTi. Nature Materials 2, 307–311.
Huang, Y., *et al*., 2015. Giant elastocaloric effect in directionally solidified Ni–Mn–In magnetic shape memory alloy. Scripta Materialia 105, 42–45.
Hultgren, R., Desai, P.D., Hawkins, D.T., Gleiser, M., Kelley, K.K., 1973. Selected values of the thermodynamic properties of binary alloys. DTIC Document.
Humbeeck, J.V., Kustov, S., 2005. Active and passive damping of noise and vibrations through shape memory alloys: Applications and mechanisms. Smart Materials and Structures 14, S171–S185. https://doi.org/10.1088/0964-1726/14/5/001.
Hutchinson, J.W., 1968. Singular behaviour at the end of a tensile crack in a hardening material. Journal of the Mechanics and Physics of Solids 16, 13–31. https://doi.org/10.1016/0022-5096(68)90014-8.
Ii, S., Yamauchi, K., Maruhashi, Y., Nishida, M., 2003. Direct evidence of correlation between {20$\bar{1}$} B19′ and {114} B2 deformation twins in Ti–Ni shape memory alloy. Scripta Materialia 49, 723–727.
Ishida, H., Hiwatari, Y., 2007. MD simulation of martensitic transformations in TiNi alloys with MEAM. Molecular Simulation 33, 459–461.
Ishida, A., Takei, A., Sato, M., Miyazaki, S. MRS Proceedings. Cambridge Univ Press, p. 381.
Jacobus, K., Sehitoglu, H., Balzer, M., 1996. Effect of stress state on the stress-induced martensitic transformation in polycrystalline Ni-Ti alloy. Metallurgical and Materials Transactions A 27, 3066–3073.
Jani, J.M., Leary, M., Subic, A., Gibson, M.A., 2014. A review of shape memory alloy research, applications and opportunities. Materials & Design 56, 1078–1113.
Janssen, J., Follon, M., Delaey, L., 1979. In: Haasenv Gerold, P., Kostorz, G. (Eds.), Strength of Metals and Alloys. Pergamon, pp. 1125–1130.

Jiang, X., *et al.*, 1997. In situ observation of stress-induced martensitic transformation and plastic deformation in TiNi alloy. Materials Science and Engineering: A 238, 303–308. https://doi.org/10.1016/S0921-5093(97)00422-X.

Jiang, F., Vecchio, K.S., 2007. Fracture of nitinol under quasistatic and dynamic loading. Metallurgical and Materials Transactions A 38, 2907–2915. https://doi.org/10.1007/s11661-007-9349-5.

Jian, L., Wayman, C.M., 1992. On the mechanism of the shape memory effect associated with (fcc) to (hcp) martensitic transformations in Fe-Mn-Si based alloys. Scripta Metallurgica et Materialia 27, 279–284. https://doi.org/10.1016/0956-716X(92)90512-D.

Jian, L., Wayman, C.M., 1994. Shape memory effect and related phenomena in a microalloyed Fe•Mn•Si alloy. Materials Characterization 32, 215–227. https://doi.org/10.1016/1044-5803(94)90091-4.

Jin, Z., Bieler, T.R., 1995. An in-situ observation of mechanical twin nucleation and propagation in TiAl. Philosophical Magazine A 71, 925–947.

Johnson, A.W., *et al.*, 2005. Analysis of multistep transformations in single-crystal NiTi. Metallurgical and Materials Transactions A 36, 919–928.

Joos, B., Duesbery, M.S., 1997. The Peierls stress of dislocations: An analytic formula. Physical Review Letters 78, 266.

Joós, B., Ren, Q., Duesbery, M.S., 1994. Peierls-Nabarro model of dislocations in silicon with generalized stacking-fault restoring forces. Physical Review B 50, 5890–5898.

Jost, N., 1999. Thermal fatigue of Fe–Ni–Co–Ti shape-memory-alloys. Materials Science and Engineering: A 273–275, 649–653. https://doi.org/10.1016/S0921-5093(99)00341-X.

Juan, J.S., Nó, M.L., Schuh, C.A., 2009. Nanoscale shape-memory alloys for ultrahigh mechanical damping. Nature Nanotechnology 4, 415–419. https://doi.org/10.1038/nnano.2009.142.

Kainuma, R., Ise, M., Jia, C.C., Ohtani, H., Ishida, K., 1996. Phase equilibria and microstructural control in the Ni-Co-Al system. Intermetallics 4, S151–S158. https://doi.org/10.1016/0966-9795(96)00034-9.

Kainuma, R., *et al.*, 2006. Magnetic-field-induced shape recovery by reverse phase transformation. Nature 439, 957–960.

Kajiwara, S., 1999. Characteristic features of shape memory effect and related transformation behavior in Fe-based alloys. Materials Science and Engineering: A 273–275, 67–88. https://doi.org/10.1016/S0921-5093(99)00290-7.

Kajiwara, S., Kikuchi, T., 1982. Dislocation structures produced by reverse martensitic transformation in a Cu ■ Zn alloy. Acta Metallurgica 30, 589–598. https://doi.org/10.1016/0001-6160(82)90240-1.

Kajiwara, S., Owen, W.S., 1977. The martensite-austenite interface and the thickness of twins in martensite in Fe3Pt. Scripta Metallurgica 11, 137–142. https://doi.org/10.1016/0036-9748(77)90293-9.

Kajiware, S., Owen, W.S., 1973. Substructure of austenite formed by a partial reverse martensitic transformation in an Fe-Pt alloy. Metallurgical Transactions 4, 1988–1990. https://doi.org/10.1007/BF02665428.

Karaca, H., *et al.*, 2013a. Effects of nanoprecipitation on the shape memory and material properties of an Ni-rich NiTiHf high temperature shape memory alloy. Acta Materialia 61, 7422–7431.

Karaca, H., Acar, E., Basaran, B., Noebe, R., Chumlyakov, Y., 2012. Superelastic response and damping capacity of ultrahigh-strength [1 1 1]-oriented NiTiHfPd single crystals. Scripta Materialia 67, 447–450.

Karaca, H., Acar, E., Tobe, H., Saghaian, S., 2014. NiTiHf-based shape memory alloys. Materials Science and Technology 30, 1530–1544.

Karaca, H.E., Karaman, I., Chumlyakov, Y.I., Lagoudas, D.C., Zhang, X., 2004. Compressive response of a single crystalline CoNiAl shape memory alloy. Scripta Materialia 51, 261–266. https://doi.org/10.1016/j.scriptamat.2004.04.002.

Karaca, H.E., Karaman, I., Lagoudas, D.C., Maier, H.J., Chumlyakov, Y.I., 2003. Recoverable stress-induced martensitic transformation in a ferromagnetic CoNiAl alloy. Scripta Materialia 49, 831–836. https://doi.org/10.1016/s1359-6462(03)00470-6.

Karaca, H., *et al.*, 2011. Compressive response of nickel-rich NiTiHf high-temperature shape memory single crystals along the [1 1 1] orientation. Scripta Materialia 65, 577–580. doi:10.1016/j.scriptamat.2011.06.027.

Karaca, H., *et al.*, 2013b. Shape memory behavior of high strength NiTiHfPd polycrystalline alloys. Acta Materialia 61, 5036–5049.

Karaman, I., Lagoudas, D.C., 2006. Magnetic Shape Memory Alloys with High Actuation Forces DTIC Document.

Karki, B., Müllner, P., Pond, R., 2020. Topological model of type II deformation twinning in 10M Ni-Mn-Ga. Acta Materialia 201, 604–616. https://doi.org/10.1016/j.actamat.2020.10.020.

Katanchi, B., Choupani, N., Khalil-Allafi, J., Tavangar, R., Baghani, M., 2018. Mixed-mode fracture of a superelastic NiTi alloy: Experimental and numerical investigations. Engineering Fracture Mechanics 190, 273–287. https://doi.org/10.1016/j.engfracmech.2017.12.027.

Khalil-Allafi, J., Dlouhy, A., Eggeler, G., 2002. Ni_4Ti_3-precipitation during aging of NiTi shape memory alloys and its influence on martensitic phase transformations. Acta Materialia 50, 4255–4274.

Khovailo, V., *et al.*, 2001. On order–disorder (L21→ B2′) phase transition in Ni2 + xMn1—xGa Heusler alloys. Physica Status Solidi ((a)) 183, R1–R3.

Kibey, S., Sehitoglu, H., Johnson, D., 2009. Energy landscape for martensitic phase transformation in shape memory NiTi. Acta Materialia 57, 1624–1629.

Kim, H.Y., Fu, J., Tobe, H., Kim, J.I., Miyazaki, S., 2015. Crystal structure, transformation strain, and superelastic property of Ti–Nb–Zr and Ti–Nb–Ta alloys. Shape memory and Superelasticity 1, 107–116.

Kim, H.Y., Hashimoto, S., Kim, J.I., Hosoda, H., Miyazaki, S., 2004. Mechanical properties and shape memory behavior of Ti-Nb alloys. Materials Transactions 45, 2443–2448.

Kim, H., Ikehara, Y., Kim, J., Hosoda, H., Miyazaki, S., 2006a. Martensitic transformation, shape memory effect and superelasticity of Ti–Nb binary alloys. Acta Materialia 54, 2419–2429.

Kim, H.Y., Jinguu, T., Nam, T.-h, Miyazaki, S., 2011. Cold workability and shape memory properties of novel Ti–Ni–Hf–Nb high-temperature shape memory alloys. Scripta Materialia 65, 846–849.

Kim, H.Y., *et al.*, 2006b. Effect of Ta addition on shape memory behavior of Ti–22Nb alloy. Materials Science and Engineering: A 417, 120–128.

Kim, J.I., Kim, H.Y., Inamura, T., Hosoda, H., Miyazaki, S., 2005. Shape memory characteristics of Ti–22Nb–(2–8) Zr (at%) biomedical alloys. Materials Science and Engineering: A 403, 334–339.

Kireeva, I., *et al.*, 2010. Orientation dependence of superelasticity in ferromagnetic single crystals $Co_{49}Ni_{21}Ga_{30}$. The Physics of Metals and Metallography 110, 78–90. https://doi.org/10.1134/s0031918x10070100.

Kirsch, S.-M., *et al.*, 2018. NiTi-based elastocaloric cooling on the macroscale: From basic concepts to realization. Energy Technology 6, 1567–1587. https://doi.org/10.1002/ente.201800152. (doi).

Kishi, Y., *et al.*, 2003. Microstructures and magnetic properties of rapidly solidified CoNiGa ferromagnetic shape memory alloys. Journal of Magnetism and Magnetic Materials 262, L186–L191. https://doi.org/10.1016/s0304-8853(03)00195-1.

Kishi, Y., *et al.*, 2008. Crossing and detwinning of fully twinned martensites in rapidly solidified CoNiGa alloy ribbons. Materials Science and Engineering: A 481–482, 442–445. https://doi.org/10.1016/j.msea.2007.03.124.

Knowles, K.M., Smith, D.A., 1981. The crystallography of the martensitic transformation in equiatomic nickel-titanium. Acta Metallurgica 29, 101–110.

Knowles, K., 1982. A high-resolution electron microscope study of nickel-titanium martensite. Philosophical Magazine A 45, 357–370.

Koch, C.C., 2007. Structural nanocrystalline materials: An overview. Journal of Materials Science 42, 1403–1414. https://doi.org/10.1007/s10853-006-0609-3.

Kockar, B., Karaman, I., Kim, J.I., Chumlyakov, Y., 2006. A method to enhance cyclic reversibility of NiTiHf high temperature shape memory alloys. Scripta Materialia 54, 2203–2208. https://doi.org/10.1016/j.scriptamat.2006.02.029.

Kockar, B., *et al.*, 2010. Role of severe plastic deformation on the cyclic reversibility of a Ti50.3Ni33.7Pd16 high temperature shape memory alloy. Acta Materialia 58, 6411–6420. https://doi.org/10.1016/j.actamat.2010.08.003.

Kohn, W., Becke, A.D., Parr, R.G., 1996. Density functional theory of electronic structure. The Journal of Physical Chemistry 100, 12974–12980.

Kotil, T., Sehitoglu, H., Maier, H., Chumlyakov, Y., 2003. Transformation and detwinning induced electrical resistance variations in NiTiCu. Materials Science and Engineering: A 359, 280–289.

Koval, Y.N., Kokorin, V.V., Khandros, L.G., 1979. Shape memory effect in Fe-Ni- Co-Ti alloys. Physics of Metals and Metallography 48, 162–164.
Kovarik, L., *et al.*, 2010. Structural analysis of a new precipitate phase in high-temperature TiNiPt shape memory alloys. Acta Materialia 58, 4660–4673. https://doi.org/10.1016/j.actamat.2010.04.039.
Ko, W.-S., Grabowski, B., Neugebauer, J., 2015. Development and application of a Ni-Ti interatomic potential with high predictive accuracy of the martensitic phase transition. Physical Review B 92.https://doi.org/10.1103/PhysRevB.92.134107. 134107.
Ko, W.-S., Maisel, S.B., Grabowski, B., Jeon, J.B., Neugebauer, J., 2017. Atomic scale processes of phase transformations in nanocrystalline NiTi shape-memory alloys. Acta Materialia 123, 90–101. https://doi.org/10.1016/j.actamat.2016.10.019.
Krishnan, M., Maji, B.C., 2001. Is the observation of {112} pseudotwins in the B2 phase of Ni-Ti-Fe shape-memory alloys a case of misidentification? Philosophical magazine letters 81, 243–249.
Krooß, P., *et al.*, 2014. Cyclic degradation mechanisms in aged FeNiCoAlTa shape memory single crystals. Acta Materialia 79, 126–137.
Kubin, L.P., Fourdeux, A., Guedou, J.Y., Rieu, J., 1982. Pseudoelasticity and slip reversibility in DO3-ordered Fe–Al single crystals by in situ experiments. Philosophical Magazine A 46, 357–378. https://doi.org/10.1080/01418618208239564.
Kudoh, Y., Tokonami, M., Miyazaki, S., Otsuka, K., 1985. Crystal structure of the martensite in Ti-49.2at% Ni alloy analyzed by the single crystal X-ray diffraction method. Acta Metallurgica 33, 2049–2056.
Kumar, P.K., Lagoudas, D.C., 2010. Experimental and microstructural characterization of simultaneous creep, plasticity and phase transformation in Ti50Pd40Ni10 high-temperature shape memory alloy. Acta Materialia 58, 1618–1628.
Kumar, P.K., *et al.*, 2011. Experimental investigation of simultaneous creep, plasticity and transformation of Ti50:5Pd30Ni19:5 high temperature shape memory alloy during cyclic actuation. Materials Science and Engineering: A 530, 117–127. doi:10.1016/j.msea.2011.09.051.
Kumar, P.K., Lagoudas, D.C., 2008. Shape Memory Alloys: Modeling and Engineering Applications. Springer. pp. 1–51.
Lagoudas, D.C., 2008a. Shape Memory Alloys: Modeling and Engineering Applications. Springer Science & Business Media.
Lagoudas, D., Hartl, D., Chemisky, Y., Machado, L., Popov, P., 2012. Constitutive model for the numerical analysis of phase transformation in polycrystalline shape memory alloys. International Journal of Plasticity 32, 155–183.
Lagoudas, D.C., 2008b. Shape Memory Alloys. Science and Business Media, LLC.
Lagoudas, D.C., *et al.*, 2006. Shape memory alloys, Part II: Modeling of polycrystals. Mechanics of Materials 38, 430–462. https://doi.org/10.1016/j.mechmat.2005.08.003.
Lai, W., Liu, B., 2000. Lattice stability of some Ni-Ti alloy phases versus their chemical composition and disordering. Journal of Physics: Condensed Matter 12, L53.
Lai, W.S., Zhang, Q., Liu, B.X., Ma, E., 2000. Structural stability and amorphization transition in the Ni–Ti system studied by molecular dynamics simulation with an n-body potential. Journal of the Physical Society of Japan 69, 2923–2937.
Leo, P.H., Shield, T.W., Bruno, O.P., 1993. Transient heat transfer effects on the pseudoelastic behavior of shape-memory wires. Acta Metallurgica et Materialia 41, 2477–2485.
LePage, W.S., Shaw, J.A., Daly, S.H., 2021. Effects of texture on the functional and structural fatigue of a NiTi shape memory alloy. International Journal of Solids and Structures 221, 150–164. https://doi.org/10.1016/j.ijsolstr.2020.09.022.
Lexcellent, C., Goo, B.C., Sun, Q.P., Bernardini, J., 1996. Characterization, thermomechanical behaviour and micromechanical-based constitutive model of shape-memory Cu-Zn-Al single crystals. Acta Materialia 44, 3773–3780. https://doi.org/10.1016/1359-6454(95)00452-1.
Lexcellent, C., Thiebaud, F., 2008. Determination of the phase transformation zone at a crack tip in a shape memory alloy exhibiting asymmetry between tension and compression. Scripta Materialia 59, 321–323. https://doi.org/10.1016/j.scriptamat.2008.03.040.
Lieberman, D.S., Wechsler, M., Read, T., 1955. Cubic to orthorhombic diffusionless phase change—experimental and theoretical studies of AuCd. Journal of Applied Physics 26, 473–484.
Lin, B., Gall, K., Maier, H.J., Waldron, R., 2009. Structure and thermomechanical behavior of NiTiPt shape memory alloy wires. Acta Biomaterialia 5, 257–267.
Liu, D.Z., Dunne, D., 2003. Atomic force microscope study of the interface of twinned martensite in copper–aluminium–nickel. Scripta Materialia 48, 1611–1616. https://doi.org/10.1016/S1359-6462(03)00140-4.
Liu, Y., McCormick, P.G., 1996. Criteria of transformation sequences in NiTi shape memory alloys. Matrials Transactions, JIM 37, 691–696.
Liu, J., Xia, M., Huang, Y., Zheng, H., Li, J., 2006a. Effect of annealing on the microstructure and martensitic transformation of magnetic shape memory alloys CoNiGa. Journal of Alloys and Compounds 417, 96–99. https://doi.org/10.1016/j.jallcom.2005.09.026.
Liu, J., Xie, H., Huo, Y., Zheng, H., Li, J., 2006b. Microstructure evolution in CoNiGa shape memory alloys. Journal of Alloys and Compounds 420, 145–157. https://doi.org/10.1016/j.jallcom.2005.10.056.
Liu, Y., Xie, Z., Van Humbeeck, J., Delaey, L., 1998. Asymmetry of stress–strain curves under tension and compression for NiTi shape memory alloys. Acta Materialia 46, 4325–4338.
Liu, Y., Xie, Z., 2003. Twinning and detwinning of< 0 1 1> type II twin in shape memory alloy. Acta Materialia 51, 5529–5543.
Liu, Z., Yu, S., Yang, H., Wu, G., Liu, Y., 2008. Phase separation and magnetic properties of Co,ÄiNi,ÄiAl ferromagnetic shape memory alloys. Intermetallics 16, 447–452. https://doi.org/10.1016/j.intermet.2007.12.004.
Liu, M., Zhang, X.M., Li, Y.Y., Chen, J.Z., Tu, M.J., 2002. High-resolution transmission electron microscope (HRTEM) study of the transformation interface and substructure in NiTiHf40 melt, Äispun ribbons. Journal of Alloys and Compounds 334, 147–153. https://doi.org/10.1016/s0925-8388(01)01762-5.
Liu, J., Zheng, H.X., Xia, M.X., Huang, Y.L., Li, J.G., 2005a. Martensitic transformation and magnetic properties in Heusler CoNiGa magnetic shape memory alloys. Scripta Materialia 52, 935–938. https://doi.org/10.1016/j.scriptamat.2004.12.034.
Liu, J., Zheng, H., Huang, Y., Xia, M., Li, J., 2005b. Microstructure and magnetic field induced strain of directionally solidified ferromagnetic shape memory CoNiAl alloys. Scripta Materialia 53, 29–33. https://doi.org/10.1016/j.scriptamat.2005.03.013.
López, H.F., Salinas-Rodríguez, A., Rodríguez-Galicia, J.L., 1996. Microstructural aspects of precipitation and martensitic transformation in a Ti-rich Ni-Ti alloy. Scripta Materialia 34, 659–664. https://doi.org/10.1016/1359-6462(95)00570-6.
Luo, J., *et al.*, 2016. Fracture properties of polycrystalline NiTi shape memory alloy. Materials Science and Engineering: A 653, 122–128. https://doi.org/10.1016/j.msea.2015.12.014.
Lu, G., Kioussis, N., Bulatov, V.V., Kaxiras, E., 2000. The peierls-nabarro model revisited. Philosophical Magazine Letters 80, 675–682.
Lu, B., Xiao, F., Yan, A., Liu, J., 2014. Elastocaloric effect in a textured polycrystalline Ni-Mn-In-Co metamagnetic shape memory alloy. Applied Physics Letters 105. 161905.
Maki, T., Kobayashi, K., Minato, M., Tamura, I., 1984. Thermoelastic martensite in an ausaged Fe-Ni-Ti-Co alloy. Scripta Metallurgica 18, 1105–1109. https://doi.org/10.1016/0036-9748(84)90187-X.
Malarría, J., Lovey, F.C., Sade, M., 2009. Two way shape memory effect in CuZnAl single crystals after pseudoelastic cycling at low temperatures. Materials Science and Engineering: A 517, 118–124.
Malarría, J., Sade, M., Lovey, F., 2001. Microstructural evolution in the pseudoelastic cycling of Cu–Zn–Al single crystals: behavior at a transition stage. Materials Science and Engineering: A 308, 88–100. https://doi.org/10.1016/S0921-5093(00)02023-2.
Malécot, P., Lexcellent, C., Foltête, E., Collet, M., 2006. Shape memory alloys cyclic behavior: Experimental study and modeling. Journal of Engineering Materials and Technology 128, 335–345. https://doi.org/10.1115/1.2204947.
Maletta, C., Sgambitterra, E., Furgiuele, F., 2013. Crack tip stress distribution and stress intensity factor in shape memory alloys. Fatigue & Fracture of Engineering Materials & Structures 36, 903–912. https://doi.org/10.1111/ffe.12055.
Maletta, C., Sgambitterra, E., Niccoli, F., 2016. Temperature dependent fracture properties of shape memory alloys: novel findings and a comprehensive model. Sci Report 6, 17. https://doi.org/10.1038/s41598-016-0024-1.
Manosa, L., Jarque-Farnos, S., Vives, E., Planes, A., 2013. Large temperature span and giant refrigerant capacity in elastocaloric Cu-Zn-Al shape memory alloys. Applied Physics Letters 103. 211904.

Manosa, L., Jarque-Farnos, S., Vives, E., Planes, A., 2013. Large temperature span and giant refrigerant capacity in elastocaloric Cu-Zn-Al shape memory alloys. Applied Physics Letters 103. 211904. https://doi.org/10.1063/1.4832339.
Mañosa, L., Planes, A., 2017. Materials with giant mechanocaloric effects: Cooling by strength. Advanced Materials 29 (11).
Manosa, L., Planes, A., Ortin, J., Martinez, B., 1993. Entropy change of martensitic transformations in Cu-based shape-memory alloys. Physical Review B (Condensed Matter) 48, 3611–3619. https://doi.org/10.1103/PhysRevB.48.3611.
Manosa, L., Planes, A., Vives, E., Bonnot, E., Romero, R., 2009. The use of shape-memory alloys for mechanical refrigeration. Functional Materials Letters 2, 73–78. https://doi.org/10.1142/S1793604709000594.
Marcinkowski, M.J., Brown, N., 1961. Theory and direct observation of dislocations in the Fe3Al superlattices. Acta Metallurgica 9, 764–786. https://doi.org/10.1016/0001-6160(61)90107-9.
Marcinkowski, M., Sree Harsha, K., 1968. Numerical analysis of deformation twin behavior. Small static twin lamellas. Journal of Applied Physics 39, 6063–6070.
Mari, D., Dunand, D.C., 1995. NiTi and NiTi-TiC composites: Part I. Transformation and thermal cycling behavior. Metallurgical & Materials Transactions A-Physical Metallurgy & Materials Science 26A, 2833–2847.
Ma, J., Karaman, I., Noebe, R.D., 2010. High temperature shape memory alloys. International Materials Reviews 55, 257–315.
Ma, J., *et al.*, 2013. The effect of nanoprecipitates on the superelastic properties of FeNiCoAlTa shape memory alloy single crystals. Acta Materialia 61, 3445–3455. https://doi.org/10.1016/j.actamat.2013.02.036.
McKelvey, A.L., Ritchie, R.O., 1999. Fatigue-crack propagation in Nitinol, a shape-memory and superelastic endovascular stent material. Journal of Biomedical Materials Research 47, 301–308.
McKelvey, A.L., Ritchie, R.O., 2001. Fatigue-crack growth behavior in the superelastic and shape-memory alloy nitinol. Metallurgical and Materials Transactions A 32, 731–743. https://doi.org/10.1007/s11661-001-1008-7.
McMeeking, R.M., Evans, A.G., 1982. Mechanics of transformation-toughening in brittle materials. Journal of the American Ceramic Society 65, 242–246. https://doi.org/10.1111/j.1151-2916.1982.tb10426.x.
Melton, K.N., Mercier, O., 1979a. Fatigue life of CuZnAl alloys. Scripta Metallurgica 13, 73–75. https://doi.org/10.1016/0036-9748(79)90393-4.
Melton, K.N., Mercier, O., 1979b. Fatigue of NITI thermoelastic martensites. Acta Metallurgica 27, 137–144. https://doi.org/10.1016/0001-6160(79)90065-8.
Melton, K., Mercier, O., 1979c. The effect of the martensitic phase transformation on the low cycle fatigue behaviour of polycrystalline NiTi and CuZnAl alloys. Materials Science and Engineering 40, 81–87.
Meng, X., Cai, W., Zheng, Y., Zhao, L., 2006. Phase transformation and precipitation in aged Ti–Ni–Hf high-temperature shape memory alloys. Materials Science and Engineering: A 438, 666–670.
Meng, X., *et al.*, 2002. Stress-induced martensitic transformation behavior of a Ti–Ni–Hf high temperature shape memory alloy. Materials Letters 55, 111–115.
Mercier, O., Melton, K., 1976. The influence of an anisotrophic elastic medium on the motion of dislocations: Application to the martensitic transformation. Scripta Metallurgica 10, 1075–1080.
Mercier, O., Melton, K., Gremaud, G., Hägi, J., 1980. Single-crystal elastic constants of the equiatomic NiTi alloy near the martensitic transformation. Journal of Applied Physics 51, 1833–1834.
Meyer, D., Maier, H.J., Dadda, J., Karaman, I., Karaca, H.E., 2006. Thermally and stress-induced martensitic transformation in Co‚ÄìNi‚ÄìAl ferromagnetic shape memory alloy single crystals. Materials Science and Engineering: A 438–440, 875–878. https://doi.org/10.1016/j.msea.2006.05.038.
Miller, D.A., Lagoudas, D.C., 2001. Influence of cold work and heat treatment on the shape memory effect and plastic strain development of NiTi. Materials Science and Engineering: A 308, 161–175.
Mirzaeifar, R., Gall, K., Zhu, T., Yavari, A., DesRoches, R., 2014. Structural transformations in NiTi shape memory alloy nanowires. Journal of Applied Physics 115. 194307.
Miyazaki, S., Imai, T., Igo, Y., Otsuka, K., 1986. Effect of cyclic deformation on the pseudoelasticity characteristics of Ti-Ni alloys. Metallurgical Transactions A (Physical Metallurgy and Materials Science) 17A, 115–120.
Miyazaki, S., Kimura, S., Otsuka, K., Suzuki, Y., 1984. The habit plane and transformation strains associated with the martensitic transformation in Ti-Ni single crystals. Scripta Metallurgica 18, 883–888. https://doi.org/10.1016/0036-9748(84)90254-0.
Miyazaki, S., Kim, H.Y., Hosoda, H., 2006. Development and characterization of Ni-free Ti-base shape memory and superelastic alloys. Materials Science and Engineering: A 438, 18–24.
Miyazaki, S., Mizukoshi, K., Ueki, T., Sakuma, T., Liu, Y., 1999. Fatigue life of Ti–50 at% Ni and Ti–40Ni–10Cu (at%) shape memory alloy wires. Materials Science and Engineering: A 273, 658–663.
Miyazaki, S., Mizukoshi, K., Ueki, T., Sakuma, T., Liu, Y., 1998. Proceedings of the International Conference on Martensitic Transformations, 7–11 Dec. ICOMAT 98. Elsevier. pp. 658–663.
Miyazaki, S., Ohmi, Y., Otsuka, K., Suzuki, Y., 1982. Characteristics of deformation and transformation pseudoelasticity in Ti-Ni alloys. Journal de Physique Colloques 43. https://doi.org/10.1051/jphyscol:1982434. C4-255-C254-260.
Miyazaki, S., Otsuka, K., Suzuki, Y., 1981. Transformation pseudoelasticity and deformation behavior in a Ti-50.6at%Ni alloy. Scripta Metallurgica 15, 287–292. https://doi.org/10.1016/0036-9748(81)90346-x.
Moberly, W.J., Proft, J.L., Duerig, T.W., Pelton, A.R., Sinclair, R., 1991. Thermomechanical strengthening of B2 intermetallics. New Orleans, LA: Minerals. In: Metals & Materials Soc.(TMS), 387.
Moberly, W.J., Proft, J.L., Duerig, T.W., Sinclair, R., 1990. Deformation, twinning and thermo-mechanical strengthening of Ti 50 Ni 47 Fe 3. Acta Metallurgica et Materialia 38, 2601–2612.
Moberly, W.J., 1991. Mechanical twinning and twinless martensite in ternary Ti50Ni (50-x) Mx intermetallics.
Moffat, D., Kattner, U., 1988. The stable and metastable Ti-Nb phase diagrams. Metallurgical Transactions A 19, 2389–2397.
Mohammed, S., Celebi, O., Sehitoglu, H., 2022. Critical stress prediction upon accurate dislocation core description. Acta Materialia 233, 117989.
Mohammed, A.S.K., Sehitoglu, H., 2020a. Martensitic twin boundary migration as a source of irreversible slip in shape memory alloys. Acta Materialia 186, 50–67.
Mohammed, A.S.K., Sehitoglu, H., 2020b. Modeling the interface structure of type II twin boundary in B19′ NiTi from an atomistic and topological standpoint. Acta Materialia 183, 93–109. https://doi.org/10.1016/j.actamat.2019.10.048.
Mohammed, A.S.K., Sehitoglu, H., 2021. Strain-sensitive topological evolution of twin interfaces. Acta Materialia 208. 116716.
Monroe, J.A., *et al.*, 2011. Determining recoverable and irrecoverable contributions to accumulated strain in a NiTiPd high-temperature shape memory alloy during thermomechanical cycling. Scripta Materialia 65, 123–126. https://doi.org/10.1016/j.scriptamat.2011.03.019.
Monroe, J.A., Karaman, I., Karaca, H.E., Chumlyakov, Y.I., Maier, H.J., 2010. High-temperature superelasticity and competing microstructural mechanisms in Co49Ni21Ga30 shape memory alloy single crystals under tension. Scripta Materialia 62, 368–371. https://doi.org/10.1016/j.scriptamat.2009.11.006.
Morii, K., Ohba, T., Otsuka, K., Sakamoto, H., Shimizu, K., 1991. Crystallography of $\beta 2 \rightarrow \gamma 2'$ martensitic transformation in Au-47.5 at% Cd and Au-47.5 at% Cd•Cu alloys. Acta Metallurgica et Materialia 39, 2719–2725. https://doi.org/10.1016/0956-7151(91)90088-I.
Morito, H., *et al.*, 2005. Effects of partial substitution of Co on magnetocrystalline anisotropy and magnetic-field-induced strain in NiFeGa alloys. Journal of Magnetism and Magnetic Materials 290–291 (Part 2), 850–853. https://doi.org/10.1016/j.jmmm.2004.11.392.
Moshref-Javadi, M., Seyedein, S.H., Salehi, M.T., Aboutalebi, M.R., 2013. Age-induced multi-stage transformation in a Ni-rich NiTiHf alloy. Acta materialia 61, 2583–2594.
Moumni, Z., Herpen, A.V., Riberty, P., 2005. Fatigue analysis of shape memory alloys: Energy approach. Smart Materials and Structures 14, S287–S292. https://doi.org/10.1088/0964-1726/14/5/017.
Moya, X., Kar-Narayan, S., Mathur, N., 2014. Caloric materials near ferroic phase transitions. Nature Materials 13, 439–450.
Müller, I., Xu, H., 1991. On the pseudo-elastic hysteresis. Acta Metallurgica et Materialia 39, 263–271. https://doi.org/10.1016/0956-7151(91)90305-K.

Müllner, P., Chernenko, V., Kostorz, G., 2003. A microscopic approach to the magnetic-field-induced deformation of martensite (magnetoplasticity). Journal of Magnetism and Magnetic Materials 267, 325–334.
Müllner, P., King, A., 2010. Deformation of hierarchically twinned martensite. Acta Materialia 58, 5242–5261.
Müllner, P., Kostorz, G., 2008. Materials Science Forum. Trans Tech Publ 583, 43–65.
Müllner, P., Romanov, A., 2000. Internal twinning in deformation twinning. Acta Materialia 48, 2323–2337.
Mura, T., 2012. Micromechanics of Defects in Solids. vol. 3. Springer Science & Business Media.
Murakami, Y., 1992. Stress Intensity Factors Handbook. vol. 3. Pergamon.
Murray, S.J., Marioni, M., Allen, S.M., O'Handley, R.C., Lograsso, T.A., 2000. 6% magnetic-field-induced strain by twin-boundary motion in ferromagnetic Ni–Mn–Ga. Applied Physics Letters 77, 886–888. https://doi.org/10.1063/1.1306635.
Mutlu, F., Anlaş, G., Moumni, Z., 2020. Effect of loading rate on fracture mechanics of NiTi SMA. International Journal of Fracture 224, 151–165. https://doi.org/10.1007/s10704-020-00450-6.
Mutter, D., Nielaba, P., 2011. Simulation of the thermally induced austenitic phase transition in NiTi nanoparticles. The European Physical Journal B 84, 109–113.
Mutter, D., Nielaba, P., 2013. Simulation of the shape memory effect in a NiTi nano model system. Journal of Alloys and Compounds 577, S83–S87.
Mutter, D., Nielaba, P., 2010. Simulation of structural phase transitions in NiTi. Physical Review B 82. 224201.
Nakahara, T., Shimeno, Y., Hashimoto, T., 2000. Low-cycle fatigue of TiNi shape memory alloy and formulation of fatigue life.
Nam, T.H., Saburi, T., Shimizu, K.i, 1990a. Cu-content dependence of shape memory characteristics in Ti–Ni–Cu alloys. Materials Transactions, JIM 31, 959–967.
Nam, T.H., Saburi, T., Nakata, Y., Shimizu, K.i, 1990b. Shape memory characteristics and lattice deformation in Ti–Ni–Cu alloys. Materials Transactions, JIM 31, 1050–1056.
Nemat-Nasser, S., Yong Choi, J., Guo, W.-G., Isaacs, J.B., Taya, M., 2005a. High strain-rate, small strain response of a NiTi shape-memory alloy. Journal of Engineering Materials and Technology 127, 83–89. https://doi.org/10.1115/1.1839215.
Nemat-Nasser, S., Choi, J.-Y., Guo, W.-G., Isaacs, J.B., 2005b. Very high strain-rate response of a NiTi shape-memory alloy. Mechanics of materials 37, 287–298.
Niclaeys, C., Ben Zineb, T., Arbab-Chirani, S., Patoor, E., 2002. Determination of the interaction energy in the martensitic state. International Journal of Plasticity 18, 1619.
Niendorf, T., *et al.*, 2015. Functional and structural fatigue of titanium tantalum high temperature shape memory alloys (HT SMAs). Materials Science and Engineering: A 620, 359–366. https://doi.org/10.1016/j.msea.2014.10.038.
Nishida, M., Honma, T., 1984. All-round shape memory effect in Ni-rich TiNi alloys generated by constrained aging. Scripta Metallurgica 18, 1293–1298. https://doi.org/10.1016/0036-9748(84)90125-X.
Nishida, M., Ohgi, H., Itai, I., Chiba, A., Yamauchi, K., 1995a. Electron microscopy studies of twin morphologies in B19′ martensite in the Ti-Ni shape memory alloy. Acta metallurgica et materialia 43, 1219–1227.
Nishida, M., Ueda, T., Toyama, Y., Chiba, A., 1990. Materials Science Forum. Trans Tech Publ. 599–604.
Nishida, M., Wayman, C.M., Chiba, A., 1988. Electron microscopy studies of the martensitic transformation in an aged Ti-51at%Ni shape memory alloy. Metallography 21, 275–291. https://doi.org/10.1016/0026-0800(88)90025-0.
Nishida, M., Wayman, C.M., Honma, T., 1986. Precipitation processes in near-equiatomic TiNi shape memory alloys. Metallurgical Transactions A 17, 1505–1515. https://doi.org/10.1007/BF02650086.
Nishida, M., *et al.*, 1998. New deformation twinning mode of B19′ martensite in Ti-Ni shape memory alloy. Scripta Materialia 39, 1749–1754.
Nishida, M., *et al.*, 2006. Crystallography of deformation twin boundaries in a B2 type Ti–Ni alloy. Materials Science and Engineering: A 438, 495–499.
Nishida, M., Yamauchi, K., Itai, I., Ohgi, H., Chiba, A., 1995b. High resolution electron microscopy studies of twin boundary structures in B19′ martensite in the Ti-Ni shape memory alloy. Acta Metallurgica et Materialia 43, 1229–1234.
Nishida, M., *et al.*, 1997. Transmission electron microscopy of twins in martensite in Ti ■ Pd shape memory alloy. Acta Materialia 45, 4847–4853. https://doi.org/10.1016/S1359-6454(97)00162-6.
Nishida, M., *et al.*, 2008. Crystallography and morphology of twins in equiatomic TiPt martensite. Materials Science and Technology 24, 884–889. https://doi.org/10.1179/174328408X302549.
Noebe, R., *et al.*, 2006. Effect of Thermomechanical Processing on the Microstructure, Properties, and Work Behavior of a Ti50.5Ni295.Pt20. Noebe, Ronald, *et al.* "Effect of thermomechanical processing on the microstructure, properties, and work behavior of a Ti50. 5 Ni29. 5 Pt20 high-temperature shape memory alloy." International Conference on Shape Memory and Superelastic Technologies. No. ASM Paper 12688.
Norfleet, D., *et al.*, 2009. Transformation-induced plasticity during pseudoelastic deformation in Ni–Ti microcrystals. Acta Materialia 57, 3549–3561.
Nye, J.F., 1985. Physical Properties of Crystals: Their Representation by Tensors and Matrices. Oxford University Press.
O'Handley, R.C., 2000. Modern Magnetic Materials. Wiley.
Oikawa, K., *et al.*, 2002. Magnetic and martensitic phase transitions in ferromagnetic Ni–Ga–Fe shape memory alloys. Applied Physics Letters 81, 5201–5203.
Oikawa, K., *et al.*, 2001. Phase equilibria and phase transformations in new B2-type ferromagnetic shape memory alloys of Co-Ni-Ga and Co-Ni-Al systems. Materials Transactions 42, 2472–2475. https://doi.org/10.2320/matertrans.42.2472.
Ojha, A., Alkan, S., Patriarca, L., Sehitoglu, H., Chumlyakov, Y., 2015. Shape memory behavior in Fe3Al-modeling and experiments. Philosophical Magazine 95, 2553–2570. https://doi.org/10.1080/14786435.2015.1066939.
Ojha, A., Sehitoglu, H., 2016a. Critical stresses for twinning, slip, and transformation in Ti-based shape memory alloys. Shape Memory and Superelasticity 2, 180–195.
Ojha, A., Sehitoglu, H., 2015. Slip resistance of Ti based high temperature shape memory alloys. Shape Memory and Superelasticity. Ahead of print.
Ojha, A., Sehitoglu, H., 2016b. Slip resistance of Ti-based high-temperature shape memory alloys. Shape Memory and Superelasticity 2, 50–61.
Ojha, A., Sehitoglu, H., 2016c. Transformation stress modeling in new FeMnAlNi shape memory alloy. International Journal of Plasticity 86, 93–111. https://doi.org/10.1016/j.ijplas.2016.08.003.
Okamoto, K., Ichinose, S., Morii, K., Otsuka, K., Shimizu, K., 1986. Crystallography of $\beta 1 \rightarrow \gamma' 1$ stress-induced martensitic transformation in a Cu ■ Al ■ Ni alloy. Acta Metallurgica 34, 2065–2073. https://doi.org/10.1016/0001-6160(86)90265-8.
Olier, P., Brachet, J., Bechade, J., Foucher, C., Guenin, G., 1995. Investigation of transformation temperatures, microstructure and shape memory properties of NiTi, NiTiZr and NiTiHf alloys. Journal de Physique IV 5.(C8-741-C748-746).
Olson, G., Cohen, M., 1982. Stress-assisted isothermal martensitic transformation: application to TRIP steels. Metallurgical Transactions A 13, 1907–1914.
Olson, G.B., Cohen, M., 1975. Thermoelastic behavior in martensitic transformations. Scripta Metallurgica 9, 1247.
Omori, T., Ando, K, Kano, M, *et al.*, 2011. Superelastic effect in polycrystalline ferrous alloys. Science 333, 68–71.
Omori, T., *et al.*, 2004. Phase transformations in Ni–Ga–Fe ferromagnetic shape memory alloys. Materials Science and Engineering: A 378, 403–408.
Omori, T., Kainuma, R., 2017. Martensitic transformation and superelasticity in Fe–Mn–Al-based shape memory alloys. Shape Memory and Superelasticity 3, 322–334.
Onda, T., Bando, Y., Ohba, T., Otsuka, K., 1992. Electron microscopy study of twins in martensite in a Ti-50.0 at% Ni alloy. Materials Transactions, JIM 33, 354–359.
Ortin, J., Planes, A., 1988. Thermodynamic analysis of thermal measurements in thermoelastic martensitic transformations. Acta Metallurgica 36, 1873.
Oshima, R., Sugiyama, M., 1982. Proceedings of the International Conference on Martensitic Transformations, ICOMAT-82, C-4 ed., August 8–12, 1982, pp. 383–388.
Ossmer, H., Chluba, C., Gueltig, M., Quandt, E., Kohl, M., 2015. Local evolution of the elastocaloric effect in TiNi-based films. Shape Memory and Superelasticity 1, 142–152. https://doi.org/10.1007/s40830-015-0014-3.
Ossmer, H., *et al.*, 2014. Evolution of temperature profiles in TiNi films for elastocaloric cooling. Acta Materialia 81, 9–20.
Otsuka, K., Ren, X., 2005. Physical metallurgy of Ti–Ni-based shape memory alloys. Progress in Materials Science 50, 511–678.
Otsuka, K., Sawamura, T., Shimizu, K., 1971. Crystal structure and internal defects of equiatomic TiNi martensite. Physica Status Solidi A 5, 457.

Otsuka, K., Shimizu, K., rsquo, ichi, 1974. Morphology and crystallography of thermoelastic Cu–Al–Ni martensite analyzed by the phenomenological theory. Transactions of the Japan Institute of Metals 15, 103–108. https://doi.org/10.2320/matertrans1960.15.103.
Otsuka, K., Wayman, C.M., 1999. Shape Memory Materials. Cambridge University Press.
Otsuka, K., Wayman, C., 1998. Mechanism of shape memory effect and superelasticity. Shape Memory Materials. 27–49.
Otsuka, K., *et al.*, 1993. The shape memory effect in a Ti 50 Pd 50 alloy. Scripta Metallurgica et Materialia 29, 1355–1358.
Otsuka, K., Wayman, C.M., Nakai, K., Sakamoto, H., Shimizu, K., 1976. Superelasticity effects and stress-induced martensitic transformations in Cu•Al•Ni alloys. Acta Metallurgica 24, 207–226. https://doi.org/10.1016/0001-6160(76)90071-7.
Otsuka, H., *et al.*, 1990. Effects of alloying additions on Fe-Mn-Si shape memory alloys. ISIJ International 30, 674–679.
Ozcan, H., *et al.*, 2018. Microstructural design considerations in Fe-Mn-Al-Ni shape memory alloy wires: Effects of natural aging. Scripta Materialia 142, 153–157.
Ozcan, H., *et al.*, 2017. Effects of cyclic heat treatment and aging on superelasticity in oligocrystalline Fe-Mn-Al-Ni shape memory alloy wires. Scripta Materialia 134, 66–70.
Özerim, G., Anlaş, G., Moumni, Z., 2018. On crack tip stress fields in pseudoelastic shape memory alloys. International Journal of Fracture 212, 205–217. https://doi.org/10.1007/s10704-018-0300-0.
O'Handley, R.C., Murray, S.J., Marioni, M., Nembach, H., Allen, S.M., 2000. Phenomenology of giant magnetic-field-induced strain in ferromagnetic shape-memory materials. Journal of Applied Physics 87, 4712–4717.
O'Donoghue, L., *et al.*, 2010. X-ray and microstructural investigation of NiTiPt alloys homogenised at intermediate to high temperatures. Nuclear Instruments and Methods in Physics Research Section B: Beam Interactions with Materials and Atoms 268, 287–290. https://doi.org/10.1016/j.nimb.2009.07.015.
Paidar, V., 1976. Generalized stacking faults in model lattice of ordered Fe-Si alloys. Czechoslovak Journal of Physics B 26, 865–874. https://doi.org/10.1007/BF01589690.
Parrinello, M., Rahman, A., 1981. Polymorphic transitions in single crystals: A new molecular dynamics method. Journal of Applied physics 52, 7182–7190.
Pataky, G.J., Ertekin, E., Sehitoglu, H., 2015. Elastocaloric cooling potential of NiTi, Ni2FeGa, and CoNiAl. Acta Materialia 96, 420–427. https://doi.org/10.1016/j.actamat.2015.06.011.
Pathak, A., Banumathy, S., Sankarasubramanian, R., Singh, A., 2014. Orthorhombic martensitic phase in Ti–Nb alloys: A first principles study. Computational Materials Science 83, 222–228.
Patoor, E., Eberhardt, A., Berveiller, M., 1996. Micromechanical modelling of superelasticity in shape memory alloys. Le Journal de Physique IV 6.(C1-277-C271-292).
Patoor, E., El Amrani, M., Eberhardt, A., Berveiller, M., 1995a. Determination of the origin for the dissymmetry observed between tensile and compression tests on shape memory alloys. Le Journal de Physique IV 5.(C2-495-C492-500).
Patoor, E., Eberhardt, A., Berveiller, M., 1995b. Micromechanical modelling of the superelastic behavior. Journal De Physique 5, 2.
Patriarca, L., Sehitoglu, H., 2015. High-temperature superelasticity of Ni 50.6 Ti 24.4 Hf 25.0 shape memory alloy. Scripta Materialia 101, 12–15.
Patriarca, L., Sehitoglu, H., Panchenko, E.Y., Chumlyakov, Y., 2016a. High-temperature functional behavior of single crystal Ni51. 2Ti23. 4Hf25. 4 shape memory alloy. Acta Materialia 106, 333–343.
Patriarca, L., Wu, Y., Sehitoglu, H., Chumlyakov, Y.I., 2016b. High temperature shape memory behavior of Ni50.3Ti25Hf24.7 single crystals. Scripta Materialia 115, 133–136. https://doi.org/10.1016/j.scriptamat.2016.01.015.
Peierls, R., 1940. The size of a dislocation. Proceedings of the Physical Society 52, 34.
Pelegrina, J., Ahlers, M., 1992. The martensitic phases and their stability in Cu-Zn and Cu- Zn- Al alloys—I. The transformation between the high temperature β phase and the 18R martensite. Acta metallurgica et materialia 40, 3205–3211.
Pelton, A., *et al.*, 2008. Fatigue and durability of Nitinol stents. Journal of the mechanical behavior of biomedical materials 1, 153–164.
Pelton, A., Huang, G., Moine, P., Sinclair, R., 2012. Effects of thermal cycling on microstructure and properties in Nitinol. Materials Science and Engineering: A 532, 130–138.
Pelton, A., 2011. Nitinol fatigue: A review of microstructures and mechanisms. Journal of Materials Engineering and Performance 20, 613–617.
Perez-Saez, R., Recarte, V., Nó, M., San Juan, J., 1998. Anelastic contributions and transformed volume fraction during thermoelastic martensitic transformations. Physical Review B 57, 5684.
Perkins, J., 1975. Shape Memory Effects in Alloys. New York: Springer Science & Business Media.
Pfetzing-Micklich, J., *et al.*, 2012. Orientation dependence of stress-induced phase transformation and dislocation plasticity in NiTi shape memory alloys on the micro scale. Materials Science and Engineering: A 538, 265–271.
Pfetzing-Micklich, J., *et al.*, 2013. On the crystallographic anisotropy of nanoindentation in pseudoelastic NiTi. Acta Materialia 61, 602–616.
Planes, A., Mañosa, L., Acet, M., 2009. Magnetocaloric effect and its relation to shape-memory properties in ferromagnetic Heusler alloys. Journal of Physics: Condensed Matter 21. 233201.
Planes, A., Mañosa, L., Saxena, A., 2005. Magnetism and Structure in Functional Materials. Springer.
Pond, R.C., 1989.Chapter – 38 In: Nabarro, (Ed.), Dislocations in Solids, vol. 8. Elsevier.
Pond, R., Celotto, S., 2003. Special interfaces: Military transformations. International materials reviews 48, 225–245.
Pond, R.C., Hirth, J.P., 2018. Topological model of type II deformation twinning. Acta Materialia 151, 229–242. https://doi.org/10.1016/j.actamat.2018.03.014.
Pond, R.C., Hirth, J.P., Knowles, K.M., 2019. Topological model of type II deformation twinning in NiTi martensite. Philosophical Magazine 99, 1619–1632. https://doi.org/10.1080/14786435.2019.1587185.
Pond, R.C., Ma, X., Chai, Y.W., Hirth, J.P., 2007. In: Nabarro, F.R.N., Hirth, J.P. (Eds.), Dislocations in Solids, vol. 13. Elsevier.
Pons, J., Chernenko, V., Santamarta, R., Cesari, E., 2000. Crystal structure of martensitic phases in Ni–Mn–Ga shape memory alloys. Acta Materialia 48, 3027–3038.
Pons, J., Sade, M., Lovey, F., Cesari, E., 1993. Pseudoelastic cycling and two-way shape memory effect in β Cu–Zn–Al alloys with γ-precipitates. Materials Transactions, JIM 34, 888–894.
Pons, J., Santamarta, R., Chernenko, V., Cesari, E., 2003. HREM study of different martensitic phases in Ni–Mn–Ga alloys. Materials Chemistry and Physics 81, 457–459.
Pons, J., Santamarta, R., Chernenko, V.A., Cesari, E., 2005. Long-period martensitic structures of Ni-Mn-Ga alloys studied by high-resolution transmission electron microscopy. Journal of Applied Physics 97. 083516.
Potapov, P.L., *et al.*, 1997. Effect of Hf on the structure of Ni-Ti martensitic alloys. Materials Letters 32, 247–250.
Pozzi, M., Airoldi, G., 1999. The electrical transport properties of shape memory alloys. Materials Science and Engineering: A 273–275, 300–304. https://doi.org/10.1016/s0921-5093(99)00359-7.
Prokoshkin, S., *et al.*, 2016. Manufacturing, structure control, and functional testing of Ti–Nb-based SMA for medical application. Shape Memory and Superelasticity. 1–15.
Pun, G.P., Yamakov, V., Mishin, Y., 2015. Interatomic potential for the ternary Ni–Al–Co system and application to atomistic modeling of the B2–L10 martensitic transformation. Modelling and Simulation in Materials Science and Engineering 23. 065006.
Qian, S., *et al.*, 2016. A review of elastocaloric cooling: Materials, cycles and system integrations. International Journal of Refrigeration 64, 1–19. https://doi.org/10.1016/j.ijrefrig.2015.12.001.
Rajagopalan, S., Little, A., Bourke, M., Vaidyanathan, R., 2005. Elastic modulus of shape-memory NiTi from in situ neutron diffraction during macroscopic loading, instrumented indentation, and extensometry. Applied Physics Letters 86. 081901.
Rajini Kanth, B., *et al.*, 2010. Effect of annealing on the martensitic transformation of a CoNiAl ferromagnetic shape memory alloy. Journal of Alloys and Compounds 491, 22–25. https://doi.org/10.1016/j.jallcom.2009.10.227.
Rao, J., Roberts, T., Lawson, K., Nicholls, J., 2010. Nickel titanium and nickel titanium hafnium shape memory alloy thin films. Surface and Coatings Technology 204, 2331–2336. https://doi.org/10.1016/j.surfcoat.2009.12.025.

Reedlunn, B., Daly, S., Hector, L., Zavattieri, P., Shaw, J., 2013. Tips and tricks for characterizing shape memory wire Part 5: Full-field strain measurement by digital image correlation. Experimental Techniques 37, 62–78.
Ren, X., Otsuka, K., 1997. Origin of rubber-like behaviour in metal alloys. Nature 389, 579–582.
Ren, G., Sehitoglu, H., 2016. Interatomic potential for the NiTi alloy and its application. Computational Materials Science 123, 19–25.
Ren, X., *et al*., 2001. A comparative study of elastic constants of Ti–Ni-based alloys prior to martensitic transformation. Materials Science and Engineering: A 312, 196–206.
Reuss, A., 1929. Berechnung der fließgrenze von mischkristallen auf grund der plastizitätsbedingung für einkristalle. ZAMM-Journal of Applied Mathematics and Mechanics/ Zeitschrift für Angewandte Mathematik und Mechanik 9, 49–58.
Rice, J.R., Thomson, R., 1974. Ductile versus brittle behaviour of crystals. The Philosophical Magazine: A Journal of Theoretical Experimental and Applied Physics 29, 73–97.
Ritter, A., Yang, N.Y.C., Pope, D.P., Laird, C., 1979. The dislocation and martensite substructures of a fatigued, polycrystalline, pseudoelastic Cu-Al-Ni alloy. Metallurgical Transactions A 10, 667–676. https://doi.org/10.1007/BF02658387.
Robertson, S.W., Mehta, A., Pelton, A.R., Ritchie, R.O., 2007. Evolution of crack-tip transformation zones in superelastic Nitinol subjected to in situ fatigue: A fracture mechanics and synchrotron X-ray microdiffraction analysis. Acta Materialia 55, 6198–6207. https://doi.org/10.1016/j.actamat.2007.07.028.
Robertson, S.W., Pelton, A.R., Ritchie, R.O., 2012. Mechanical fatigue and fracture of Nitinol. International Materials Reviews 57, 1–37. https://doi.org/10.1179/1743280411y.0000000009.
Robertson, S.W., Ritchie, R.O., 2007. In vitro fatigue–crack growth and fracture toughness behavior of thin-walled superelastic Nitinol tube for endovascular stents: A basis for defining the effect of crack-like defects. Biomaterials 28, 700–709. https://doi.org/10.1016/j.biomaterials.2006.09.034.
Rodriguez, P.L., Condo, A.M., Lovey, F.C., 1996. Quantitative analysis of dislocations in relation with the martensitic transformation in Cu-Zn-Al alloys. Physica Status Solidi ((b)) 197, 279–292. https://doi.org/10.1002/pssb.2221970202.
Roitburd, A., Kurdjumov, G., 1979. The nature of martensitic transformations. Materials Science and Engineering 39, 141–167.
Romero, R., Lovey, F., Ahlers, M., 1988. Plasticity in β phase Cu-Zn-Al alloys. Philosophical Magazine A 58, 881–903. https://doi.org/10.1080/01418618808214421.
Saburi, T., Inada, Y., Nenno, S., Hori, N., 1982. Stress-induced martensitic transformations in Cu-Zn-Al and Cu-Zn-Ga alloys. Le Journal de Physique Colloques 43.(C4-633-C634-638).
Saburi, T., Nenno, S., Fukuda, T., 1986. Crystal structure and morphology of the metastable X phase in shape memory Ti-Ni alloys. Journal of the Less Common Metals 125, 157–166.
Potirniche, G., Horstemeyer, M., Gullett, P., Jelinek, B., 2006. Proceedings of the Royal Society of London A: Mathematical, Physical and Engineering Sciences. The Royal Society, 462,pp. 3707–3731.
Patoor, E., El Amrani, M., Eberhardt, A., Berveiller, 1995. J. de Physique 5, C2 495–500.
Saburi T., Nenno, S., 1981. The shape memory effect and related phenomena. In: Aaronson, H.I., Laughlin, D.E., Serkeka, R.E., Wayman, C.M. (Eds.), Proc. Int. Conf., Solid-Solid Phase Transformations, pp. 1455–1479. Pittsburgh, P.A.
Sade, M., Hornbogen, E., 1988. Fatigue of single- and polycrystalline -CuZn-base shape memory alloys. Zeitschrift fur Metallkunde 79, 782–787.
Sade, M., *et al*., 2007. Fatigue and martensitic transitions in Cu–Zn–Al and Cu–Al–Ni single crystals: Mechanical behaviour, defects and diffusive phenomena. Smart Materials and Structures 16, S126.
Sade, M., Rapacioli, R., Ahlers, M., 1985. Fatigue in Cu ■Zn■ Al single crystals. Acta Metallurgica 33, 487–497. https://doi.org/10.1016/0001-6160(85)90091-4.
Sade, M., Uribarri, A., Lovey, F., 1987. An electron-microscopy study of dislocation structures in fatigued Cu-Zn-Al shape-memory alloys. Philosophical Magazine A 55, 445–461. https://doi.org/10.1080/01418618708209908.
San Juan, J., Nó, M., 2003. Damping behavior during martensitic transformation in shape memory alloys. Journal of Alloys and Compounds 355, 65–71.
San Juan, J., Perez-Saez, R.B., 2001. 5.4 transitory effects. Materials Science Forum 366–368, 416–436. https://doi.org/10.4028/www.scientific.net/MSF.366-368.416.
Sandu, A., Tsuchiya, K., Yamamoto, S., Todaka, Y., Umemoto, M., 2006. Influence of isothermal ageing on mechanical behaviour in Ni-rich Ti–Zr–Ni shape memory alloy. Scripta Materialia 55, 1079–1082.
Sanjabi, S., Cao, Y.Z., Barber, Z.H., 2005. Multi-target sputter deposition of $Ni_{50}Ti_{50-x}Hf_x$ shape memory thin films for high temperature microactuator application. Sensors and Actuators A: Physical 121, 543–548. https://doi.org/10.1016/j.sna.2005.04.006.
Santamarta, R., *et al*., 2013. TEM study of structural and microstructural characteristics of a precipitate phase in Ni-rich Ni–Ti–Hf and Ni–Ti–Zr shape memory alloys. Acta Materialia 61, 6191–6206.
Sateesh, V.L., Senthilkumar, P., Satisha, Dayananda, G.N., 2014. Low cycle fatigue evaluation of NiTi SESMA thin wires. Journal of Materials Engineering and Performance 23, 2429–2436. https://doi.org/10.1007/s11665-014-1062-0.
Sato, A., Chishima, E., Soma, K., Mori, T., 1982. Shape memory effect in $\gamma \rightleftarrows \epsilon$ transformation in Fe-30Mn-1Si alloy single crystals. Acta Metallurgica 30, 1177–1183. https://doi.org/10.1016/0001-6160(82)90011-6.
Sato, A., Chishima, E., Yamaji, Y., Mori, T., 1984. Orientation and composition dependencies of shape memory effect in Fe-Mn-Si alloys. Acta Metallurgica 32, 539–547.
Sato, A., Mori, T., 1991. Development of a shape memory alloy Fe-Mn-Si. Materials Science and Engineering: A 146, 197–204.
Sato, T., Saitoh, K.-i, Shinke, N., 2006. Molecular dynamics study on microscopic mechanism for phase transformation of Ni–Ti alloy. Modelling and Simulation in Materials Science and Engineering 14, S39.
Sawaguchi, T., *et al*., 2016. Design concept and applications of Fe–Mn–Si-based alloys—from shape-memory to seismic response control. Materials Transactions 57, 283–293.
Schetky, L.M., 1991. Shape memory alloy applications in space systems. Materials & Design 12, 29–32.
Schmidt, M., *et al*., 2015. Thermal stabilization of NiTiCuV shape memory alloys: Observations during elastocaloric training. Shape Memory and Superelasticity 1, 132–141. https://doi.org/10.1007/s40830-015-0021-4.
Schmid, E., Boas, W., 1950. Plasticity of Crystals. A. Hughes and Co.
Schroeder, T., Wayman, C., 1979. Pseudoelastic effects in Cu ■ Zn single crystals. Acta Metallurgica 27, 405–417.
Schryvers, D., Tirry, W., Yang, Z., 2006. Measuring strain fields and concentration gradients around Ni_4Ti_3 precipitates. Materials Science and Engineering: A 438, 485–488.
Sedlak, P., Frost, M., Benešová, B., Zineb, T.B., Šittner, P., 2012. Thermomechanical model for NiTi-based shape memory alloys including R-phase and material anisotropy under multi-axial loadings. International Journal of Plasticity 39, 132–151.
Sedmák, P., *et al*., 2016. Grain-resolved analysis of localized deformation in nickel-titanium wire under tensile load. Science 353, 559–562.
Sedmák, P., Šittner, P., Pilch, J., Curfs, C., 2015. Instability of cyclic superelastic deformation of NiTi investigated by synchrotron X-ray diffraction. Acta Materialia 94, 257–270.
Seguí, C., Cesari, E., Pons, J., Chernenko, V., 2004. Internal friction behaviour of Ni–Mn–Ga. Materials Science and Engineering: A 370, 481–484. https://doi.org/10.1016/j.msea.2003.07.008.
Sehitoglu, H., *et al*., 2000. Compressive response of NiTi single crystals. Acta Materialia 48, 3311–3326.
Sehitoglu, H., Efstathiou, C., Maier, H., Chumlyakov, Y., 2005. Magnetization, shape memory and hysteresis behavior of single and polycrystalline FeNiCoTi. Journal of Magnetism and Magnetic Materials 292, 89–99.
Sehitoglu, H., Gall, K., 1999. Role of texture in tension-compression asymmetry of polycrystalline NiTi. International Journal of Plasticity(UK) 15, 69–92.
Sehitoglu, H., Patriarca, L., Wu, Y., 2017a. Shape memory strains and temperatures in the extreme. Current Opinion in Solid State and Materials Science 21, 113–120.
Sehitoglu, H., Wang, J., Maier, H., 2012. Transformation and slip behavior of Ni2FeGa. International Journal of Plasticity 39, 61–74.
Sehitoglu, H., *et al*., 2002. Shape memory behavior of FeNiCoTi single and polycrystals. Metallurgical and Materials Transactions A: Physical Metallurgy and Materials Science 33, 3661–3672.
Sehitoglu, H., *et al*., 2001a. Shape memory and pseudoelastic behavior of 51.5%Ni-Ti single crystals in solutionized and overaged state. Acta Materialia 49, 3609–3620. https://doi.org/10.1016/S1359-6454(01)00216-6.
Sehitoglu, H., *et al*., 2001b. Deformation of NiTiCu shape memory single crystals in compression. Metallurgical and Materials Transactions A 32, 477–489.

Sehitoglu, H., Karaman, I., Zhang, X.Y., Chumlyakov, Y., Maier, H.J., 2001c. Deformation of FeNiCoTi shape memory single crystals. Scripta Materialia 44, 779–784.
Sehitoglu, H., Wu, Y., Patriarca, L., 2017b. Shape memory functionality under multi-cycles in NiTiHf. Scripta Materialia 129, 11–15.
Sehitoglu, H., *et al.*, 2017c. Superelasticity and shape memory behavior of NiTiHf alloys. Shape Memory and Superelasticity 3, 168–187.
Sehitoglu, H., *et al.*, 2003. Detwinning in NiTi alloys. Metallurgical and Materials Transactions A 34, 5–13.
Sehitoglu, H., Hamilton, R., Maier, H., Chumlyakov, Y., 2004. Journal de Physique IV (Proceedings). EDP Sciences,115, pp. 3–10.
Sehitoglu, H., 2001. Compressive response of NiTi single crystals, by H. Sehitoglu, I. Karaman, R. Anderson, X. Zhang, K. Gall, HJ Maier and Y. Chumlyakov, originally published in Acta Materialia, Volume 48 (13), pp. 3311–3326, 2000. Acta Materialia 49, 747–747.
Sehitoglu, H., Y, W., Alkan, S., Ertekin, E., 2017d. Plastic deformation of B2-NiTi – Is it slip or twinning? To Appear in Philosophical Magazine Letters.
Sgambitterra, E., *et al.*, 2019. Effects of temperature on fatigue crack propagation in pseudoelastic NiTi shape memory alloys. Shape Memory and Superelasticity 5, 278–291.
Sgambitterra, E., Maletta, C., Furgiuele, F., Sehitoglu, H., 2018. Fatigue crack propagation in [0 1 2] NiTi single crystal alloy. International Journal of Fatigue 112, 9–20.
Shaw, J.A., Kyriakides, S., 1995. Thermomechanical aspects of NiTi. Journal of the Mechanics and Physics of Solids 43, 1243–1281.
Shaw, J.A., 2000. Simulations of localized thermo-mechanical behavior in a NiTi shape memory alloy. International Journal of Plasticity 16, 541–562.
Shield, T.W., 1995. Orientation dependence of the pseudoelastic behavior of single crystals of Cu ■ Al ■ Ni in tension. Journal of the Mechanics and Physics of Solids 43, 869–895. https://doi.org/10.1016/0022-5096(95)00011-7.
Shivasiddaramaiah, A.G., Mallikarjun, U.S., Jeevan, Prashantha, S., 2018. Synthesis and evaluation of fracture behaviour of Cu-Al-Be-Mn quaternary shape memory alloy. Materials Today: Proceedings 5, 24457–24465. https://doi.org/10.1016/j.matpr.2018.10.242.
Sidharth, R., Wu, Y., Brenne, F., Abuzaid, W., Sehitoglu, H., 2020a. Relationship between functional fatigue and structural fatigue of iron-based shape memory alloy FeMnNiAl. Shape Memory and Superelasticity 6, 256–272.
Sidharth, R., Abuzaid, W., Vollmer, M., Niendorf, T., Sehitoglu, H., 2020b. Fatigue crack initiation in the iron-based shape memory alloy FeMnAlNiTi. Shape Memory and Superelasticity 6, 323–331.
Sih, G.C., 1973. Handbook of Stress-Intensity Factors : Stress-Intensity Factor Solutions and Formulas for Reference4. Institute of Fracture and Solid Mechanics, Lehigh University.
Simon, T., Kröger, A., Somsen, C., Dlouhy, A., Eggeler, G., 2010. On the multiplication of dislocations during martensitic transformations in NiTi shape memory alloys. Acta Materialia 58, 1850–1860.
Sinclair, R., Mohamed, H.A., 1978. Lattice imaging study of a martensite-austenite interface. Acta Metallurgica 26, 623–628. https://doi.org/10.1016/0001-6160(78)90114-1.
Sittner, P., *et al.*, 2014. Youngs modulus of austenite and martensite phases in superelastic NiTi wires. Journal of Materials Engineering and Performance 23, 2303–2314.
Soboyejo, W.O., Srivatsan, T., 2006. Advanced Structural Materials: Properties, Design Optimization, and Applications. CRC press.
Söderberg, O., Ge, Y., Sozinov, A., Hannula, S., Lindroos, V., 2005. Recent breakthrough development of the magnetic shape memory effect in Ni–Mn–Ga alloys. Smart Materials and Structures 14, S223.
Sohmura, T., Oshima, R., Fujita, F.E., 1980. Thermoelastic FCC-FCT martensitic transformation in Fe-Pd alloy. Scripta Metallurgica 14, 855–856. https://doi.org/10.1016/0036-9748(80)90304-X.
Solomon, V.C., *et al.*, 2005. Magnetic domain configurations in spark-eroded ferromagnetic shape memory Ni-Mn-Ga particles. Applied Physics Letters 86, 2503.
Sozinov, A., Likhachev, A., Lanska, N., Ullakko, K., 2002. Giant magnetic-field-induced strain in NiMnGa seven-layered martensitic phase. Applied Physics Letters 80, 1746–1748.
Soolshenko, V., Lanska, N., Ullakko, K., 2003. Journal de Physique IV (Proceedings), 112, 947–950.
Sozinov, A., Likhachev, A.A., Ullakko, K., 2001. Proceedings of the SPIE's 8th Annual International Symposium on Smart Structures and Materials, 4333, pp. 189–196.
Stam, G., van der Giessen, E., 1995. Effect of reversible phase transformations on crack growth. Mechanics of Materials 21, 51–71. https://doi.org/10.1016/0167-6636(94)00074-3.
Stebner, A., Brinson, L.C., 2013. Explicit finite element implementation of an improved three dimensional constitutive model for shape memory alloys. Computer Methods in Applied Mechanics and Engineering 257, 17–35.
Stebner, A., Brown, D., Brinson, L., 2013. Young's modulus evolution and texture-based elastic–inelastic strain partitioning during large uniaxial deformations of monoclinic nickel–titanium. Acta Materialia 61, 1944–1956.
Stebner, A.P., *et al.*, 2014. Transformation strains and temperatures of a nickel-titanium-hafnium high temperature shape memory alloy. Acta Materialia 76, 40–53. https://doi.org/10.1016/j.actamat.2014.04.071.
Straka, L., Novák, V., Landa, M., Heczko, O., 2004. Acoustic emission of Ni–Mn–Ga magnetic shape memory alloy in different straining modes. Materials Science and Engineering: A 374, 263–269.
Stroh, A.N., 1958. Dislocations and cracks in anisotropic elasticity. Philosophical Magazine 3, 625–646.
Sugiyama, M., Oshima, R., Fujita, F.E., 1984a. Martensitic transformation in the Fe-Pd alloy system. Transactions of the Japan Institute of Metals 25, 585–592.
Sugiyama, M., Oshima, R., Fujita, F.E., 1984b. Transmission electron microscopy of FCC-FCT thermoelastic martensite transformation in Fe-Pd alloys. Journal of the Japan Institute of Metals 48, 881–889.
Sun, W., Liu, J., Lu, B., Li, Y., Yan, A., 2016. Large elastocaloric effect at small transformation strain in Ni 45 Mn 44 Sn 11 metamagnetic shape memory alloys. Scripta Materialia 114, 1–4.
Surikova, N.S., Chumlyakov, Y.I., 2000. Mechanisms of plastic deformation in titanium nickelide single crystals. Fizika Metallov i Metallovedenie (The Physics of Metals and Metallography) 89, 98–107.
Sutou, Y., *et al.*, 2004. Stress-strain characteristics in Ni–Ga–Fe ferromagnetic shape memory alloys. Applied physics letters 84, 1275–1277.
Suzuki, H., 1962. Segregation of solute atoms to stacking faults. Journal of the Physical Society of Japan 17, 322–325.
Tadaki, T., Nakata, Y., Shimizu, K.i, Otsuka, K., 1986. Crystal structure, composition and morphology of a precipitate in an aged Ti-51 at% Ni shape memory alloy. Transactions of the Japan Institute of Metals 27, 731–740.
Tadaki, T., Nakata, Y., Shumizu, K., 1987. Thermal cycling effects in an aged Ni-Rich Ti-Ni shape memory alloy. Transactions of the Japan Institute of Metals 28, 883–890.
Tadaki, T., Wayman, C., 1982. Electron microscopy studies of martensitic transformations in Ti50Ni50–xCux alloys. Part I. Compositional dependence of one-third reflections from the matrix phase. Metallography 15, 233–245.
Tadmor, E.B., Miller, R.E., 2011. Modeling Materials: Continuum, Atomistic and Multiscale Techniques. Cambridge University Press.
Tahara, M., Kim, H.Y., Hosoda, H., Miyazaki, S., 2009. Shape memory effect and cyclic deformation behavior of Ti–Nb–N alloys. Functional Materials Letters 2, 79–82.
Takahashi, E., Sakurai, T., Watanabe, S., Masahashi, N., Hanada, S., 2002. Effect of heat treatment and Sn content on superelasticity in biocompatible TiNbSn alloys. Materials Transactions 43, 2978–2983.
Tanaka, K., Sato, Y., 1986. Analysis of superplastic deformation during isothermal martensitic transformation. Res Mechanica 17, 241–252.
Tang, T., Kim, S., Horstemeyer, M., 2010. Fatigue crack growth in magnesium single crystals under cyclic loading: Molecular dynamics simulation. Computational Materials Science 48, 426–439.
Tang, W., Sandström, R., Wei, Z., Miyazaki, S., 2000. Experimental investigation and thermodynamic calculation of the Ti-Ni-Cu shape memory alloys. Metallurgical and Materials Transactions A 31, 2423–2430.
Taylor, G.I., 1928. The deformation of crystals of β-brass. Proceedings of the Royal Society of London A: Mathematical, Physical and Engineering Sciences 118, 1–24.
Teng, Y., Zhu, S., Wang, F., Wu, W., 2007. Electronic structures and shape-memory behavior of Ti 50 Ni 50 − xCux (x= 0, 6.25, 12.5, 18.75 and 25.0 at%) by density functional theory. Physica B: Condensed Matter 393, 18–23.
Thamburaja, P., Anand, L., 2001. Polycrystalline shape-memory materials: effect of crystallographic texture. Journal of the Mechanics and Physics of Solids 49, 709–737.
Thumann, M., Hornbogen, E., 1988. Thermal and mechanical fatigue in Cu-base shape memory alloys. Zeitschrift fur Metallkunde 79, 119–126.

Tickle, R.J., 2000. Ferromagnetic Shape Memory Materials. University of Minnesota.
Timofeeva, E., Panchenko, E.Y., Chumlyakov, Y.I., Maier, H., 2012. Development of thermoelastic martensitic transformations in ferromagnetic [011]-oriented NiFeGa single crystals in compression. Russian Physics Journal. 1–4.
Tirry, W., Schryvers, D., 2005. Quantitative determination of strain fields around Ni_4Ti_3 precipitates in NiTi. Acta materialia 53, 1041–1049.
Tobushi, H., Shimeno, Y., Hachisuka, T., Tanaka, K., 1998. Influence of strain rate on superelastic properties of TiNi shape memory alloy. Mechanics of Materials 30, 141–150.
Tong, C.-J., *et al*., 2005a. Microstructure characterization of AlxCoCrCuFeNi high-entropy alloy system with multiprincipal elements. Metallurgical and Materials Transactions A 36, 881–893. https://doi.org/10.1007/s11661-005-0283-0.
Tong, Y., Chen, F., Tian, B., Li, L., Zheng, Y., 2009. Microstructure and martensitic transformation of $Ti_{49}Ni_{51-x}Hf_x$ high temperature shape memory alloys. Materials Letters 63, 1869–1871. https://doi.org/10.1016/j.matlet.2009.05.069.
Tong, Y., Liu, Y., Miao, J., 2008. Phase transformation in NiTiHf shape memory alloy thin films. Thin Solid Films 516, 5393–5396. https://doi.org/10.1016/j.tsf.2007.07.015.
Tong, Y., Liu, Y., Miao, J., Zhao, L., 2005b. Characterization of a nanocrystalline NiTiHf high temperature shape memory alloy thin film. Scripta Materialia 52, 983–987. https://doi.org/10.1016/j.scriptamat.2005.01.030.
Treppmann, D., Hornbogen, E., 1995. The effect of dislocation substructure and decomposition on the course of diffusionless transformations. Le Journal de Physique IV (Journal de Physique IV) 5.(C2-211-C212-216).
Tseng, L., *et al*., 2015a. The effect of precipitates on the superelastic response of [100] oriented FeMnAlNi single crystals under compression. Acta Materialia 97, 234–244.
Tseng, L., *et al*., 2015b. Superelastic response of a single crystalline FeMnAlNi shape memory alloy under tension and compression. Acta Materialia 89, 374–383.
Tseng, L.W., Ma, J., Wang, S.J., Karaman, I., Chumlyakov, Y.I., 2016. Effects of crystallographic orientation on the superelastic response of FeMnAlNi single crystals. Scripta Materialia 116, 147–151.
Tyumentsev, A., *et al*., 2004. Mechanism of deformation and crystal lattice reorientation in strain localization bands and deformation twins of the B2 phase of titanium nickelide. Acta Materialia 52, 2067–2074.
Ullakko, K., Huang, J.K., Kantner, C., O'Handley, R.C., Kokorin, V.V., 1996. Large magnetic-field-induced strains in Ni2MnGa single crystals. Applied Physics Letters 69, 1966–1968. https://doi.org/10.1063/1.117637.
Umakoshi, Y., Yamaguchi, M., Yamane, T., 1985. In: Suzuki, H., Ninomiya, T., Sumino, K., Takeuchi, S. (Eds.), Dislocations in Solids: Proceedings of Yamada Conference IX. University of Tokyo Press, pp. 81–84.
Van Humbeeck, J., Delaey, L., 1981. The influence of strain-rate, amplitude and temperature on the hysteresis of a pseudoelastic Cu-zn-al Single Crystal. Journal de Physique Archives 42.(C5-1007-C1005-1011).
Van Humbeeck, J., 2001. 5.3 the martensitic transformation. Materials Science Forum 366–368, 382–415. https://doi.org/10.4028/www.scientific.net/MSF.366-368.382.
Van Humbeeck, J., 2003. Damping capacity of thermoelastic martensite in shape memory alloys. Journal of Alloys and Compounds 355, 58–64. https://doi.org/10.1016/S0925-8388(03)00268-8.
Venkateswaran, S., Nuhfer, N., De Graef, M., 2007. Magnetic domain memory in multiferroic Ni 2 MnGa. Acta Materialia 55, 5419–5427.
Verbeken, K., Van Caenegem, N., Raabe, D., 2009. Identification of υ martensite in a Fe-based shape memory alloy by means of EBSD. Micron 40, 151–156.
Vinals, J., Torra, V., Planes, A., Macqueron, J.L., 1984. Effect of atomic order on the thermodynamic properties of the martensitic transformation in CuZn and CuZnAl alloys. Philosophical Magazine A: Physics of Condensed Matter, Structure, Defects and Mechanical Properties 50, 653–666.
Vishnu, K.G., Strachan, A., 2010. Phase stability and transformations in NiTi from density functional theory calculations. Acta Materialia 58, 745–752.
Vives, E., *et al*., 2011. Temperature contour maps at the strain-induced martensitic transition of a Cu–Zn–Al shape-memory single crystal. Applied Physics Letters 98. 011902.
Vivet, A., Lexcellent, C., 1999. Observations and analysis of martensitic phase transformation on CuZnAl single crystals. Le Journal de Physique IV 9.(Pr9–411-Pr419–418).
Voigt, W., 1928. Lehrbuch der kristallphysik (mit ausschluss der kristalloptik). Springer-Verlag.
Vollmer, M., *et al*., 2019. On the microstructural and functional stability of Fe-Mn-Al-Ni at ambient and elevated temperatures. Scripta Materialia 162, 442–446.
Vollmer, M., *et al*., 2016. Cyclic degradation in bamboo-like Fe–Mn–Al–Ni shape memory alloys — The role of grain orientation. Scripta Materialia 114, 156–160. https://doi.org/10.1016/j.scriptamat.2015.12.007.
Vollmer, M., *et al*., 2017a. Cyclic degradation behavior of <001>-oriented Fe–Mn–Al–Ni single crystals in tension. Shape Memory and Superelasticity 3, 335–346.
Vollmer, M., Krooß, P., Karaman, I., Niendorf, T., 2017b. On the effect of titanium on quenching sensitivity and pseudoelastic response in Fe-Mn-Al-Ni-base shape memory alloy. Scripta Materialia 126, 20–23.
Vollmer, M., *et al*., 2015. On the effect of gamma phase formation on the pseudoelastic performance of polycrystalline Fe–Mn–Al–Ni shape memory alloys. Scripta Materialia 108, 23–26. https://doi.org/10.1016/j.scriptamat.2015.06.013.
Wagner, M.-X., Windl, W., 2008. Lattice stability, elastic constants and macroscopic moduli of NiTi martensites from first principles. Acta Materialia 56, 6232–6245.
Wagner, M.F.-X., Windl, W., 2009. Elastic anisotropy of Ni_4Ti_3 from first principles. Scripta Materialia 60, 207–210.
Waitz, T., Antretter, T., Fischer, F., Simha, N., Karnthaler, H., 2007. Size effects on the martensitic phase transformation of NiTi nanograins. Journal of the Mechanics and Physics of Solids 55, 419–444.
Waitz, T., Kazykhanov, V., Karnthaler, H., 2004. Martensitic phase transformations in nanocrystalline NiTi studied by TEM. Acta Materialia 52, 137–147.
Waitz, T., Spišák, D., Hafner, J., Karnthaler, H., 2005. Size-dependent martensitic transformation path causing atomic-scale twinning of nanocrystalline NiTi shape memory alloys. EPL (Europhysics Letters) 71, 98.
Wang, H.Y., Liu, Z.H., Wang, Y.G., Duan, X.F., Wu, G.H., 2005. Microstructure of martensitic phase in the Co39Ni33Al28 shape memory alloys revealed by transmission electron microscopy. Journal of Alloys and Compounds 400, 145–149. https://doi.org/10.1016/j.jallcom.2005.03.055.
Wang, J., Sehitoglu, H., 2013. Twinning stress in shape memory alloys: Theory and experiments. Acta Materialia 61, 6790–6801.
Wang, J., Sehitoglu, H., 2014a. Dislocation slip and twinning in Ni-based L12 type alloys. Intermetallics 52, 20–31.
Wang, J., Sehitoglu, H., 2014b. Modeling of pseudotwinning in Fe3Ga. Modelling and Simulation in Materials Science and Engineering 22. 055008.
Wang, J., Sehitoglu, H., 2014c. Modelling of martensite slip and twinning in NiTiHf shape memory alloys. Philosophical Magazine 94, 2297–2317. https://doi.org/10.1080/14786435.2014.913109.
Wang, J., Sehitoglu, H., Maier, H.J., 2014. Dislocation slip stress prediction in shape memory alloys. International Journal of Plasticity 54, 247–266. https://doi.org/10.1016/j.ijplas.2013.08.017.
Wang, J., Sehitoglu, H., 2012. Resolving quandaries surrounding NiTi. Applied Physics Letters 101. 081907.
Wang, J., Sehitoglu, H., 2014d. Martensite modulus dilemma in monoclinic NiTi-theory and experiments. International Journal of Plasticity 61, 17–31.
Wang, X., Xu, B., Yue, Z., Tong, X., 2008. Fracture behavior of the compact tension specimens in NiTi shape memory alloys. Materials Science and Engineering: A 485, 14–19. https://doi.org/10.1016/j.msea.2007.07.056.
Wang, Y., Zheng, Y., Cai, W., Zhao, L., 1999. The tensile behavior of Ti36Ni49Hf15 high temperature shape memory alloy. Scripta Materialia 40, 1327–1331.
Wang, L., *et al*., 2019. Superelastic effect in Ti-rich high entropy alloys via stress-induced martensitic transformation. Scripta Materialia 162, 112–117. https://doi.org/10.1016/j.scriptamat.2018.10.035.
Warlimont, H., Delaey, L., 1974. Martensitic transformations in Cu-, Ag- and Au-based alloys. Progress in Materials Science 18.(160 p).
Wayman, C.M., 1964. Introduction to the Crystallography of Martensitic Transformations. Macmillan.
Wayman, C.M., 1993. International Conference on Martensitic Transformations (ICOMAT 92), 104p.
Webster, P., Ziebeck, K., Town, S., Peak, M., 1984. Magnetic order and phase transformation in Ni2MnGa. Philosophical Magazine B 49, 295–310.
Webster, J., 2006. Smart structures and materials. In: Industrial and Commercial Applications of Smart Structures Technologies, 61710F. International Society for Optics and Photonics.

Wechsler, M.S., Lieberman, D.S., Read, T.A., 1953. On theory of formation of martensite. Journal of Metals 5, 1503–1515.
Williams, M.L., 1957. On the stress distribution at the base of a stationary crack. Journal of Applied Mechanics 24, 109–114. https://doi.org/10.1115/1.4011454.
Wollmershauser, J.A., Kabra, S., Agnew, S.R., 2009. In situ neutron diffraction study of the plastic deformation mechanisms of B2 ordered intermetallic alloys: NiAl, CuZn, and CeAg. Acta Materialia 57, 213–223. https://doi.org/10.1016/j.actamat.2008.08.066.
Wu, Y., Ojha, A., Patriarca, L., Sehitoglu, H., 2015. Fatigue crack growth fundamentals in shape memory alloys. Shape Memory and Superelasticity 1, 18–40.
Wu, Y., Patriarca, L., Sehitoglu, H., Chumlyakov, Y., 2016. Ultrahigh tensile transformation strains in new Ni50.5Ti36.2Hf13.3 shape memory alloy. Scripta Materialia 118, 51–54. https://doi.org/10.1016/j.scriptamat.2016.03.009.
Wu, M.H., Perkins, J., Wayman, C.M., 1989. Long range order, antiphase domain structures, and the formation mechanism of α1 ("Bainite") plates in A Cu-Zn-Al alloy. Acta Metallurgica 37, 1821–1837. https://doi.org/10.1016/0001-6160(89)90067-9.
Wu, Y., *et al.*, 2019. Deshielding effects on fatigue crack growth in shape memory alloys-A study on CuZnAl single-crystalline materials. Acta Materialia 176, 155–166.
Xiangyang, Z., Qingping, S., Shouwen, Y., 2000. A non-invariant plane model for the interface in CuAlNi single crystal shape memory alloys. Journal of the Mechanics and Physics of Solids 48, 2163–2182. https://doi.org/10.1016/S0022-5096(99)00102-7.
Xiao, F., Fukuda, T., Kakeshita, T., 2013. Significant elastocaloric effect in a Fe-31.2Pd (at%) single crystal. Applied Physics Letters 102. 161914. https://doi.org/10.1063/1.4803168.
Xiao, F., Jin, M., Liu, J., Jin, X., 2015. Elastocaloric effect in Ni 50 Fe 19 Ga 27 Co 4 single crystals. Acta Materialia 96, 292–300.
Xie, Z., Liu, Y., Van Humbeeck, J., 1998. Microstructure of NiTi shape memory alloy due to tension–compression cyclic deformation. Acta Materialia 46, 1989–2000.
Xie, Z.L., Liu, Y., 2004. HRTEM study of⟨ 011⟩ type II twin in NiTi shape memory alloy. Philosophical Magazine 84, 3497–3507.
Xiong, F., Liu, Y., 2007. Effect of stress-induced martensitic transformation on the crack tip stress-intensity factor in Ni–Mn–Ga shape memory alloy. Acta Materialia 55, 5621–5629. https://doi.org/10.1016/j.actamat.2007.06.031.
Xu, G.-f, Yin, Z.-m, Mou, S.-z, Luo, F.-h, Oikawa, K., 2006. Martensitic and magnetic transformation of Co41Ni32Al24Sb3 and Co41Ni32Al27 alloys. Transactions of Nonferrous Metals Society of China 16, 776–782. https://doi.org/10.1016/s1003-6326(06)60325-7.
Yaacoub, J., Sehitoglu, H., 2019. 9th ECCOMAS Thematic Conference on Smart Structures and Materials, SMART. International Center for Numerical Methods in Engineering. pp. 837–843.
Yamaguchi, M., Pope, D.P., Vitek, V., Umakoshi, Y., 1981. Planar faults and dislocation dissociations in body-centred-cubic-derivative ordered structures. Philosophical Magazine A 43, 1265–1275. https://doi.org/10.1080/01418618108236155.
Yamaguchi, M., Umakoshi, Y., 1984. In: Paidar, V., Lejcek, L. (Eds.), The Structure and Properties of Crystal Defects. Elsevier, p. 131.
Yamaguchi, M., Umakoshi, Y., 1990. The deformation behaviour of intermetallic superlattice compounds. Progress in Materials Science 34, 1–148. https://doi.org/10.1016/0079-6425(90)90002-Q.
Yamaguchi, M., Umakoshi, Y., 1983. In: Paidar, V., Lejcek, L. (Eds.), The Structure and Properties of Crystal Defects. Elsevier.
Yamakov, V., *et al.*, 2016. Multiscale modeling of sensory properties of Co–Ni–Al shape memory particles embedded in an Al metal matrix. Journal of Materials Science 51, 1204–1216.
Yamauchi, K., Ohkata, I., Tsuchiya, K., Miyazaki, S., 2011. Shape Memory and Superelastic Alloys: Applications and Technologies. Elsevier.
Yang, F., *et al.*, 2013. Structure analysis of a precipitate phase in an Ni-rich high-temperature NiTiHf shape memory alloy. Acta Materialia 61, 3335–3346.
Yang, N.Y.C., Laird, C., Pope, D.P., 1977. The cyclic stress-strain response of polycrystalline, pseudoelastic Cu-14.5 wt pct Al-3 wt pct Ni alloy. Metallurgical Transactions A 8, 955–962. https://doi.org/10.1007/BF02661579.
Yang, W.S., Mikkola, D.E., 1993. Ductilization of Ti-Ni-Pd shape memory alloys with boron additions. Scripta Metallurgica et Materialia 28, 161–165. https://doi.org/10.1016/0956-716x(93)90556-8.
Yang, J.H., Wayman, C.M., 1994. On the formation mechanism of Ni5Al3 in NiAl-base alloys: Part I. Microstructures. Intermetallics 2, 111–119. https://doi.org/10.1016/0966-9795(94)90005-1.
Yasuda, H.Y., *et al.*, 2005. Effect of Al concentration on pseudoelasticity in Fe3Al single crystals. Acta Materialia 53, 5343–5351. https://doi.org/10.1016/j.actamat.2005.08.011.
Yasuda, H.Y., Nakajima, T., Umakoshi, Y., 2007. Temperature dependence of pseudoelasticity in Fe3Al single crystals. Intermetallics 15, 819–823. https://doi.org/10.1016/j.intermet.2006.10.006.
Yasuda, H.Y., Nakano, K., Ueda, M., Umakoshi, Y., 2003. Orientation dependence of pseudoelasticity in Fe3Al single crystals. Materials Science Forum 426–432, 1801–1806.
Yasuda, H.Y., Umakoshi, Y., 2010. Pseudoelastic behaviour of Fe3Al single crystals with D03 structure. Intermetallics 18, 1273–1278. https://doi.org/10.1016/j.intermet.2010.01.007.
Ye, Y., Chan, C., Ho, K.M., 1997. Structural and electronic properties of the martensitic alloys TiNi, TiPd, and TiPt. Physical Review B 56, 3678.
Yin, H., He, Y., Sun, Q., 2014. Effect of deformation frequency on temperature and stress oscillations in cyclic phase transition of NiTi shape memory alloy. Journal of the Mechanics and Physics of Solids 67, 100–128.
Yin, H., Yan, Y., Huo, Y., Sun, Q., 2013. Rate dependent damping of single crystal CuAlNi shape memory alloy. Materials Letters 109, 287–290. https://doi.org/10.1016/j.matlet.2013.07.062.
Yi, S., Gao, S., 2000. Fracture toughening mechanism of shape memory alloys due to martensite transformation. International Journal of Solids and Structures 37, 5315–5327. https://doi.org/10.1016/s0020-7683(99)00213-9.
Yi, S., Gao, S., Shen, L., 2001. Fracture toughening mechanism of shape memory alloys under mixed-mode loading due to martensite transformation. International Journal of Solids and Structures 38, 4463–4476. https://doi.org/10.1016/s0020-7683(00)00283-3.
Yu, H.J., Fu, H., Sun, J.X., Wang, Z.G., Zu, X.T., 2009a. Transformation temperatures in polycrystalline Ni56.5,âíxFe17 Ga26.5Gex ferromagnetic shape memory alloys. Journal of Alloys and Compounds 477, 628–631. https://doi.org/10.1016/j.jallcom.2008.10.137.
Yu, H.J., *et al.*, 2009b. Phase transformations and magnetocaloric effect in NiFeGa ferromagnetic shape memory alloy. Journal of Alloys and Compounds 477, 732–735. https://doi.org/10.1016/j.jallcom.2008.10.143.
Zaki, W., Moumni, Z., 2007. A three-dimensional model of the thermomechanical behavior of shape memory alloys. Journal of the Mechanics and Physics of Solids 55, 2455–2490.
Zamora, R., Baker, K., Warner, D., 2015. Illuminating the chemo-mechanics of hydrogen enhanced fatigue crack growth in aluminum alloys. Acta Materialia 100, 232–239.
Zarinejad, M., Liu, Y., Tong, Y., 2009. Transformation temperature changes due to second phase precipitation in NiTi-based shape memory alloys. Intermetallics 17, 914–919. https://doi.org/10.1016/j.intermet.2009.03.022.
Zarinejad, M., Liu, Y., White, T.J., 2008. The crystal chemistry of martensite in NiTiHf shape memory alloys. Intermetallics 16, 876–883. https://doi.org/10.1016/j.intermet.2008.04.004.
Zarkevich, N.A., Johnson, D.D., 2014. Shape-memory transformations of NiTi: Minimum-energy pathways between austenite, martensites, and kinetically limited intermediate states. Physical review letters 113. 265701.
Zayak, A., Entel, P., Enkovaara, J., Ayuela, A., Nieminen, R., 2002. First-principles investigations of homogeneous lattice-distortive strain and shuffles in Ni2MnGa. Journal of Physics: Condensed Matter 15, 159.
Zayak, A., Entel, P., Enkovaara, J., Ayuela, A., Nieminen, R.M., 2003. First-principles investigation of phonon softenings and lattice instabilities in the shape-memory system Ni_2MnGa. Physical Review B 68. 132402.
Zayak, A., Entel, P., 2004. Role of shuffles and atomic disorder in Ni–Mn–Ga. Materials Science and Engineering: A 378, 419–423.
Hatcher, N., Kontsevoi, O.Y., Freeman, A.J., 2009. Structural stabilities, elastic constants, generalized stacking fault energetics, and the martensitic transformation mechanisms for the $Ni_{50-x}TiPt_x$ ($x = 0 - 30$) ternary system: ab initio investigation Proceedings of the European Symposium on Martensitic Transformations. EDP Sciences, Articel No. 02010.
Zayak, A., Entel, P., Hafner, J., 2003. Journal de Physique IV (Proceedings). EDP Sciences 112, 985–988.
Zener, C., 1938. Internal friction in solids II. General theory of thermoelastic internal friction. Physical Review 53, 90.

Zhang, X., Feng, P., He, Y., Yu, T., Sun, Q., 2010. Experimental study on rate dependence of macroscopic domain and stress hysteresis in NiTi shape memory alloy strips. International Journal of Mechanical Sciences 52, 1660–1670.
Zhang, X., Sehitoglu, H., 2004. Crystallography of the B2→ R→ B19′ phase transformations in NiTi. Materials Science and Engineering: A 374, 292–302.
Zhang, J., *et al*., 2012. Leaf-like dislocation substructures and the decrease of martensitic start temperatures: A new explanation for functional fatigue during thermally induced martensitic transformations in coarse-grained Ni-rich Ti–Ni shape memory alloys. Acta Materialia 60, 1999–2006. https://doi.org/10.1016/j.actamat.2011.12.014.
Zhang, Y., *et al*., 2017. Experimental and theoretical investigation of the frequency effect on low cycle fatigue of shape memory alloys. International Journal of Plasticity 90, 1–30. https://doi.org/10.1016/j.ijplas.2016.11.012.
Zhang, L., 1999. Twin-intersection-related nanotwinning in a heavily deformed gamma-TiAl-based alloy. Philosophical Magazine Letters 79, 49–54.
Zheng, Y., Zhang, J., Zhao, L., Ye, H., 1999. HREM studies on the microstructure of severely cold-rolled TiNi alloy after reverse martensitic transformation. Materials Letters 41, 9–15.
Zhong, Y., Gall, K., Zhu, T., 2011. Atomistic study of nanotwins in NiTi shape memory alloys. Journal of Applied Physics 110. 033532.
Zhong, Y., Gall, K., Zhu, T., 2012. Atomistic characterization of pseudoelasticity and shape memory in NiTi nanopillars. Acta Materialia 60, 6301–6311.
Zhou, X., Li, X.Y., Lu, K., 2018. Enhanced thermal stability of nanograined metals below a critical grain size. Science 360, 526.
Zhu, Y., Dui, G., 2010. Micromechanical modeling of stress, Äistrain behaviors with intermartensitic transformation in NiFeGa alloys. Mechanics of Materials 42, 429–434. https://doi.org/10.1016/j.mechmat.2010.02.003.
Zou, N., *et al*., 2018. Plastic deformation of Ni–Mn–Ga 7M modulated martensite by twinning & detwinning and intermartensitic transformation. International Journal of Plasticity 100, 1–13. https://doi.org/10.1016/j.ijplas.2017.07.006.